Development of an Innovative Biomechanical Model for Clinical Gait Analysis

Thesis submitted to University College London for the degree of

Doctor of Philosophy

Matthew James Thornton

[redacted]

Division of Surgery and Interventional Science

Institute of Orthopaedic and Musculoskeletal Science

May 2022

I Matthew James Thornton confirm that the work presented in this thesis is my own. Where information has been derived from other sources, I can confirm that this has been indicated in the thesis.

Abstract

Work contained in this thesis describes a new biomechanical model for clinical gait analysis. Identified problems with current models are related to the subjective reasonableness of their underlying modelling assumptions and used to guide development of a new model.

Gait scores were developed to evaluate alternative modelling solutions in terms of cycle average position, range, inter-cycle variability and movement pattern. An overly simple pro-forma model was developed to facilitate evaluation of the effects of complexity from alternative modelling approaches, both existing and newly developed.

A clinical interpretation of Euler angles, widely used to describe joint orientations and movements, is presented. Leading directly from this interpretation, simple, joint-specific rules are derived that ensure calculated angles match clinical terminology. Other identified concerns are tackled on a per body-segment basis, with each segment presenting a different challenge.

Identified problems with current trunk models were related to difficulties of orientating and tracking movement of the whole based on a selected sub-region. This was solved via the development of a more holistic solution, which additionally reduces the need for patient upper body exposure.

For the pelvis and thigh segments, excessive soft tissue cover was identified as the major issue and resolved by the amalgamation of published methods with the novel introduction of fixed length thigh segments and a bespoke axial alignment calibration procedure.

Foot model accuracy was improved by the application of bespoke calibration(s) that relates a defining flat foot posture to the position of surface markers, thus reducing the requirement for accurate placement over bony landmarks. Existing multi-segment foot models were grouped by a novel complexity index. Analysis of each group revealed an optimal balance with hind, medial forefoot, and lateral forefoot divisions. A model with this configuration was developed and outputs related to existing clinical terminology describing the foot shape.

Impact Statement

The original aim for this thesis was to develop methods of transforming the output signals from gait analysis into clinically meaningful scores that could form the basis of a machine learning approach. These scores were intended to represent clinically meaningful gait characteristics, that could be directly comparable between different individuals. Key to this comparability, was that each score represented a measurable physical quantity. Initial development served to illustrate that the required inter-subject comparability was not sufficiently robust in the gait signal on which the scores were based. On analysis, it quickly became apparent that the scores were not objectively meaningful because the surface marker movements did not sufficiently reflect those of the underlying bones, and that this mismatch was particularly apparent for the transverse plane kinematics.

Work contained in this thesis describes a surface marker configuration developed to overcome the theoretical and demonstrable weaknesses of currently employed methods. In addition to providing a foundation for future research, including the originally envisaged machine learning approach, the new biomechanical model has significantly improved clinical outputs from the RNOH gait analysis service. Comparison of segmental orientations with equivalent video images have anecdotally provided both a driving force for development, and a validation of the final solution. We are currently in discussion with Vicon, the predominate manufacturer of clinical motion capture systems, as to how the model might best be made more widely available. I have additionally been selected as a finalist for the DePuy Best Bioengineering Project Award, to be presented at the Institute of Mechanical Engineers this June.

From a patient perspective, the model development philosophy of finding a minimally complex solution capable of representing the required anatomy, has resulted in additional utility benefits over current solutions. No surface markers are located over the upper thigh regions, such that these regions need not be exposed for accurate data collection. Similarly, for the trunk segment, the proposed model can do away with thoracic surface markers and concomitant undressing requirement.

From the clinician’s perspective, the requirement for unrealistically accurate surface marker placement to represent bony axes, is replaced by the introduction of segment-specific static calibrations. For the hind and forefoot segments, rather than the representation of anatomical axis by surface markers, neutral axes are defined and related to the surface marker locations during a neutral trial. The full model calibration is then performed in a crouched posture, both minimising deviation from this calibration position during gait, and providing full weight bearing static information about the knee joint axis orientation, required to accurately model the thigh segments.

Taken together, the described improvements have resulted in a novel biomechanical model with greater accuracy than currently available solutions.

Acknowledgements

The duration of this PhD has spanned a period of both personal and world turbulence, that I would not have survived without the generous support from many other people. Top of this list must be Professor Roger Woledge, whose recognition provided the confidence necessary to embark on such an ordeal so late in my career. Although Roger was sadly lost to a horse-riding accident early in his retirement and my studies, his embedded influence continued to have profound influence on my thought process throughout.

Thanks are also due to Professor Gordon Blunn, who provided the opportunity for me to register for the PhD, and to Professor Rui Loureiro and Dr Steve Taylor for maintaining this registration on Gordon's move to Portsmouth University. I am especially indebted to Dr Lynsey Duffell, who was able to interpret my clinical conclusions into the discernible structure that holds this thesis together – Thank you.

The commencement of these studies coincided with a restructuring of RNOH clinical services, during which the old gait laboratory was amalgamated into a newly formed therapies division. Praise is due to my constant companions, Roisin Delaney and Professor Deborah Eastwood for their insightful feedback throughout, and who kept the clinical service on track while I was pre-occupied with delivering the technical advantages envisaged for the first UK clinical, treadmill-based gait laboratory. Special thanks are also due to our laboratory technician, Olivia McVeigh-Mellor, whose patient listening, and shrewd questioning were critical to the creation of a coherent concept.

Last, but by no means least, I must acknowledge the sacrifice and support of my wife Claire and son Zachary, who have both given up large chunks of family life to allow me to bring this thesis to fruition. You are my world.

Table of Contents

Table of Figures

Table of Tables

Abbreviations List

2D	2-Dimmentional
3D	3-Dimmentional
AJC	Ankle Joint Centre
AMD	Absolute Mean Difference
Ant	Anterior
ARF	Anatomical Reference Frame
asis	anterior superior iliac spine
BMC	Baseline Model Concept
BMI	Body Mass Index
calc	calcaneus
CAST	Calibration Anatomical System Technique
CGA	Clinical Gait Analysis
CGM	Conventional Gait Model
CMAS	Clinical Motion Analysis Society
Cor	Coronal
dist	distal
DK	Direct Kinematic
Epi	Epicondyle
FD	Forward Dynamic
fib	fibula
fore	forefoot
GPS	Gait Profile Score
GT	Greater Trochanter
GVS	Gait Variable Score
Harr	Harrington
HBM	Human Body Model
head1	first metatarsal head
head5	fifth metatarsal head
HFMM	Heidelberg Foot Measurement Method
hind	hind foot
HJC	Hip Joint Centre
Hor	Transverse
ID	Inverse Dynamic
IK	Inverse Kinematic
inf	Inferior
IOMS	Institute of Orthopaedics and Musculoskeletal Science
ISB	International Society of Biomechanics
JCS	Joint Coordinate System
JN	Jugular Notch
KAD	Knee Alignment Device
KJC	Knee Joint Centre
L	Left
L1-5	Spinous Process of Lumber Vertebrae
Lat	Lateral
Mal	Malleolus
Med	Medial
MEMS	Micro Electro-Mechanical System
MFM	Milwaukee Foot Model
mid	middle
MLL	Motor Learning Lab
mm	millimetre
mo-cap	motion capture
mOFM	modified Oxford Foot Model
MRI	Magnetic Resonance Imaging
MSFM	Multi-Segment Foot Model
OFM	Oxford Foot Model
PiG	Plug in Gait
prox	proximal
psis	posterior superior iliac spine
r	Correlation coefficient
R	Right
R^2	Coefficient of Determination
RMS	Root Mean Square
RNOH	Royal National Orthopaedic Hospital
Sag	Sagittal
SHCG	Shriners Hospital for Children Greenville
STA	Soft Tissue Artefact
sup	Superior
T1-12	Spinous Process of Thoracic Vertebrae
TRF	Technical Reference Frame
UCL	University College London
UEL	University of East London
UK	United Kingdom
USA	United States of America
wrt	with respect to
XP	Xiphisternal

1 Chapter 1 – General Introduction

Clinical gait analysis involves the assessment of an individual's walking pattern from data collected under controlled conditions. Motion capture (mo-cap) technology is commonly employed to estimate skeletal segment orientations, based on the tracked positions of reflective markers fixed to the skin surface (Baker et al., 2016, Wren et al., 2011). The set of rules and assumptions applied to achieve this transformation are contained within a biomechanical model. This chapter identifies issues with current modelling approaches, sets objectives for the development of a new model, and provides background information on which the development of this model at the Royal National Orthopaedic Hospital (RNOH) is based, and which is described in subsequent chapters.

1.1 Four Modelling Paradigms

Throughout the thesis, appropriate combinations of up to four biomechanical modelling approaches are compared. The conventional gait model (CGM), refers to the currently widely used model, which remains largely unchanged since its inception during the late 1980's. The technical ability of early mo-cap systems to track surface markers, required CGM to make several concessions to model accuracy in favour of utility; most notable of these is the avoidance of medial marker locations required to define body segment planes in a direct manner. This concession asks clinicians to locate additional lateral markers over the thigh and shank segments that, with other surface markers, would represent the same coronal plane as a medial marker. The inevitable random error that this indirect definition of body segment introduces, is addressed in chapter 2, as part of a baseline model concept (BMC) development. BMC represents the simplest, most direct method of modelling each body segment's principal plane, making no concessions to either model utility or tracking accuracy. These latter issues are then addressed in subsequent chapters on a segment-by-segment basis. Each of these chapters present an RNOH modelling solution as an optimised balance of anatomical, utility and tracking considerations for a clinical gait model. Finally, the Calibrated Anatomical System Technique (CAST) modelling technique represents a modelling philosophy where surface markers employed to define

segment anatomical orientation during a static trial, are not re-employed to track that orientation through dynamic movements. Alternative markers located to avoid unwanted soft tissue wobble, are instead calibrated to the anatomical marker locations, such that they may perform the dynamic tracking function but continue to report this movement around the segment's anatomical axis. The CAST paradigm is the major alternative to CGM currently available.

1.2 Seminal Papers in Gait Analysis

During the mid-1990s, as a mature physiotherapy student, I was introduced to instrumented gait analysis by Dr Matt Morrissey, who was busy establishing the inaugural biomechanics laboratory at the University of East London (UEL). Matt was keen for me to apply my technical mechanical engineering background to some of their clinical studies. At this early time in clinical gait analysis development, two issues were prevalent in the published literature. The first issue concerned the representation of 3D joint angles in the clinical setting and was exemplified by two published papers, both now considered seminal (Chao, 1980, Grood and Suntay, 1983). The second issue concerning configuration of surface marker location was exemplified by two more, both now also considered seminal (Davis et al., 1991, Kadaba et al., 1990). At that time, I found all of these publications technically complex for what at first glance was a seemingly simple problem. To me it seemed reasonable that joint angles during gait, could be measured frame by frame from orthogonal video images, that this identification might be enhanced by the application of target markers on the subject's skin surface, and that the process might be made less labour intensive, and the requirement for the video to be orthogonal removed, by the emerging and increasingly commercially available motion capture (mo-cap) technology.

1.3 The RNOH Gait Analysis Laboratory –aging equipment

Following my undergraduate studies, I embarked on a short clinical career away from gait analysis. Prior to this I was able to make a small contribution to the field, concerning the inherent tracking accuracy of the UEL system (Thornton et al., 1998). I was reintroduced to the subject when a position became available at RNOH in 2005. Shortly before this, my good friend and mentor Professor Roger

Woledge, had retired from heading up UCL's Institute of Human Performance, based on the RNOH site, which had consequently transitioned into the more clinical role of the hospital's gait laboratory. For the next ten years the resident clinical physiotherapist, Roisin Delaney, and myself nursed the already aged equipment to provide a clinical gait analysis service under the auspices of CGM variant provided by the manufacturer. This variant was unusual in its application of wands to capture the segmental movements (Figure 1-1).

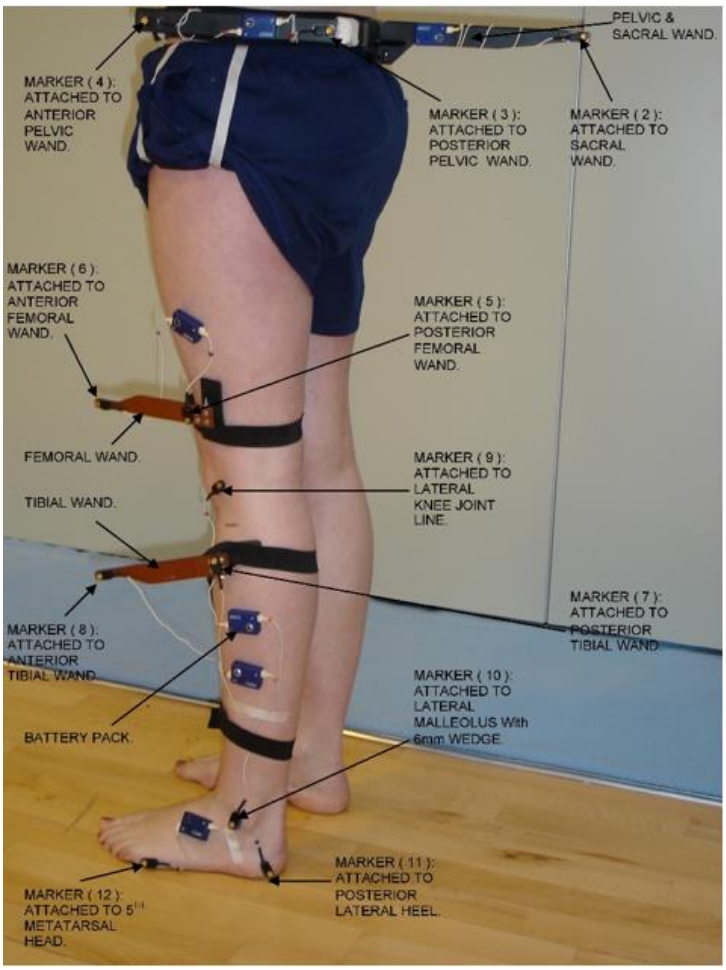

Figure 1-1 CGM marker-set promoted by Manufacturer Charnwood Dynamic

Harwoods CODA-motion gait analysis system. This CGM interpretation is unusual it its extensive use of marker wands, which must be calibrated to point in the anterior direction of their respective shank, thigh and pelvis body segments. Image from Monaghan et al. (2007).

As part of the model calibration procedure, the tibial and femoral wands were required to point anteriorly, thus setting the neutral transverse plane orientation of these segments. For the tibial wand this was facilitated by use of a jig that

aligned with the inter-malleoli ankle axis to provide a floor based visual reference to guide the required wand direction. For the femoral wand, we devised an alignment protocol such that, with the patient seated on a bench, we axially rotated the thigh to make the knee joint axis horizontal. This was judged by the vertical plane movement of the distal shank segment during passively applied knee movement; in the resulting position the femoral wand was set to vertical.

Anecdotally, these protocols had largely protected us from the excessive coronal plane knee range of motion that, without correction, were commonly reported as an issue from laboratories employing more traditional CGM variants. We had however become increasingly suspicious of the ability of these wands to capture, in particular, the transverse plane component of the required movements. Wand wobble during gait was a visible phenomenon, and the wands were also highly susceptible to being knocked out of the calibrated position during the data collection process.

1.4 Gait Cycle Divisions – a modern consensus

Regardless of the details of the marker configuration employed to capture body segment movements during gait, all clinical laboratories report this data in the form of a typical (or mean) gait cycle. The gait cycle is conventionally defined for each leg, between successive ground contact events; the left and right cycle are therefore synonymous with the left and right strides. Further temporal division of this cycle is useful for descriptive purposes. Within each cycle, the period from initiation to loss of ground contact is termed ‘stance’ phase and the period when the foot is off the ground as ‘swing’ phase. For typically developing gait, stance occupies approximately five-eighths of the cycle duration and swing three-eighths. The first and last eights of stance phase approximate periods of loading and unloading transition, as the body weight is progressively transferred from one leg to the other. Between these double support sub-phases, the stance leg enters single support, while the other leg is in swing. During a conversation with Prof Richard Baker (CMAS conference 2011 – London), I remarked, that it was not sensible that the clinical gait community described the single support period for the stance leg by two sub-divisions (mid and terminal stance), but the same

period for the swing leg by three sub-divisions (early, mid and late swing) (Perry, 1992). Prof Baker agreed with this, and pointed out that he made the same case in his soon to be published text book (Baker, 2013). This reference divides the single support period into equal early, middle, and late sub-division that match the divisions for the swing leg (Figure 1-2).

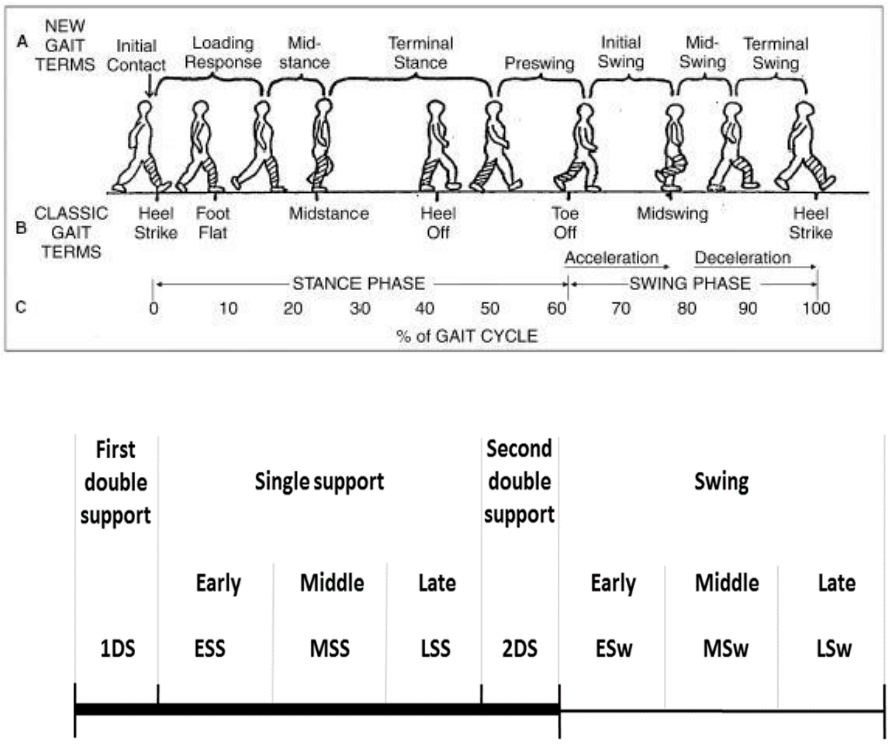

Figure 1-2 Two alternative divisions of the gait cycle

The diagram (top) shows temporal divisions of the gait cycle as traditionally employed Perry (1992), and (bottom) the alternative more equal arrangement proposed by Baker (2013).

Required foot contact and lift events may be identified by any revealing characteristic from any collected signal. Data from force-plates is most easy to interpret as the transition from no-force to force occurs almost instantaneously. When suitable ground force data is not available, gait events may alternatively be identified from a kinematic signals (Zeni et al., 2008). At their simplest, these techniques are based on the foot being at its most forward position at ground contact and most backward at foot lift. This kinematic approach only requires the reasonably smooth formation of left and right steps. In the clinical environment, this assumption is generally more robust than the need for clean left and right

force data, with each foot only making floor contact over its dedicated force-plate. Despite this robustness, there can be significant synchronisation discrepancy between contact events identified by kinematic and the gold standard kinetic signals. For these reasons, I have more recently found it best to specify clinical gait cycles by a hybrid approach, whereby cycles identified via a suitable kinematic signal, are shifted to the precise moment of contact or lift, by comparison with a small sample of kinetic equivalents.

1.5 The RNOH Motor Learning Lab (MLL) – a new beginning

At around the same time as I discussed gait cycle division with Prof Baker, the RNOH Gait Laboratory was facing a new threat. The old UCL building in which we were still situated was designated for demolition to make way for a much overdue hospital rebuild. At this time, a focus with the cost per square metre of hospital space, provided an opportunity to transition the service towards an emerging technological solution centred on treadmill walking. This solution requires far less space than a traditional walkway. To this date, there remains only one company providing a serious commercial solution for treadmill-based gait analysis (Motek Medical BV). Their system promoted a new marker-set (van den Bogert et al., 2013), termed the Human Body Model (HBM). The HBM model is optimised to facilitate real-time calculation and feedback of joint kinematics.

The Motek system is able to integrate the HBM kinematic outputs with continuous left and right ground force records, as the subjects walk on an instrumented dual belt treadmill. The system also provides a 180° screen surrounding the front of the treadmill such that the subject walks in a partially immersive environment. Lab mounted video cameras provide front, back, left, and right images of the subject, which remain fully orthogonal through the gait trail (Figure 1-3).

Figure 1-3 The RNOH Motor Learning Lab (MLL)

Equipment is a GRAIL system by Motek Medical B.V. Houton, Netherlands. The central treadmill includes right and left belts over separate force plates. A 10 camera Vicon Bonita mocap-system is temporally and spatially synchronised to the force record. Orthogonal video cameras collect front, back, left and right images while the subject views a projected environment on a 180° surround screen.

Comparison of the HBM marker set to PiG, showed them to be almost identical, with HBM addition of thigh markers over the greater trochanter, formalisation of the inclusion of medial ankle markers, and replacement of the central toe marker by separate medial and lateral markers. HBM has since been shown to produce a different coronal and transverse plane kinematic to traditional CGM solutions (Flux et al., 2020). At the time we purchased our new system, it was our assumption, or at least hope, that this update would solve the underlying problems we were suffering with our outdated equipment.

1.6 Gait Analysis Data Transformations – a shift in study focus

The process of gait analysis may be regarded as a series of data transformations, from captured surface marker locations, to a skeletal representation of human movement via a biomechanical model, and finally, to some form of clinically relevant score or interpretation (Figure 1-4).

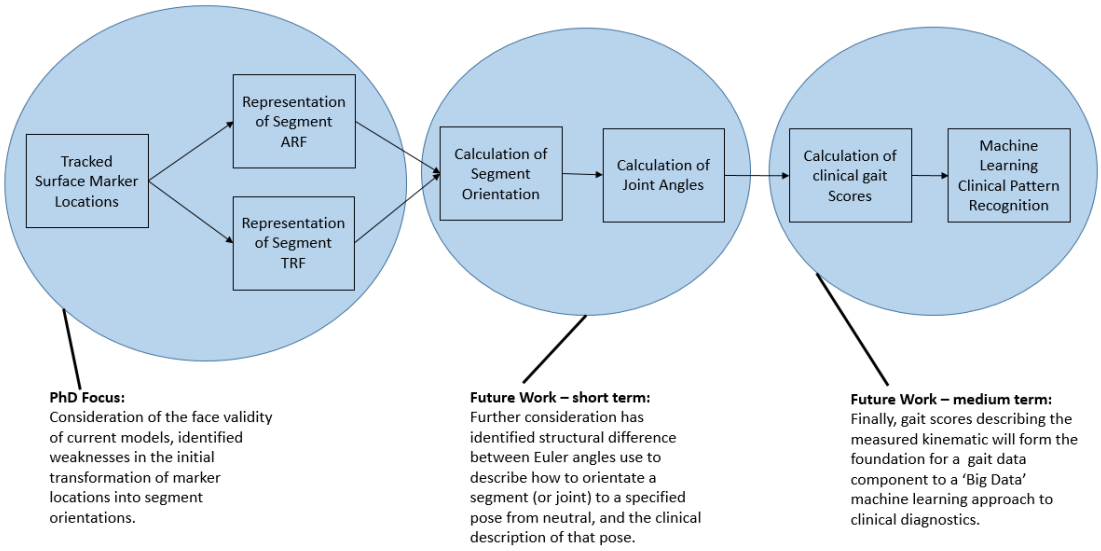

Figure 1-4 Clinical gait analysis as a series of data transformations

> *First, the locations of surface markers collected using mo-cap technology must be interpreted as segmental orientations. Development of a new biomechanical for this purpose has been the focus of this thesis. Consideration of an orientation with respect to that of the proximal segment, allows for the expression of the intervening joint angle. Careful consideration of the Euler rotation sequence used to calculate these angles at each joint has aimed to best match clinical terminology. Future work may attempt to derive angles that provide a precise match. The final transformation in this data chain is to clinical interpretation.*

Under the guidance of Professor Gordon Blunn, who at the time, headed Biomechanics at the UCL Institute of Orthopaedics and Musculoskeletal Science (IOMS), my initial studies were directed towards the final transformations in this chain. This work took the form of gait score developments intended to form the basis of a machine learning approach to the analysis of gait data. These scores were similar in nature to those used to describe whole gait cycles throughout this thesis, but applied individually to the eight functional gait phases, and therefore termed 'OctoScores'.

Our early experiments with PiG/HBM marker-sets however, revealed similar data deficits to that from our old gait laboratory. Although the calculated 'OctoScores' provided good representations of each measured kinematic, in terms of average position, range, movement, and inter-cycle variation, there was a clear discrepancy between the measured kinematic and expert interpretation of the newly abundant orthogonal video images. As before, this difference was

particularly noticeable in the transverse plane kinematic. Scores relating the transverse orientation of the thigh segments with respect to the lab for example, were unreliable in their ability to identify subject with clear squinting or frog-eyed patella, as observed from the front facing video image. Similarly, freeze frame observation of heel, flat or toe ground contact of the foot segment from the side video, did not always correlate with its measured sagittal kinematic with respect to the ground.

Over time, it became clear that, like our old laboratory, the new data was only clinically usefully in conjunction with expert opinion that could account for the likely marker misplacement and soft tissue influences of the individual subjects under consideration. Anecdotally, it seemed that the data remained insufficiently robust as an independent gait measure, and that this was particularly true for the transverse plane measurements. Following this, and somewhat driven by Prof Woledge's proclivity to 'reinventing the wheel', the focus of my studies shifted from the generation of clinically meaningful gait scores to the other end of the data transformation chain; the initial specification of mo-cap surface marker locations and subsequent transformation into skeletal orientations. Four major issues are identified with current methods employed for this transformation.

1.7 Issue 1 – Representation of Joint Angles – the Euler rotation sequence

The first issue identified with current methods concerns the mathematical specification of three-dimensional (3D) angles, such that they will match clinical terminology.

1.7.1 Euler Angles provide a Mathematically Robust, User Friendly description of 3D orientation.

The problem of describing 3D orientation of an object is ubiquitous. In the aviation industry for example, a mathematical frame is commonly embedded with one axis along the fuselage of an aircraft and another pointing along a wing. Rotation around each of the axis can then be specified, such that they correspond with industry terminology of the aircraft's yaw (heading), pitch (elevation) and roll (banking) angles. The heading component describes the aeroplane's destination

direction, pitch is the height of its nose with respect to its tail, and roll, the height of one wing with respect to the other. These angles are interpreted as *sequential* rotations from a neutral orientation.

To match Euler descriptors with industry terminology, the axis aligned with the aircraft's fuselage is designated as principal. In the sequence of three rotations, the first points the principal axis towards its destination; the second also moves the principal axis in space - describing if it points upward, downward or is level. The final rotation in the sequence then spins the now oriented principal axis to describe the plane's bank angle. This consensus between calculated angles and accepted terminology, is only maintained when the rotations are applied in the stated sequence (yaw-pitch-roll). It should be emphasised that the three sequential orientation angles only *describes* the plane's orientation from a neutral orientation (level and pointing north); it is of course unlikely that the plane actually achieved its orientation by three distinct rotations in this way.

The above example serves to illustrate that Euler angles do not behave like vectors, in that the sequence of application is critical to maintain their link with industry terminology. It further demonstrates a relationship between the designation of an object's principal axis and the rotation sequence that will correspond to its intuitively meaningful orientation angles.

1.7.2 Specification of a Euler Rotation Sequence is critical to angles matching Clinical Terminology

Although Euler angles are employed in multiple fields, application in the clinical field to describe orientation of body segments has been somewhat troublesome. Unlike the aviation example, the choice of principal axis for individual body segments in not always self-evident. The pelvis for example, may be considered as the inferior end of the spine with a vertical principal axis, or an interconnector of the left and right hip joints with a horizontal principal axis. Similarly, the hind-foot may be modelled as vertically aligned with the shank, or an antero-posterior transition to the mid and forefoot regions. Many current models have avoided these complexities by the specification of a sagittal, coronal, and then transverse rotation sequence for all segments regardless of their principal axis assignment.

This sequence however, is known not to replicate clinical terminology at the pelvis (Baker, 2001), and there is poor agreement amongst current models on the required rotation sequence to maintain clinical terminology around the foot (Bishop et al., 2012). The resulting confusion has led to suggestions that the Euler method is somehow insufficiently robust for clinical use (Simon et al., 2006, Wren and Mitiguy, 2007) despite its wide acceptance throughout engineering and physics applications.

1.7.3 Segment Orientation is specified by an Embedded Anatomical Reference Frame (ARF)

For the purpose of expressing 3D orientation in biomechanics, it is a common mathematical practice to represent each assumed rigid body, as an orthogonal frame consisting of three mutually perpendicular axes emerging from a common origin. For the calculation of joint angles without translation, specification of the origin location becomes superfluous; it remains important however, that the axes are aligned parallel with the clinical expectation of joint axes. This requirement is in addition to specification of an appropriate rotation sequence. Unless both requirements are met the resultant output angles will not correspond to clinical movement terminology such as flexion-extension or ab-adduction. Appropriate clinical axes are commonly defined in terms of mo-cap surface marker locations over bony landmarks, either directly, or from derived virtual locations. When the clinical alignment requirement is met, the resulting frame is referred to as an anatomical reference frame (ARF). Unaligned frames used to describe the segment orientation with respect to an arbitrary reference system are referred to as technical reference frames (TRF). Without the constraint of having to define an *anatomical* plane, TRF may be optimised for movement tracking, for example by avoiding marker locations with excessive soft tissue wobble. With both ARF and TRF surface markers in place, the TRF orientation may be related to than of the ARF during a static calibration trial.

1.7.4 True non-orthogonality of bony axis dictates the long axis as Principal

Defining a segment's orientation equates to describing the orientation of one of its principal planes; sagittal, coronal or transverse. As all planes are modelled as

mutually perpendicular, orientation of the remaining two planes can then be computed (Zatsiorsky, 1998a). The three orthogonal axes that intersect these planes form the segment's ARF (Figure 1-5). It should be observed that the clinically described axes of biological entities such as body segments are not truly orthogonal; the clinical medio-lateral knee axis of the thigh segment for example, will not be exactly perpendicular to the segment long axis between knee and hip joint centres. Application of the Euler method therefore requires orientation of one axis to be prioritised as principal, and model the other axis orthogonal to it. If the knee flexion axis was *wrongly* selected as the principal axis of the thigh, the resulting perpendicular long axis emanating from its midpoint, would likely miss its intersection with the true hip joint centre by some margin. In order to minimise this type of modelling error, it is generally best to assign the long axis of a segment as principal.

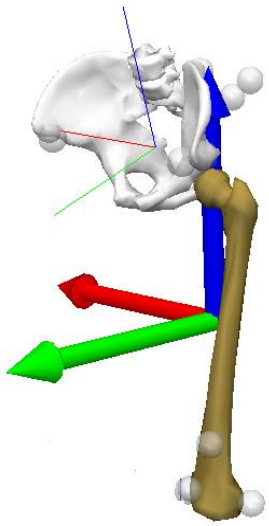

Figure 1-5 Anatomical Reference Frame for the Thigh

In this example, the vertical principal axis of the ARF is aligned with the long axis of the segment between hip and knee joint centres (blue). The modelled medio-lateral axis (red) is a good approximation of the true knee flexion axis. Had the medio-lateral alignment been prioritised, the much longer vertical axis would likely have missed the hip joint centre by significant margin.

1.7.5 A Mechanical Arrangement Appeared to Bypass the Rotation Sequence Issue at the Knee

One of the identified seminal publication concerning clinical joint orientation measurement, reports an attempt to measure dynamic three-dimensional (3D) joint kinematics at the knee, by the use of a tri-axial goniometer (Chao, 1980). An axis embedded in one half of the goniometer was aligned with the knee joint axis and strapped to the distal thigh. The other half of the goniometer strapped around the long axis of the shank such that these axes also aligned. The third axis was designed to mechanically float mutually perpendicular to the other two (Figure 1-6).

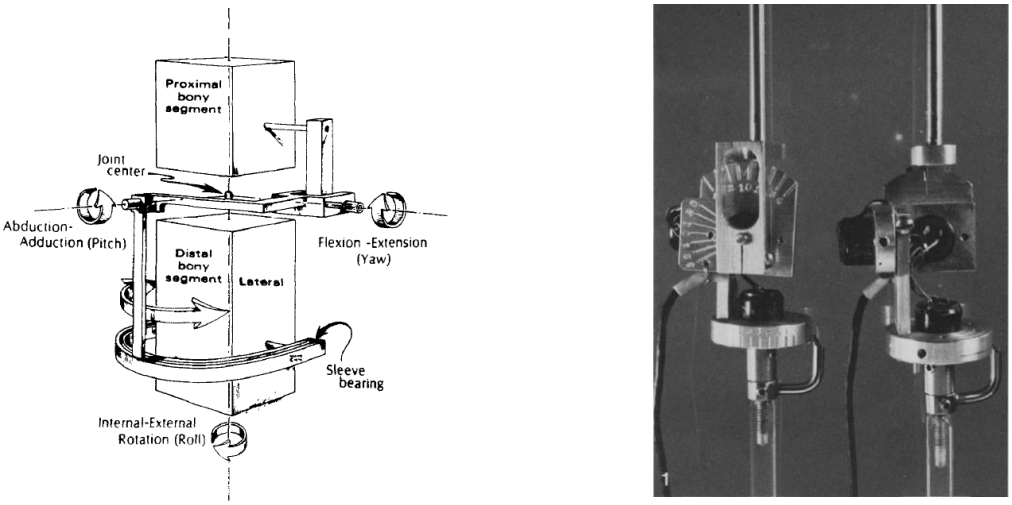

Figure 1-6 Chao's tri-axial goniometer

In idealised form (left) and as would be strapped to the lateral aspect of a body joint (right). A medio-lateral axis is fixed to the proximal segment and a longitudinal axis to the distal segment; a third axis mechanically 'floats' between the other two. Electrical potentiometers independently report the position of each axis, which do not remain mutually perpendicular as the joint moves.

Electrical potentiometers attached to each goniometer axis reported their instantaneous configuration, which in turn corresponded to the joint position. Critically, these outputs were independent of each other and outputs from each potentiometer corresponded to the clinical terminology of flexion-extension from

the thigh fixed axis, internal-external rotation from the shank fixed axis, and varus-valgus from the floating axis. The goniometer itself, however, was an intrusive electro-mechanical device, difficult to align and cumbersome to wear. Because of this, there was significant risk of poor fitting and a consequential loss of accuracy.

1.7.6 Joint Coordinate System (JCS) as a virtual representation of Chao's Mechanical Solution

The advent of mo-cap technology facilitated measurement of the instantaneous location of small reflective markers that could be individually attached directly to a subject's skin surface via bi-adhesive tape (Sutherland and Hagy, 1972). This made it possible to define a virtual segment axis between marked surface locations, either directly, or via the creation of derived virtual points, typically to represent joint rotation centres. No longer constrained by the physicality of a mechanical goniometer, it became as easy to mathematically embed a longitudinal or antero-posterior axis in the thigh as it was a medio-lateral one. Similarly, the shank axis need not be longitudinally orientated, as the choice was no longer dictated by the physical design of a goniometer. Crucially, the effect of this axes choice dictates the three angular outputs used to describe the joint position. The second identified seminal publication on this issue (Grood and Suntay, 1983) showed that, only the configuration that mimics Chao's tri-axial goniometer, results in angular outputs for the knee that correspond with clinical terminology. From this finding, it was widely inferred that clinical terminology itself referred to non-orthogonal angles. The arrangement was thus coined a Joint Coordinates System (JCS) to distinguish it from the orthogonal Cartesian reference frames employed by the Euler method. JCS was later adopted by the International Society of Biomechanics' (ISB) Standardization and Terminology Committee to be employed as a 'common output filter' to aid communication of knee kinematics between different laboratories (Wu and Cavanagh, 1995). They also recognised that expression of kinetic data in a non-orthogonal system would be problematic and announced that several subcommittees had been formed to establish recommended standards for kinematic reporting at other joints.

1.7.7 JCS Extended to all Lower Extremity Joints

Twenty-five ISB member experts from various medical fields divided themselves into nine permutations of ISB subcommittees to report on ankle, hip, spine, shoulder, elbow, hand, wrist, TMJ and whole-body kinematics. Seven years on, they reported part I of their recommendations concerning the spine, hip and ankle joints (Wu et al., 2002). For these purposes the spine was not considered as a single trunk segment as might be employed in a gait model, but instead as individual intervertebral motion unit. Here, recommendations mimicked that of the JCS for the knee, with a medio-lateral axis embedded in the proximal vertebra, a longitudinal axis embedded in the distal vertebra, and an intervening 'floating' axis. The same mimicry was recommended by the hip subcommittee - which again recommends a medio-lateral axis embedded in the proximal pelvic segment, a longitudinal axis embedded in the distal thigh segment and the obligatory floating axis perpendicular to both. Even at the ankle joint, where the antero-posterior orientation of the distal foot segment might be expected to require a different axis configuration, the subcommittee instead defined a vertical axis hind-foot segment and employed the now common JCS configuration.

Following the publication of ISB recommendations part 1 there was concern by some within the gait community, that blanket application of the JCS as described resulted in angles that do not always correspond to clinical terminology (Baker, 2003). A case in point was the pelvis segment. In keeping with clinical description of this segment, its orientation is commonly expressed with respect to the laboratory frame. Tilt and obliquity angles are therefore reported with respect to a true horizontal datum, and rotation with respect to true vertical. Baker's previous work had shown that in order to maintain clinical terminology, pelvic orientation required a different configuration than that for the hip and knee joints (Baker, 2001). He did not, however, express these differences in terms of an axis configuration, but via the more widely employed specification of a rotation sequence. To make Euler angle outputs consistent with clinical terminology at the pelvis, the reverse rotation sequence to that at the hip and knee is required.

1.7.8 JCS debunked as Equivalent to a Specific Rotational Sequence

The JCS as described, with a medio-lateral axis embedded in the distal segment and longitudinal axis in the proximal is now widely acknowledged to be equivalent to an Euler rotation sequence of sagittal-coronal-transverse (Allard et al., 2003, Baker, 2003). This rotation sequence is usually interpreted as three separate rotations around orthogonal axes embedded in the *distal* segment (an intrinsic angle). In common with the JCS, reference frames representing the orientation of proximal and distal joint segments are initially aligned. At the knee for example, the first rotation in the descriptive angular sequence occurs around a medio-lateral axis causing the shank to move with respect to the thigh in the sagittal plane (knee flexion/extension). The second rotation occurs around the now rotated antero-posterior shank axis to cause movement in the local coronal plane (knee varus/valgus). The final rotation causes the shank to spin around its now fully orientated longitudinal axis (knee internal/external rotation).

Equivalence of the JCS requirement for specification of proximal and distal axes, and Euler angle requirement for specification of a rotation sequence has since been unequivocally established (MacWilliams and Davis, 2013). The two systems are simply different paradigms of the same mathematical solution. The claimed advantages of the JCS in communicating joint angles in the clinical setting, relate to the mind-set of clinicians only. The claimed rotation-sequence independence (Grood and Suntay, 1983) had proven bogus; the choice of a sequence was simply hidden from the maths by the design of the measurement equipment (Chao, 1980). Given the outlined development history, it is unsurprising that the JCS has subsequently been shown to lack robustness outside of a limited range of joint orientations (Dabirrahmani and Hogg, 2017).

The ISB initial response to Bakers concerns was largely dismissive (Allard et al., 2003); while acknowledging the equivalence of Cardan and JCS methods for the description of joint rotation, JCS was defended as a ‘necessary compromise’ derived from the collective opinion of people from many disciplines. JCS was further promoted as a robust method to describe joint translational movements in a clinically meaningful way. This point, however, is not clear. Unlike rotations, translation movements are true vector quantities, commutative across addition

and therefore not subject to the complexities of requiring a sequence specification for interpretation. Imposition of a non-orthogonal axis system for translational movement is therefore counterintuitive. Given the stated motivation for such an imposition to maintain a connection with the rotational components of the movement, it would surely make more sense to adopt the orthogonal Euler paradigm for both?

1.8 Issue 2 - Configuration of Surface Markers - the conventional gait model

1.8.1 Conventional Gait Model (CGM) emerges as a Gait Analysis Solution

As the technical challenges of making mo-cap equipment clinically viable were met, attention turned to the creation of a biomechanical model suitable for gait analysis. For this purpose, two near identical models, independently emerged from the Helen Hayes Hospital in New York USA (Kadaba et al., 1990), and the Children's Hospital in Newington USA (Davis et al., 1991) at about the same time. These models balanced the need to keep markers within view of the limited number of cameras available to mo-cap systems of the era, with the requirement to construct 3D axis systems to represent hip, knee, and ankle joints. Both publications acknowledge unresolved problems. Sensitivity analysis in the Kadaba publication uncovers problems with coronal and transverse plane kinematic patterns and offsets. At the time, this offset problem was overcome by assuming a neutral posture during the calibration trial, with an admission that the assumption would not hold in many clinical situations. Similar problems are also highlighted in the Davis publication, which anticipated that some aspects of the model will 'soon be replaced'. The emphasis of these papers was on producing a technically simple system that employs a small number of surface markers. The simultaneous emergence of virtually the same model from two unrelated laboratories, reflects that this solution was considered an optimal balance of technical and clinical considerations for the era.

Subtle variations to this model have since been promoted by various manufacturers of mo-cap equipment under various banners including the Kadaba, Davis, Helen Hayes and Newington models. The most widely used variant, Plug-in Gait (PiG), still widely in use, is produced by the Vicon division of

Oxford Metric UK (Figure 1-7). More recently there has been a move to group all variants under a common banner of the Conventional Gait. Model (CGM (Baker, 2018)).

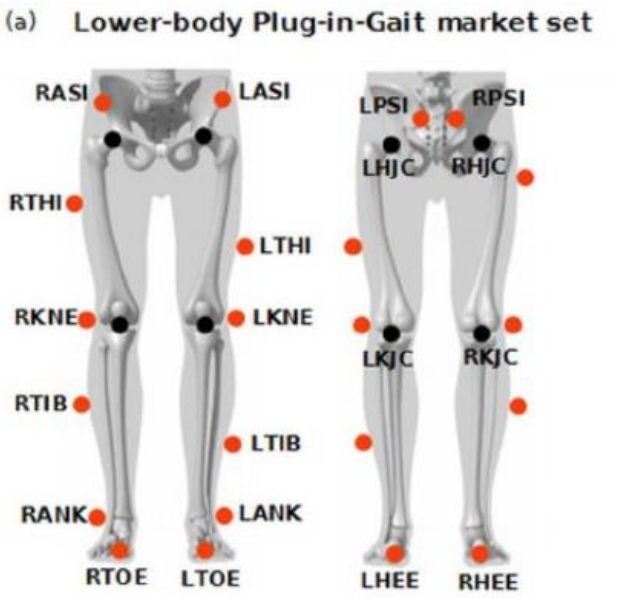

Figure 1-7 CGM marker-set promoted by Manufacturer Vicon (the PiG marker-set)

> *Surface marker locations for the PiG lower extremity model are depicted in red with virtual hip and knee joint locations in black. Lateral thigh and shank markers are purposely asymmetric, with right side markers purposely higher. This asymmetry helps software automatically orientate the model. Image from Baudet et al. (2014).*

1.8.2 CGM Indirect Specification of the Thigh (and Shank) Principal Planes

Although CGM recognised an internationally agreed principal plane specification of the thigh, from a proximal HJC location to a distal inter-epicondyle knee axis (Wu et al., 2002), it does not specify this axis directly by surface markers. Right (RKNE) and left (LKNE) knee markers of the PiG marker-set, are located at lateral epicondyle locations only (Figure 1-7). Absence of a medial knee marker requires that the mid-epicondyle knee joint centre locations are calculated by indirect means. PiG estimates these joint centre locations at half the measured knee width from the lateral marker, in the plane defined by the lateral thigh marker (RTHI or LTHI) and the hip joint centre (RHJC or LHJC) The HJC locations themselves, are estimated form the pelvic surface markers. This indirect defining of the thigh principal plane, is inevitably subject to a significant increase in error.

In practice, a similar situation at the ankle is commonly avoided by inclusion of both lateral and medial joint markers (Nair et al., 2010). Here the medial marker is far less susceptible to being dislodged during gait, than at the knee.

An early version of the PiG manual assigned responsibility for accurate placement of the lateral thigh substitute markers with the clinician, stating that:

"it is the responsibility of clinical staff to use their anatomical knowledge to position markers such that the model is able to make as good an approximation to the joint centres as possible"

…… also noting that it is:

"*almost impossible to obtain an independent measure of hip rotation in a standing subject, so a non-zero hip rotation may either be real or due to incorrect thigh marker placement" (Vicon, 1999).*

The current PiG manual continues to instruct users to:

"adjust the antero-posterior position of the lateral thigh marker such that it lies in a plane that contains the hip joint centres and the knee flexion axes" (Vicon, 2017b).

As none of these structures are easily envisaged from the skin surface, significant inaccuracy in the placement of this marker is a widely acknowledged problem (Schache et al., 2006). In recognition of these difficulties, the PiG manual goes on to recommend use of a Knee Alignment Device (KAD), to facilitate software adjustment of the lateral thigh marker representation into the desired plane.

The KAD is described by its manufacturer as a light-weight spring loaded G-clamp with an adjustable jaw bridge; the user is instructed to align the jaw with the knee flexion axis (Motion Lab Systems, 1998). Markers fixed to the lateral aspect of the KAD then act as a projection of this axis (Figure 1-8). Advantages of this approach over the direct placement of medial and lateral surface markers relies on the user being able to more accurately envisage and then represent the

required axis. The manufactures do not provide any evidence to support this presumption.

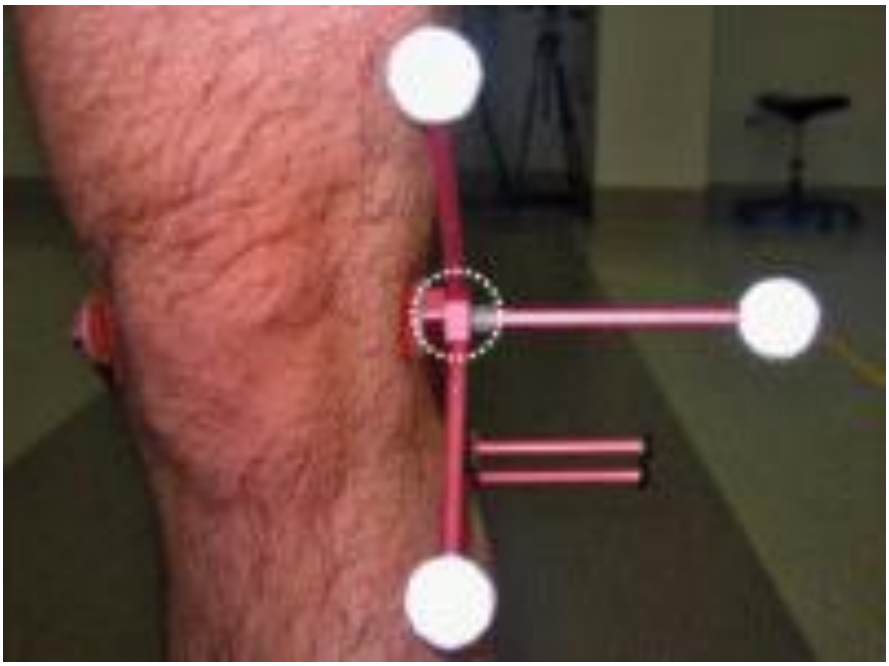

Figure 1-8 The Knee Alignment Device (KAD)

The orthogonal reference frame described by the three fixed markers is aligned with the knee joint axis. This alignment provides no more information than the placement of medial and lateral epicondyle markers to represent the same axis. In conjunction with the calculated HJC location, software is then able to virtually adjust the position of the lateral thigh marker into the desired plane. The KAD is removed for dynamic trials, and the lateral jaw position replaced with a surface marker.

With the KAD correctly placed, PiG software adjusts the location of the lateral thigh marker to a virtual location in the required plane. This adjustment also employs the HJC location from the pelvis. Post calibration, the KAD is removed, and the user instructed to place a lateral knee marker at the exact position from which the lateral KAD pad was removed. Overall, the difficulties of locating and fixing the KAD in the correct position, and of consistently re-identifying the required lateral knee location, have been shown to suffer similar reliability problems to that of the manual marker placement method (Schache et al., 2006). More recently, there has been an acknowledgment within the CGM community that the KAD alignment cannot provide any more information to the model than

the simple and direct identification of the epicondyle axis by surface markers alone (Leboeuf et al., 2019).

The unmet challenge of accurately locating a lateral thigh marker either directly or virtually, has resulted in widespread use of post collection data manipulation. Several published algorithms are available for this purpose; all adjust the marker position to minimise the amplitude of the coronal plane knee kinematic (Schache et al., 2006, Baker, 1999, Baudet et al., 2014). Some laboratories manually adjust the marker to achieve this objective. In attempting to relate the modelled knee joint axis to movement created by the shape of the knee joint articular surface during gait, they are commonly forced to base this relationship on the large swing phase movement. During swing, however, the joint is at it least congruent (Hohe et al., 2002) and surface markers will also be subject to maximal dynamic STA components.

While these post data collection manipulations may provide a cosmetic fix for the measured kinematic, they are not truly part of that measurement. The effective assumption of minimally lax knee joint, acting as a single degree of freedom hinge, may not hold true for some pathological gait patterns. In these cases, the correction risks contamination of a properly identified abnormal kinematic. Alternatively, subjects exhibiting a stiff-knee gait pattern will show low amplitude knee kinematics in all planes regardless of axial alignment; here poor axial rotation measurement of the thigh will not be highlighted by an abnormally large coronal knee kinematic, and post collection correction will not be possible. Any discrepancy between graphical and video appearance must then be either ignored, subjectively resolved by manual adjustment, or caveated in the clinical report.

1.9 Issue 3 – Representation of skeletal movement by Surface Markers

1.9.1 The Soft Tissue Artefact

A re-examination of the literature, some 20 years after my introduction to clinical gait analysis, revealed little clinical uptake of published advancements on the first two identified issues, and the emergence of a third. This new issue concerns the difference between the measured movement of skin mounted surface markers,

and that of the underlying skeletal structures they represent. These differences are a real phenomenon caused by deformation of intervening soft tissue. Within the context of regarding this difference as a source of error, it is commonly referred to as a soft-tissue *artefact* (STA).

Following advancements in equipment accuracy, STA is now widely acknowledged as the primary source of mo-cap error (Andriacchi and Alexander, 2000, Baker, 2006, Camomilla et al., 2017b). It is reported to consist of 3 independent components; skin sliding, inertial effects, and additional deformation due to muscle contraction (Leardini et al., 2005, Bonci et al., 2014). The skin sliding component has been shown to act predominantly around the joint regions at the ends of each segment, causing an underestimate of the true skeletal range of motion (Bonci et al., 2014). Physics dictates that the inertial effects will operate along the vector of applied accelerations that predominate around foot-ground contact events. STA caused by muscle contractions is likely to have localised effects over the active muscle bellies. These dynamic components often cause en-bloc movement of the entire skin surface over the underlying bone (Taylor et al., 2005).

1.9.2 STA influences in Gait Analysis

Direct measurement of skeletal movements requires either exposure to ionising radiation, or the insertion of bone-pins through the skin surface. The invasive nature of these techniques makes them unsuitable for routine clinical use. Mo-cap technology is therefore commonly employed to track the three-dimensional location of surface markers fixed to the patient's skin surface. From these locations, the orientation of the underlying bones are estimated. Markers that define a segment's anatomical plane are generally located over palpable bony landmarks, i.e. locations with reduced soft-tissue cover (Wu et al., 2002). Perhaps counterintuitively, these regions often suffer considerable sliding of soft tissue over skeletal structures during movement. Lack of skin-skeletal attachments around the knee joint for example, can result in up to 40mm of skin sliding over the epicondyles (Cappozzo et al., 1996). The same study reports typical levels of skin sliding over many bony landmarks of 10-30mm during gait. For the lower extremity, STA generally increases from the distal foot to proximal pelvic segment

(Cereatti et al., 2017). Finding solutions to accurately track movement of the thigh and pelvic segments in the general population is therefore inherently challenging (Leardini et al., 2005).

1.9.3 Difficulty of Capturing Transverse Plane movement is Long Recognised

All clinical gait models must balance a multitude of technical and utility considerations. This is highlighted when contemplating an early attempt to accurately measure transverse plane movements, that required the construction of a glass roof over the biomechanics laboratory at the University of California (Eberhart and Inman, 1951). The transverse plane movements of subcutaneous bone pins were studied from mirror reflections as subjects walked across the roof (Figure 1-9).

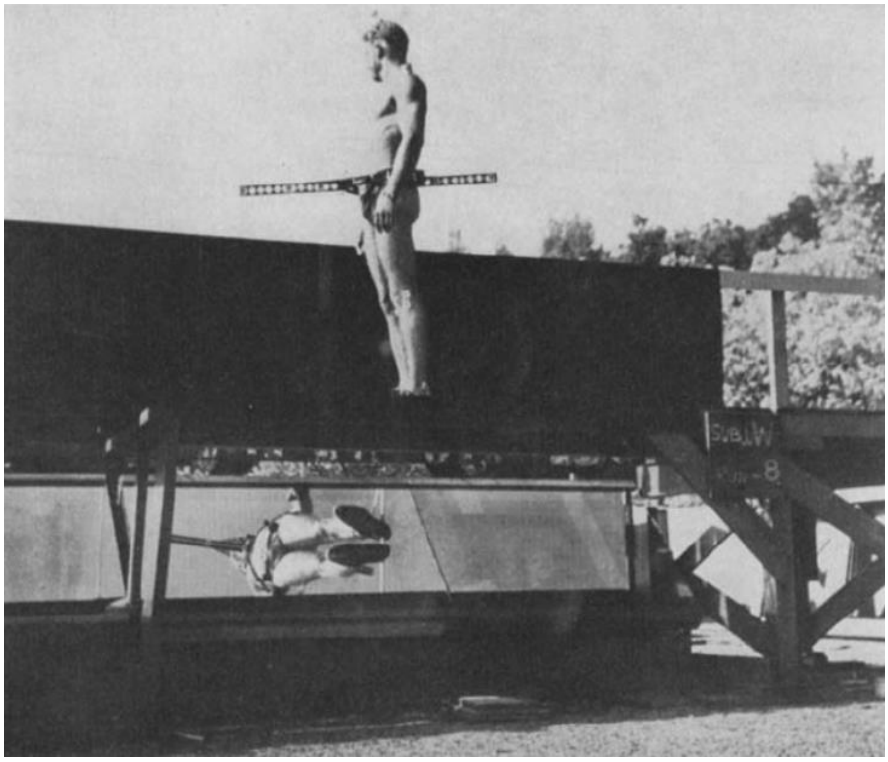

Figure 1-9 Early attempts at 3D gait analysis

> *The subject walked along a glass walkway and movement was recorded from the end of the platform. A second camera recorded side and underside views by means of a mirror placed at 45˚ to the platform (Eberhart and Inman, 1951).*

As technological advances were made, the emergence of multi-camera systems capable of tracking the position of multiple surface markers, seemingly replaced

the need for such elaborate laboratory set-ups, as surface marker locations could be *virtually* reconstructed to *any* view point (Abdel-Aziz, 1971). These technical developments however, appear to have superseded efforts to minimise the influence of soft tissue movement, a problem that has only recently regained prominence in the published literature (Camomilla et al., 2017b).

1.9.4 CGM is Not optimised to minimise STA errors

For PiG (Figure 1-7), right (RTHI) and left (LTHI) lateral thigh markers are located at different heights on the segments, with the right thigh marker significantly higher than the left (Vicon, 2017b). As the anterior-posterior position of this marker is critical in locating the knee joint axis, this height difference can only make reliable, symmetrical identification of the required plane more difficult. Pragmatically, the majority of clinical laboratories are force to amend the model, by manipulating the position of the lateral thigh markers post data collection, under the assumption of constraining the knee to a hinge type function. These markers are additionally employed to track the segment's movement, particularly affecting the transverse plane component. Here again, the height difference between right and left segments must make one of these markers better in this regard. In consideration of the increased soft tissue cover thickness over the higher right sided marker, it seems reasonable to expect better performance from the left configuration. Further consideration of the soft tissue insulation to skeletal movement on both sides, might reasonably give rise to low expectations bilaterally. The two other surface markers employed to track the thigh are located over the lateral epicondyle, a known high STA location(Cappozzo et al., 1996), and the HJC location, which will inherit STA from the pelvic surface markers. A similar situation is also evident for the shank segments. Here however, mitigations are easily conceived by inclusion of the less affected medial ankle marker (Nair et al., 2010), and the presence of the potential tracking regions with minimal soft tissue cover (Peters et al., 2009).

1.9.5 Reduction of STA influence - the CAST technique

A few years after publication of the CGM, the Calibrated Anatomical System Technique (CAST) emerged from the Rizzoli gait laboratory in Bologna, as a way

to reduce STA effects (Cappozzo et al., 1995). Contrary to the CGM philosophy of re-employing anatomical markers to also track segment movements, the CAST method purposefully separates these functions via specification of easily viewable secondary TRF markers.

Orientation of ARF with respect to TRF for each body segment, are established during a static calibration trial in which the subject is stationary, and all markers are viewed simultaneously. Model Calibration allows expression of TRF movement around ARF axes. Post calibration, the ARF orientation from dynamic trials can be reconstructed from only the TRF marker positions. Any difficulties of viewing ARF locations during this calibration, may be resolved by instead identifying anatomical landmarks using a pointer device (Figure 1-10).

Figure 1-10 Mo-cap system digitised pointer – used to identify anatomical locations

The pointer may be employed to identify anatomical locations during a static calibration. The pointer tip location is conveyed to the software via the easily viewed reflective markers located along the pointer shaft. This sophisticated version is sprung loaded, such that marker movement when the shaft is compressed, informs the software that the tip of the pointer is in the required anatomical location.

The reference frame of the pointer is described by rigidly attached markers; the tip location can then be used to identify anatomical landmarks during a static calibration and related to the location of the segment's tracking markers. Within the constraints of avoiding collinear cluster configurations (Cappozzo et al., 1997), the CAST technique allows complete freedom in the choice of tracking marker locations. This characteristic therefore has the potential to reduce STA influences in the movement tracking solution for each segment.

CAST tracking solutions for the thigh and shank segments generally employ a lateral mid segment cluster of 3 or 4 surface markers, either individually attached, or fixed via a rigid plate (Cappozzo et al., 1997). The mid-segment location separates these tracking clusters from the skin sliding STA components caused by joint movements at the segment extremities. For the thigh however, the cluster will inevitably be subject to the known high STA levels which affect the whole segment (Barre et al., 2017), and particularly affects the transverse plane measurement (Fiorentino et al., 2017).

Tracking both the anatomical and tracking cluster markers during the static calibration trial is generally not too technically challenging. As the anatomical markers are no longer required during the dynamic trials, only the TRF clusters need be tracked; anatomical markers may therefore be removed from the subject post calibration. Arguably, the advent of CAST was therefore not driven by improvements in the technical capabilities of mo-cap systems to track a greater number of markers; it simply represents a different paradigm in the clinical setting.

1.9.6 Reduction of STA influence - Double Calibration

Measuring of ARF movement by an alternative TRF, can be affected by non-rigidity of the underlying body segment; if the segment were truly rigid all reasonably non-collinear tracking solutions would show good agreement. As it is, this agreement between the body's ARF and TRF is defined during the static calibration trial, and true agreement is only achieved at this posture. During the subsequent dynamic gait trials, as the subject moves away from this position, STA and other modelling errors will inevitably cause this spatial synchronisation to be lost. Even at the calibration posture, the dynamic STA components of inertial and muscle contraction during gait will prevent the TRF from being a perfect representation the ARF. These dynamic errors aside, increasing differences between ARF and TRF orientation of each body segment, as the subject moves away from the calibration posture, are an expression of that segment's violation of its modelled rigid body assumption.

Some authorities have advocated the use of an averaged double calibration that covers the range of segment orientations under investigation (Cappello et al.,

2005, Stagni et al., 2006, Stagni et al., 2009). While the technique has been shown to improve accuracy, it is not widely adopted within the clinical environment, where capturing even a single static pose with all markers in view can sometimes be challenging. An alternative approach to minimising segment ARF and TRF differences might be to calibrate the subject in a mid-movement crouched posture, rather than the traditional use of an upright standing posture.

1.10 Issue 4 – Expansion of Gait models to include More Body Segments

Over 50% of the body mass is included in the torso and upper limb body segments above the pelvis. Although not directly involved in locomotion, movement of these segments is clearly related to the biomechanical aims of ambulation. Various representations with gait models are becoming increasingly common, often as a relatively rigid thorax segment. Chapter 3 challenges the philosophy of this approach, in favour of a more encompassing approach able to report the orientation of the shoulder girdle with respect to the pelvic girdle by a minimal number of surface markers.

At the other end of the kinematic chain, there has been a move to model complexity of the foot, by division into multiple sub-regions. Here again there is little consensus of how this is best achieved. An extensive review of the literature in Chapter 6, suggests a three-segment approach with hind, medial and lateral forefoot subdivisions. From this basis an optimised solution is developed.

1.11 Derivation of Research Questions

This section summarises the challenges presented by each of the identified Clinical Gait Analysis (CGA) issues, prior to formal statement of the thesis aims and objective in the next section.

Issue 1 concerns a longstanding dialogue on the selection of an appropriate joint specific Euler rotation sequence, to maintain clinical terminology of calculated 3D orientation. A simple philosophy, relating the neutral orientation of each segment's principal axis to the required sequence is presented in chapter 2. This development is incorporated into that of a novel modelling approach termed the

‘Baseline Model Concept’ (BMC). The BMC represents the absolute simplest representation of human anatomy required for CGA. This approach allows the BMC to bypass the complexity of current models, at the expense of requiring medially located surface markers to define the required segment anatomical planes, and making no concession to STA effects. BMC outputs are posited to provide un-optimised versions of fundamentally correct kinematics.

Issue 2 concerns the minimal evolution of the CGM marker-set since its inception over 30 years ago. Improved measurement techniques are often presented in the literature in isolation. There is however a pragmatic technical barrier to incorporation of these improvements into a CGA system provided by a mo-cap manufactured as a complete system. Reluctance of manufactures to modify what has become their legacy solution combined with clinicians’ reluctance to climb the required technical barriers, will have contributed to the current status quo. Conservatism in the clinical environment is often defended as a method of maintaining comparability with legacy datasets. In reality, CGM failure to minimise or account for STA effects, serves to invalidate comparisons between subjects with different soft tissue characteristics. While technological improvements that allow more accurate marker tracking have been rightly accepted without questions, constraints to the placements of markers, largely dictated by technological limitations that no longer hold true, have persisted. Change is necessary however. The emergence of micro electromechanical system (MEMS) accelerometer and magnetometer technologies have the potential to grossly capture body segment orientations in far more functional situations than a gait analysis laboratory, and at a much-reduced cost.

Optically based mo-cap via surface markers retain two innate advantages over these rival technologies. First, the measurements are equally accurate in all planes. This is not the case for MEMS devices, which track vertical movement components with respect to the local gravitation field, but are reliant on the far less reliable magnetic north as a horizontal reference. Although the relatively small amplitude of transverse plane movement make measurement challenging for mo-cap systems also, these difficulties are exacerbated by current marker configurations failure to minimise STA effects.

The second accuracy advantage of surface marker approach over solid-state devices is in the identification of bony landmark locations. This feature allows mo-cap systems to create meaningful neutral orientation for each body segment. The problems of accurately fixing MEMS devices to a body segment in a small region that represents movement of the whole, and aligning its axes to match clinical expectations of the segment, are non-trivial and unresolved.

Issue 3 acknowledges the re-emergence of STA as a recognised serious threat to CGA accuracy, and again highlights CGM failure to address this. Since the emergence of the CGM solution, the CAST method has demonstrated that surface markers required to define each body segment's anatomy, need not also be employed to track the segment's movement. Inclusion of additional surface markers solely for this purpose, opens the possibility of locating these markers in locations less affected by STA.

In order to leverage the innate advantages of mo-cap technology over cheaper solid-state alternatives, optimal marker configuration for the pelvis and thigh segments are developed in chapters 4 and 5 respectively. Leveraging these advantages will require refinement to both ARF and TRF segment definitions for each body segment.

Finally, **issue 4** addressed the inclusion of a new body segment since the CGM inception. A simple trunk segment, evolved from the simplistic BMC solution (Chapter 2) is presented in Chapter 3, and a multi-segment approach integrated into a 3D whole foot representation in chapter 6.

1.12 Aims and Objectives of this Study

Existing methods of analysing gait are subject to limitations and have not been updated in line with advances in technology. The overarching aim of the work presented in this thesis is to evaluate the advantages and limitations of existing gait models in the context of individual body segments, and derive bespoke segment-specific marker solutions. Taken together, these solutions aim to provide an integrated non-invasive surface marker-based clinical gait model that

can demonstrate improved validity over conventional methods, whilst maintaining clinical utility.

I have tackled this ambitious aim by addressing the following objectives:

i) Derive a theoretical baseline model concept to provide the simplest representation of a gait model with predictable strengths and weakness.
ii) Evaluate existing clinical models against the conceptual model for each body segment
iii) Derive unique marker solutions for each body segment that are reliable and valid, as well as clinically practical.

Following the General Introduction (this chapter) my thesis outlines the Baseline Model Concept (BMC, Chapter 2), then uses the BMC reference values in a segment-by-segment investigation of modelling solutions (Chapters 3-6, also containing chapter-specific introductions and methods). Finally, I conclude with a chapter providing a summary and suggestions for potential future work based on the findings of my PhD research (Chapter 7).

1.13 Development of a New Gait Model – Background Information

1.13.1 An Integrated Development Approach

Simultaneous development all segment solutions into a complete gait analysis model, allows for the distribution of any required modelling assumptions across adjacent segments. This approach facilitates the amalgamation of individual concepts from published literature into a single coherent solution. Specific assumptions already accepted for the modelling of one segment may then be leveraged to the benefit of another, increasing the usefulness of the model without the introduction of new inaccuracies.

1.13.2 Model Calculation Method is Pragmatically Dictated by choice of Software

Established Newtonian physics link the forces acting on a rigid body to its instantaneous acceleration, and the body's velocity to the accumulative effects of its acceleration history. Calculations and methods that start with measured forces

and output joint angles and displacements are referred to as forward dynamic (FD). Clinical gait analysis employs the opposite approach, termed inverse dynamic (ID), where movements are measured, from which imposing forces can be calculated. Integration of ground reaction force data, generated from force plates, provide acceleration of the whole-body centre of mass location, such that joint moments can then be calculated by the subtraction of contributions by distal segments.

Movements captured as a set of marker trajectories may be modelled on a 'per segment' basis, and resultant joint angles calculated as a direct kinematic (DK). Alternatively, all segment markers may be considered together, and the model's joint angles adjusted to find the best overall fit for all markers. The latter global optimisation approach is referred to as inverse kinematic (IK). Application of DK or IK is largely dictated by the choice of software. While most CGM applications, including Vicon's PiG (Oxford Metric, UK) have persisted with the simple DK approach, bespoke biomechanical modelling software packages including OpenSim (Delp et al., 2007) and AnyBody (Damsgaard et al., 2006) have promoted IK as a method of reducing the overall STA effect on the model. An IK approach (Lu and O'Connor, 1999) is also integral to the Visual3D software (C-Motion, Germantown MD, USA) used throughout this thesis. It should be noted that the choice between DK and IK method for kinematic calculations, has far less influence on outputs than that of the underlying biomechanical model employed (Kainz et al., 2016).

1.13.3 Precision and Accuracy in Gait Analysis

Regardless of the calculation method employed to calculate outputs from a bio-mechanical model, these outputs need to demonstrate both precision and accuracy. Precision concerns the ability of model outputs to give exactly the same result consistently, under identical test conditions. This tight grouping is indicative of controlling sources of random error in the measurement process and is synonymous with test reliability. Regardless of the tightness of grouping of repeat measurement, it is important that the average of these measures reflects the true value of interest. This ability of the measure to avoid bias associated with systematic error is termed its accuracy.

An often-used archery metaphor relates precision to the tight grouping of multiple arrows fired at a target (Figure 1-11). Accuracy is then the closeness of the *average* arrow position to the bullseye, at the target centre. This average position may not reflect the location of any actual arrow which may, for example, be evenly distributed around the target's outer ring. In this way it is quite possible for a measure to be accurate without being precise or vice versa.

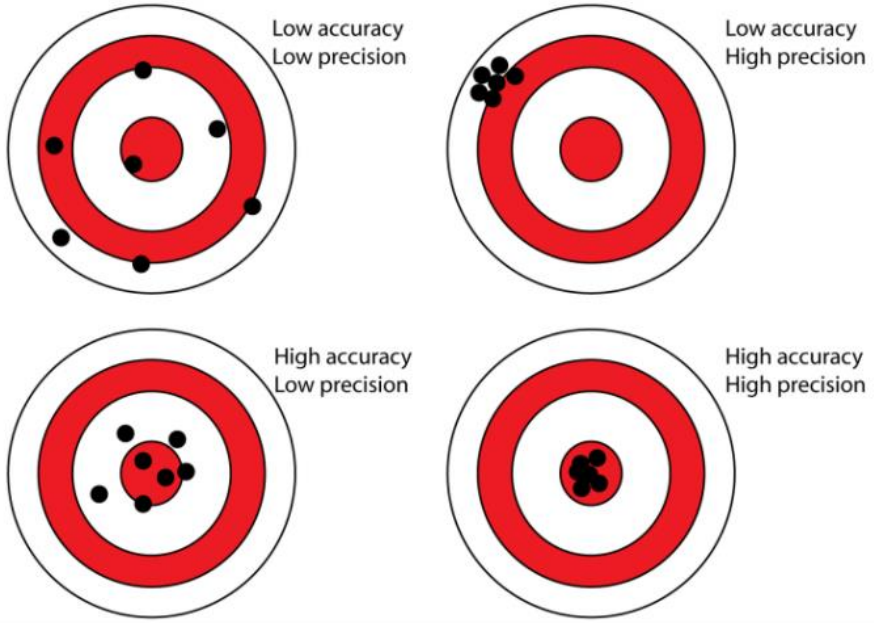

Figure 1-11 Precision and Accuracy

The concepts of precision (reliability) and accuracy can be represented by arrows (shown in black) aimed at a target (shown in red). Precision requires the tight grouping of the arrows not necessarily at the target centre. Accuracy concerns the average position of all arrows.

Within the field of gait analysis, the precision of a model output is often reported as the inter-cycle standard deviation of the measure averaged over one gait cycle, and accuracy as the root-mean-squared difference between the measured subject-value and reference-value over one gait cycle (Figure 1-12). The requirement for a comparative reference value to establish accuracy/validity, makes it a much harder measurement characteristic to establish than precision/accuracy. Ideally the required accuracy reference value would take the form of a gold standard measure.

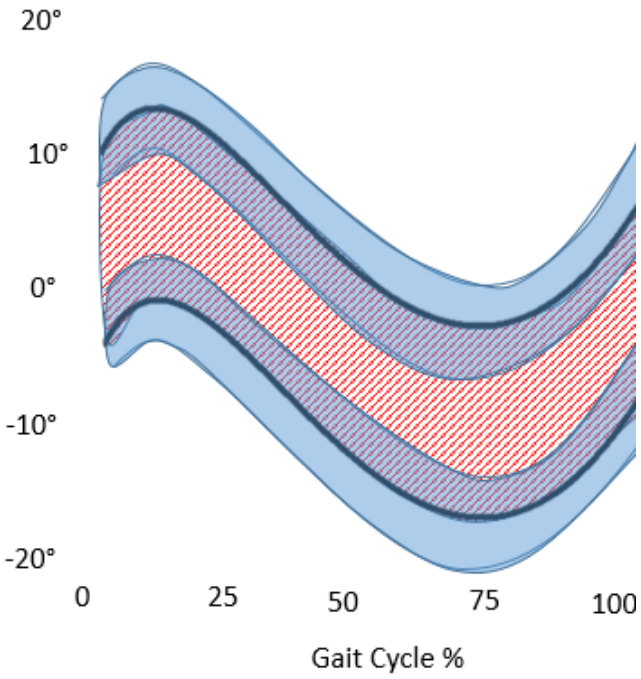

Figure 1-12 Schematic Difference between Two Gait Kinematics

Image shows two measures of a single kinematic with an approximate 12° offset difference. Precision of each measurement is depicted by their inter-cycle variability (blue regions) and relative accuracy between the two measurements by their mean difference (red region).

1.13.4 Direct Measurement of Skeletal Movement

Soft tissue obscuration of skeletal movement from skin mounted surface markers, makes the establishment a true gold-standard measure for this movement necessarily invasive. Two approaches are possible – both are non-trivial and unsuited to routine clinical use.

The most direct measurement method requires the insertion of intra-cortical bone pins, through the soft tissue structures, such that the required skeletal movement may be tracked via a small surface marker cluster attached to the external end of the pin. For obvious reasons there have been a limited number of subjects willing to volunteer for this type of in vivo study. The technique is best suited to applications within the foot, where minimal soft tissue covering masks subtle intra-articular movement but allows reliable identification of bony structure by palpation (Lundgren et al., 2008, Nester et al., 2007a). More proximal in vivo application at the shank and thigh segments have also been validated (Maiwald

et al., 2017), but requires care in the insertion of the bone-pin to minimise soft-tissue damage (Ramsey et al., 2003). Other studies have avoided these bone-pin insertion issues, by instead adopting the ex-vivo approach, of imposing simulated gait on cadaveric specimens (Nester et al., 2007b, Zhu et al., 2020). Alternatively, dynamic in-vivo imaging of skeletal bone movements by low dose ionizing radiation is becoming an increasingly attractive research tool (Strauss, 2019, Hill et al., 2018).

1.13.5 Gait Analysis Validity

The concept of validity is concerned with whether a measure is actually reporting what it purports to measure. It is somewhat related to accuracy. While validity infers the authenticity of the measure to the required quantity, accuracy describes its freedom from error. The difference between validity and accuracy therefore reflects the confidence in the gold-standard comparator. If an invasive direct skeletal movement is available for this purpose, the validity of the underlying construct of a biomechanical model may be inferred by its measurement accuracy. In this case, developed hypotheses generally predict a correlation (convergent validity) rather than a non-correlation (discriminate validity) with the gold standard measure.

A major obstacle to the development of new segment tracking solutions has been the difficulty in establishing a true ‘gold standard’ to evaluate the alternatives (Cereatti et al., 2017, Flux et al., 2020, Schache et al., 2008). In the absence of suitable reference measure, a hypothesis may alternatively be based on the ability of the measure to distinguish between individuals with and without a characteristic of interest; this sensitivity may contribute to an overall assessment of model validity. However assessed, construct validity gets to the heart of the question of whether a test measures what it is says it does. In this respect, an important aspect of achieving construct validity is in ensuring all model outputs are appropriately labelled (Hulleman et al., 2010).

Construct validity is the accumulation of evidence to support the interpretation of what a measure reflects. Proof of construct validity by comparison against an acknowledged gold standard measure provides the best evidence to support the

use of a biomechanical model. This paradigm cannot, however, drive development of the underlying model constructs. It would be neither practicable nor efficient for example, to develop a new biomechanical model by testing all possible surface marker configurations, in various patient groups, against an agreed gold standard measure, and then simply choose the best performing. Selection of an appropriate model is better guided by first establishing other forms of validity. In this respect it is worth noting that the identified issues raised against CGM were largely acknowledged from its inception (Davis et al., 1991, Kadaba et al., 1990) and accepted as a necessary compromise to the technical and knowledge constraints of the era. Results from subsequent studies comparing surface marker movements against a skeletal gold standard measure, confirm significant STA effects consistent with the identified CGM issues (Stagni et al., 2005, Garling et al., 2007, Lundgren et al., 2008, Andersen et al., 2012, Dumas et al., 2014, Barre et al., 2017, Bonnet et al., 2017, Camomilla et al., 2017a, Camomilla et al., 2017b, Fiorentino et al., 2017, Richard et al., 2017). This conformation, made possible by intellectual and technological advancements, only quantified what was already subjectively apparent.

Subjective model validity concerns its content validity, which includes both sampling validity and face validity components (Hulley, 2001). While sampling validity concerns the ability to account for all components of a measure, face validity is an even more subjective characteristic, concerning the measure's intuitive correctness. All biomechanical models aim to increase understanding by simplifying real situations. Face validity relates to the perceived reasonableness of the modelling assumptions applied to achieve this simplification. Poor assumptions will cause the model to misrepresent reality. Only after consideration of a measures content validity, can construct validity be established by testing the empirical and theoretical constructs, or underlying modelling assumptions of the developed model. Evidence should therefore be collected to corroborate rather than derive best practice.

In order to avoid the invasive nature of establishing a true gold standard measure of skeletal movement, many published studies have instead used an established CGM solution to provide a reference validity measure (Duffell et al., 2014, Flux et

al., 2020, Kainz et al., 2017, Leboeuf et al., 2019, Mentiplay and Clark, 2018, Samala et al., 2020, Stief et al., 2013). The identified CGM issues, however, questions its true validity against skeletal movements, and therefore the value of these comparisons. This approach also tends to perpetuate the legacy solution by repeatedly affirming CGM as the gold standard. Difficulties in measuring true bone movements have led many multi-segment foot models to claim validity on the basis of serial repeatability studies alone (Leardini et al., 2019).

1.13.6 CGM 1.1 fails to address the identified CGM issues

Over time, CGM improvements may have logically arisen from technological advancements in marker tracking ability (equipment improvements), refinement in the representation of anatomical axis in the model to better represent clinical expectations (ARF improvements), or placement of surface markers to better capture bone movements around these axes (TRF improvements). Of these possible sources of error, only equipment improvements of newer systems have been promoted by manufacturers and accepted by clinicians. In an attempt to address this imbalance, a Vicon (Oxford Metrics UK)-funded study recently proposed a CGM1.1 update to overcome some acknowledged problems with the current PiG implementation (Leboeuf et al., 2019). Perhaps influenced by commercial concerns, CGM 1.1 promotes an evolutionary approach, tinkering at the edges of the current implementation rather than modifying its core. This approach is justified against the claim that CGM is widely understood by its users. Two obvious improvements implemented by CGM1.1, allow the use of a medial knee marker to define the principal plane of the thigh segment, and correction of the Euler rotation sequence applied at the pelvis. No efforts are suggested to improve the individual segment tracking solutions. Validity of these modifications is somehow inferred by showing minimal difference from traditional PiG outputs for the healthy population.

Another CGM 1.1 modification involves simplification of a PiG-specific complexity in modelling the shank segment. This includes correction of a related, newly discovered data processing error within the Vicon software. A secondary, un-torsioned, shank segment within the original PiG model was originally intended to insulate knee kinematics from torsional influence of the shank segment malleoli

axis. This duality, however, puts PiG out of line with other implementations of CGM, which report torsional knee kinematics with an offset that also reflects tibial torsion. This feature of the PiG method is not widely appreciated and complicates clinical interpretation of the resulting model outputs. While the hip kinematic includes any bony deformation offset caused by the thigh, the output knee kinematic is insulated from deformation of the shank. In addition, an error in the PiG implementation uncovered during CGM1.1 development, showed inconsistent use of these reference frames when remodelling an absent heel marker for the dynamic trials (Leboeuf et al., 2019). The error is shown to produce aberrant eversion of the foot during swing. That the error went unnoticed until this decomposition of the model for CGM 1.1 development, suggests that while the general anatomical definition employed by CGM are widely understood, the specifics of the PiG implementation are not.

The final modification proposed by CGM 1.1 is less widely accepted in the literature, and involves blanket acceptance of JCS for calculation of joint moments (Schache and Baker, 2007). This inclusion is all the more surprising, as the main opponent to blanket application of JCS for joint kinematics (Baker, 2003), is also an author on the suggestion to use JCS for joint moments. This approach is promoted on the grounds of consistency with expression of kinematic data, while acknowledging that discussion in the literature is not extensive (Schache et al., 2007). It should however be noted that expression of joint moments along JCS axis was specifically warned against in the closing statements of the original ISB recommendations:

"*A joint coordinate system (which might better be called a joint rotation convention) is defined for each joint individually. This system allows rotations about axes which can be anatomically meaningful at the sacrifice of establishing a reference frame with non-orthogonal axes. As long as forces and moments are* ***not*** *resolved along these non-orthogonal axes, this does not present a problem. This approach allows the preservation of an important linkage with clinical medicine where the use of independent paired rotations (ab/ad, internal/external, etc.) is common usage……" (Wu and Cavanagh, 1995)*

The published comparison of different reference frames, also suggests that a solution for clinical interpretation requires less rigor than the orthogonal solution required for calculations such as joint power (Schache and Baker, 2007). Despite this disclaimer, others have promoted implementation of JCS for joint moments on the grounds that this provides a link between joint angles and the individual motor torques and power from which they originate (Passmore and Sangeux, 2018). In reality, this connection is folly, as the whip-like action of induced accelerations allow any muscles in the kinematic chain to generate torque at any joint – even those it does not physically cross. (Zajac and Gordon, 1989).

1.13.7 Technical Considerations aside, Data Collection must also work clinically

In addition to precision, accuracy and validity, an important aspect of any 'clinical' gait model, is the practicality of its application in a clinical environment. Markers must be placed in locations that achieve their technical objectives and that can be easily tracked even in subjects demonstrating a pathological gait pattern. An optimal balance should not make unreasonable modelling assumptions during the data processing or place unrealistic demand for precision in marker placement during data collection.

1.14 Premises on which development of a New RNOH_model is based

This chapter closes by outlining three main premises on which the development of a new biomechanical model might be based. First rationale for optimisation on a per body segment, rather than body joint, are presented. Second currently available methods to model the shank segment are defended as a useful foundation for further development. The third premise states that this development is deterministic – that the ability of surface markers to capture bony movement can be reasonably predicted through knowledge of the underlying anatomy and model geometry.

1.14.1 A Segment-by-Segment Approach

Human gait is characterised by the co-ordinated movement of hip, knee and ankle joints, with the aim of supporting the body's centre-of-mass, while propelling it forward. These joint movements describe the relative orientation of a distal

segment with respect to a proximal one (Zatsiorsky, 1998b). The description of joint positions, and ultimately human gait, is therefore synonymous with the accumulated descriptions of the orientation of the skeletal structure of the proximal and distal segments of each joint. It follows that, if the orientation of all body segments are properly represented within a model, so too will be the intervening joint angles. The practical benefit of developing the model on a body segment rather than joint basis, is that identified errors no longer need to be attributed to separate proximal and distal sources.

1.14.2 Identified CGM Issues do not Fundamentally Affect the Shank Segment

ISB recommendation (Wu et al., 2002) for the principal axis of the shank differ from that commonly employed by CGM. ISB define the proximal end of the axis between medial and lateral tibial condyles, whereas CGM employs the mid-point of the femoral epicondyle. CGM deviation from ISB recommendations is partly explained by chronology of its development, but also facilitates easier and anecdotally more reliable location of bony landmarks; joining the shank and thigh segments at a single point in the model also facilitates calculation of knee joint moments and power. Both solutions define the segment ARF via a coronal principal plane through the distal malleoli ankle axis.

Published literature looking at knee kinematics have attempted to quantify STA at thigh and shank segments against gold standard measures of cortical bone pins (Cappozzo et al., 1996, Holden et al., 1997, Reinschmidt et al., 1997, Manal et al., 2003, Taylor et al., 2005, Benoit et al., 2006), external fixation devices (Cappozzo et al., 1996) and fluoroscopy (Stagni et al., 2005). All studies show that shank STA effects are around one-third those at the thigh segment. A cortical bone pin study also suggested that ankle kinematics were more affected by STA associated with the hind-foot than shank segment (Reinschmidt et al., 1997). Optimal tracking of the shank segment via surface markers requires locations of minimal STA. Anecdotal and marker cluster rigidity measures (Peters et al., 2009) supports re-employment of the anatomical ankle axis markers at the medial and lateral malleoli locations, plus proximal and distal markers on the antero-medial shin aspect. Personal experience additionally suggests that a marker over the

head of the fibular bone provides useful non-collinear redundancy, should remodelling of any of the other marker locations be required.

The relatively uncontroversial ARF and TRF definitions already available for the shank provide an excellent starting point for development of a new model. It should be noted that although PiG officially substitutes the medial malleoli surface marker for a lateral shank marker, synonymous with the thigh definition, this is widely ignored within the clinical community, and use of the medial ankle marker in shank anatomical and tracking solutions is wide spread (Nair et al., 2010).

1.14.3 Other segment development assumes a Link between Face and Construct validity

Development of solution for body segments other than the shank is based on the premise that face validity may be subjectively judged by listing required modelling assumptions. Known discrepancies between true skeletal movements and CGM estimates are related to face validity deficits in the CGM model and detailed under the four main issue headings previously outlined. These deficits might be expressed as a list of assumptions inherent to the modelling approach that must be accepted in order that model outputs may be considered valid. It is further asserted that this face validity will likely relate to the solutions construct validity/accuracy. This focus prioritises model validity concerns over those of the much easier to assess model reliability.

Numerous publications have demonstrated model reliability of subtly different surface marker configurations employed in gait analysis (Decavel et al., 2019, Kainz et al., 2017, McCahill et al., 2021, McDermott et al., 2010, Mentiplay and Clark, 2018). The dearth of studies showing unreliable solutions may be partly explained by a general publication bias against negative results (Johnson and Dickersin, 2007, Hasenboehler et al., 2007, Rockwell et al., 2006). None the less, it is unsurprising that similar models, employing surface markers over a limited number of available bony landmarks, and avoiding poor planar tracking solutions related to skinny triangular marker configurations, all demonstrate similar levels of reliability.

Model development is also premised on there being a link between the modelling assumptions applied in order to simplify reality (Nagymate and Kiss, 2019), and resultant face validity reflecting the subjective reasonableness of the solution (Hulley, 2001). This paradigm makes it possible to make an educated guess as to the useful scope of a given biomechanical model, by consideration of its underlying assumptions against a particular patient group. The BMC and CGM pelvis for example, tracks pelvic movements via surface markers located over the ASIS and PSIS bony landmarks, which are known to suffer significant STA effects (see Chapter 4). This approach might therefore not be best suited to a study of pelvic ranges in obese patients. More generally, the attractiveness of a simple modelling approach is in the need to make fewer assumptions, in this case just the requirement for low STA. More complex modelling may be based on the application of several assumptions. In these cases, face validity will require a judgement as to whether the accumulative error of these assumptions is less than that of the alternatives. Model development should therefore aim to employ modelling assumptions with the widest possible scope, over the widest range of patients. Disputes over the subjective reasonableness of these assumptions, either generally or for a specific patient group, may be resolved by formal testing of the underlying model constructs. Establishing construct validity however, generally requires comparison against a gold-standard measure, which for skeletal movement can only be achieved via invasive methods – either mechanical or via ionizing radiation. The costs and complexity of these techniques suggests that model face validity should be established, at least as a precursor to more objective evaluation.

2 Chapter 2 – The Baseline Model Concept (BMC)

2.1 Introduction

Substantive and acknowledged deficits in the current CGM solution (see Chapter 1) make it a poor reference point for the development of a new model. The BMC is introduced here to represent the simplest biomechanical model capable of describing segment orientations by a minimal number of surface markers. It includes 8 body segments, including left and right foot, shank and thigh segments joined by a pelvis segment which, in turn, carries the trunk. The BMC aims to directly represent segment anatomical orientations by surface marker locations, without the need to employ a neutral joint position calibration assumption. Developed modelling alternatives to achieve the same aim, should justify complexity above that of BMC against improved outputs or utility.

2.1.1 Model Complexity should Prioritise Increased Accuracy over Increased Utility

Proponents advocating the use of the simplest possible solution to a problem, generally caveat the approach by stating that complexity should not be accepted without reason. Here a simplistic biomechanical model of a required anatomy is developed. Comparison with the widely used CGM, reveals that CGM complexity is not justified by improvements in accuracy, but more likely derived from clinical utility constraints imposed by technical limitations of the era. BMC outputs are therefore expected to outperform CGM. Normative reference values for the BMC are established and a set of scores developed to characterise the average cycle position, range of cyclic movement and inter-cycle variability. Additional scores are developed to evaluate movement pattern difference and overall root-mean-squared (RMS) difference of biomechanical models with respect to the BMC approach. These scores provide a point of comparison for the development of segment specific modelling solutions in the subsequent chapters.

Table 2-1 Philosophical links between simplicity and accuracy.

*"plurality should not be posited **without necessity***"	Occam's razor Circa 1347
"*No more causes of natural things should be admitted than are both true **and sufficient** to explain their phenomena*"	Newton, Isaac, Andrew Motte, and N. W Chittenden. Newton's Principia. 1687
*"Everything should be made as simple as possible, **but no simpler**".*	Widely attributed to Albert Einstein Circa 1933 (Calaprice, 2000)

In the somewhat lofty examples presented in Table 2-1, the authors were seeking understanding of a profound truth, and complexity is only justified against improvements in accuracy. In the development of a biomechanical model for clinical gait analysis, this truth is represented by the skeletal frame of a walking patient, and the aim is to report the instantaneous orientation of each skeletal segment through the gait cycle, via the movement of skin mounted surface markers.

2.1.2 BMC prioritises Simplicity over Accuracy as a pro forma for further Development

The BMC aims to model the orientation of thorax, pelvis, thigh, shank and whole-foot segments, such that these may be reported using clinical terminology. This aim is in accordance with the stated primary objectives of both the original JCS application at the knee (Grood and Suntay, 1983), and subsequent application at other joints (Wu et al., 2002). Within these aims, development will be characterised by the prioritisation of model simplicity over accuracy. This remit

encompasses segment ARF definition in the most direct method possible and development of a strategy for segment-specific application of Euler rotation sequences. No consideration will be given to reducing STA by the development of separate segment TRF solutions, or to modifications aimed at improving clinical utility. Model outputs are therefore expected to represent non-optimised versions of measures that are fundamentally correct in form. Against this background, a clinical model employing ARF refinement or TRF development, should justify any increased complexity against improvements in model outputs or clinical utility benefits.

As modern mo-cap systems claim sub-millimetre accuracy in the capture of surface marker locations (Topley and Richards, 2020, Raghu et al., 2019, Eichelberger et al., 2016, Aurand et al., 2017), the primary cause of mo-cap measurement error is now generally acknowledged as the difference between the movement measured at the skin surface, and that of the underlying skeletal structures (Andriacchi and Alexander, 2000, Camomilla et al., 2017b, Leardini et al., 2005). From this, it seems reasonable, that the reduction of STA effects should be a primary justification for the introduction of model complexity. Model development therefore involves balancing the introduction of complexity over and above that of the BMC solution, against an increased ability to represent skeletal movement. To finish this introduction with one more quote, the English statistician George Box, succinctly acknowledged this balance between complexity and inevitable modelling errors by his famous quote:

"All models are wrong but some are useful" (Box, 1976).

2.2 BMC Development

2.2.1 Specification of Euler Angles

Long before the advent of CGM, Leonhard Euler (1707 – 1783) worked out the mathematics of describing the 3D orientation of a 3D axis system with respect to a reference neutral position by three intuitively meaningful angles. Each axis system is commonly referred to as a frame and consists of 3 mutually perpendicular axes with a common origin. When the frame is anatomically orientated within a body segment and embedded to move with the segment it

forms an ARF. The ARF facilitates description of that object's orientation as equivalent to that of the frame's axes.

2.2.1.1 *Joint Angles generally express Orientation of a Distal Segment with respect to Proximal*

When the ARF of the proximal and distal segments are aligned, the intermediate joint is, by definition, in a neutral position. The Euler method is then employed to describe joint orientation away from neutral, by the specification of 3 intuitive angles.

Euler angles describing a segment's orientation may be expressed with respect to a global laboratory frame, or more commonly, as a joint angle relative to the adjacent proximal segment. The former informs on the functional contribution of each segment to the formation of step length, width, and height; joint angles inform on the applied change in length of soft tissue structures that cross the joint at a specified aspect and radius. Regardless of this calculation choice, the angles may be expressed around the proximal segment ARF (extrinsic Euler angles) or around the distal segment ARF (intrinsic Euler angles). Mathematically this choice is trivial, as an intrinsic-to-extrinsic conversion is achieved by simple reversal of the elemental rotation sequence. From a clinical mind-set, joint angles are generally regarded as movement of the distal segment around axes embedded in that segment (intrinsic).

2.2.1.2 *The Sequence of Rotations around Distal ARF Axis is critical to their Numeric Values.*

Consider an Euler rotation sequence consisting of a flexion movement at the hip followed by external rotation. In this sequence both angles maintain their clinical meaning. If, however, these rotations were applied in the reverse sequence, the joint would not end up in the expected clinical position; the act of applying external rotation first would introduce an element of abduction to the subsequent flexion movement. If this sequence were employed, this unwanted abduction component would need to be 'undone' by a third rotation, in order to describe the required orientation. The resulting three angles could then perfectly describe the desired

thigh orientation, but they would not correspond with the clinical hip angle descriptors. Logically there are 12 possible rotation sequences that may be employed to describe any joint orientation by the application of 3 sequential rotations around 3 possible axes. While all rotation sequences are mathematically accurate, only one specification will yield angles that corresponds with clinical terminology such as flexion-extension ad-abduction and internal-external rotation.

2.2.1.3 Clinical Rotation Sequence can be Restricted to Six Cardan Options

A potential problem with the Euler method, referred to as gimbal lock, occurs when the second rotation in the sequence aligns the axis for the third rotation parallel to that already employed by the first. When this occurs only two rotations are effectively specified, and the reported angles becomes unstable. Fortunately, anatomical constraints to movement at all lower extremity joints prevent gimbal lock configurations; gimbal lock need not therefore be a factor in the selection of a suitable rotation sequence in expressing orientation at these joints. Interestingly, at the more mobile upper extremity shoulder joint, the intrinsic rotation sequence that avoids gimbal lock is transverse followed by coronal followed by transverse (An et al., 1991). This two-axis sequence, where the first and third rotations are around a common axis, which gets re-orientated by the second, can still be matched to clinically acceptable terminology. In this case, the first rotation in the sequence specifies an elevation plane, the second an elevation amount, and third the spin orientation of the arm around its long axis. Clinical terminology for the orientation of all lower extremity joints, specifies rotations around all three available axes. Rotation in the sagittal plane is generally termed flexion-extension, coronal plane movement is termed adduction-abduction and transverse internal-external rotation. This sub-set of Euler rotation sequence solutions that employ all three axes, are termed Cardan angles.

2.2.1.4 Appropriate Cardan Sequence depends on Neutral Orientation of Distal Principal Axis

In both clinical examples just presented, one of the angles specified axial rotation of the distal segment around its principal axis. For a segment with a vertical

neutral principal axis (thigh or shank) this rotation is the transverse plane internal-external rotation. As illustrated in the hip joint example, application of this rotation prior to the flexion-extension or ad-abduction rotations, would tend to muddy the clinical meaning of these latter rotations. This mismatch with clinical terminology is avoided by reserving the axial spin movement of the distal segment as the final rotation in the sequence. In ordering the first two rotations, it makes sense that the largest movement takes advantage of the purity of being defined from the neutral starting position; this movement generally creates movement in the sagittal plane. Application of this logic to a vertically aligned distal principal axis (thigh or shank segments) confirms the sagittal-coronal-transverse sequence universally accepted for application at the hip and knee joints. For a medio-laterally aligned axis the rotation sequence that answers the above logic is transverse-coronal-sagittal, thus confirming the now widely agreed required sequence for the pelvic segment (Baker, 2001, Collins et al., 2009b, Leboeuf et al., 2019). Further extension of this logic to an anterior-posterior principal axis, as might be encountered within the foot, strongly suggests that the required rotation sequence here, is sagittal-transverse-coronal.

2.2.1.5 Extension of ISB recommendations to Upper Extremity supports the Derived Premise

The ISB initial defence for blanket application of the JCS, or its equivalent sagittal-coronal-transverse Euler sequence, at all joints, was eventually relinquished in consideration of the upper extremity joints (Wu et al., 2005). The relative complexity of these joints appears to have necessitated specification on a per joint basis. A general pattern emerges that confirms the appropriateness of a sagittal-coronal-transverse (Sag-Cor-Hor) pattern for joints where the distal segment has a vertical neutral orientation, and the reverse sequence, transverse-coronal-sagittal (Hor-Cor-Sag) for when it has a medial-lateral orientation. These recommendations together with those for the lower extremity joints are collated in table 2-2.

Table 2-2 ISB and related recommendations for the reporting of joint kinematic data.

JOINT	PROXIMAL		DISTAL		EQUIVALENT EULER ROTATION SEQUENCE
	SEGMENT	JCS AXIS	SEGMENT	JCS AXIS	
Pre ISB Recommendations on JCS definitions (Baker, 2001)					
Pelvis	Global	Superoinferior	Pelvis	Medio-lateral	Hor-Cor-Sag
Initial ISB Recommendations on JCS definitions (Wu and Cavanagh, 1995)					
Knee	Thigh	Medio-lateral	Shank	Superoinferior	Sag-Cor-Hor
ISB Recommendations on JCS definitions Part I (Wu et al., 2002)					
Ankle	Shank	Medio-lateral	Hind-foot	Superoinferior	Sag-Cor-Hor
Hip	Pelvis	Medio-lateral	Thigh	Superoinferior	Sag-Cor-Hor
Spine	Proximal Vertebra	Medio-lateral	Distal Vertebra	Superoinferior	Sag-Cor-Hor
ISB Recommendations on JCS definitions Part II (Wu et al., 2005)					
Thorax	Global	Medio-lateral	Thorax	Superoinferior	Sag-Cor-Hor
Sternoclavicular	Thorax	Superoinferior	Clavicle	Medio-lateral	Hor-Cor-Sag
Acromioclavicular	Clavicle	Superoinferior	Scapular	Medio-lateral	Hor-Cor-Sag
Glenohumeral	Scapular	Superoinferior	Upper Arm	Superoinferior	Hor-Cor-Hor
	Thorax	Superoinferior	Clavicle	Medio-lateral	Hor-Cor-Sag
	Thorax	Superoinferior	Scapular	Medio-lateral	Hor-Cor-Sag
	Thorax	Superoinferior	Upper Arm	Superoinferior	Hor-Cor-Hor
Elbow	Upper Arm	Medio-lateral	Forearm	Superoinferior	Sag-Cor-Hor
Humeroulnar	Upper Arm	Medio-lateral	Ulna	Superoinferior	Sag-Cor-Hor
Radioulnar	Ulna	Antero-posterior	Radius	Superoinferior	Cor-Sag-Hor
Interphalangeal, metacarpophalangeal, inter-carpal, radiocarpal, and carpometacarpal	Various	Medio-lateral	Various	Superoinferior	Sag-Cor-Hor

The ISB recommended rotation sequence for all joints with a medio-lateral distal axis is transverse-coronal-sagittal sequence. With the exception of the shoulder joint representation, which adopts the expected anti-gimbal-lock rotation sequence, all other joints with a vertical distal axis adopt a sagittal-coronal-transverse rotation sequence. The only joint sequence not following these general rules was at the radioulnar joint. Here the ulnar and radius bones run vertically side by side to form the bony skeleton of the forearm. The major movement between them rotates the radius around the ulnar to supinate or pronate the orientation of the distal hand segment. For this joint the suggested rotation sequence is coronal-sagittal-transverse. Although there is no equivalent movement in the lower extremity, this example also serves to confirm the general

rule, that clinical terminology is maintained by placing the axial spin movement as the final component in the rotation sequence.

Whatever the motivation or mathematical justification employed by the various ISB sub-committees in deriving these recommendations, this decomposition provides strong evidence for the general link between the neutral orientation of the distal segment and the required rotation sequence to maintain clinical terminology.

2.2.2 Specification of Segment ARF

2.2.2.1 Segment ARF are specified by extension of a Principal Axis into a Principal Plane

In addition to indicating the required rotation sequence, defining a segment's principal axis goes a long way to defining the complete ARF. In order to complete this definition, the spin orientation of this principal axis must also be specified via the orientation of one other axis. Pragmatically, this second axis will point in an anatomically identified direction to define a named aspect of the segment; for a vertical principal axis, the secondary axis may point either antero-posteriorly or medio-laterally to define the segment's local sagittal or coronal plane respectively. Defining a segment's ARF is therefore synonymous with specifying two locations that define a principal axis, plus a third non-collinear location that extends this definition to a principal plane.

2.2.2.2 ARF for Pelvis and Thigh segments are provided by ISB Recommendation

Principal planes for each body segment required by a clinical gait model have largely been agreed via International Society of Biomechanics (ISB) recommendations (Table 2-2). The pelvic ARF is based on the crest plane between left and right ASIS locations and a posterior mid-PSIS location. The recommendation does not specify which of several published regression equations should be employed to model the hip joint centres with respect to this plane. Moving distally, principal planes of left and right thigh segments are defined between their respective hip joint centres and a knee joint flexion-extension axis between medial and lateral epicondyle locations. Knee joint

centres are defined as the mid-epicondyle locations with the principal axis then running up to the hip joint centres.

2.2.2.3 A suitable ARF for the Shank Segment is also Widely Accepted

In the previous section, a complete absence of suitable bony landmarks around the proximal thigh segment, forced ISB recommendations to inherit the HJC location from the pelvic segment. For the shank, ISB recommendations avoid dependence on the adjacent thigh segment, and the proximal end of the principal axis is defined as the mid-point of medial and lateral tibial condyles. Difficulty in locating these landmarks by surface palpation, however, makes this definition unsuitable for clinical gait analysis. The CGM solution to this, mimics the definition of the thigh segment and introduces a dependence on the proximal segment. In this case, the knee joint centre is inherited as the proximal end of the shank principal axis. Specification of the distal end of the shank segment is maintained as the inter-malleoli axis.

2.2.2.4 ARF for Trunk and Foot segments are derived from Postural Alignment definitions.

Unfortunately, ISB recommendations do not extend to defining suitable principal planes for a proximal trunk or distal feet segments. Clinically however, the trunk is considered to be in a neutral posture when the shoulder line is vertically above the hip line (Kendall et al., 1993); a clinically relevant principal plane can therefore be defined between left and right acromial markers at the shoulder tips, and a mid-hip location. Similarly, if the foot ARF is to describe the segment's orientation with respect to the ground in terms of, toe-up/down, medial/lateral contact, the principal plane must reflect that of the plantar surface. The triangular shape of this surface dictates two anterior markers over the medial and lateral metatarsal heads and a single posterior marker at the heel. Theoretically, surface markers may be located at a common height above the required surface on the dorsal surface of the lateral metatarsal, medial surface of the medial metatarsal and posterior surface of the heel.

2.2.3 Specification of Segment TRF

In keeping with the philosophical prioritising of simplicity over accuracy, all BMC segment movements are tracked via the same three locations employed to define their ARF. This is also true of the CGM solution.

2.2.4 Specification of Marker Set

The BMC aims to represent the specified uncontroversial segment ARF definitions with the application of a minimal number of modelling assumptions. Required ARFs are defined via surface markers, either directly or via the definition of internal virtual joint locations.

2.2.4.1 Eight Body Segments are represented by 19 Surface Markers.

Each body segment requires 3 specified locations to define its 3D orientation via specification of a principal plane. The BMC employs left and right acromial markers plus a mid-hip location to clinically define and track a trunk segment. The addition of left and right ASIS markers in combination with a mid-PSIS markers also define a pelvis principal plane, from which HJC locations are calculated via one of the available regression equations. In typically developing subjects where a leg length measurement is available, the Hara publication presents a strong case for its use as the preferred option (Hara et al., 2016). Alternatively, a similar location may be estimated via pelvic dimensions (Harrington et al., 2007). Either way, both segments are defined with just 5 surface markers. The principal plane of left and right thigh segments reemploys these HJCs locations together with additional markers over their medial and lateral epicondyles. Similarly, virtual mid-epicondyle locations, plus the addition of surface markers over medial and lateral malleoli at each ankle define the left and right shank segments. This minimalist approach employs just 13 surface markers to define all required body segments excluding the feet. Use of the mid-malleoli location to define the proximal end of the foot segment principal axis is problematic; with the foot flat to the floor, this axis inevitably shows a significant plantar flexion orientation toward a mid-toe location. To avoid this misrepresentation, the BMC models the foot principal plane between heel, 1st metatarsal head and 5th metatarsal head surface markers. Each

foot is therefore represented by 3 dedicated markers, giving the BMC a total of 19 markers (Figure 2-1).

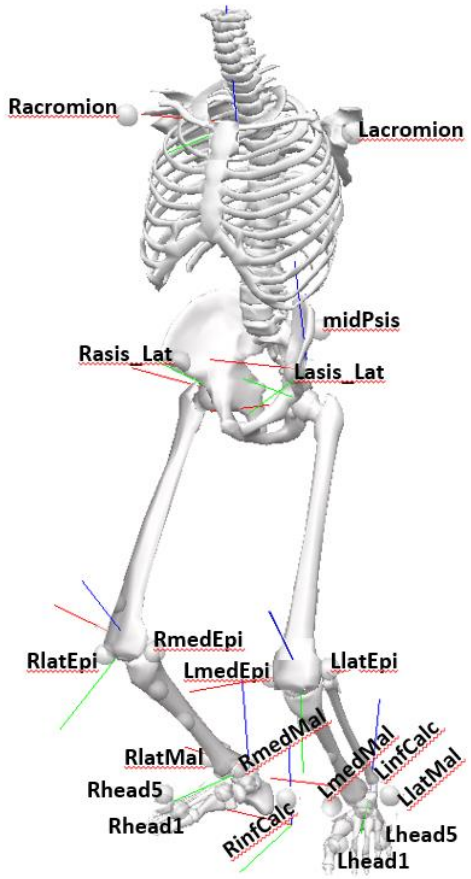

Figure 2-1 Nineteen surface marker locations use to define the BMC model

The BMC model employs 19 surface markers to represent left and right feet, shank, and thigh segments. Above these pelvis and trunk body segments are also included.

2.2.4.2 Standard Segment Mass Distribution are Adopted

In preparation for kinetic calculations, a proportion of the subject's total body mass was assigned to each body segment. Similar to CGM, these percentage values were taken from a long established study based on the average of eight dismembered cadaveric specimens recorded as white and male (Dempster, 1955). Stated ages (age for two of the subjects was not recorded on the death certificate) averaged 68 years with a range from 52 to 83 years. BMI statistics (mean +/- standard deviation) were 20.8 +/- 1.9 kg/m^2. Establishing the validity of

these mass distributions for subjects outside of these demographics remains an unresolved issue.

2.2.5 Specification of Model Outputs

2.2.5.1 Spatial Outputs - Required Model Segments

Clinical expression of segment orientation angles through the gait cycle are commonly presented with respect to the ARF of the proximal segment as a joint angle. Calculation of these angles therefore inherits error from measurement of both the proximal and distal segment orientations. Alternatively, segment orientations may be expressed with respect to a global laboratory frame, with axes pointing in the forward direction of travel, vertically upward, and laterally. These angles represent the projections of the segment axes onto the sagittal, coronal, and transverse planes of the laboratory frame. Projection angles allow evaluation of the measurement of individual segments. Kinematic outputs for the orientation of trunk, pelvis, thigh, shank, and foot segments with respect to the laboratory frame are presented. Optimisation of segment projection angles are then assumed to also optimise modelling of joint angles between adjacent segments. Because the coronal knee kinematic is renowned for being sensitive to the transverse plane orientation of the proximal thigh segment (Piazza and Cavanagh, 2000), this single joint kinematic is also presented. The knee joint kinematic expresses the orientation of the shank with respect to the proximal thigh segment.

2.2.5.2 Temporal Outputs - Defining the Gait Cycles

For the purpose of defining gait events, ground contact and lift events are most simply detected via the presence or absence of a force record. One advantage of collecting walking data on an instrumented treadmill, is that this kinetic record is collected continuously. For the typically developing cohort, used to establish the reference BMC data, the right and left support periods occured cleanly over separate force plates, and the resultant kinetic record was all that was required for gait cycles identification.

2.2.6 Development of Gait Scores

Presented scores describe reference cycle average position, range of motion and inter-cycle variability characteristics. Conceptual scores are also outlined for overall difference and movement pattern scores based on the subtraction of BMC values from alternative modelling approaches developed in subsequent chapters. In addition to comparison of modelling approaches, these scores might also be used to compare a patient's gait pattern with a mean value from a typically developed cohort. As this application is arguably less abstract of the two uses, clinical examples are usefully included as part of each score description.

All of the developed scores are expressed in angular degree units (°).

2.2.6.1 Calculation of cycle Overall difference score

The accuracy of a particular measurement protocol is often measured as the RMS average of its cyclic difference to an agreed gold standard measure. Here, the same calculation method is employed to generate an overall difference score between proposed measurement protocol(s) and BMC reference values.

The root-mean-squared (RMS) difference between two kinematics, is also commonly adopted to score the difference between a patient's gait pattern and the mean of a typically developing cohort collected. In this case the individual kinematic values are termed 'gait variable scores' (GVS). GVS from the 3D pelvis and hip kinematic, sagittal knee and ankle kinematics, and transverse plane foot kinematics may then be combined by secondary RMS averaging, into the commonly quoted GPS, or 'gait profile score' (Baker et al., 2012, Baker et al., 2009). The GPS claims to be a mathematically rigorous measure of overall gait pathology. It does not however account for the proportion of individual GVS contributions, or their compensatory effects; for example, it is functionally much better to walk with overly flexed hips and knees, than to exhibit abnormal flexion at one level only. GVS are also unable to account for which parts of the cycle are most different from their reference values. Use of RMS averaging tends to exaggerate the influence of regions of maximal difference in the GVS scores. Aggregation of GVS into the GPS score by RMS averaging then also increases

the weighting of the most aberrant GVS scores. The resultant biases help the GPS reflect position, range and movement pattern component differences into a single score. This representation, however, comes at the expense of reducing its detailed interpretability as to the source of those differences.

2.2.6.2 *Calculation of separate cycle Average Position, Variability and Range of Motion scores*

Walking is a cyclic action requiring a repetitive movement pattern at each joint. Small, inter-cycle variations in these patterns allow the typically developing subject to cope with changes in the external environment and vary internal loads. In non-typically developing subjects, variability may be further increased by reduced neurological control (Latash et al., 2002). In either case, a treadmill may be employed to promote a steady state walking environment over a large number of cycles (Hollman et al., 2016); residual variability will then reflect the subject's ability to perform the defined task plus that caused by measurement error.

For cycle average position, and inter-cycle variability scores, the mean cycle is calculated, after interpolation of all individual cycles to a standard duration representing 0 to 100% of a gait cycle. The average cycle position score is then calculated as the mean ordinate value of this mean gait cycle. At each instance of this cycle, the inter-cycle variability is expressed as a standard deviation. An inter-cycle variability score is calculated as the arithmetic mean of the standard deviation values throughout the entire cycle.

The range score could similarly be calculated by subtraction of the mean-cycle maximum ordinate from the minimum ordinate values. This approach, however, would tend to under-estimate the true mean value of the individual cycle ranges. The discrepancy would be caused by inevitable small temporal shifts in the occurrence of minimum and maximum values between cycles. To maintain the purity and sensitivity of the range score, it is instead calculated on a per cycle basis, and then the mean of all individual cycle ranges calculated. This approach has a similar effect to temporally registering the signal prior to calculating the mean (Sadeghi et al., 2000), but bypasses the need for identification of cyclic

registration characteristics, which can be challenging – particularly in non-typically developing gait pattern.

The cycle position, range and variability scores of each individual kinematic provide an absolute value expressed in angular degrees. Values from alternative modelling approaches may be directly compared with BMC reference values presented in this chapter.

2.2.6.3 Calculation of cycle Movement Pattern difference score.

The RMS overall difference scores reflect differences in both average cycle position and movement pattern, including the range difference, for each individual model output. In order to isolate just the movement pattern difference, both the signal of interest and the reference signal must be shifted, such that they both share a common mean cycle value. This is most simply achieved by subtraction of each cycles position score from all ordinate values, such that both resulting signals oscillates around a mean zero value. With the fixed difference between two signals accounted for, the average ordinate difference between the two signals becomes a measure of difference in movement pattern only. Care is required in making this average calculation; if a signal underestimates the reference value during some parts of the cycle, and overestimates in others, these differences will tend to cancel each other out.

One obvious mathematical solution to this polarity problem, is to employ an RMS average - identical to the GPS averaging approach. RMS averages are calculated as the square root of the mean squared differences through the cycle. The act of squaring the difference before calculating this mean, weights the RMS average towards ordinate values showing the largest difference. In the case of the GPS, this approach allows a single score to be influenced by both the average and peak (range of motion) values of this difference (Chai and Draxler, 2014). The aim here however, is to develop a score representing the average difference only, for which the absolute value of the mean ordinate difference (AMD) is the appropriate metric (Willmott and Matsuura, 2005). While AMD provides a pure measure of movement difference it is also less mathematically robust than RMS (e.g. for AMD minus 5 is not truly equal to plus 5, but for RMS $\sqrt{(-5^2)}$is truly equal

to $\sqrt{(5^2)}$). AMD based scores should not therefore be used as a basis of further calculation (Norman and Streiner, 2000).

2.3 Experiment 2A – Establishing BMC reference Gait Scores

2.3.1 Aim

Data will be collected to establish BMC reference signals from which gait scores will be calculated for typically developing subjects representing a range of BMI values. These scores provide a useful reference for the evaluation of alternative, more complex, modelling approaches considered in subsequent chapters.

2.3.2 Hypothesis

> Hypothesis 2A_I - BMC gait scores reflecting average cycle position, range of motion and inter-cycle variability, from left and right versions of each body segments, will show good symmetry.

This in turn, will justify the subsequent comparison of left side results only.

2.3.3 Methods

2.3.3.1 BMC Model Specification

Details of the BMC biomechanical model are summarised in table 2-3 (next page). This includes specification of the required left (L) and right (R) surface markers, calculation of virtual points, including joint centres from the surface marker locations, input or calculated anthropometric values used to scale the model to the individual subject, definition of segmental ARF in terms of the proximal and distal principal-axis locations, and specification of a third location to create a principal plane. For completeness, the final section additionally specifies the segment mass distributions.

Table 2-3 Formal Specification of the BMC

PREFIX*	NAME	PLACEMENT / CALCULATION
Surface Markers		
L or R	acromion	Acromial Process at the tips of each shoulder.
L or R	asis_Ant	Over anterior aspect of pelvic ASIS bony landmark.
	midPsis	At midpoint between pelvic PSIS bony landmark.
L or R	medEpi	Centre of medial epicondyle bony prominence at the knee.
L or R	latEpi	Centre of lateral epicondyle bony prominence at the knee.
L or R	medMal	Tip of medial malleoli bony prominence at the ankle.
L or R	latMal	Tip of lateral malleoli bony prominence at the ankle.
L or R	infCalc	Posterior surface of hind foot at same height as head1 and head5 markers.
L or R	head1_Med	1st metatarsal head bony prominence on medial foot surface at same height as head5.
L or R	head5	5th metatarsal head bony prominence on dorsal surface of foot.
Virtual Markers		
	midAcromion	Mid-point of Lacromion and Racromion surface markers.
	midAsis	Mid-point of Lasis_Ant and Rasis_Ant surface markers.
L or R	hipHara	Posterior, lateral and inferior offsets from midAsis as provided by the Hara regression equation (Hara et al., 2016).
	midHara	Mid-point of LhipHara and RhipHara.
L or R	midEpi	Mid-point of latEpi and medEpi surface markers.
L or R	midMal	Mid-point of latMal and medMal surface markers.
L or R	midHead	Mid-point of head1 and head5 surface markers.
Subject Metrics		
	Mass	Subject body mass.
	Shoulder_Widt	Distance between Lacromion and Racromion surface markers.
	Pelvic_Width	Distance between Lasis_Ant and Rasis_Ant surface markers.
	Pelvic_Depth	Distance between midASIS and midPSIS landmarks.
	Hip_Width	Distance between LhipHara and RhipHara landmarks.
L or R	knee_Width	Distance between medEpi and latEpi surface markers.
L or R	ankle_Width	Distance between medMal and latMal surface markers.
L or R	foot_Width	Distance between head1 and head5 surface markers.
Anatomical Reference Frame (ARF)		
	Torso	Principal axis from midHara to mid Acromion with Racromion defining principle coronal plane.
	Pelvis	Principal axis from LhipHara to RhipHara with midPsis_Offset defining principle transverse plane.
L or R	thigh	Principal axis from hipHara to midEpi with latEpi defining principle coronal plane.
L or R	shank	Principal axis from midEpi to midMal with latMal defining principle coronal plane.
L or R	foot	Principal axis from infCalcl to midHead with head1 defining principle transverse plane.
Body Mass Distribution		
	Torso	53.60% as truncated cone with a proximal diameter equal to the Pelvic_Width and distal diameter equal to the Shoulder_Width.
	Pelvis	14.20% as an elliptic cylinder with antero-posterior diameter equal to 2*Pelvic_Depth, and supero-inferior diameter equal to Pelvic_Depth.
L or R	thigh	10.00% (*2) as truncated cone with a proximal diameter equal to the hip_Width and distal diameter equal to knee_Width.
L or R	shank	4.65% (*2) as truncated cone with proximal diameter equal to the knee_Width and distal diameter equal to ankle_Width.
L or R	foot	1.45% (*2) as cone with proximal apex at midMal and distal diameter equal to foot_Width.
		**** L or R corresponds to left or right side respectively***

2.3.3.2 Laboratory Set-up

Testing was performed on the treadmill-based gait analysis system (GRAIL – Motek Medical B.V. Houton, Netherlands; Figure 1-3) within the Motor Learning

Lab based at the Royal National Orthopaedic Hospital (Stanmore, United Kingdom). Left and right treadmill belts run over independent force plates that provide 3D force vectors representing the ground contact force from each foot at a sampling rate of 1000Hz. In addition, the system incorporates a 10-camera mo-cap system (VICON Bonita, Oxford, United Kingdom) employed to simultaneously track the dynamic position of retro-reflective surface markers (14mm diameter, B&L Engineering, Santa Ana, CA), fixed by bi-adhesive tape to the walking subject. Mo-cap data was collected at 100Hz. Temporal synchronisation of the force and mo-cap data was automatically managed by the D-Flow integration software (Sinitski et al., 2015), which is integral to the Motek system.

Prior to each data collection session, the system was calibrated according to manufacturer's recommendations. Briefly, this consisted of the spatial synchronisation of all cameras by agreement of views of a standardised wand with fixed surface markers (Figure 2-2). The wand was waved through the calibration volume until the software indicated synchronisation had been achieved.

Figure 2-2 Mo-cap system calibration wand – used for spatial synchronisation

Active markers on the wand define a fixed frame. Simultaneous viewing from multiple cameras as the wand is waved through the collection volume, allow the system to agree a common technical reference frame.

The same wand was then located at a fixed horizontal position, at the centre of the treadmill surface, to define the origin and orientation of laboratory ARF. This alignment defines the positive direction of the global X axis to the right, the Y axis forwards and the Z axis vertically upwards. Following this the spatial synchronisation of the force-plates was visually confirmed via a pole test (Collins et al., 2009a).

2.3.3.3 Test Subjects

The study was approved by the UCL Ethics Committee (Ref Number 6860/007), and all subjects gave their written consent to participate.

Twelve healthy adults, aged 18 years or older, were recruited to the study. All subjects reported no problems with walking or any cognitive impairment. Two to three subjects were individually tested per data collection session, with sessions spread over a 6-week period. Prior to testing, the subject's height and weight were measured to allow calculation of BMI (Table 2-4).

Table 2-4 Study Subject Characteristics.

Subject Number	Mass (kg)	Height (m)	BMI (kg/m^2)	Sex
1	46.8	1.69	16.4	Female
2	50.6	1.65	18.6	Female
3	51.8	1.65	19.1	Female
4	66.8	1.74	22.2	Male
5	69.8	1.73	23.3	Female
6	61	1.61	23.5	Female
7	79	1.82	23.9	Male
8	72.8	1.71	24.9	Female
9	80.6	1.8	25	Male
10	97.4	1.95	25.6	Male
11	71	1.64	26.4	Female
12	72.4	1.64	26.9	Female

Healthy BMI values are considered to range between 19 and 25. This cohort therefore provide 2 underweight subjects, 7 spanned through the healthy range and 3 overweight.

2.3.3.4 Data Collection

All subjects wore lightweight sports clothing. Surface markers were applied to foot, shank and thigh and trunk segments, as per the BMC model specification with the subject in a seated position. The subject then stood, and the pelvic crest area was over-wrapped in tight-fitting elasticated bandage (Coban™, 3M Berkshire, UK) to provide a firm surface on which to fix pelvic surface markers. All surface markers were 14mm diameter fixed using medical grade double-sided adhesive tape (3M - Parafix Tapes and Conversion Ltd).

Prior to the dynamic walking trial, data was collected during a static calibration pose with all surface markers in view. This allowed TRF for all segments to be calibrated to their ARF alignment. Following common practice, subjects were instructed to hold static pose for a few seconds, during which the positions of all motion capture surface markers were recorded. Unlike common practice, this calibration did not employ an upright standing pose, but instead, had the subject crouched with approximately 40° of knee flexion; they were also encouraged to keep their torso upright, such that the anterior pelvic markers did not become obscured from view. Calibration in a mid-range posture reduces potential drift between ARF and TRF alignment during the dynamic trials. All of the healthy adults reported on here were easily able to adopt this pose independently. From a clinical utility perspective, experience has shown very few patients are unable to meet this requirement; it is far more common to encounter patient that are unable to full straighten their knees. If required, patients suffering weakness or balance problems are encouraged to partially weigh bear through the treadmill handrail during this calibration.

Dynamic walking trials were routinely collected at three walking speeds, representing slow, mid, and fast walking speeds of typically developing young adults. These speeds were fixed at 0.8, 1.2 and 1.6m/s for all subjects. Each subject was provided a short warm-up period at each speed (typically a couple of minutes at the start of each session and less than 1 minute between changes in speed). For each subject at each walking speed, data collection only commenced when an apparent steady state walking condition had been attained.

2.3.4 Data analysis

Following collection, data markers were labelled via standard software tools provided by the Vicon Nexus software (Version 2.7.1). Out of view gaps in the data were rare and easily interpolated via the same software. The clean and complete marker position and synchronised force data was then exported to biomechanics model building software Visual3D (v6.01.36, C-Motion, Germantown, MD, USA) in the form of industry standard (www.C3D.org) files on a per trial basis.

2.3.4.1 Signal Processing

Within the Visual3D software, a fourth order low-pass Butterworth filter with a 6Hz cut-off value was applied to all surface marker data prior to calculations. The orientation of trunk, pelvic, thigh shank and foot segments were then calculated with respect to the laboratory frame. Additionally, knee joint angles were calculated as the orientation of shank segment with respect to the adjacent thigh. Segments with a vertical principal axis (truck, thigh and shank), employed a sagittal-coronal-transverse Cardan rotation sequence. The pelvis, with a medio-lateral principal axis, employed a transverse-coronal-sagittal rotation sequence. Finally, the foot, with an antero-posterior principal axis, employed a sagittal-transverse-coronal rotation sequence. Angular outputs were generally signed to make sagittal flexion, coronal adduction, and transverse internal rotation positive. It should be noted that the positive direction for each segment was inherited from the proximal joint; thigh flexion is therefore associated with hip flexion and acts in the opposite direction to flexion at the knee and shank. At the pelvis and trunk, anterior tilt, upward (medial) obliquity and forward rotation were signed as positive. Positive directions for the foot segments corresponded to ankle dorsi-flexion, supination (inversion) and adduction (in-toeing).

Gait cycles for all signals were defined between respective right and left ground contact events identified from the force data. All cycles were interpolated to 101 data points and average position, range of motion and inter-cycle variability scores calculated as per the developed protocol.

2.3.4.2 Statistics

Initial analysis confirmed few right-left differences in the kinematics of this typically developing subject group (Table 2-5). Only left sided data is therefore subsequently presented.

BMC position, range and variability gait scores for both the right and left body segments were calculated for their respective gait cycles. Equivalence scores are compared via paired t-test.

Following this, calculated gait scores presented for the left sided segments only are presented.

Finally, individual scores are investigated for BMI effects by calculation of coefficients of determination against subject BMI value (Table 2-4).

2.3.5 Results

Table 2-5 shows paired t-test results for the left-right symmetry evaluation. Statistically significant differences (P<=0.05) are highlighted in bold.

Table 2-5 Comparison (T-test p-value) of left and right segment gait scores.

		SAGITTAL			CORONAL			TRANSVERSE		
		Position	**Range**	**Variability**	**Position**	**Range**	**Variability**	**Position**	**Range**	**Variability**
TRUNK	**SLOW**	0.90	0.47	0.19	0.64	0.58	0.40	0.97	0.71	0.24
	MIDSPEED	0.25	0.50	0.79	0.49	0.84	0.88	0.83	0.74	0.49
	FAST	0.21	0.17	0.29	0.39	0.56	0.42	0.59	0.57	0.75
PELVIS	**SLOW**	0.90	0.55	0.28	0.89	0.39	0.26	0.41	0.34	0.10
	MIDSPEED	0.13	0.98	0.37	0.97	0.88	0.68	0.38	0.95	0.64
	FAST	0.46	0.68	0.37	0.68	0.46	0.92	0.66	0.88	0.46
THIGH	**SLOW**	0.84	0.62	0.13	0.58	0.90	0.32	0.78	0.78	0.16
	MIDSPEED	0.47	0.91	0.32	0.30	0.39	0.98	0.66	0.46	0.96
	FAST	0.83	0.25	0.96	0.40	0.87	0.66	0.99	0.36	0.62
KNEE	**SLOW**	0.52	0.31	0.14	0.83	0.50	0.46	0.82	0.17	0.09
	MIDSPEED	0.59	0.80	0.22	0.81	0.53	0.17	0.66	0.14	0.48
	FAST	0.55	0.60	0.97	0.71	0.56	0.89	0.84	**0.05***	0.62
SHANK	**SLOW**	0.40	0.38	0.15	0.41	0.72	0.27	0.59	0.91	0.29
	MIDSPEED	0.98	0.85	0.37	0.42	0.13	0.49	0.38	0.37	0.78
	FAST	0.32	0.24	0.75	0.57	0.31	0.83	0.77	0.12	**0.03***
FOOT	**SLOW**	0.33	0.92	0.09	**0.03***	0.98	0.19	0.13	0.65	0.74
	MIDSPEED	0.86	0.61	0.27	**0.03***	0.40	0.90	0.11	0.57	0.59
	FAST	0.51	0.07	0.71	**0.04***	0.40	0.50	0.17	0.83	0.13

Asymmetry in the coronal plane foot position probably reflects difficulty in judging the positioning of the Head1 and Head5 surface markers to an equal height above the plantar surface of the foot. The only other identified asymmetry shows a difference in inter-cycle variability of the transverse plane shank kinematic, likely also responsible for the difference in the measured transverse plane knee ranges.

Overall, left and right scores show good symmetry, and hypothesis 2A-I is accepted. Further analysis is therefore based on values from the left leg only.

2.3.5.1 Kinematic Position, Range and Variability Scores

BMC reference scores for average cycle position, cyclic range of motion, and inter-cycle variability are presented via a horizontal bar chart format for the sagittal (Figure 2-3), coronal (Figure 2-4) and transverse (Figure 2-5) kinematic at slow, mid and fast walking speeds.

	Position (°)	Range (°)	Variability (°)
Slow	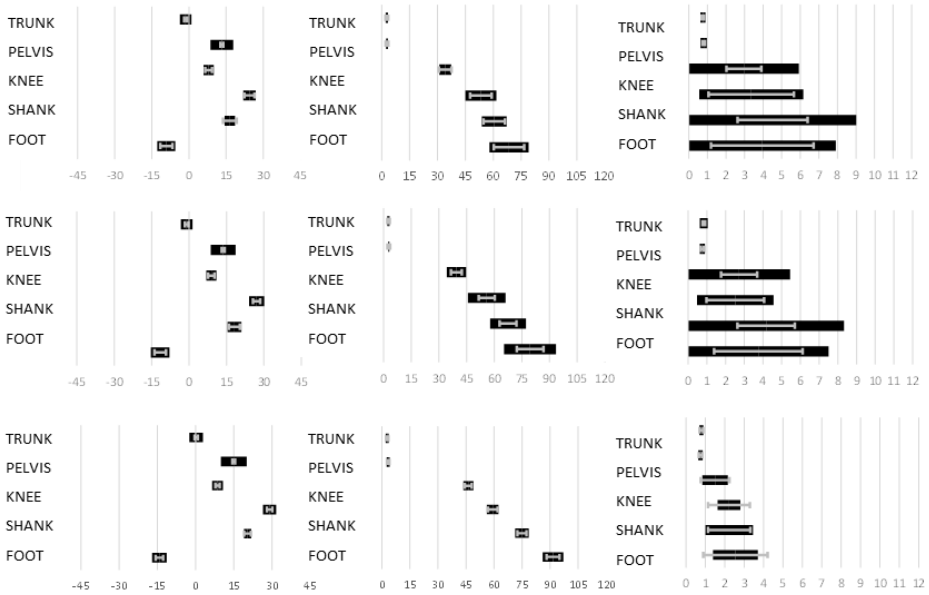		
Mid-speed			
Fast			

Figure 2-3 Sagittal plane BMC reference scores

Sagittal plane BMC reference scores for average cycle position, cyclic range of motion, and mean inter-cycle standard deviation at slow, mid and fast walking speeds. Positive directions for position scores are trunk forward flexion, pelvic anterior tilt, thigh knee and shank flexion, and foot dorsi-flexion.
All values calculated from left gait cycles of left sided segments.

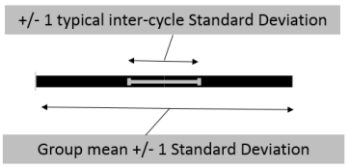

The left column shows the average cycle position of each body segment. Sagittal inter-subject variability in the average position of each body segment is greatest for the pelvis and foot segments. For the trunk and pelvis, positional inter-cycle variability is small; below this level, positional inter-cycle variability is of a similar order to the inter-subject variability.

The trunk and pelvis exhibit comparatively little sagittal plane oscillation (range). Below this level there is a clear proximal to distal increase in segmental movement. At the slow and fast walking speeds inter-cycle variability in range of movement is of a similar degree to the inter-subject variability, with a clear decrease in variability at the fast-walking speed. At the mid-speed walking, inter-

subject variation in range is increased, perhaps reflecting the approximation of this speed to that that would be self-selected (Theunissen et al., 2021, Song et al., 2020).

The specific inter-cycle variability scores show low values at the trunk and pelvis at all walking speeds, and much reduced variability below these levels at the fast-walking speed. For fast walking, typical inter-cycle variability was generally greater than the inter-subject variability, indicating that the envelope of kinematic solutions available for the fast-walking task was highly restricted.

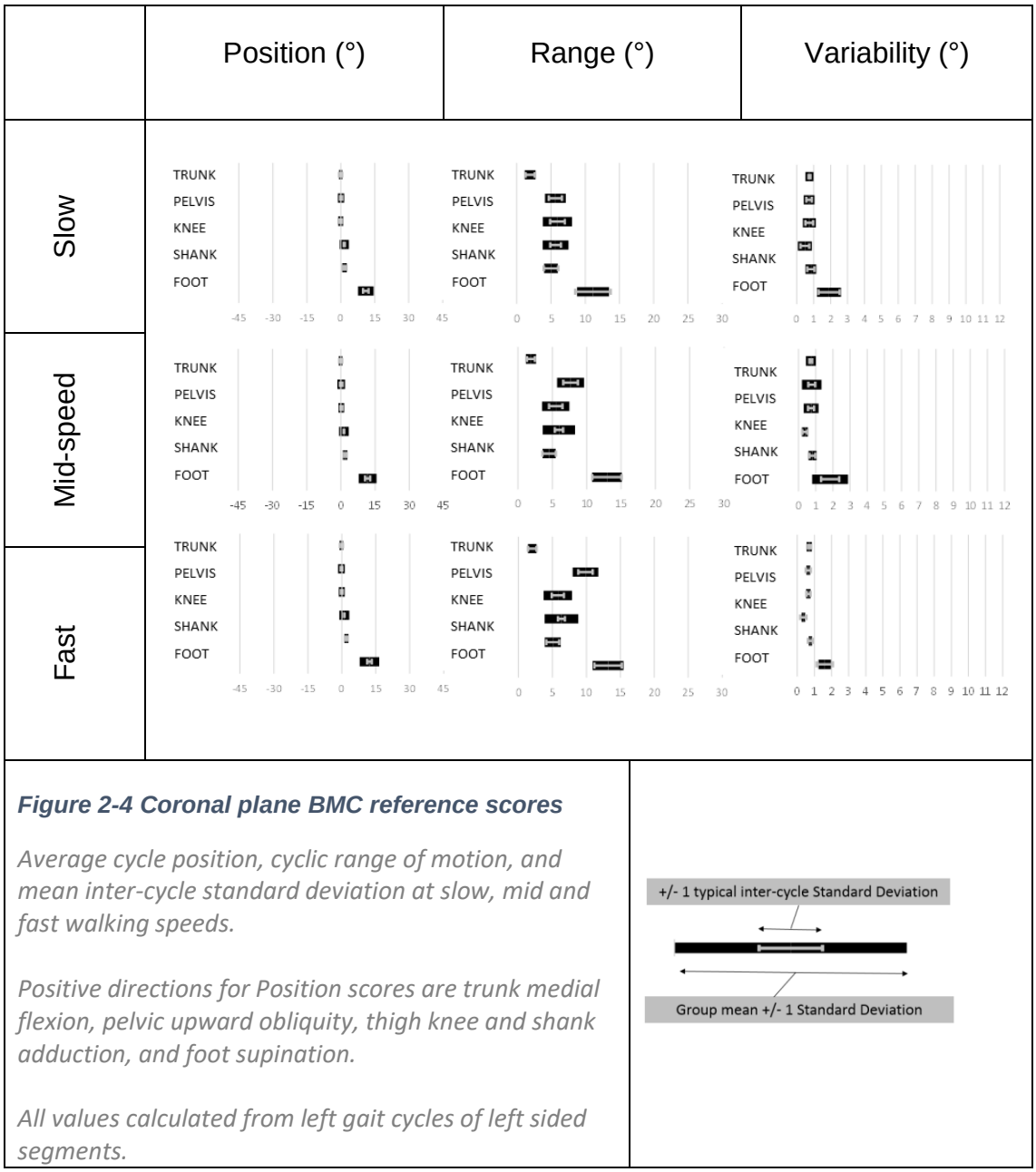

Figure 2-4 Coronal plane BMC reference scores

Average cycle position, cyclic range of motion, and mean inter-cycle standard deviation at slow, mid and fast walking speeds.

Positive directions for Position scores are trunk medial flexion, pelvic upward obliquity, thigh knee and shank adduction, and foot supination.

All values calculated from left gait cycles of left sided segments.

Near neutral average coronal plane position at all segments are consistent with an upright posture in this plane. At the slow walking speed similarly small angular ranges of motion are observed at the pelvis, thigh, and shank segments, with about double this amount of movement, and a commensurate increase in variability, at the foot. Speed related increases in coronal plane range are evident at the pelvis and foot segments.

	Position (°)	Range (°)	Variability (°)
Slow	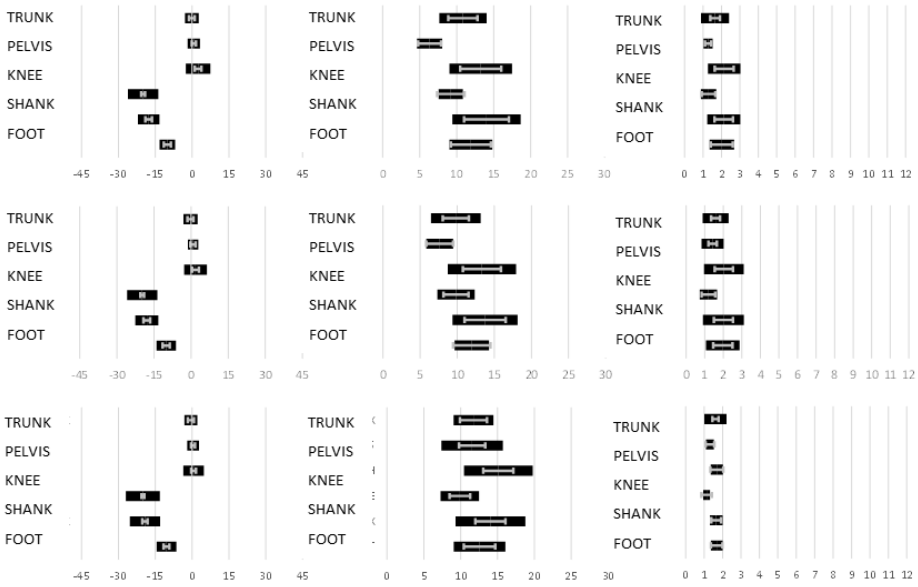		
Mid-speed			
Fast			

Figure 2-5 Transverse plane BMC reference scores

Average cycle position, cyclic range of motion, and mean inter-cycle standard deviation at slow, mid and fast walking speeds.

Positive directions for Position scores are trunk and pelvic forward rotation, thigh knee shank and foot internal rotation.

All values calculated from left gait cycles of left sided segments.

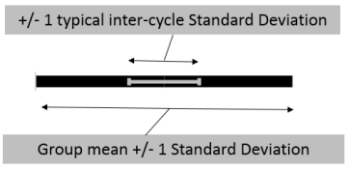

The trunk, pelvis and thigh segments hold near neutral average transverse plane position throughout the gait cycle. External rotation of the shank segment reflects

the posterior displacement of the lateral ankle marker with respect to its medial counterpart. A portion of this external rotation is inherited by the transverse plane foot alignment.

Some movement range is evident at all levels, with the largest movements at the thigh and shank segments. A much smaller movement range at the knee joint, indicates that these proximal and distal segments often move together in the same direction. There is a clear increase in the pelvic range of movement at the fast-walking speed.

Like the other planes, both inter-cycle and inter-subject variability generally decreases with increased walking speed.

2.3.5.2 Graphical Kinematic for Movement and RMS score reference.

Graphical kinematics, from which the position, range and variability gait score were derived, are presented for visual confirmation, and to show the reference kinematic pattern that will be employed for movement difference and overall RMS difference gait scores in the subsequent chapters. Figure 2-6 shows kinematic graphs for the orientation of the trunk and pelvis segments.

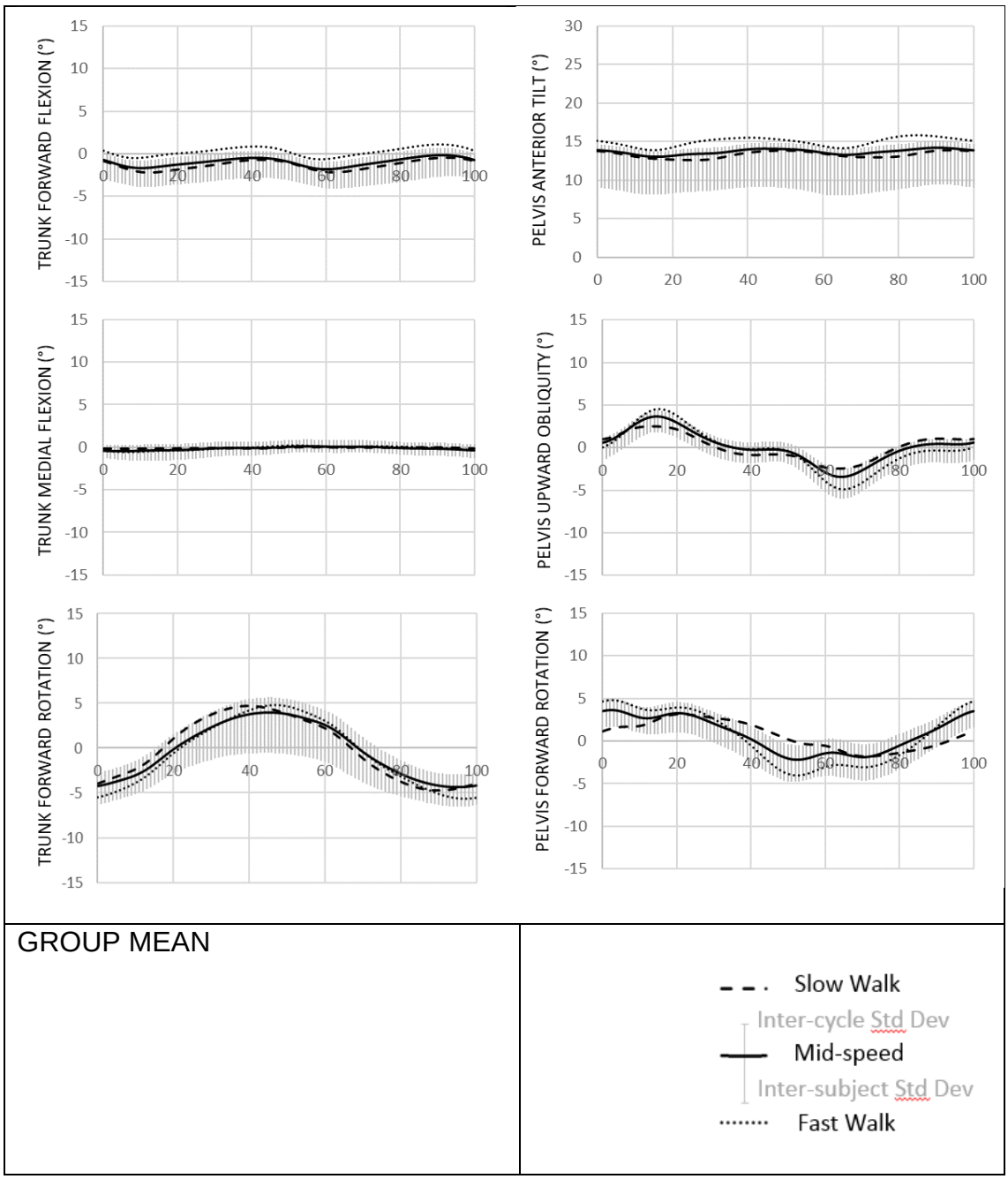

Figure 2-6 BMC Trunk and Pelvic Kinematic wrt Laboratory Frame

Trunk (left column) and pelvis (right column) group average orientation for sagittal (top), coronal (middle) and transverse (bottom) cycle kinematics from BMC data. All calculated segments were taken from the left sided data. Fast, mid and slow data are depicted with dotted, solid and dashed lines respectively. Standard deviations on the mid-speed average show typical inter-cycle standard deviation above the line and inter-subject standard deviation below. All graphs plot their ordinate value against a gait cycle % abscissa representing 0 to 100% of the left gait cycle.

The trunk segment leans a few degrees more forward when walking fast (figure 2-6 top left). No other speed related changes are noted; cyclic movement predominates in the transverse plane (bottom left) which broadly shows the shoulder line counter rotating the transverse pelvic movement (bottom right).

There is little pelvic sagittal plane movement (top right) but anterior tilt increases by a degree or two at the fast walking speed. The coronal kinematic shows an oscillatory drop on offloading double support and concomitant lift on loading (middle right). A few degrees of transverse plane forward rotation at initial contact contributes to step length; this strategy is not employed at the slow walking speed (bottom right).

Figure 2-7 shows graphs for the thigh segments orientation, and resultant knee joint angle.

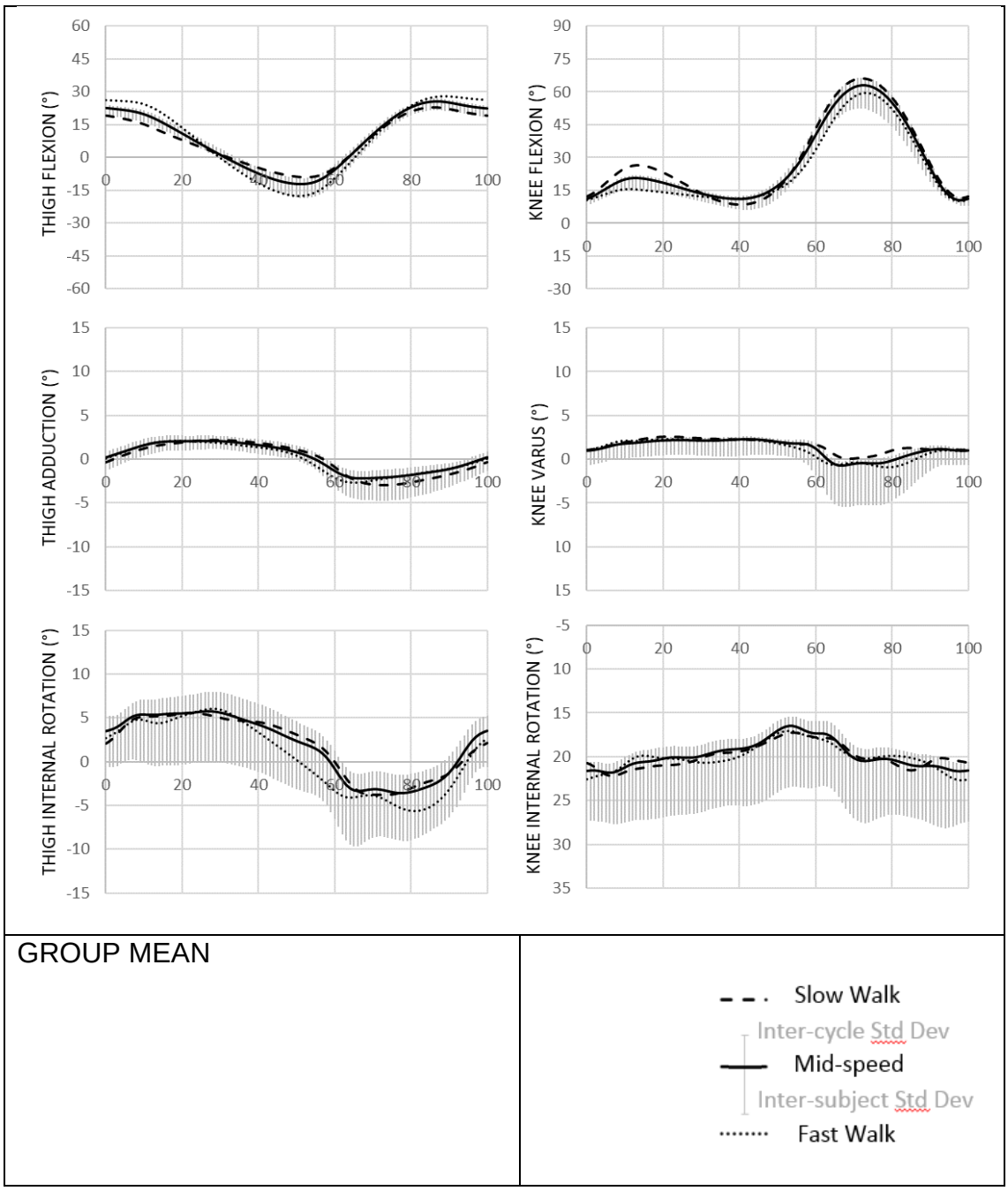

Figure 2-7 BMC Thigh Segment and Knee Joint Kinematic

Thigh (left column) and knee (right column) group average orientation for sagittal (top), coronal (middle) and transverse (bottom) cycle kinematics from BMC data. All calculated values were taken from the left sided data. Fast, mid and slow data are depicted with dotted, solid and dashed lines respectively. Standard deviations on the mid-speed average show typical inter-cycle standard deviation above the line and inter-subject standard deviation below. All graphs plot their ordinate value against a gait cycle % abscissa representing 0 to 100% of the left gait cycle.

Progressive extension of the thigh through stance is reversed through early and mid-swing and the position held in late swing (Figure 2-7 top left). In the coronal (middle left) and transverse (bottom left) planes there is a transition from a slightly adducted and internally rotated position in stance, to slight abduction and external rotation through swing.

The BMC sagittal knee kinematic shows the classic small stance and large swing flexion wave pattern (top right). The amplitude of these waves shows a small speed related increase. The coronal kinematic remains reasonably flat in a near neutral position throughout the cycle (right middle).

Transverse plane internal rotation shows an approximate 5° progressive decrease through stance, which is recovered through swing (right bottom).

Figure 2-8 shows kinematic graphs for the orientation of the shank and foot segments.

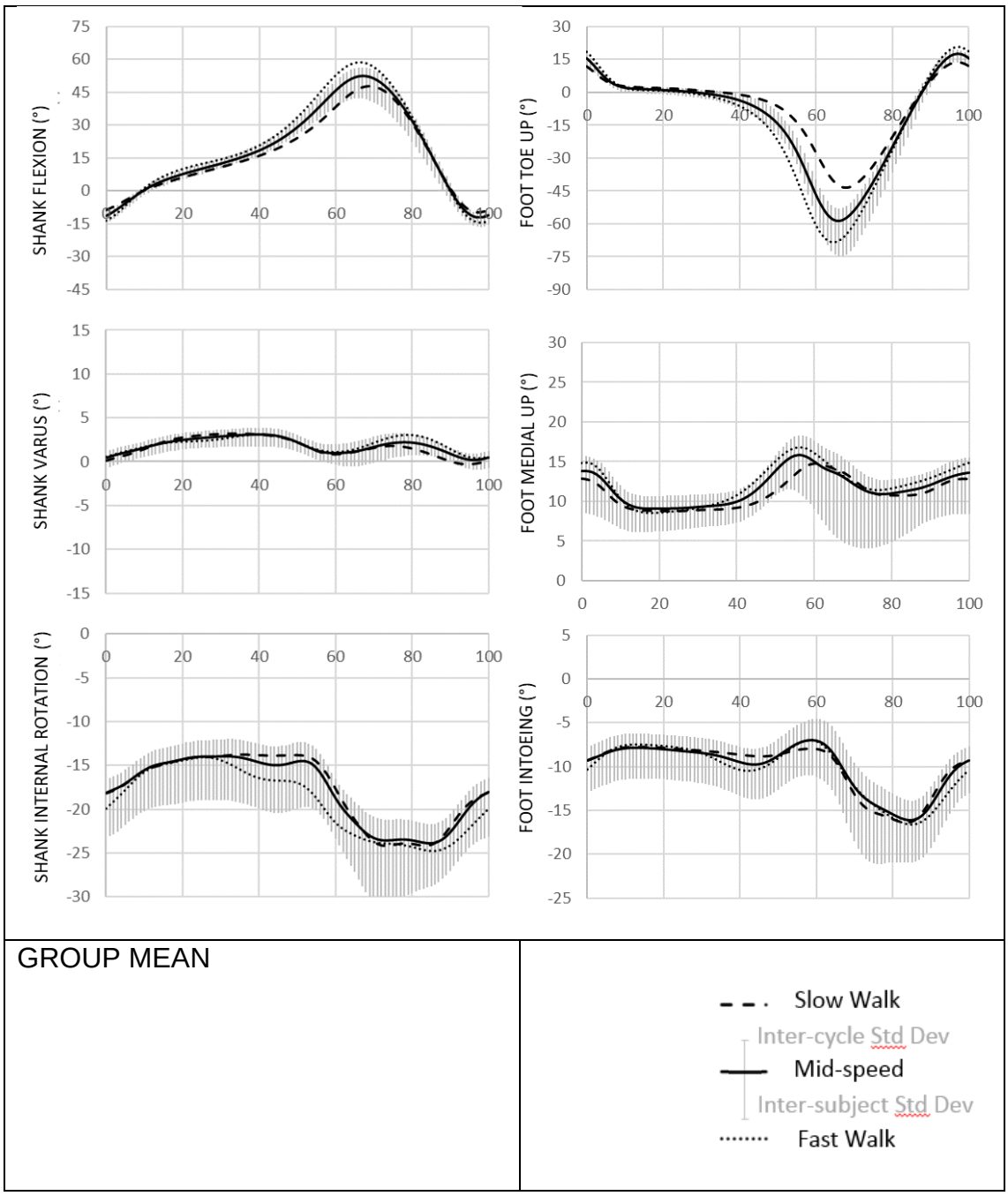

Figure 2-8 BMC Shank and Foot Kinematic wrt Laboratory Frame

Shank (left column) and foot (right column) group average orientation for sagittal (top), coronal (middle) and transverse (bottom) cycle kinematics from BMC data. All calculated segments were taken from the left sided data. Fast, mid and slow data are depicted with dotted, solid and dashed lines respectively. Standard deviations on the mid-speed average show typical inter-cycle standard deviation above the line and inter-subject standard deviation below. All graphs plot their ordinate value against a gait cycle % abscissa representing 0 to 100% of the left gait cycle.

With the shank in slight extension at initial contact (Figure 2-8 top left), the foot makes heel contact with ground and moves to flat through loading (top right) as the shank becomes vertical. Up to approximately 30% of the gait cycle, further tibial advancement is countered at the ankle keeping the foot flat to the floor. Further advancement through single support sees some speed related heel lift. At the end of stance, off-loading coincides with a strong plantar flexion movement of the foot and continued tibial advancement. During swing, the two segments move almost as one back toward their neutral orientation.

In the coronal plane, the shank holds a slight varus positioning throughout the cycle with little movement (left middle). The measured coronal foot position is not credible, showing a significant medial side up (supinated) posture throughout the cycle (right middle). This is likely caused by the difficultly of placing 1st and 5th metatarsal surface markers at a common height above the plantar surface as highlighted in the symmetry analysis (Table 2-5). The coronal movement pattern links loading plantarflexion with pronation and offloading plantarflexion with supination.

With little transverse plane movement range available from the ankle joint complex, the shank (left bottom) and foot (right bottom) follow a similar course. With the foot essentially fixed to the ground through stance there is very little movement. On offloading external rotation plateaus during the first half of swing but is then recovered in conjunction with foot dorsiflexion in the latter half.

2.3.5.3 Correlation of subject BMI statistic to BMC Gait Scores

To investigate sensitivity of the BMC to subject BMI, correlation coefficient from individual subject scores with their BMI value were calculate (Table 2-6). Correlations above $|r|=0.5$ ($R^2 =0.25$), explaining at least 25% of the signal variance are highlighted.

Table 2-6 Correlation of subject BMI with their position, range and variability scores.

		SAGITTAL			CORONAL			TRANSVERSE		
		Position	**Range**	**Variability**	**Position**	**Range**	**Variability**	**Position**	**Range**	**Variability**
TRUNK	**SLOW**	-0.05	**-0.67***	0.15	0.11	-0.08	0.22	0.38	-0.19	0.10
	MIDSPEED	-0.02	**-0.59***	-0.13	0.19	0.03	-0.04	0.31	0.08	-0.22
	FAST	0.08	**-0.62***	0.14	0.29	0.02	0.21	0.41	0.23	0.19
PELVIS	**SLOW**	0.14	-0.42	-0.16	-0.09	-0.48	0.22	0.49	**-0.71***	-0.17
	MIDSPEED	0.11	-0.29	-0.25	-0.18	-0.17	-0.27	0.44	-0.26	-0.22
	FAST	0.14	**-0.61***	-0.01	-0.07	-0.38	0.33	0.46	0.24	0.33
THIGH	**SLOW**	-0.28	-0.22	0.20	-0.36	0.31	0.08	0.02	-0.14	0.03
	MIDSPEED	-0.43	0.29	-0.21	**-0.56***	**0.57***	-0.28	-0.07	0.03	-0.39
	FAST	-0.31	-0.03	-0.08	**-0.57***	0.35	0.16	0.04	-0.18	-0.49
KNEE	**SLOW**	-0.30	-0.40	0.23	0.31	-0.31	0.29	-0.19	-0.31	0.07
	MIDSPEED	0.01	0.17	-0.18	0.30	-0.14	0.13	-0.20	-0.21	-0.31
	FAST	-0.15	-0.04	0.04	0.31	-0.12	-0.09	-0.03	-0.43	-0.33
SHANK	**SLOW**	-0.08	-0.34	0.18	0.21	-0.33	0.09	-0.31	0.00	-0.11
	MIDSPEED	0.33	0.21	-0.15	0.27	0.19	-0.25	-0.42	0.31	-0.42
	FAST	0.18	-0.26	0.15	0.11	0.00	-0.07	-0.09	-0.04	-0.49
FOOT	**SLOW**	0.32	-0.33	0.24	**0.61***	-0.08	-0.19	**-0.53***	0.03	-0.11
	MIDSPEED	-0.14	0.27	-0.14	**0.69***	0.07	**-0.55***	**-0.53***	0.44	-0.30
	FAST	-0.01	-0.19	0.08	**0.68***	-0.08	**-0.66***	-0.38	0.01	-0.47

Correlations relating the average position of the foot segment to subject BMI may be yet another indicator of the difficulties of representing the required plane by the 3 surface markers. A decrease in transverse plane inter-cycle variability in subjects with increased BMI is possibly associated with greater marker separations in larger feet reducing the sensitivity of angular calculations to individual marker movements.

Speed related BMI effects at the pelvis and thigh suggest an interplay between skin sliding and dynamic STA components.

At all walking speeds the measured range of sagittal trunk movement appears to decrease with increased subject BMI. This may be a genuine effect showing that larger individuals do not need to lean forward as much in order to shift their centre of mass towards the direction of travel, or a modelling effect reflecting the difficulties of accurately locating the HJC-shoulder-line plane in subjects with higher BMI.

2.4 Discussion

This chapter has described the specification of the BMC modelling solution, developed to avoid CGM complexity caused by the prioritisation of utility considerations over accuracy. Comparison of the two solutions identifies CGM substitution of the difficult to track medial knee and ankle markers, for lateral thigh and shank segments in the equivalent planes, as a major difference.

2.4.1 BMC Direct specification of Thigh Principal Plane by a Medial Knee Marker

Complexity of the indirect specification of the required thigh plane by the CGM method leads to an inevitably increased measurement error. CGM attempts to counter this error by use of the KAD calibration alignment jig, or cosmetic correction to the kinematic post data collection adds further complexity. Benefits of avoiding this complexity by direct specification of the required plane for the shank segment are well established (Nair et al., 2010). BMC implementation of the same solution at for the thigh showed similarly good results, exhibiting virtually none of the tell-tale excessive range of coronal plane knee kinematic, indicating malalignment (Figure 2-7).

CGM avoidance of medially placed markers at the knee and ankle axis, was likely driven by their susceptibility to dislodgment during the gait trails. As development (Davis et al., 1991, Kadaba et al., 1990) predated the intellectual separation of segmental ARF and TRF solutions introduced by the CAST method (Cappozzo et al., 1995), the only available solution was to introduce the substitute planar markers. As both markers are likely subject to similarly high STA affects (Barre et al., 2017, Cappozzo et al., 1996), there is probably little to choose between the BMC and the CGM tracking abilities.

Here, data is collected in a typically developing cohort on a treadmill-based system fully surrounded by mo-cap cameras. In this relatively small collection volume, tracking of these medial markers was not problematic. This situation was further enhanced by the typically developing subject cohort not expected to exhibit any scissoring gait characteristics, and the use of a split-belt treadmill, which is acknowledged to promote a tendency towards a slightly wider stepped

gait pattern, thus increasing the knee separation distance (Sloot et al., 2014, Hollman et al., 2006, Tesio and Rota, 2008, Zeni and Higginson, 2010, Altman et al., 2012, Oude Lansink et al., 2017).

2.4.2 BMC Scores Provide an Absolute Reference for Evaluation of more Complex Solutions.

Through the prioritising of segmental solutions directly related to underlying definitions, the BMC represents the *absolute* simplest model capable of representing the required anatomy of a gait model. The BMC itself is not, however, advocated for clinical use. It gives no consideration to minimising the influence of soft tissue wobble or to improved clinical utility. It therefore provides an absolute reference point from which to compare all other modelling approaches that do tackle these issues. These models will necessarily be more complex than the BMC and should therefore justify this complexity by conferring a specified tracking or utility benefit, ideally without introducing a loss of accuracy or reliability. It is by this measure that the CGM fails to provide a suitable reference for the evaluation of new solutions.

2.4.3 Interpretation of BMC Scores for Model Development

Scores to compare competing modelling solutions with BMC reference values for average cycle position, cyclic range of movement, inter-cycle variability and movement pattern difference have been developed. An additional RMS difference score provides a mathematically robust overview score. For the position and range scores, the mean and standard deviation metrics are easily interpreted as measures of central tendency and inter-cycle variability. Similarly, for the variability score, the inter-cycle mean of the intra-cycle variability may be interpreted at the typical line thickness required to represent small variations over multiple cycles. Inter-cycle variability may arise form a genuinely variable subject or a noisier measurement solution. Concurrent collection of data by different modelling solutions on the same subjects, facilitates control of external sources of variance.

2.4.3.1 Average Cycle Position Score

The simplicity of the BMC solution is expected to result in a non-optimised version of a fundamentally correct solution. In this regard the average cycle position scores are expected to approximate required values, and low difference (after subtraction of BMC reference values) should be interpreted as a good score.

2.4.3.2 Cyclic Range of Motion Score

By way of contrast, the BMC solution is not concerned with minimising the STA effects predominated by skin sliding (Bonci et al., 2014). These effects are found to reduce the range of skeletal motion captured by surface markers (Fiorentino et al., 2017). BMC range scores are therefore expected to underestimate required values, and high positive values of these scores, after subtraction of BMC reference values, should be interpreted as good. One possible exception to this general rule is if dynamic STA effects secondary to soft tissue inertia cause surface markers to overestimate bony landmark positions, at periods of maximum acceleration experienced during directional changes. If present, this exception might be identifiable by an increased predominance at the fast-walking speed and in subjects with higher BMI values.

2.4.3.3 Inter-cycle Variability Score

A fundamental principle of the BMC reference values is that the increased complexity of the proposed solution should be justified, primarily against accuracy benefits, or secondarily against utility benefits. These more sophisticated modelling solutions will generally require more input signals (extra surface markers), each of which will contribute both noise and signal to the solution. Accumulation of the noise component is expected to be reflected as an increase in the inter-cycle variability scores. Too large an increase may indicate unfavourable signal to noise ratio of one or more input signals, making the resultant calculation less stable. In this regard, low inter-cycle variability scores, (after subtraction of BMC reference values), should be interpreted as good.

2.4.3.4 Movement Pattern Score

Positional difference between BMC and alternative solutions may be removed by subtraction of cycle mean values from each dataset. Calculation of an absolute mean difference average from the resulting difference signal, as opposed to an RMS average, heavily dilutes the influence of range difference, by giving equal weight to all points of the gait cycle. Nonetheless, the resultant movement pattern score will suffer some contamination from changes in the measured range. It is not possible to change the range of motion without an associated change in the movement pattern. Following subtraction of BMC reference values, residual positive scores may be justified against differences in movement pattern that result in a desirable increase in measured range. This justification may be facilitated by visual inspection of the kinematic cycle in graphical format.

2.4.3.5 Overall Difference RMS Score

RMS scores from equivalent kinematics from BMC and alternative solution, reflect position, range and movement pattern differences. These scores are akin to the GVS components of GPS scores employed to show difference between patient and typically developed cohorts in the clinical setting (Baker et al., 2012, Baker et al., 2009). Calculated in isolation these scores are insufficiently sensitive to provide understanding of the difference between different modelling solutions by subtly different surface marker configurations.

2.4.4 Sensitivity of the Position, Range and Variability Gait Scores

Clinically, slow walking may emphasise any temporal asymmetry and additionally tests a subject's ability to balance with reduced inertial effects (Hof et al., 2005). Increased variability at slow walking speeds is consistent with the known difficulty of automating this task (Park et al., 2017). Fast walking can unmask tonal anomalies and tests coordinated muscular control (Neptune et al., 2008).

The ability of a score to detect subtle difference at different speeds of walking is indicative of good sensitivity (Slater et al., 2018).

Here, the presented BMC reference gait scores were able to demonstrate speed related changes to the sagittal pelvic position score and, also to the inter-cycle variability score at all levels below the pelvis. (Figure 2-3). In the coronal plane, speed related changes were evident in the foot position score, pelvic and foot range scores and the inter-cycle variability score at all levels. (Figure 2-4). There were also some speed-related changes in the transverse plane range scores for the trunk and pelvis and inter-cycle variability scores of all segments except the trunk (Figure 2-5).

Admittedly, at general low correlation coefficient, data also suggested speed independent BMI related effects in the coronal plane foot position and trunk range of motion, and BMI related effects in the coronal thigh position, coronal foot variability and transverse foot position scores at two of the three walking speeds.

Taken together, the ability of these scores to detect and attribute kinematic differences caused by changes in the walking speed and subject BMI are supportive of their use to evaluate tracking solutions, likely to produce similarly small differences.

2.4.5 TRF evaluation is Primarily Concerned with Range and Movement-Pattern scores

When simultaneously testing alternative segment tracking solutions against each other, all are synchronised to an agreed neutral orientation, as defined by the anatomical markers during the static calibration trial. As the subject moves away from the calibration posture, the inevitable effects of soft tissue sliding over skeletal structures, causes a mismatch between the desired and measured orientation. This mismatch is further exacerbated by soft tissue deformations caused by inertial and muscle contraction; these are the three components of STA.

Complex interactions between STA components make interpretation of the resultant divergence difficult. For example, one tracking solution may be particularly sensitive to movement away from the calibration posture in the coronal plane, while another is sensitive to transverse plane movement. In this

case, the positional offset of each solution is as much a function of the chosen calibration posture, as it is the ability to track the underlying movement.

It follows that, positional offset scores (and overall-difference RMS scores of which they are a component) have limited value in the evolution of movement tracking solutions, where the primary focus should be on the ability to accurately capture range and movement pattern.

3 Chapter 3 – The Trunk

3.1 Introduction

At the top of the lower extremity and pelvic segments directly involved in locomotion, sits the torso, head and upper limb body segments. The torso can be further divided into neck, thorax and abdominal regions. Together these segments account for just over half of the total body mass (Dempster, 1955). At a time of early gait analysis development, Dr Jacquelin Perry (Rancho Los Amigos Rehabilitation Centre, California) suggested that these segments might be regarded as a simple 'passenger unit' in gait function, using the term 'trunk' to describe the combined abdominal and thoracic components (Perry, 1992).

3.1.1 Trunk Anatomy dictates a Non-rigid Segment

The lumbo-sacral articulation, between the pelvis and lumber spine, is located just above and forward of the pelvic mid-PSIS location. The lumber spine itself, consists of five articulated vertebrae, identifiable at individual surface locations, corresponding to their posterior spinous process. These locations are labelled L1 to L5 from top to bottom. Above this, twelve articulated thoracic vertebrae provide similarly labelled surface markings T1 to T12. Additional articulations either side of the thoracic vertebrae join left and right rib bones to the spine. The ribs in turn, curve anteriorly, joining together at the sternum with relatively rigid articulations to form the thoracic cage. Anteriorly, the xiphisternal landmark (XP) at the bottom of the sternum, and the jugular notch (JN) at the top of the sternum provide conveniently identifiable surface location to facilitate consistent marker placement. The JN presents as a small depression between the proximal ends of left and right clavicle bones; distal ends of these bones articulate with the scapular bones of their respective shoulder joints at acromial-clavicular articulations; together each clavicle and scapular pair form left and right shoulder girdles. Independent gliding of the scapular against the thoracic cage gives each shoulder much greater mobility than that afforded to the hips by the comparatively rigid pelvic girdle. Finally, the upper limbs articulate with their scapular at the gleno-humeral joints, just below the acromial process of each scapular. The

acromial processes themselves, are identifiable as surface locations at the lateral tips of each shoulder joint (Figure 3-1).

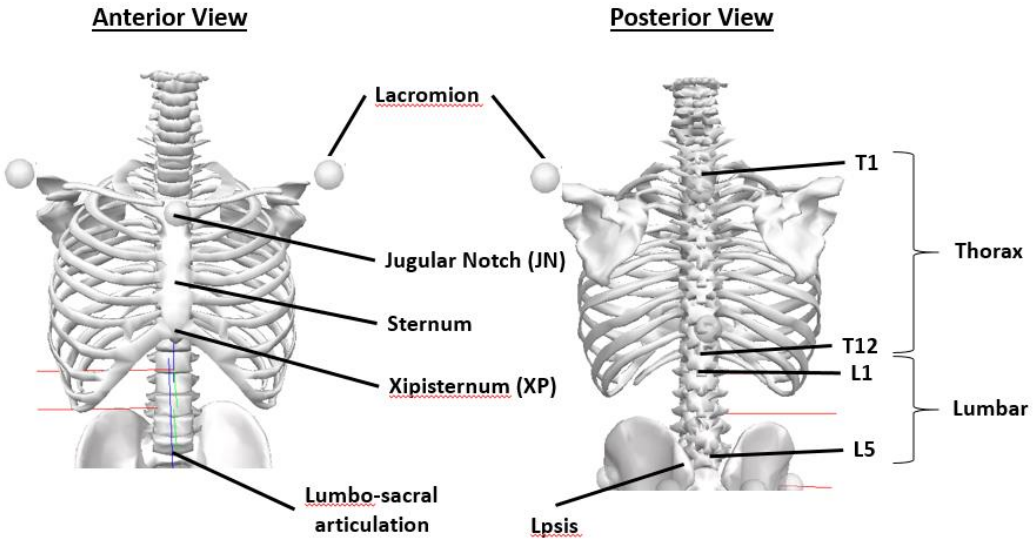

Figure 3-1 Trunk Segment Anatomical Landmark Locations

The non-rigid articulated nature of the trunk segment provides multiple identifiable bony landmark surface locations.

3.1.2 Single Segment representation of a Non-rigid Segment is complex

When a non-rigid body such as the trunk is modelled as rigid, the tracking solution must contend with deformation occurring within the underlying skeleton, in addition to the usual STA effects. In these cases, the normal approach of selecting minimal STA locations for the TRF markers may no-longer be warranted. In specific cases, the choice of marker location may be directed by a clinical question concerning the movement of a particular sub-region (Leardini et al., 2009). If the clinical question concerns multiple sub-regions, the required model will similarly require a multi-segment approach. For general use in a clinical gait analysis modelling, the trunk segment is historically omitted, or increasingly included as a single segment entity.

The BMC modelling approach, developed in chapter 2, tracks a single segment trunk over its entire length, via the same markers used to define the segments ARF. This all-encompassing approach, that prioritises simplicity over accuracy,

avoids the need to select a particular sub-region to represent movement of the whole.

3.1.3 The original single segment CGM Trunk also represented the Shoulder-Line Orientation

Of the two originating CGM publications, only one included a segment above the pelvis to account for the mass of the trunk (Davis et al., 1991). Surface markers for this representation were restricted to the upper thorax with surface markers at the neck, and the tips of both shoulders. These markers were carefully located to define a local transverse principal plane parallel to the C7 vertebra posteriorly and the JN location anteriorly. As is also common for the pelvic segment, the orientation of this plane was reported with respect to the laboratory frame rather than as a joint angle. Despite the resulting discontinuity between measured trunk and pelvis segments, the orientation of this upper thoracic region would reflect angular contributions from the un-modelled, but intervening, lumber/abdominal and lower thoracic regions. It therefore seems clear that the kinematic aim of this trunk segment was to represent the orientation of the shoulder line, at the end of a continuous kinematic chain extending back to the separately reported pelvis orientation. In general, the orientation of a distal region of a multi-segment chain represents the accumulative effect of all segment orientations within that chain, back to the reference ARF.

3.1.4 The current CGM Trunk is represented by a Thorax sub-region

More recently there has been a move to model the trunk by a single segment thorax region (Armand et al., 2014, Gutierrez et al., 2003, Leardini et al., 2011). The earliest of these (Gutierrez et al., 2003) has also been adopted within the latest PiG implementation (Vicon, 2017a). All of these models define a principal plane between superior and inferior marker pairs. Anterior markers are invariably located at the JN and XP bony sternal landmarks. There is less agreement for the precise location of posterior markers, which may be over a lower cervical or upper thorax spinous process superiorly and anywhere between T8 and T10 inferiorly. This variation will cause minor differences to the location of the segment's principal axis, defined between the mid-points of the superior and

inferior marker pairs. Unlike BMC, none of these variations correspond with a clinically recognised neutral orientation; they are as much a function of the shape of an individual's thoracic cages, as they are to its orientation. Individual variations in the shape of the thoracic cage are known to vary with sex (Bellemare et al., 2003), age (Well et al., 2007) and deformity (Kuru et al., 2016).

3.1.5 Evaluation of Trunk Segment Modelling Approaches

A legitimate motivation for shortening of the kinematic trunk segment to exclude the shoulder line would be to facilitate separate segmentation of the left and right shoulder girdles (Wu et al., 2005). This does not however, appear to have been the primary motivation for the prevalence of thorax only approach. Of the three identified thorax only variants, only one also account for the shoulder movement by the calculation a separate vector (Leardini et al., 2011). A more likely motivation for the primary output of thoracic orientation is revealed within one of the other models (Armand et al., 2014); this publication sought a thoracic TRF solution of three markers, best able to capture the movement of a full section of 11 thoracic markers. Optimisation of the marker-set in this way bypasses the fundamental question of which sub-region of the non-rigid segment is of primary interest. It is akin to modelling a non-rigid foot segment by mid-foot markers only, on the grounds that the mid-foot is more rigid than the whole foot. For both non-rigid segments, if the model output is intended to represent the orientation of the whole, then a non-rigid TRF that spans the whole segment may better suited. For the trunk segment, the shoulder line movement might be regarded as either integral to the trunk or artefactual (Leardini et al., 2009); its inclusion however, allows for modelling of a single segment comprised of multiple problematic sub-regions, but which together form a functional link between the kinematic chains of the upper and lower extremities. In addition, inclusion of the shoulder line in the trunk solution paves the way for its separation as an upper thorax sub-segment in the event of requiring a multi-segment modelling approach. This combined with the ability to provide a meaningful neutral orientation, plus the clinical utility benefits of requiring less upper body exposure, all support employment of the BMC_Trunk as the basis for development of the RNOH_Trunk solution.

3.2 Development of the RNOH_Trunk model

BMC results from chapter 2 show transverse plane counter rotations of the trunk segment shoulder line and pelvic inter-hip line. As the pelvis rotates forward contributing to ipsi-lateral step length at ground contact, the shoulder line counter rotates to help keep the upper thorax neck and head pointing in the direction of forward movement. The BMC tracking solution employs the same locations to track the trunk segment, as those used to define its principal plane; these are the left and right acromial markers at either end of the shoulder line, and the mid hip location inherited from the pelvic segment. These locations are well placed to capture the shoulder-line rotation of the upper trunk sub-region but insulated from counter rotation of lower thorax via its attachment to the pelvis.

By not accounting for the pelvic driven counter rotation, the BMC tracking solution is expected to overestimate transverse plane rotation of the trunk segment. Substitution of the pelvic mid-hip tracking location for a mid-PSIS location, which better represents the true lumbosacral articulation between trunk and pelvic segments, may therefore restore the lumbar counter rotation contribution, and in turn, the transverse plane kinematic. This anatomical modelling anomaly may also be responsible for the lack of appreciable coronal plane movement captured by the BMC_Trunk kinematic. The resulting solution from this minor modification to the BMC truck is termed the RNOH_Trunk segment. RNOH_Trunk maintains the clinical utility benefit of the BMC solution; as the mid-PSIS location is already available from the adjacent pelvic segment, no additional surface markers are required.

3.3 Experiment 3A - Dynamic Gait Trials

3.3.1 Aim

The primary aim of the experiment is to investigate the kinematic effect of the RNON_Trunk modification to the simplistic BMC reference scores developed in chapter 2. Against this background, a CGM_Thorax tracking solution will also be scored, and benefits/pitfalls of its relatively high utility costs discussed.

3.3.2 Hypothesis

Primary hypothesis 3A_I - The RNOH_Trunk will provide similar kinematic result to the BMC reference values but decrease the range of transverse plane movement by better representation of lumbar spine counter rotation in the tracking solution. As a secondary consideration this modification may also restore some coronal plane range.

Secondary hypothesis 3A-II - In the tested typically developing cohort, the CGM_Thorax will provide a reasonable representation of the holistic RNOH_Trunk solution. This will be demonstrated by the similarities in gait scores between the two solutions, indicating counter movements of the omitted superior and inferior regions by the CGM solution.

3.3.3 Methods

3.3.3.1 Model Specification

No additional markers were required for calculation of the RNOH_Trunk solution, over the concurrent BMC data collection described in chapter 2. Additional surface markers, located over the thoracic sub-region, were required to represent a typical CGM tracking solution. These were fixed at the jugular notch between the proximal ends of the left and right clavicle bones anteriorly (one location), and at the T3 and T10 spinous processes (two locations) posteriorly (Figure 3-2).

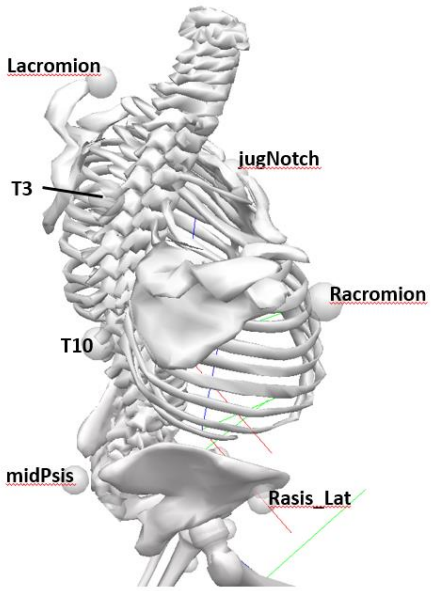

Figure 3-2 Trunk segment Surface Markers Locations

> *Left and right acromial markers facilitate definition of a clinically meaningful ARF between the intervening shoulder line and a mid-hip location. Additional tracking markers, anteriorly at the jugular notch and posteriorly over the T3 and T10 spinous processes, are employed as a CGM tracking solution of the thoracic region only.*

CGM and RNOH versions of the trunk segment, shared a common ARF, defined as part of the BMC specification. This definition maintains the shoulder-line between surface acromial markers, directly above the modelled hip joint centres as a neutral posture. Employing a common ARF for all segments, facilitates direct planar comparison of each tracking solution. Prior to dynamic testing, a single static trial (described in chapter 2), was conducted, during which the TRF for each of the three tracking solutions (BMC, CGM and RNOH) were spatially synchronised to the ARF. This simple experimental design facilitates evaluation of the three TRF solutions, while controlling all intra and inter-subject variance.

3.3.3.2 Laboratory Set-up

Data was collected concurrently with that for the BMC reference values presented in chapter 2.

3.3.4 Data Analysis

3.3.4.1 Signal Processing

Kinematics for each of the three trunk solutions were calculated as Euler angles with respect to the global laboratory frame. All orientations were calculated using a sagittal-coronal-transverse rotation sequence. Outputs were signed to make forward flexion, left side medial flexion (equivalent to upward pelvic obliquity), and left side forward rotations positive. Signal processing and gait score calculations for average cycle position, cycle range, and inter-cycle variability followed the procedure described for the BMC reference values (chapter 2).

For the CGM and RNOH solutions, an overall BMC difference score was additionally calculated as the RMS cyclic mean value. Calculation of CGM and RNOH movement scores followed a similar but slightly more complicated format. First the mean cycle was position normalised by subtraction of the mean cycle value. The movement pattern score was than calculated as the arithmetic average of the absolute difference between this cycle and the similarly zero-mean adjusted BMC reference cycle. This approach gives equal weighting to each ordinate value while preventing cancellation of negative and positive differences.

Finally, BMI effects were investigated by calculation of individual scores against subject BMI.

3.3.4.2 Statistics

For each tracking solution under investigation, paired t-test were applied across all gait scores, to identify statistically significant differences with BMC reference values.

Correlation coefficients were calculated for each gait score, against subject BMI. Correlations above 0.5 ($R^2 > 0.25$) were highlighted in a solution designated colour.

3.3.5 Results

For each tracking solution in each plane of movement, the full kinematic is presented in graphical format. Mid-speed walking data is depicted by a solid line, slow and fast data are shown by dotted and dashed lines respectively. As for the chapter 2 presentation, cycle variability is illustrated for the mid-speed trial only; error bars above the line represent typical inter-cycle variability, and those below the line represent inter-subject variability.

Below the graphical kinematic, Box plots are presented with BMC reference values for position, range and variability scores on the left, and comparative values for the alternate tracking method on the right. Figures showing the alternate values are highlighted in a solution specific colour (CGM – green, RNOH – blue). Secondary scores are also presented to represent movement-pattern difference and overall difference with the BMC solution. No standard deviations are presented for these metrics, which will have inherited variability from both solutions.

Finally, paired t-test statistics for the group mean metrics are tabulated. Results that show a statistically significant difference with BMC reference values are highlighted in the appropriate colour.

It is worth re-emphasising, that data for all solutions was collected concurrently with the BMC reference data, and that all solutions employed identical segment ARF. Any observed difference can therefore be attributed to differences in the TRF tracking of each solution.

3.3.5.1 RNOH Tracking Solution

Figures 3-3 present the gait score comparisons for the RNOH_Trunk and BMC reference values in the sagittal plane.

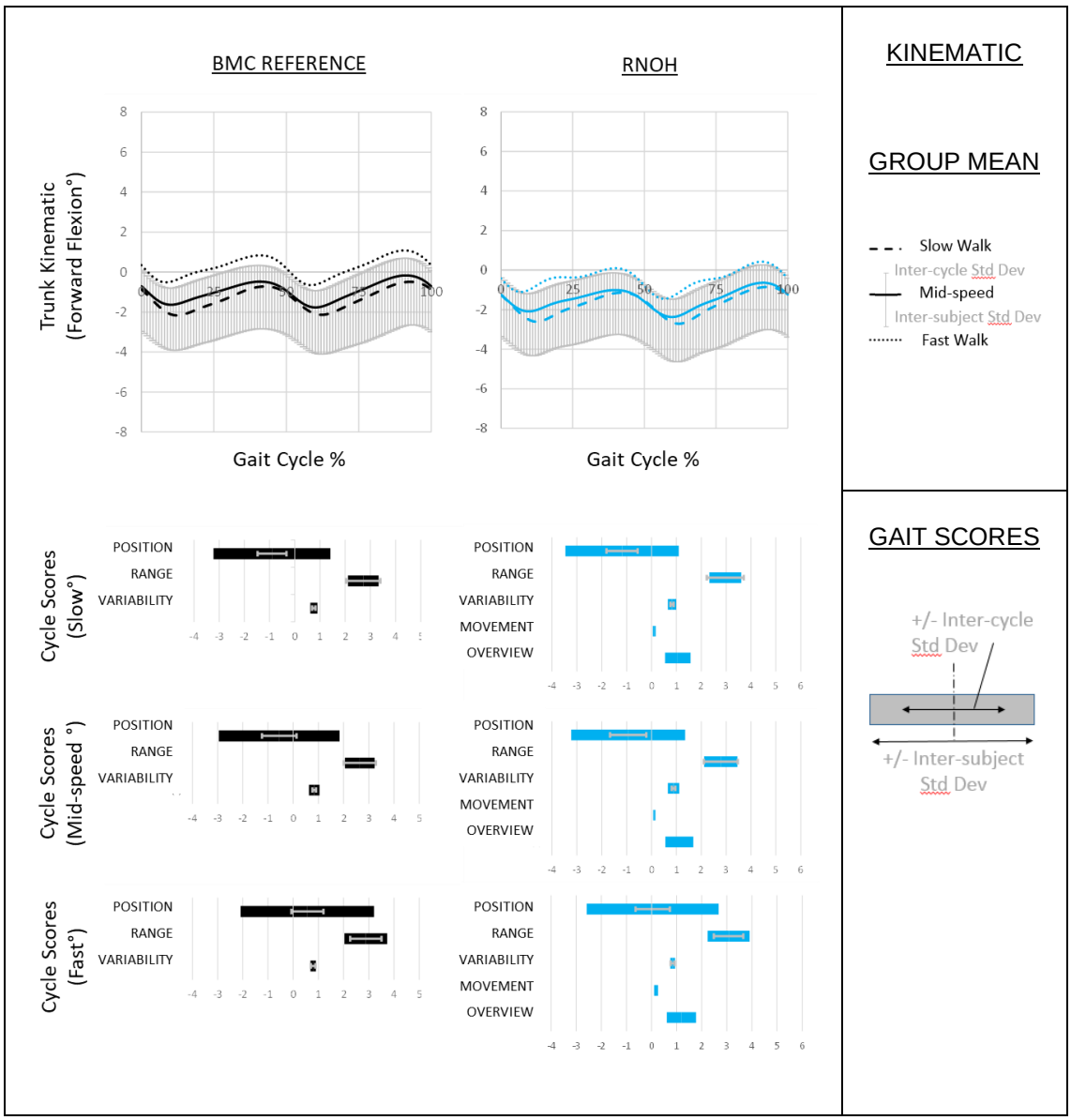

Figure 3-3 Trunk Gait Scores RNOH Tracking Solution -Sagittal

Sagittal plane comparison of RNOH tracking solution (right column) with BMC reference (left column).

Top row shows graphical kinematic for slow (dashed line), mid-speed (solid line) and fast (dotted line) walking as depicted in the legend (right). The mid-speed typical inter-cycle, and inter-subject standard deviations are shown above and below the mid-speed graph line respectively.

Subsequent rows depict speed specific gait scores as per the legend (right bottom). Cycle position, range and variability scores represent absolute values from zero. Movement pattern and overview scores measure the difference between comparative and BMC reference values.

Figure 3-4 shows similar data for the coronal plane kinematic.

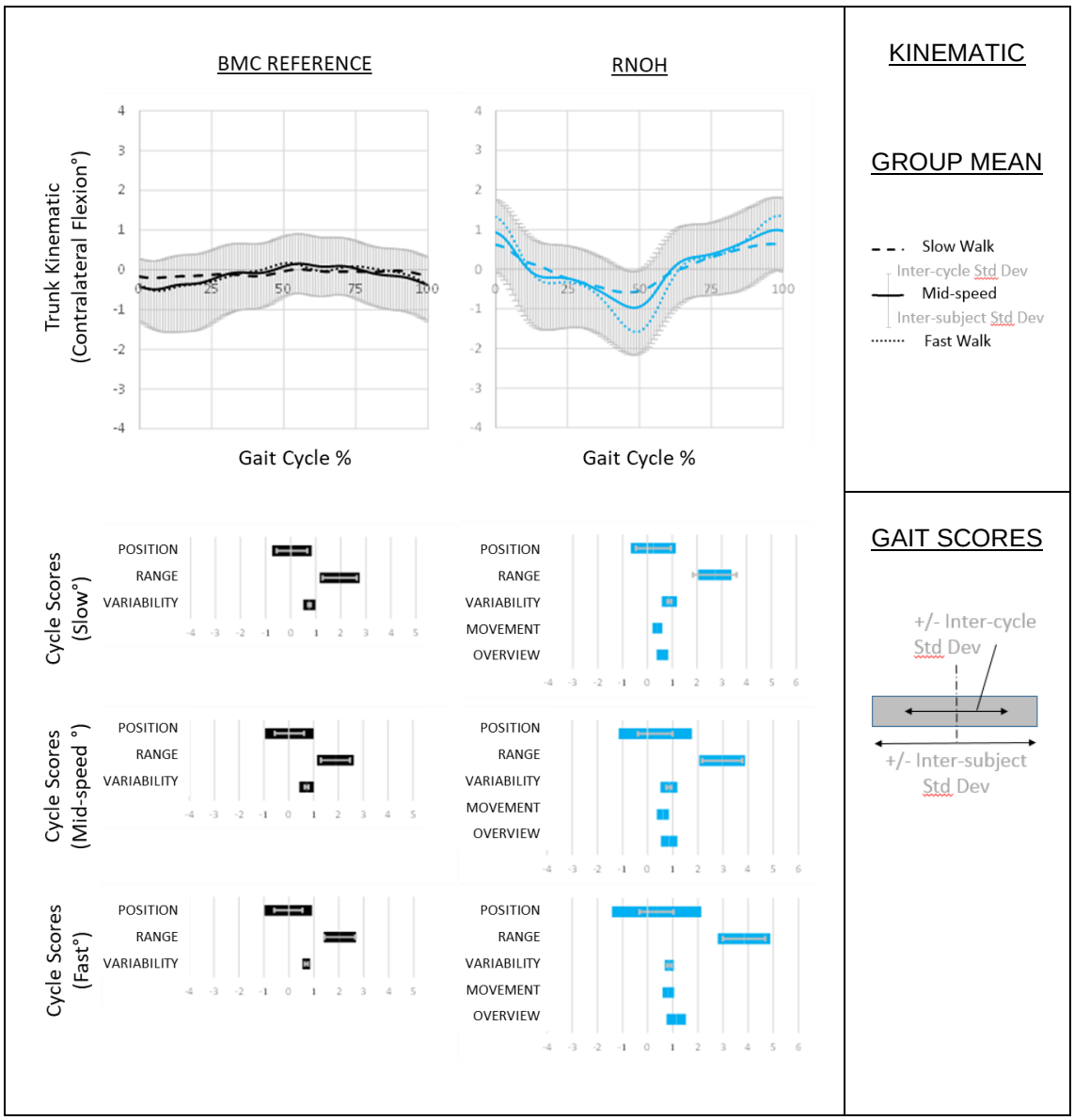

Figure 3-4 Trunk Gait Scores RNOH Tracking Solution -Coronal

Coronal plane comparison of RNOH tracking solution (right column) with BMC reference (left column).

Top row shows graphical kinematic for slow (dashed line), mid-speed (solid line) and fast (dotted line) walking as depicted in the legend (right). The mid-speed typical inter-cycle, and inter-subject standard deviations are shown above and below the mid-speed graph line respectively.

Subsequent rows depict speed specific gait scores as per the legend (right bottom). Cycle position, range and variability scores represent absolute values from zero. Movement pattern and overview scores measure the difference between comparative and BMC reference values.

Data from the RNOH_Trunk is completed with the transverse plane kinematic, figure 3-5.

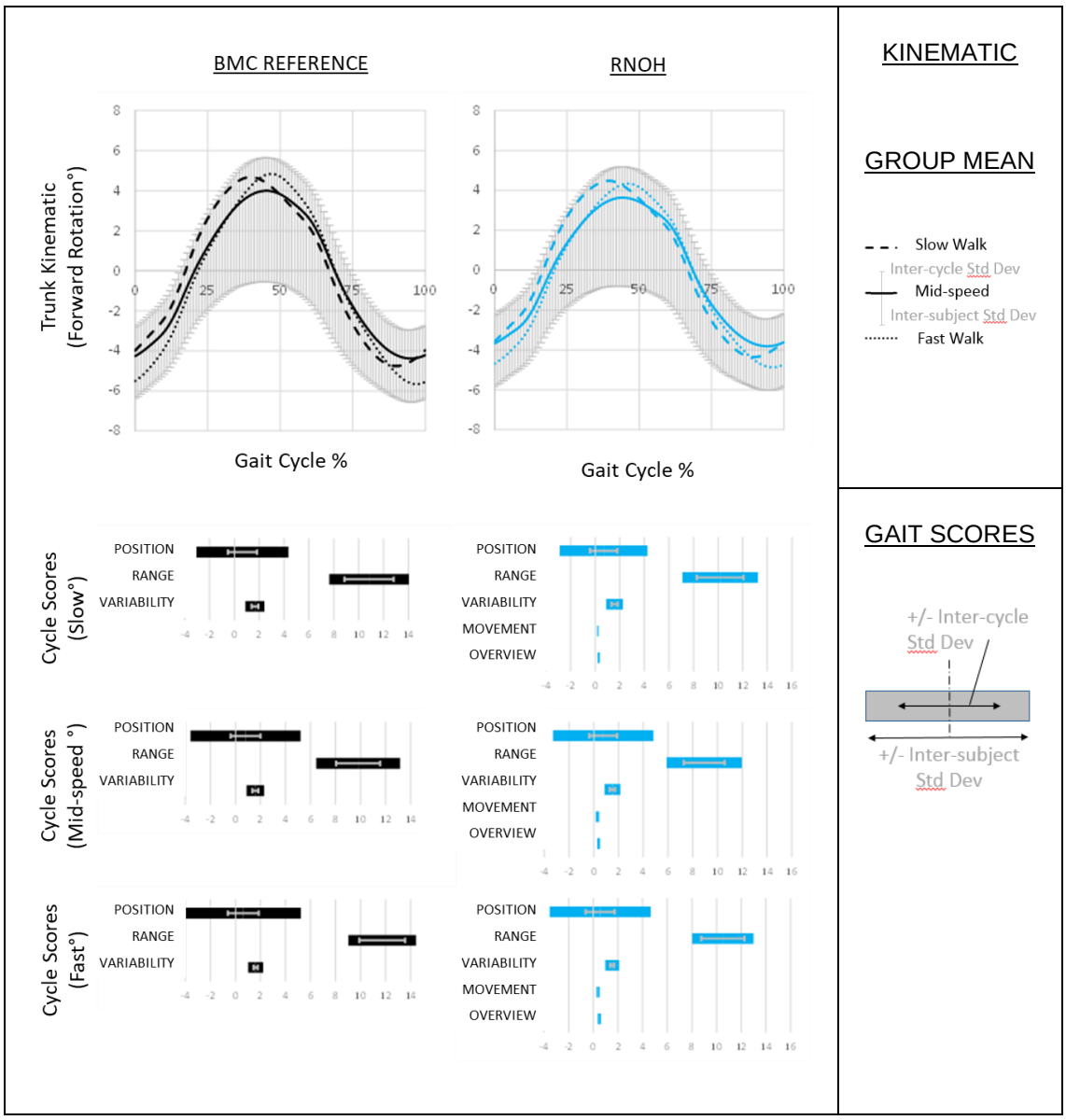

Figure 3-5 Trunk Gait Scores RNOH Tracking Solution -Transverse

Transverse plane comparison of RNOH tracking solution (right column) with BMC reference (left column).

Top row shows graphical kinematic for slow (dashed line), mid-speed (solid line) and fast (dotted line) walking as depicted in the legend (right). The mid-speed typical inter-cycle, and inter-subject standard deviations are shown above and below the mid-speed graph line respectively.

Subsequent rows depict speed specific gait scores as per the legend (right bottom). Cycle position, range and variability scores represent absolute values from zero. Movement pattern and overview scores measure the difference between comparative and BMC reference values.

The next section employs the same format to show the CGM comparison to the BMC solution.

3.3.5.2 CGM Tracking Solution

The CGM_Trunk sagittal comparison is shown in figure 3-6.

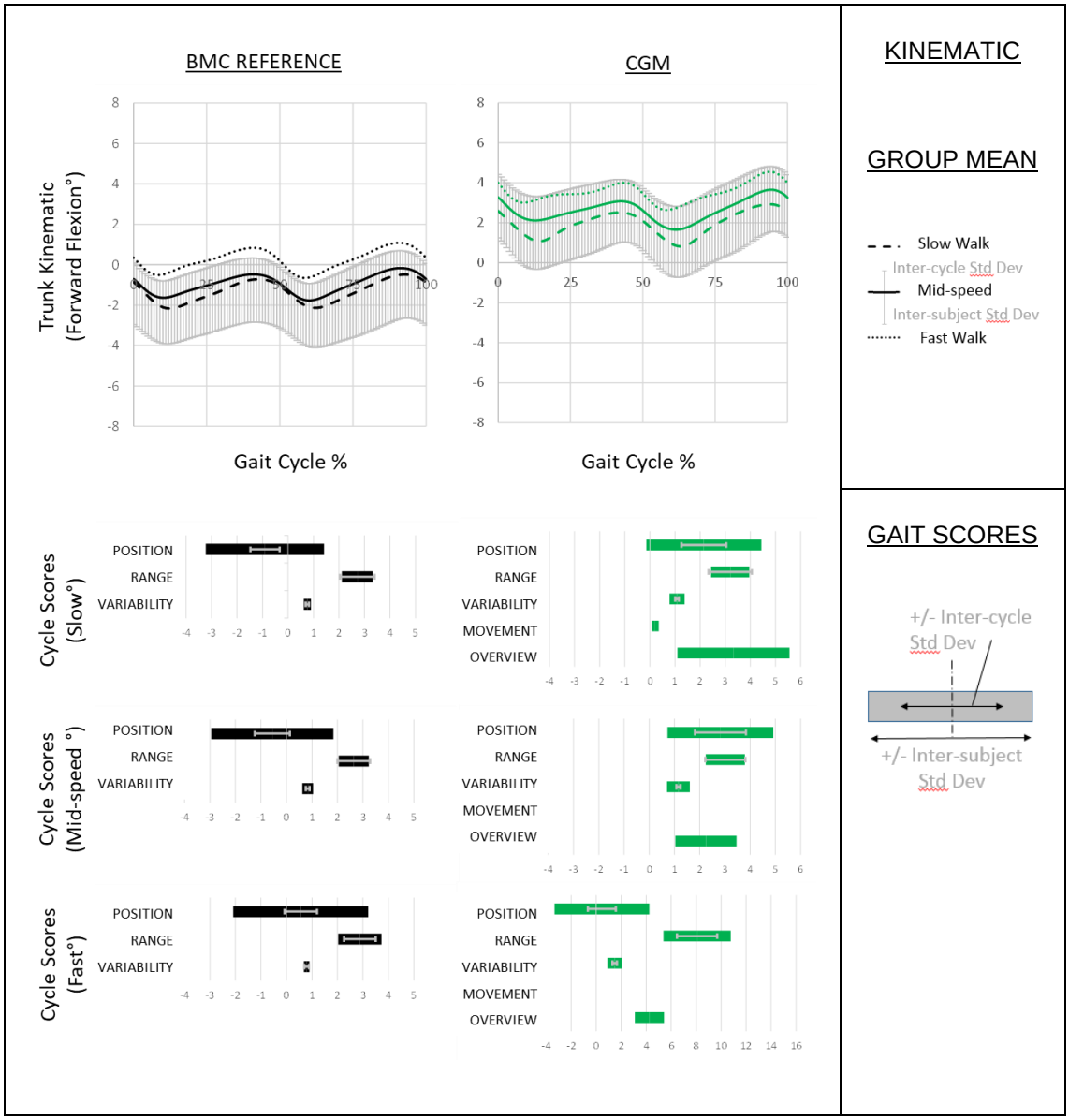

Figure 3-6 Trunk Gait Scores CGM Tracking Solution -Sagittal

Sagittal plane comparison of CGM tracking solution (right column) with BMC reference (left column).

Top row shows graphical kinematic for slow (dashed line), mid-speed (solid line) and fast (dotted line) walking as depicted in the legend (right). The mid-speed typical inter-cycle, and inter-subject standard deviations are shown above and below the mid-speed graph line respectively.

Subsequent rows depict speed specific gait scores as per the legend (right bottom). Cycle position, range and variability scores represent absolute values from zero. Movement pattern and overview scores measure the difference between comparative and BMC reference values.

Figure 3-7 shows the CGM coronal comparison to BMC reference values.

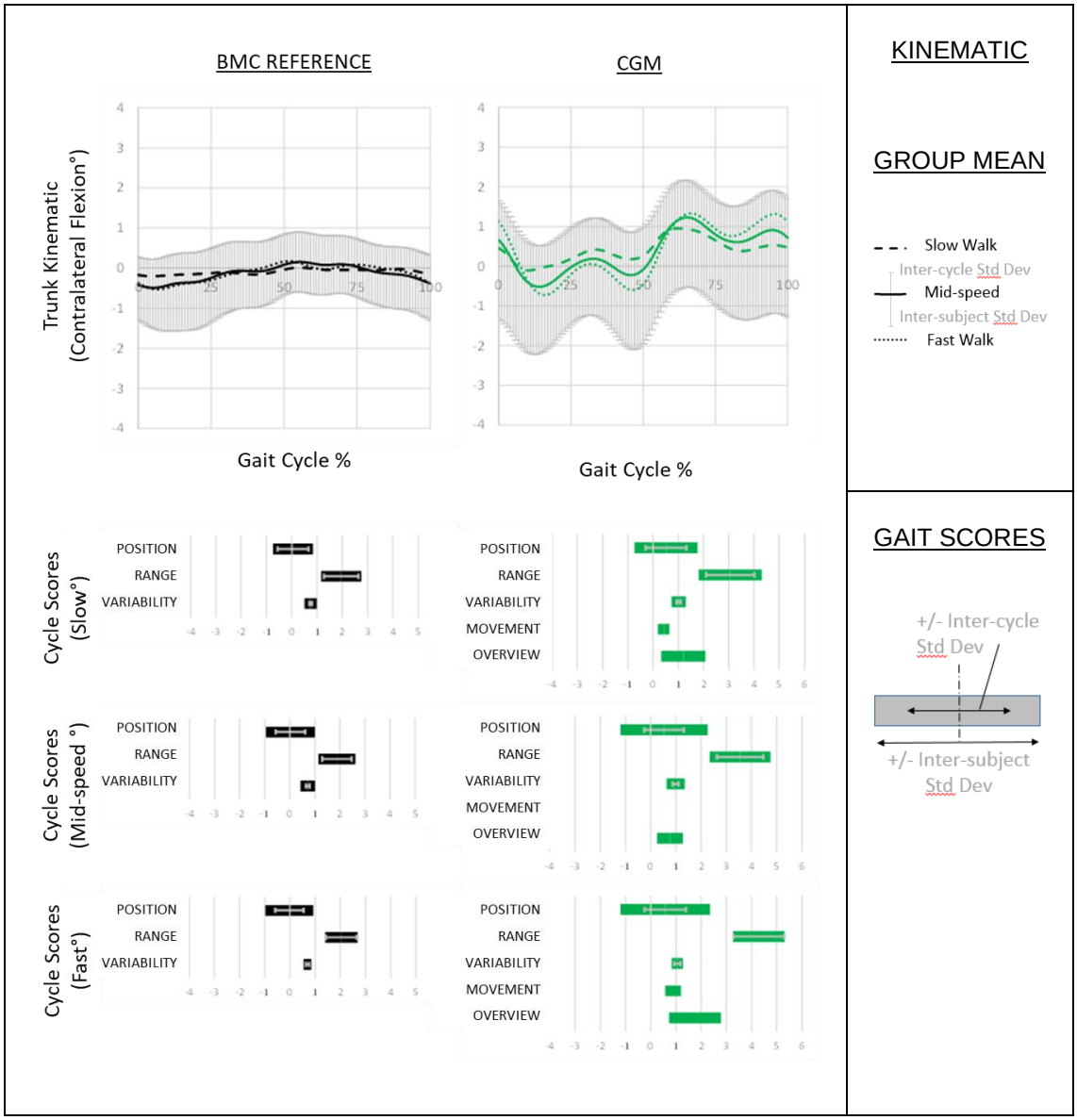

Figure 3-7 Trunk Gait Scores CGM Tracking Solution -Coronal

Coronal plane comparison of CGM tracking solution (right column) with BMC reference (left column).

Top row shows graphical kinematic for slow (dashed line), mid-speed (solid line) and fast (dotted line) walking as depicted in the legend (right). The mid-speed typical inter-cycle, and inter-subject standard deviations are shown above and below the mid-speed graph line respectively.

Subsequent rows depict speed specific gait scores as per the legend (right bottom). Cycle position, range and variability scores represent absolute values from zero. Movement pattern and overview scores measure the difference between comparative and BMC reference values.

Finally again, the transverse plane CGM kinematic is outlined in figure 3-8.

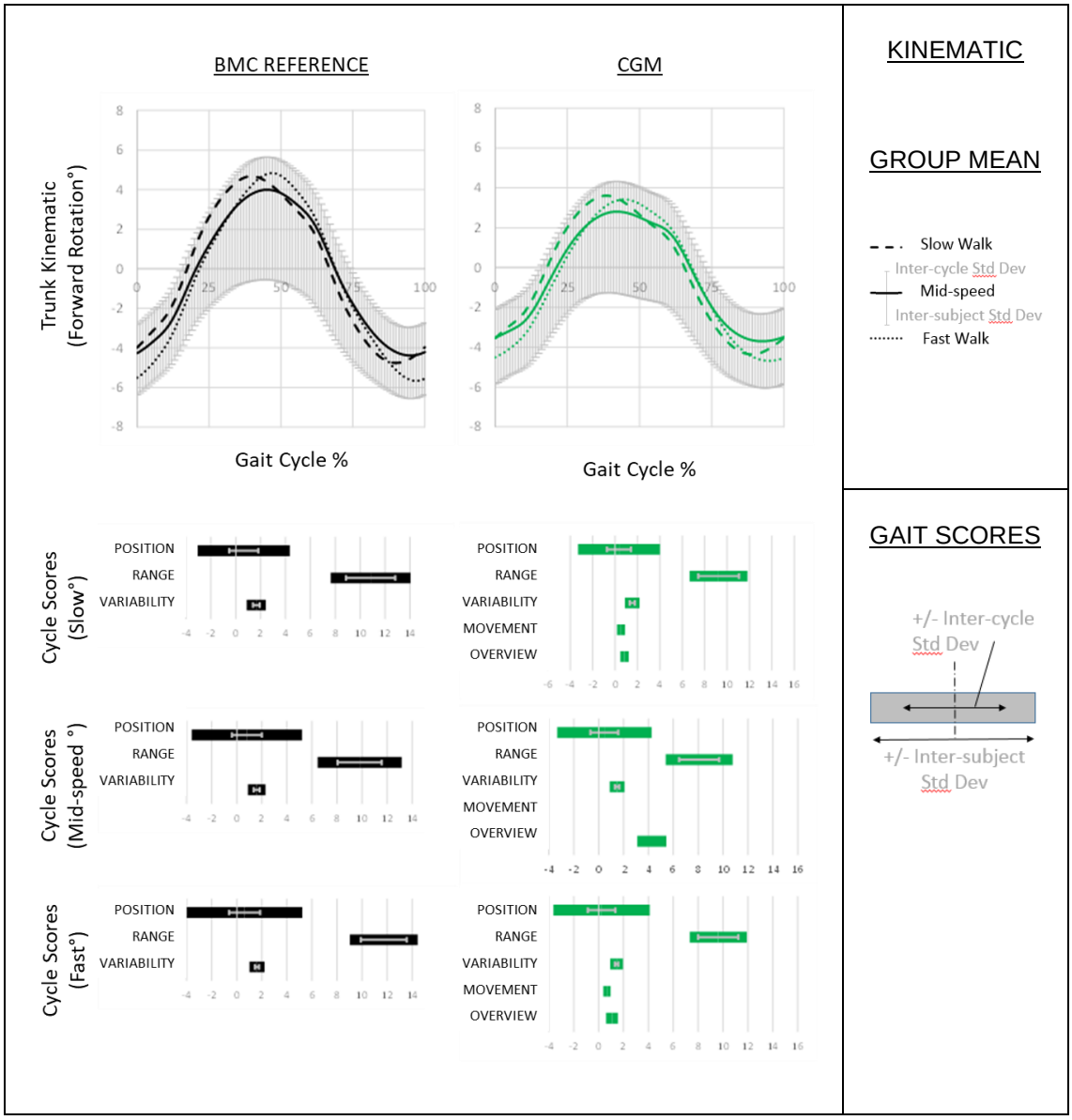

Figure 3-8 Trunk Gait Scores CGM Tracking Solution -Transverse

Transverse plane comparison of CGM tracking solution (right column) with BMC reference (left column).

Top row shows graphical kinematic for slow (dashed line), mid-speed (solid line) and fast (dotted line) walking as depicted in the legend (right). The mid-speed typical inter-cycle, and inter-subject standard deviations are shown above and below the mid-speed graph line respectively.

Subsequent rows depict speed specific gait scores as per the legend (right bottom). Cycle position, range and variability scores represent absolute values from zero. Movement pattern and overview scores measure the difference between comparative and BMC reference values.

3.3.5.3 BMI Effects

Sensitivity of the BMC sagittal plane range to subject BMI, also noted in chapter 2, is maintained by the RNOH modification (Table 3-3). This effect is therefore likely connected to inclusion of the common shoulder-line in both solutions. It remains unclear if this is a genuine effect or secondary to increased measurement error in subjects with higher BMI. The only slightly smaller correlations seen with the CGM solution, which does not include the shoulder-line, is consistent with there being a genuine element. At the fast-walking speed, when STA effects are expected to be maximal, the CGM solution appears susceptible to a change in movement pattern score in the sagittal plane, whereas the RNOH solution is most susceptible in the coronal plane movement pattern.

Table 3-3 Gait score correlations with individual subject BMI values.

Sagittal

	Position			Range			Variability		
	Slow	MidSpeed	Fast	Slow	MidSpeed	Fast	Slow	MidSpeed	Fast
BMC	-0.05	-0.02	0.08	-0.67	-0.59	-0.62	0.15	-0.13	0.14
CGM	-0.20	-0.24	-0.14	-0.54	-0.44	-0.47	-0.08	-0.27	-0.02
RNOH	-0.24	-0.20	-0.06	-0.62	-0.52	-0.60	0.13	-0.18	-0.19

	Movement			Overview		
	Slow	MidSpeed	Fast	Slow	MidSpeed	Fast
CGM	-0.43	-0.24	-0.59	-0.16	-0.19	-0.26
RNOH	0.07	0.41	0.48	-0.21	-0.07	0.04

Coronal

	Position			Range			Variability		
	Slow	MidSpeed	Fast	Slow	MidSpeed	Fast	Slow	MidSpeed	Fast
BMC	0.11	0.19	0.29	-0.08	0.03	0.02	0.22	-0.04	0.21
CGM	0.13	0.22	0.18	0.02	0.43	0.28	0.15	-0.08	0.17
RNOH	0.11	0.18	0.26	0.27	0.57	0.46	0.27	0.05	0.33

	Movement			Overview		
	Slow	MidSpeed	Fast	Slow	MidSpeed	Fast
CGM	-0.20	0.39	0.20	0.09	0.23	0.17
RNOH	0.33	0.70	0.57	0.33	0.64	0.48

Transverse

	Position			Range			Variability		
	Slow	MidSpeed	Fast	Slow	MidSpeed	Fast	Slow	MidSpeed	Fast
BMC	0.38	0.31	0.41	-0.19	0.08	0.23	0.10	-0.22	0.19
CGM	0.30	0.19	0.28	-0.37	-0.13	-0.05	0.08	-0.31	0.14
RNOH	0.37	0.30	0.39	-0.24	0.02	0.13	0.07	-0.25	0.17

	Movement			Overview		
	Slow	MidSpeed	Fast	Slow	MidSpeed	Fast
CGM	0.11	0.36	0.21	0.50	0.35	0.03
RNOH	0.19	0.52	0.41	0.05	0.50	0.36

3.3.5.4 Hypothesis Testing

The RNOH_Trunk tracking modification to the BMC reference created the expected decrease in the measured transverse plane range, and a similar increase in the coronal plane range (Table 3-2).

Table 3-1 Gait scores for the RNOH trunk kinematic

	Position (°)			Range (°)			Variability (°)		
	Sagittal	Coronal	Transverse	Sagittal	Coronal	Transverse	Sagittal	Coronal	Transverse
SLOW	-0.41	0.14	0.11	0.25	0.76	-0.67	0.07	0.14	-0.07
p-value	0.234	0.265	0.031	0.001	0.001	0.000	0.000	0.000	0.017
MIDSPEED	-0.51	0.18	0.11	0.15	1.08	-0.89	0.05	0.13	-0.08
p-value	0.162	0.215	0.048	0.020	0.003	0.000	0.001	0.000	0.003
FAST	-0.67	0.15	0.14	0.19	1.79	-1.23	0.05	0.16	-0.08
p-value	0.068	0.328	0.019	0.058	0.000	0.000	0.009	0.000	0.001

	Movement (°)			Overview (°)		
	Sagittal	Coronal	Transverse	Sagittal	Coronal	Transverse
SLOW	0.11	0.40	0.22	1.06	0.61	0.30
MIDSPEED	0.11	0.61	0.31	1.12	0.86	0.40
FAST	0.18	0.83	0.39	1.19	1.14	0.50

Other statistically significant differences were all less than 1° in magnitude. Visual comparison of the sagittal (Figure 3-3), coronal (Figure 3-4) and transverse (Figure 3-5) planar kinematics do not reveal any other structure differences between the two solutions. The primary hypothesis for this chapter (Hypothesis 3A_I) is therefore accepted.

The CGM solution, which tracks the thorax sub-region only, sees even greater decreases in the transverse plane range and increase in the coronal plane range (Table 3-3). This structural similarity between the RNOH_Trunk and CGM_Trunk gait scores, is consistent with the transverse plane rotation of the shoulder line above the CGM solution being partially countered by rotation of the lumber spine below the CGM solution. Overall, the CGM mid-segment tracking provides a reasonable representation of the whole. The secondary hypothesis for this chapter (Hypothesis 3A_II) is therefore also accepted.

Table 3-2 Gait scores for the CGM trunk tracking

	Position (°)			Range (°)			Variability (°)		
	Sagittal	Coronal	Transverse	Sagittal	Coronal	Transverse	Sagittal	Coronal	Transverse
SLOW	3.28	0.49	-0.32	0.48	1.10	-1.60	0.32	0.27	-0.12
p-value	0.000	0.223	0.052	0.002	0.000	0.001	0.000	0.000	0.022
MIDSPEED	3.59	0.50	-0.23	0.38	1.66	-1.73	0.33	0.27	-0.10
p-value	0.000	0.286	0.190	0.018	0.000	0.001	0.005	0.000	0.044
FAST	3.28	0.56	-0.21	0.25	2.25	-2.12	0.27	0.35	-0.17
p-value	0.001	0.249	0.369	0.173	0.000	0.000	0.007	0.000	0.001

	Movement (°)			Overview (°)		
	Sagittal	Coronal	Transverse	Sagittal	Coronal	Transverse
SLOW	0.21	0.42	0.53	3.33	1.20	0.84
MIDSPEED	0.25	0.56	0.59	3.69	1.43	0.91
FAST	0.33	0.89	0.68	3.40	1.76	1.08

In addition to these effects, the CGM solution measures a significant increase in the average forward flexed position of the segment at all walking speeds.

3.4 Discussion

The opening decision to represent the known flexible trunk, as single rigid segment, largely moots any sensible discussion about model construct validity. The underlying non-rigidity will cause all sub-regions to move differently, and this is likely a major contributor to differences seen between different tracking solutions. In this regard, validity may be inferred on different model outputs by carefully labelling to reflect the sub-region they represent.

For the CGM solution the trunk output is typically labelled as the thorax, which correctly reflects placement of the TRF tracking markers. This, however, is not the only requirement in making model outputs intelligible. If the orientation of this segment is reported with respect to the proximal pelvis segment for example, it becomes unclear if the orientation angle originates from movements of the lumbar spine, between the two segments, or movement/deformation of the thoracic spine, within the thorax. It is similarly difficult to interpret the thoracic orientation if it is reported with respect to the laboratory frame – as it commonly is.

The RNOH_Trunk overcomes this ambiguity, by inclusion of the lumber spine region, together with the thorax, in a single trunk segment. The segment is also extended distally to include the shoulder line. In this way the output is able to describe the orientation of the shoulder-line with respect to the pelvis. Use of the

label ‘trunk’ then infers validity on the model output by not suggesting the ability to distinguish between different regions of truncal movement that achieve this (Hulleman et al., 2010).

From the above analysis, it may seem that face validity enjoyed by the RNOH solution might be inferred on the CGM solution, simply by relabelling the output segment as the trunk, and defining this segment as the combination of lumber and thoracic segments excluding the shoulder line. The modelled segment would then appear to form a continuous chain with the proximal pelvis segment. Despite this appearance however, failure of the TRF to span the newly defined anatomical extent, would inevitably lead to a discrepancy between TRF and ARF alignment as the non-rigid segment moves away from the calibration posture in which they were synchronised. This effect is evident in the sagittal plane average cycle position of the CGM solution (Table 3-3) and reflects an inability of the CGM thoracic markers to truly represent movement originating over the entire trunk segment.

Multiple articulations within the trunk segment, together with normal STA effects, makes kinematic of this segment complex. The proposed RNOH_Thorax solution bypasses this complexity, by not attempting to account for inter-segment deformations; flexibility of the segments is thereby well modelled through the flexibility of the TRF solution itself. Additional benefits of this holistic approach, includes the incorporation of a clinically meaningful neutral orientation into the model and the requirement for just two segment specific, easily placed markers at the tips of each shoulder.

4 Chapter 4 – The Pelvis

4.1 Introduction

This chapter investigates modelling orientation of the pelvis at the proximal start of the lower limb kinematic chains.

4.1.1 Pelvic Orientation is expressed with respect to a Laboratory Frame

The principal plane of the pelvis is defined by the left and right ASIS locations anteriorly, and a mid-PSIS location posteriorly. International Society of Biomechanics (ISB) recommendations promote translation of this plane postero-inferiorly such that the principal-axis coincides with HJC locations; (Wu et al., 2002). In keeping with clinical terminology, pelvic orientation is described with respect to a global laboratory frame. Rotation around the medio-laterally oriented principal axis is termed pelvic tilt; anterior tilt drops the anterior of the pelvis and is signed as the positive direction (Figure 4-1). Rotation around the antero-posterior axis, which divides the segment into left and right halves, is termed pelvic obliquity. Lifting one side of the pelvis necessitates dropping of the opposite side; specification of obliquity therefore includes the pelvic side with the lifting direction signed as positive. Similarly, rotation around the mutually perpendicular vertical axis, termed *pelvic-rotation*, requires specification of the left or right side; here the forward direction is signed as positive.

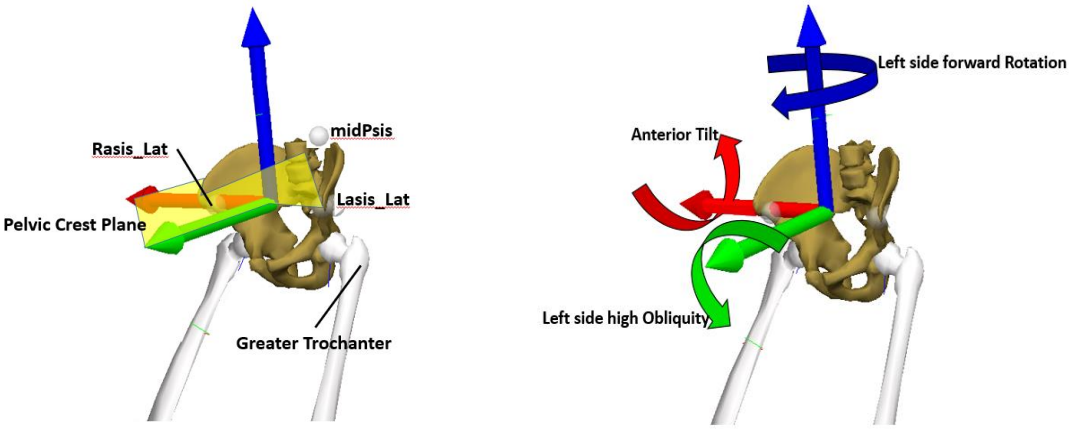

Figure 4-1 Pelvic ARF

The left diagram shows the pelvic crest plane defined by left (Lasis_Lat) and right (Rasis_Lat) anterior ASIS markers and a posterior mid PSIS location (midPsis). The horizontal axis of the ARF are orientated to this plane. Terminology used to describe positive directions of pelvic orientation from neutral is depicted on the right diagram.

4.1.2 Hip Joint Centre Locations may be estimated from Surface Landmarks

Representation of the HJC locations deep within the pelvis by surface markers is non-trivial. The only available bony landmark from the distal thigh segment is the greater trochanter at the lateral end of the femoral neck. This location is a poor predictor of the femoral head location at the medial end, as the orientation and length of the femoral neck is known to vary with age (Kong et al., 2018), sex (Braten et al., 1992) and pathology (Davids et al., 2003). The HJC location must therefore be modelled with respect to the proximal pelvic plane defined by available ASIS and PSIS surface marker locations.

The two originating CGM publications employed different regression equations to estimate the HJC locations with respect to the pelvic crest plane, defined by surface marker locations. The variant from the Helen Hayes hospital in New York (Kadaba et al., 1990) employed a simple solution that derived lateral, posterior and inferior offsets from a mid-ASIS origin as fractions of the ASIS separation distance. This regression equation was developed from measurements extracted from the X-ray images of 7 healthy adult male subjects (Bell et al., 1990). The other CGM variant (Davis et al., 1991) estimated the same offset quantities by a

more complex regression equation, which included terms for pelvic width and depth measurements and also the subject's leg length. This equation was based on 25 subjects and remains the default setting for Vicon's PiG implementation of the CGM. Other manufacturers, including the CODA system employed in the old RNOH gait laboratory, opted to implement the simpler Bell solution, which has since proven to be the more robust of the two solutions (Kiernan et al., 2015).

4.1.3 HJC Offsets from a mid-ASIS Location are Highly Correlated with Leg Length

More recently, both the Davis and Bell regression equations have been superseded by a new model (Harrington et al., 2007), which has proven more accurate (Mantovani et al., 2016, Fiorentino et al., 2016). The Harrington study presents two alternative equations with similar performance. The equations were derived from MRI images of 14 healthy children, and then validated across adults as well as children affected by cerebral palsy. The optimal equation included terms for pelvic width and depth in the lateral offset, pelvic depth only for the posterior offset and pelvic width and leg length for the inferior offset.

Table 4-1 Hip joint centre regression models

	Pelvic Width Multiple	Pelvic Depth Multiple	Leg Length Multiple	+ Constant (m)
Bell Regression Coefficients (Bell et al., 1990)				
Lateral	0.36	0	0	0
Posterior	0.19	0	0	0
Inferior	0.3	0	0	0
Harrington Simple Regression Coefficients (Harrington et al., 2007)				
Lateral	0.33	0	0	0.0073
Posterior	0	0.24	0	0.0099
Inferior	0.3	0	0	0.0109
Harrington Optimised Regression Coefficients (Harrington et al., 2007)				
Lateral	0.16	0.28	0	0.0079
Posterior	0	0.24	0	0.0099
Inferior	0.16	0	0.04	0.0071
Hara Regression Coefficients (Hara et al., 2016)				
Lateral	0	0	0.086	0.008
Posterior	0	0	0.063	-0.011
Inferior	0	0	0.078	0.009

Lateral posterior and inferior pelvic frame offsets from mid-ASIS location for 4 published regression equations.

Most recently it has emerged that the Harrington method can be closely replicated by a regression equation that employs leg length terms only for all three offset values (Hara et al., 2016). This comprehensive study was based on historic computer tomography images of cadavers from 27 children and 120 adults, all typically developing. The study further demonstrates that this simple leg length-based solution remained valid across all age ranges and both sexes. The Hara solution therefore appears to outperform other methods for both accuracy and simplicity in the typically developing population. Offset coefficients from all models are collated in table 4-1.

At first glance, it seems surprising that Hara's use of leg length is a better predictor of HJC location than pelvic dimensions. The female pelvis for example is generally wider than the male to facilitate child birth (Nwoha, 1995): how can a leg-length measurement alone account for this? Counterintuitively, this example illustrates a weakness of the pelvic-based solutions. Although the birth canal and measured ASIS width are wider in the female subject, smaller femoral heads result in a similar hip separation distance to the equivalent male pelvis (Warrener et al., 2015). This anatomical arrangement also facilitates an efficient gait pattern without the previously presumed need for increased abductor strength to hold the pelvis level during contralateral single support periods in females (Wittman and Wall, 2007). The leg length measure is able to bypass this complication by leveraging high correlations between the hip separation distance and leg length in both male and female subjects.

4.1.4 The Entire Pelvic Surface suffers Significant STA

Although numerous studies have attempted to address the general STA challenge (Camomilla et al., 2017b), there are few studies addressing STA around the pelvis. Invasive bone-pin and fluoroscopy studies have limited application here, as the segment shares visceral, central nervous system as well as locomotive functions. A single early bone-pin study indicated that pelvic STA is of a similar extent to that around the thigh, and that ASIS markers are more affected than PSIS (Rozumalski, 2008).

More recently, high speed dual fluoroscopy (dynamic X-ray) has also been used to track pelvic and thigh movement during walking in normal BMI subjects (Fiorentino et al., 2017). This research focussed on output of the hip joint rather than pelvis segment kinematics, but confirms that STA around the pelvis is generally less than that of the thigh segments. The most profound finding of the Fiorentino study, however, was that surface markers always *underestimate* true bone movement; supporting the notion that skin sliding is the primary STA component (Bonci et al., 2014). This finding suggests an under-appreciated mechanism whereby different tracking solutions may be rank ordered by their range scores.

4.1.5 Current Tracking Solutions fail to address the STA Issue present during Dynamic Gait

Comprehensive soft tissue cover, over the entire pelvic surface, makes accurate tracking of this segment particularly challenging. Accurate tracking of the pelvic bones by surface markers would therefore seem impossible. The commonly used CGM pelvis is no more evolved in this respect than the simplicity prioritised BMC solution. While the employed tracking markers give comprehensive cover of the ARF span, they are known to suffer significant movement related STA, particularly over the ASIS locations.

The alternative clinical approach of employing a CAST tracking cluster, avoids the most STA affected ASIS pelvic regions, using these markers just to define segment orientation during a static trial. One commonly applied tracking cluster design comprises the left and right PSIS markers with a centrally placed more inferior sacral marker. The resulting sacral cluster, approximating an equilateral triangle, has previously been shown to be more reliable than CGM tracking (Borhani et al., 2013). As ASIS locations are known to suffer more STA than PSIS, this solution may well be optimal within a paradigm of constraining tracking markers to the segment of interest. Others have advocated use of a lateral marker cluster over the iliac crest primarily to increase clinical utility (Liew et al., 2016, McClelland et al., 2010). While either of these sub-regions may reduce STA effects by avoidance of the ASIS regions, the generally high STA levels over the entire segment dictates that significant residual inaccuracies will remain.

4.2 Development of the RNOH_Pelvis model

4.2.1 Matching surface ASIS Identification to Bony Locations employed by HJC regression

In the majority of subjects, significant soft tissue cover naturally accumulates over the ASIS locations. This soft tissue prevents accurate representation of the true bony location expected by the HJC regression equation developed from skeletal imagery, by a single surface marker. Each bony location was therefore identified with both anterior and lateral markers, such that an internal intersection location could be specified (Figure 4-2). This *novel* technique facilitates specification of any pelvic asymmetry within the model, which can be significant even in the healthy population (Preece et al., 2008).

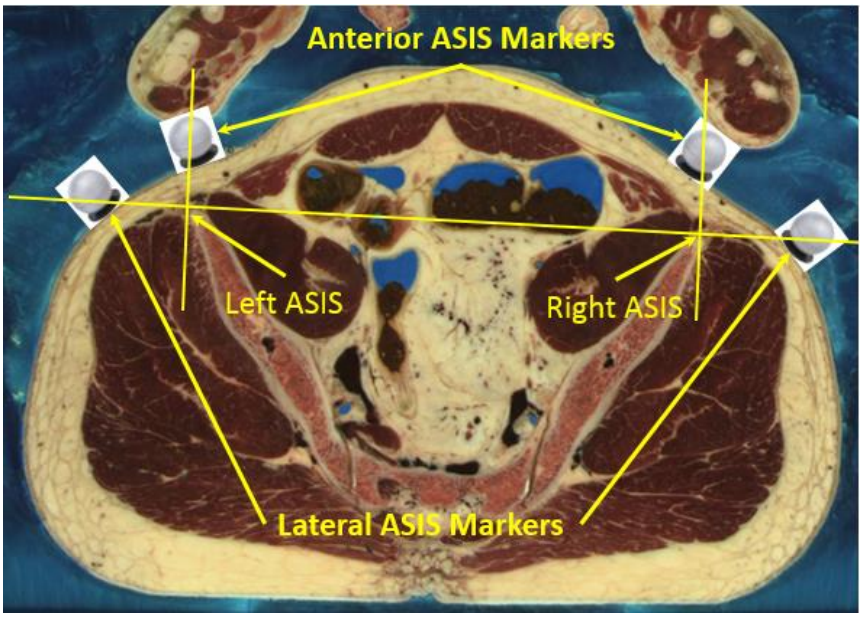

Figure 4-2 Transverse Pelvic Cross-section relating Surface Locations to Bony ASIS Landmarks

Image from the Visible Human Project – Male Data (Courtesy of the U.S. National Library of Medicine – this image may not reflect the most current/accurate data available).

The original image has been illustrated to show dual marker identification of true ASIS bony locations via anterior and lateral palpation.

4.2.2 Pseudo Dynamic Testing

Pseudo dynamic testing is a technique that involves spatial re-calibration of the ARF to the TRF at multiple static poses, in which inertial and muscle contraction

STA components are eliminated. This re-calibration is intended to account for any ARF-TRF mismatch during the motion caused by STA or other modelling errors. The required re-identification of bony landmarks between poses can however, be prone to significant intra-operator error (Della Croce et al., 1999). Despite this, the technique has been successfully employed at the pelvis to confirm the relative prevalence of pelvic skin sliding STA at ASIS locations (Hara et al., 2014).

The susceptibility of ASIS markers to STA was also highlighted in a study using the same multiple static calibration method but that also employed a complex MRI model of each subject's pelvis to better fit palpated landmarks to the underlying bones (Camomilla et al., 2017a). This study additionally found that modelled orientations of the pelvis are *less* affected by STA than that of the thigh segment. Although the accuracy of landmark identification was improved, the added complexity of the MRI imaging restricted this study to just five subjects, three within a normal BMI range, one overweight and one obese. A close look at their data does not demonstrate their implied progressive correlation between STA effects and BMI, but does find that the two high BMI subjects generally suffered more STA.

4.2.3 Development of a Pseudo Dynamic Gold Standard measure of Pelvic Obliquity

An experimental construct for a gold standard measure of pelvic obliquity is proposed. A pseudo-dynamic approach was employed to eliminate inertial and muscle contraction STA components, leaving just the primary skin sliding component active. Errors normally associated with re-identification of bony landmarks between static poses, are bypassed by tracking the required HJC locations that define the pelvic principal axis via the thigh segments. The remaining challenge was then to constrain experimental conditions such that skin sliding STA arising from the thigh segment was also eliminated. For this I reasoned that skin-sliding STA occurs when soft tissues slide over skeletal structures around moving joints. A proximal thigh tracking cluster would therefore be most susceptible to hip derived skin sliding. As hip movement was integral to the pelvic orientation under investigation, a distal thigh cluster was instead employed. Minimising STA effects on this cluster requires the knee to be held at a fixed angle. This was achieved by placing subjects in a kneeling posture with

vertical thigh segments. From this position, pelvic obliquity could be applied to the test subject, by simply lifting and blocking the left and right knees to different heights. Direct calculation of the applied obliquity angle from the differential height of the inserted blocks would be prone to errors caused by block compression and failure of the subject to keep their thigh segments absolutely vertical. These errors were avoided by instead calculating the differential height of left and right HJC locations tracked by the distal thigh marker clusters.

$$Applied\ Obliquity = \ \mathrm{asin}(RHJC_Z - LHJC_Z / Hip_{Width})$$

Equation 4.1

Calculation for gold standard obliquity orientation of pelvis principal axis during the static trials, where RHJC and LHJC are the co-ordinates of the proximal end of the right and left thigh segments. The Z subscripts denote the upward laboratory frame component.

The resulting measurement of the pelvis principal axis is completely independent of pelvic STA, as no pelvic markers are employed. The pseudo dynamic nature of the method also eliminates the possibility of either inertia or muscle contraction STA from the thigh. Skin sliding STA around the distal thigh HJC tracking clusters are minimised by the adoption of a static kneeling pose, with the knee fixed in approximately 90°of flexion. With all possible source of STA substantially mitigated by experimental constraints, this theoretic construct was assumed to act as a non-invasive gold standard measure of pelvic obliquity against alternative tracking solutions (Figure 4-3).

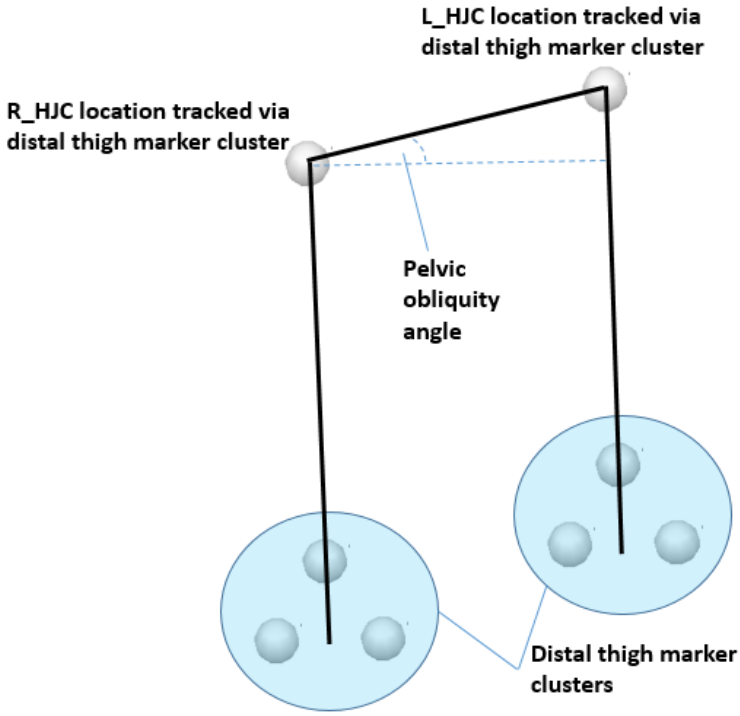

Figure 4-3 Gold standard measure of static pelvic obliquity

With knee fixed, tacking marker clusters over the distal thigh regions are assumed to suffer minimal STA due to skin sliding. Dynamic STA effects caused by inertia and muscle contraction are eliminated through the pseudo-dynamic experimental approach.

4.2.4 Kisho Fukuchi application of the HJC locations in the Pelvic tracking solution.

In an attempt to bypass STA from the pelvic surface, another study has also suggested using HJC locations tracked via the adjacent thigh segments as pelvic tracking locations (Kisho Fukuchi et al., 2010). With the principal axis of the segment defined between these points, only a single non-collinear pelvic marker was required to track the axial spin (anterior/posterior tilt) movement. This approach is relatively complex; each HJC requires 3 thigh-based surface markers to track its location. Further, as the thigh is generally more STA affected than the pelvis (Camomilla et al., 2017a) the solution remains highly susceptible to measurement error. In the typically developing cohort tested, the authors note differences between their kinematic and that of the CGM solution but recommend use of their model as a means of avoiding the ASIS locations. In addition to being particularly susceptible to STA affects, these markers are prone to camera view fallout as the upper limbs swing back and forth.

Examination of supplementary data included with the Kisho Fukuchi publication shows that the technique captured more range of motion than their comparative CGM data (Figure 4-4).

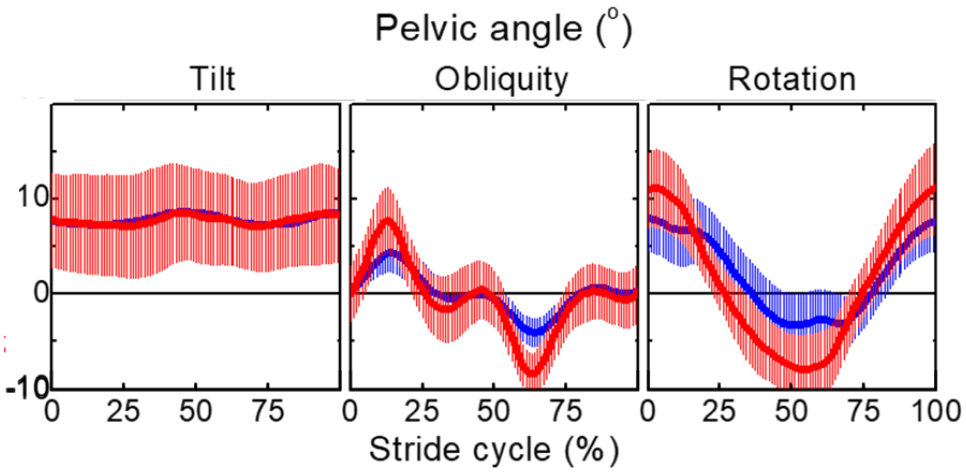

Figure 4-4 Supplementary material from Kisho Fukuchi et al. (2010)

Pelvic kinematic pattern for a tracking solution employing HJC locations tracked via thigh segments (red) and a standard CGM pelvic markers in (blue). The HJC tracking captures more obliquity and rotation range than CGM

In light of the more recent fluoroscopy finding that CGM always underestimates the true bony movement at the pelvis (Fiorentino et al., 2017), these findings might be reinterpreted as indicating the Kisho Fukuchi method as superior to CGM.

The thick covering of soft tissue over the proximal thigh region, makes it unlikely that a tracking marker cluster located in this region will reliably satisfy the criteria for low STA tracking of the HJC location. Relocation of the tracking cluster more distally, reduces the thickness of soft tissue cover, but also magnifies the effects of the inevitable angular orientation errors in establishing this target HJC locations. In this case, as thigh-based STA is known to have a predominant en bloc component along its longitudinal axis (Barre et al., 2017), the increased rotational and obliquity range may well have thigh STA as its source. Overall, the complexity of the Kisho Fukuchi tracking solution makes it unattractive for use in

a clinical setting, where maintaining interpretability of measured pathological gait patterns is key.

4.2.5 Development of the RNOH_Pelvis tracking solution.

As the HJC location may be tracked via the proximal pelvis segment, or the distal thigh, so too may the KJC location be tracked by either the thigh or the shank segment. As STA effect over the shank is relatively low, this provides a mechanism whereby the distal end of the thigh segment might be made available to a pelvic tracking solution at a low STA cost. The RNOH_Pelvis leverages this advantage by maintaining a fixed length between shank tracked KJC locations and interim pelvis tracked HJC locations. For this purpose, STA influences over the ASIS location are avoided by employing a CAST sacral tracking cluster. The resulting new HJC's are modelled at a fixed length along the KJC/interim-HJC vector, anchored to the KJC end. Identical to the Kisho Fukuchi method, the third pelvic tracking location, required to monitor axial spin of the inter-hip axis is then taken as the mid-PSIS location.

4.3 Experiment 4A - Pseudo Dynamic Validation of RNOH_Pelvis

4.3.1 Aim

This experiment aims to evaluate the BMC (CGM equivalent), CAST sacral marker cluster, and the RNOH_Pelvic tracking solutions against the developed, highly constrained, gold standard measure of pseudo-dynamic pelvic obliquity.

4.3.2 Hypothesis

Hypothesis 4A_I - The RNOH_Pelvis will capture more obliquity movement than either of the pelvic based tracking solutions, and thereby better match the gold standard measure.

4.3.3 Methods

4.3.3.1 Model Specification

The principal plane of the pelvis was anatomically defined by the right and left bony ASIS locations and the mid-point of left and right PSIS markers (Figure 4-

2). Each ASIS location was identified by a lateral (asis_Lat) and anterior (asis_Ant) marker as per the developed method (see Section 4.2.1). Posterior, lateral and downward offsets to estimate the hip joint centre (HJC) locations from the mid-ASIS point, were calculated using the Hara regression equation (Hara et al., 2016). A trio of additional surface markers were fixed over the left and right anterior distal thigh regions, to act as a gold standard tracking solution for the HJC locations of the respective thigh segments. Knee joint centre (KJC) locations, required by the RNOH-pelvis, were calculated as the mid-point of medial and lateral epicondyle surface marker locations. For this testing these locations did not require shank-based tracking, which would have been difficult to implement in the kneeling subject. Formal specifications of the employed models are outlined in table 4-2.

Table 4-2 Formal specification of pelvic biomechanical models employed in this section

PREFIX*	NAME	PLACEMENT / CALCULATION
Surface Markers		
L or R	asis_Ant	In common with BMC, over anterior aspect of pelvic ASIS bony landmark.
L or R	medEpi	In common with BMC, at centre of medial epicondyle bony prominence at the knee.
L or R	latEpi	In common with BMC, at centre of lateral epicondyle bony prominence at the knee.
L or R	asis_Lat	Over lateral aspect of pelvic ASIS bony landmark to define true inter-ASIS bony line.
L or R	psis	Over pelvic PSIS landmarks as an alternative to a single mid-PSIS BMC marker.
	Sacrum	A few cm below mid-PSIS location to form posterior CAST tracking cluster.
L or R	antThigh	Gold standard HJC tracking 1 of 3 - On anterior aspect of thigh a few cm above patella.
L or R	medThigh	Gold standard HJC tracking 2 of 3 - On antero-medial aspect of thigh a few cm above antThigh.
L or R	latThigh	Gold standard HJC tracking 3 of 3 - On antero-lateral aspect of thigh a few cm above antThigh.
Virtual Markers		
L or R	midEpi	In common with BMC, at mid-point of latEpi and medEpi surface markers.
L or R	asis_True	Projection of asis_Ant marker onto Lasis_Lat – Rasis_Lat line.
	midAsis	Mid-point of Lasis_True and Rasis_True.
L or R	hipHarr	Posterior, lateral and inferior offsets from midAsis provided by the Harrington regression equation (Harrington et al., 2007) during the initial neutral position test; this location tracked between tests by the Lpsis, Rpsis and Sacrum cluster.
L or R	hipGold	hipHarr location from initial neutral position test, tracked via antThigh, medThigh and latThigh marker cluster which are STA insulated by the experimental design.
L or R	_HJC	Proximal end of thigh Length vector from midEpi to hipHarr.
Subject Metrics		
L or R	thigh Length	Distance from midEpi to hipHarr established during the initial neutral position test.
Anatomical Reference Frame (ARF)		
	Pelvis (All versions)	Principal axis from Lasis_True to Rasis_True with midPsis defining principal transverse plane.
Technical Reference Frame (ARF)		
	Pelvis_Gold	LhipGold, RhipGold and midPSIS virtual marker location.
	Pelvis_CGM	Pelvic crest surface markers at Lasis_Ant, Lpsis, Rasis_Ant, and Rpsis.
	Pelvis_CAST	Posterior cluster consisting of Lpsis, Rpsis and Sacrum surface markers.
	Pelvis_RNOH	L_HJC, R_HJC and midPSIS virtual marker locations.
		**** L or R corresponds to left or right side respectively***

4.3.3.2 Test Subjects

Data was collected alongside the dynamic data and concurrently with the BMC reference data (presented in Chapter 2). One extra individual participated in this experiment, who did not contribute to the dynamic data. Results from this individual are identified as subject number ‘extra’ in the results table.

4.3.3.3 Data Collection

Each subject adopted an unimpeded kneeling posture. In this position, with the knee fixed, the KJC was assumed to be accurately tracked as the mid-point of the epicondyle surface markers. Six semi-rigid blocks 200mm * 300mm and 50mm thick (Yogamatter, UK) and a single unbranded swim float (25mm thick), were used to apply differential block heights under each knee during a series of 13 static kneeling pose positions, corresponding to 7 gross levels of applied pelvic obliquity (Figure 4-5).

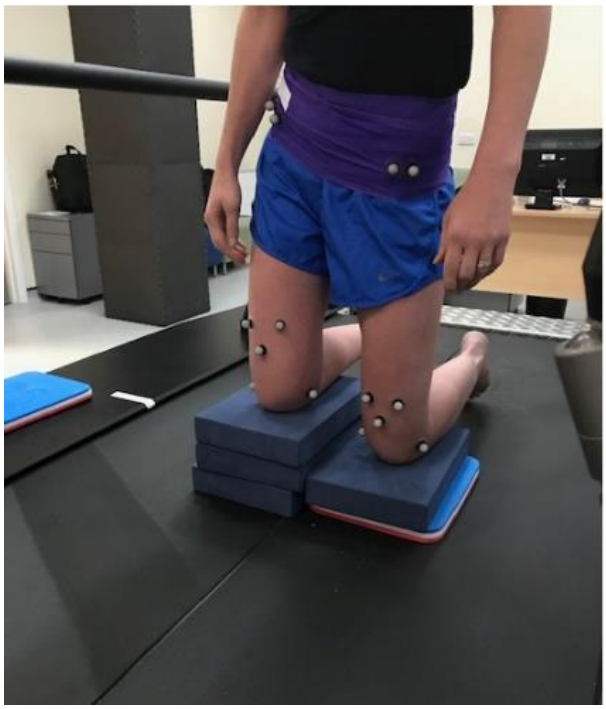

Figure 4-5 Experimental setup for the pseudo-dynamic Pelvic Trials

Pelvic obliquity was applied by application of differential block heights under each knee of an upright kneeling subject. With minimal knee movement, the distal thigh marker cluster, is assumed to accurately track the proximal HJC locations.

The initial test was with full 150mm block height under both knees. During this test the fixed KJC to HJC distance required by the RNOH_Pelvis solution for all tests was evaluated. The differential block heights were then adjusted in 25mm increments (Table 4-3).

Table 4-3 Obliquity condition for each pseudo-dynamic test

Test	1	2	3	4	5	6	7	8	9	10	11	12	13
Side	↔	R↓	R↓	R↓	R↓	R↓	↔	L↓	L↓	L↓	L↓	L↓	↔
mm	0	25	50	75	50	25	0	25	50	75	50	25	0

R↓=Right side down, ↔ = knees level, L↓=Left side down.

At each pose, mo-cap marker locations were recorded for a few seconds. Spotters to the left and right of the subject, then adjusted the block heights to the next required level and encouraged the subject to maintain the thighs as vertical as possible while the measurements were taken.

4.3.4 Data analysis

4.3.4.1 Signal processing

Three anatomically identical copies of the pelvis segment were modelled, each tracked by a different method. For the BMC (CGM equivalent) pelvis, a mid-PSIS plus left and right anterior ASIS markers were employed. The CAST pelvis was tracked via the two PSIS surface markers plus a sacrum marker. The resulting sacral cluster was also used to track the position of the interim HJC locations required by the RNOH tracking solution; corrected versions of the HJC locations which maintained a constant KJC-HJC separation distance, plus the mid-PSIS location, were employed to track the RNOH pelvis (Figure 4-6)

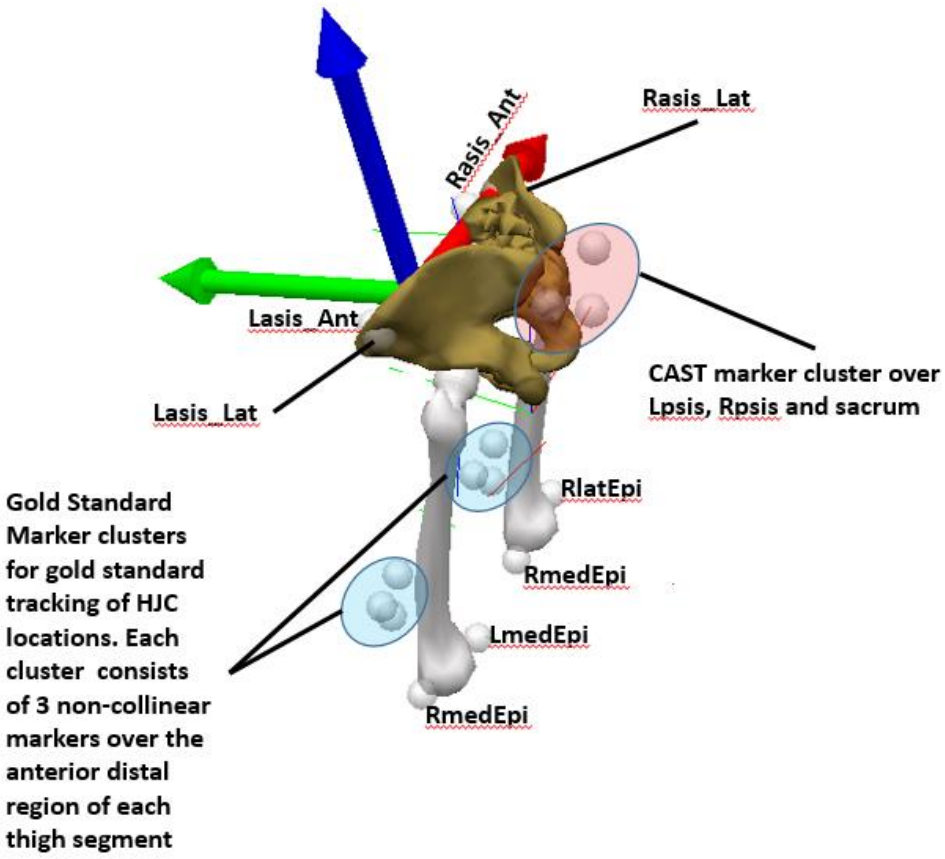

Figure 4-6 Pelvic obliquity tracking solutions employed by BMC, CAST and gold-standard tracking solutions

The BMC solution mimic that of CGM, employing a combination of ASIS and PSIS tracking markers. CAST avoids the ASIS locations by using the PSIS markers in combination with a centrally placed sacral marker. The gold standard measure employs distal thigh marker clusters to track HJC locations.

For each of the 13 obliquity conditions, the mean pelvic obliquity of each subject by each of the three tracking solutions were calculated. Using equation 4-1, the mean gold standard measure for each obliquity measure was also calculated.

4.3.4.2 Statistics

For each subject, obliquity calculated by each of the three tracking solutions was then plotted against this gold standard measure. Coefficients of regression were calculated to show the linearity of each solution against the gold standard; the gradient of these regression lines was interpreted as the accuracy (percentage

of applied obliquity captured) of each solution. Finally, outputs were investigated for correlation between subject BMI and the accuracy of each tracking solution.

4.3.5 Results

4.3.5.1 Obliquity Accuracy

Results are presented in table 4-4.

All three tracking solutions showed near perfect linearity (r>0.99) with the gold-standard measure. Gradient of these regression lines were interpreted as the accuracy of each solution. Correlation coefficients for individual subject accuracy against their BMI statistic were also calculated (Figure 4-7).

Table 4-4 Tabulated results from pseudo – dynamic obliquity test

		Test	Accuracy wrt Gold Standard (Fraction)		
BMI	**Subject**	**Range (°)**	**BMC/CGM**	**CAST**	**RNOH**
16.4	**1**	45.73	0.72	0.72	0.88
18.6	**2**	41.69	0.75	0.76	0.92
19.1	**3**	42.24	0.78	0.66	0.87
20.5	extra	44.57	0.73	0.71	0.97
22.2	**4**	45.02	0.75	0.69	0.91
23.3	**5**	39.84	0.76	0.75	0.93
23.5	**6**	32.77	0.99	0.89	1.12
23.9	**7**	38.42	0.75	0.73	0.91
24.9	**8**	43.58	0.72	0.66	0.90
25	**9**	39.99	0.76	0.69	0.86
25.6	**10**	41.38	0.62	0.71	0.89
26.4	**11**	43.48	0.82	0.74	0.91
26.9	**12**	43.06	0.69	0.62	0.69
Mean		41.67	0.76	0.72	0.90
Standard Deviation		3.43	0.08	0.06	0.09
r wrt BMI		-0.27	-0.02	-0.14	-0.21
r^2		0.07	0.00	0.02	0.05

Subject 6 exhibited an abnormally low range of applied obliquity angles, indicating a failure to keep the thigh segments vertical during the test. For this subject, the RNOH pelvis uncharacteristically overestimated the gold standard measure, while similar increases in accuracy for the CGM and CAST solutions made them

perform uncharacteristically very well. Except for this subject, the RNOH pelvis tracking solution was consistently closer to the gold standard measure than either CGM or CAST. Over all subjects, RNOH-pelvis accuracy (mean +/- standard deviation) averaged 90.4 +/- 9.1% in comparison to 76.3+/- 7.6% for CGM and 71.2 +/- 6.9% for CAST Figure 4-7.

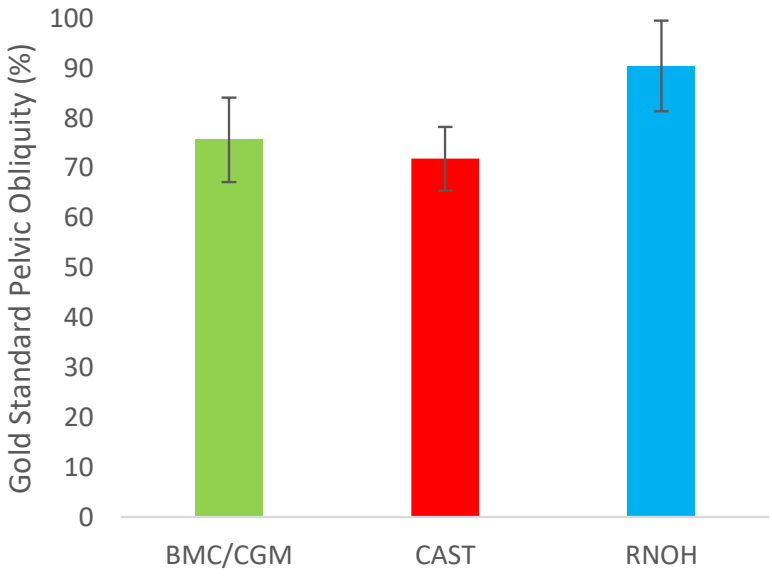

Figure 4-7 Mean obliquity error of three pelvic tracking solutions

Percentage of gold standard obliquity measure, captured by BMC, CAST and RNOH tracking solutions.

4.3.5.2 BMI Effects

No significant BMI effects were identified (Table 4-4). This suggests that dynamic STA components, not active during this testing, are most likely responsible for any BMI related segment tracking effects.

4.3.6 Hypothesis Testing

The primary hypothesis 4A_I, that the RNOH_Pelvis will capture more obliquity movement than either of the pelvic based tracking solutions, is accepted.

4.4 Experiment 4B – Dynamic Gait Trials

4.4.1 Aims

This experiment aims to evaluate the CAST, CGM and RNOH pelvic solutions against the BMC reference values established in chapter 2, during dynamic gait.

4.4.2 Hypothesis

Primary hypothesis 4B_I The RNOH_Pelvis solution will capture more coronal plane range than any of the other pelvic based tracking solutions.

Secondary hypothesis 4B_II The RNOH_Pelvis solution will demonstrate a similar pattern of movement to the other pelvis-based tracking solutions.

4.4.3 Methods

4.4.3.1 Model Specification

In order to facilitate the CAST solution, an additional tracking cluster was formed with markers at the left and right PSIS location, plus a centrally located sacral marker. The CGM tracking solution was directly represented by the BMC pelvic markers. For the RNOH_Pelvis, the required left and right KJC location were estimated at the mid-epicondyle points during a static calibration trial, and tracked via a low STA shank solution (Peters et al., 2009) as discussed in chapter 1. Full details of the model specification are outlined in table 4-5.

Table 4-5 Biomechanical model specification for dynamic testing of pelvic tracking solutions

PREFIX	NAME	PLACEMENT / CALCULATION
Surface markers		
L or R	asis_Ant	In common with BMC, over anterior aspect of pelvic ASIS bony landmark.
L or R	medEpi	In common with BMC, at centre of medial epicondyle bony prominence at the knee.
L or R	latEpi	In common with BMC, at centre of lateral epicondyle bony prominence at the knee.
L or R	medMal	In common with BMC, at centre of medial malleoli bony prominence at the ankle.
L or R	latMal	In common with BMC, at centre of lateral malleoli bony prominence at the ankle.
L or R	asis_Lat	Over lateral aspect of pelvic ASIS bony landmark to define true inter-ASIS bony line.
L or R	psis	Over pelvic PSIS landmarks as an alternative to a single mid-PSIS BMC marker.
	Sacrum	A few cm below mid-PSIS location to form posterior CAST tracking cluster.
L or R	fibHead	Low STA KJC tracking marker over fibular head bony landmark.
L or R	proxShin	Low STA KJC tracking marker on proximal anteromedial aspect of bony shin.
L or R	distShin	Low STA KJC tracking marker on distal anteromedial aspect of bony shin.
Virtual markers		
L or R	midEpi	In common with BMC, at mid-point of latEpi and medEpi surface markers.
L or R	asis_True	Projection of asis_Ant marker onto Lasis_Lat – Rasis_Lat line.
	midAsis	Mid-point of Lasis_True and Rasis_True.
L or R	hipHarr	Posterior, lateral and inferior offsets from midAsis provided by the Harrington regression equation (Harrington et al., 2007) during an initial static calibration; this location tracked via the Lpsis, Rpsis and Sacrum cluster.
L or R	_HJC	Proximal end of thigh_Length vector from midEpi to hipHarr.
L or R	_KJC	midEpi location from initial static calibration tracked via the fibHead, proxShin, distShin, medMal and latMal cluster.
Subject metrics		
L or R	Thigh_Length	Distance from midEpi to hipHarr established during the initial static calibration trial.
Model segments – anatomical orientation		
	Pelvis (All versions)	Principal axis from Lasis_True to Rasis_True with midPsis defining principal transverse plane.
Model segments – tracking solution (all tests)		
	Pelvis_CGM	Pelvic crest surface markers at Lasis_Ant, Lpsis, Rasis_Ant, and Rpsis.
	Pelvis_CAST	Posterior cluster consisting of Lpsis, Rpsis and Sacrum surface markers.
	Pelvis_RNOH	L_HJC, R_HJC and midPSIS virtual marker locations.

L or R corresponds to left or right side respectively

4.4.3.2 Laboratory Set-up

Data was collected concurrently with that for the BMC reference values presented in chapter 2.

4.4.3.3 Data Collection

Markers in addition to BMC requirements were applied with the subject in a seated posture Figure 4-8.

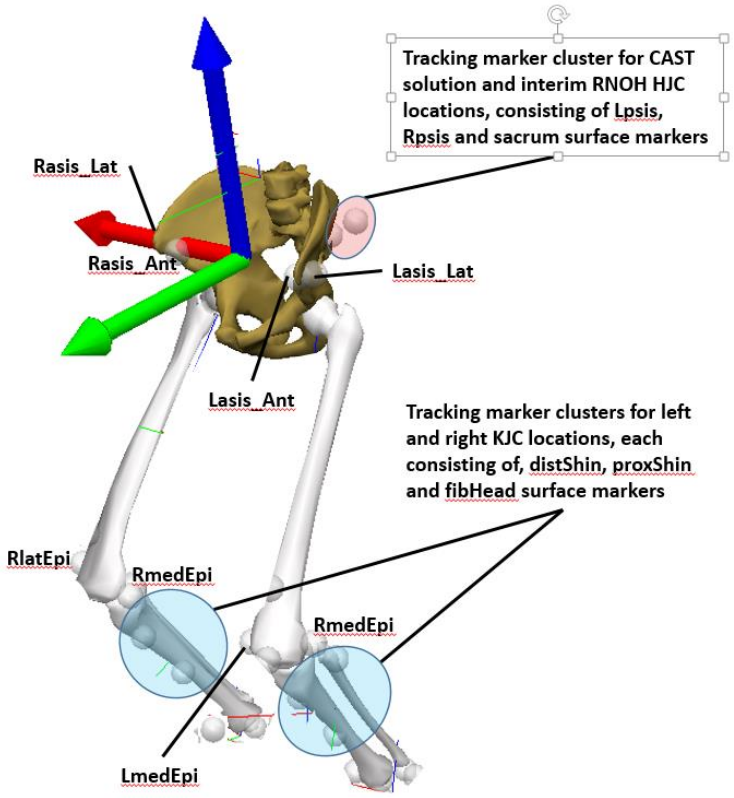

Figure 4-8 Surface marker employed during dynamic gait trial for pelvic tracking solution

BMC and CAST track the pelvis via different arrangements of pelvic surface markers. The CAST methods avoid the ASIS locations which are known to suffer high STA affects. The RNOH method tracks an interim HJC locations from the CAST tracking cluster and the KJC via shank tracking clusters. The actual HJC is then modelled along a line between the two, at a fixed distance from the KJC location.

Prior to dynamic testing, a calibration procedure was performed. HJC and KJC locations derived from surface marker locations, were related to location of markers forming pelvic and shank tracking clusters respectively. These clusters were located in the specified low STA regions, with the aim of improving the accuracy of joint centre tracking during the dynamic trials.

4.4.4 Data Analysis

4.4.4.1 Signal Processing

For each subject at each of the three walking speeds, the pelvic orientation from each of the three tracking solutions was calculated. Cardan angles for all pelvis solutions employed a rotation-obliquity-tilt sequence and were signed to make left side forward, left side high and anterior tilt positive. Force signals from the instrumented treadmill were used to identify left foot contact events. From this, all calculated signals were then divided into left gait cycles, defined between heel-strike events. Cycles were normalised to 101 time points. Finally mean cycle data for each tracking solution for all subjects were calculated, from which the metrics presented in the results section were extracted.

4.4.5 Statistics

For each tracking solution under investigation. Paired t-test were applied across all gait scores, in order to identify statistically significant differences with BMC reference values.

Correlation coefficients were calculated for each gait score, against subject BMI. Correlations above 0.5 (R2 > 0.25) are highlighted in the solution designated colour.

4.4.6 Results

4.4.6.1 CAST Tracking Solution

Figure 4-9 compares the sagittal kinematic from the CAST tracking solution, against the BMC reference.

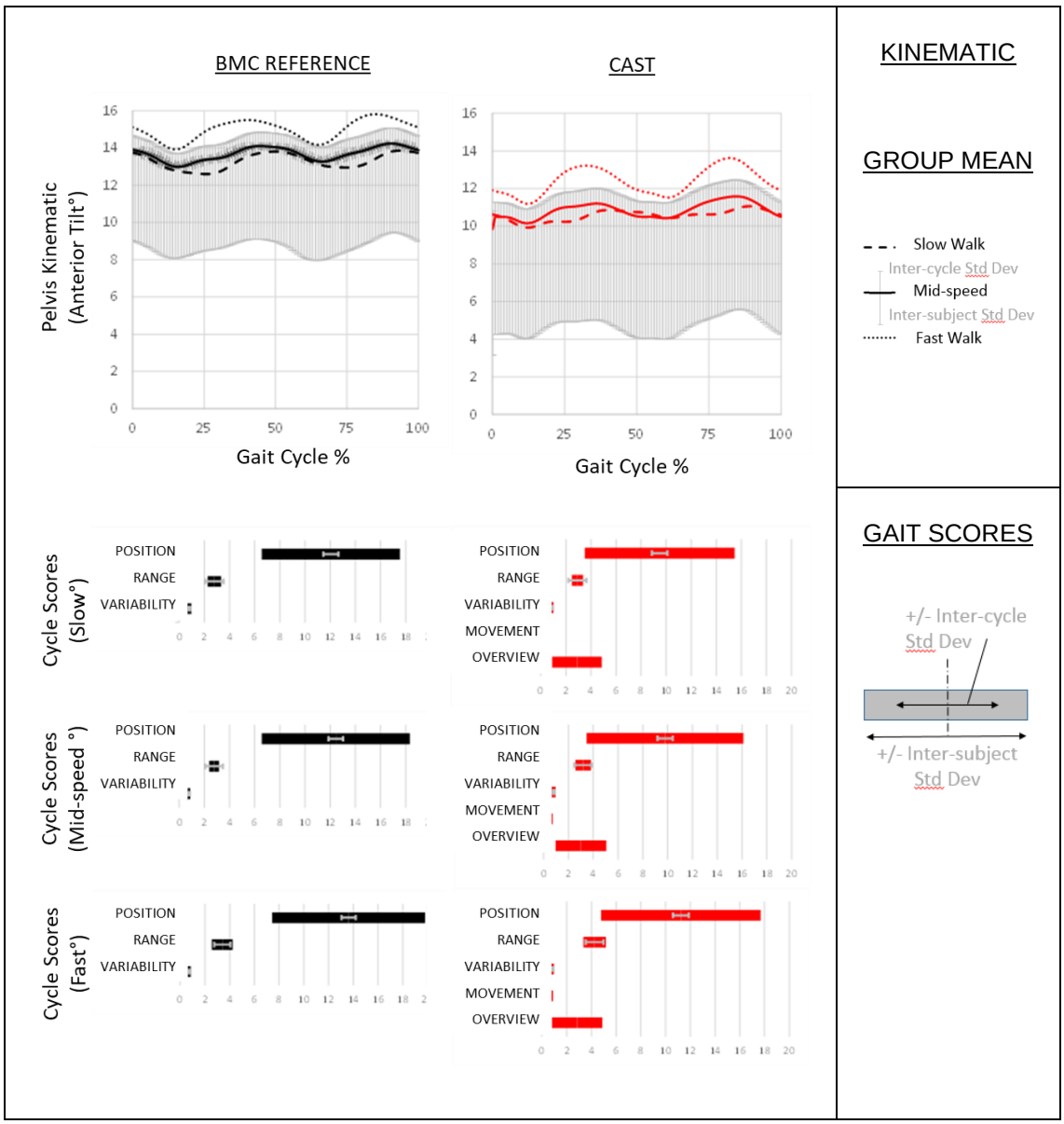

Figure 4-9 CAST tracking solution for pelvis - Sagittal

Sagittal plane comparison of CAST tracking solution (right column) with BMC reference (left column).

Top row shows graphical kinematic for slow (dashed line), mid-speed (solid line) and fast (dotted line) walking as depicted in the legend (right). The mid-speed typical inter-cycle, and inter-subject standard deviations are shown above and below the mid-speed graph line respectively.

Subsequent rows depict speed specific gait scores as per the legend (right bottom). Cycle position, range and variability scores represent absolute values from zero. Movement pattern and overview scores measure the difference between comparative and BMC reference values.

The largest sagittal difference appears to be a positional offset, with the CAST solution less anteriorly tilted. Figure 4-10, shows the coronal plane comparison.

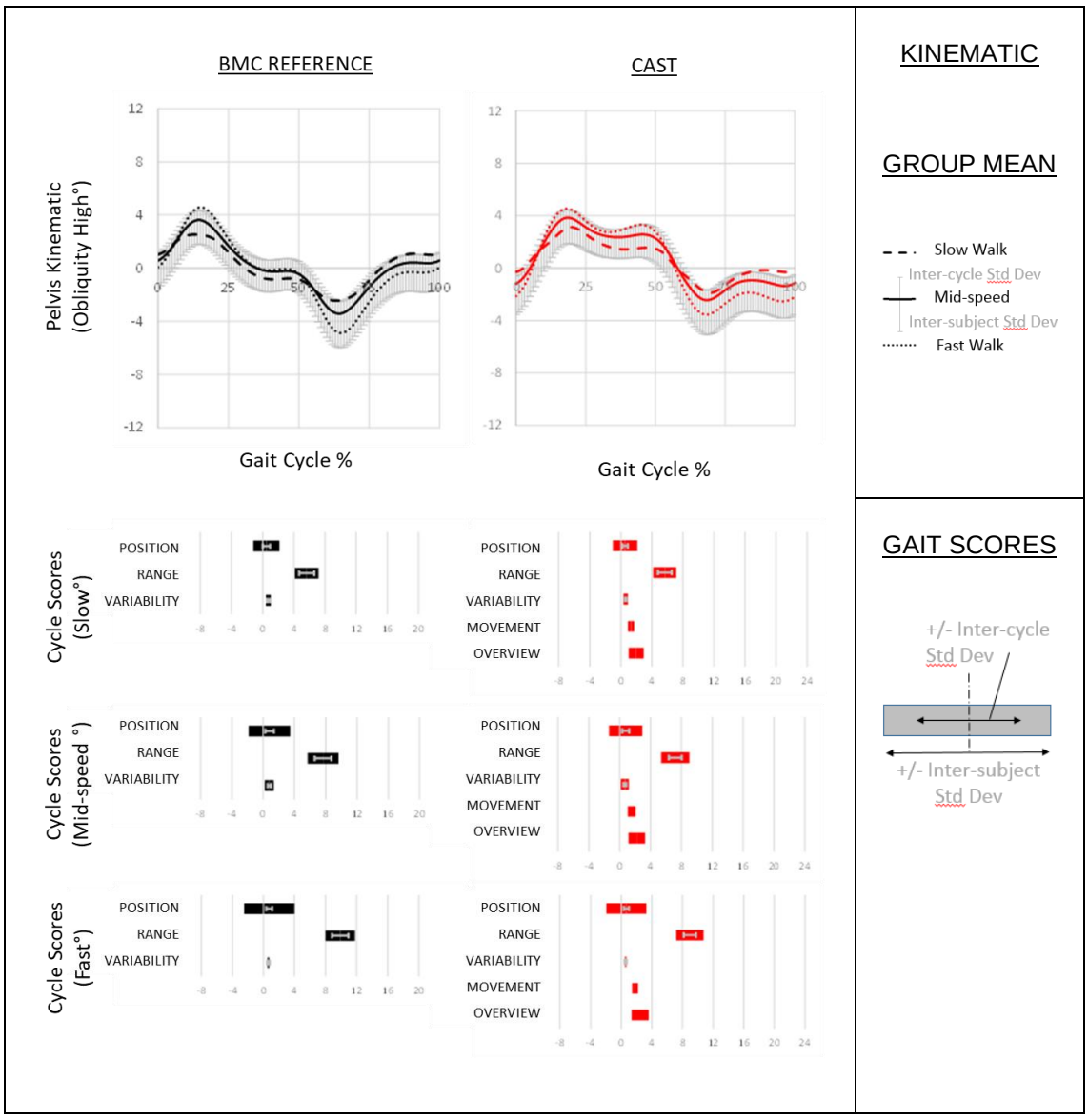

Figure 4-10 CAST tracking solution for pelvis - Coronal

Coronal plane comparison of CAST tracking solution (right column) with BMC reference (left column).

Top row shows graphical kinematic for slow (dashed line), mid-speed (solid line) and fast (dotted line) walking as depicted in the legend (right). The mid-speed typical inter-cycle, and inter-subject standard deviations are shown above and below the mid-speed graph line respectively.

Subsequent rows depict speed specific gait scores as per the legend (right bottom). Cycle position, range and variability scores represent absolute values from zero. Movement pattern and overview scores measure the difference between comparative and BMC reference values.

A mid-single-support plateau in the coronal obliquity of the CAST solution, is not evident in the BMC reference. Figure 4-11 shows the transverse plane comparison.

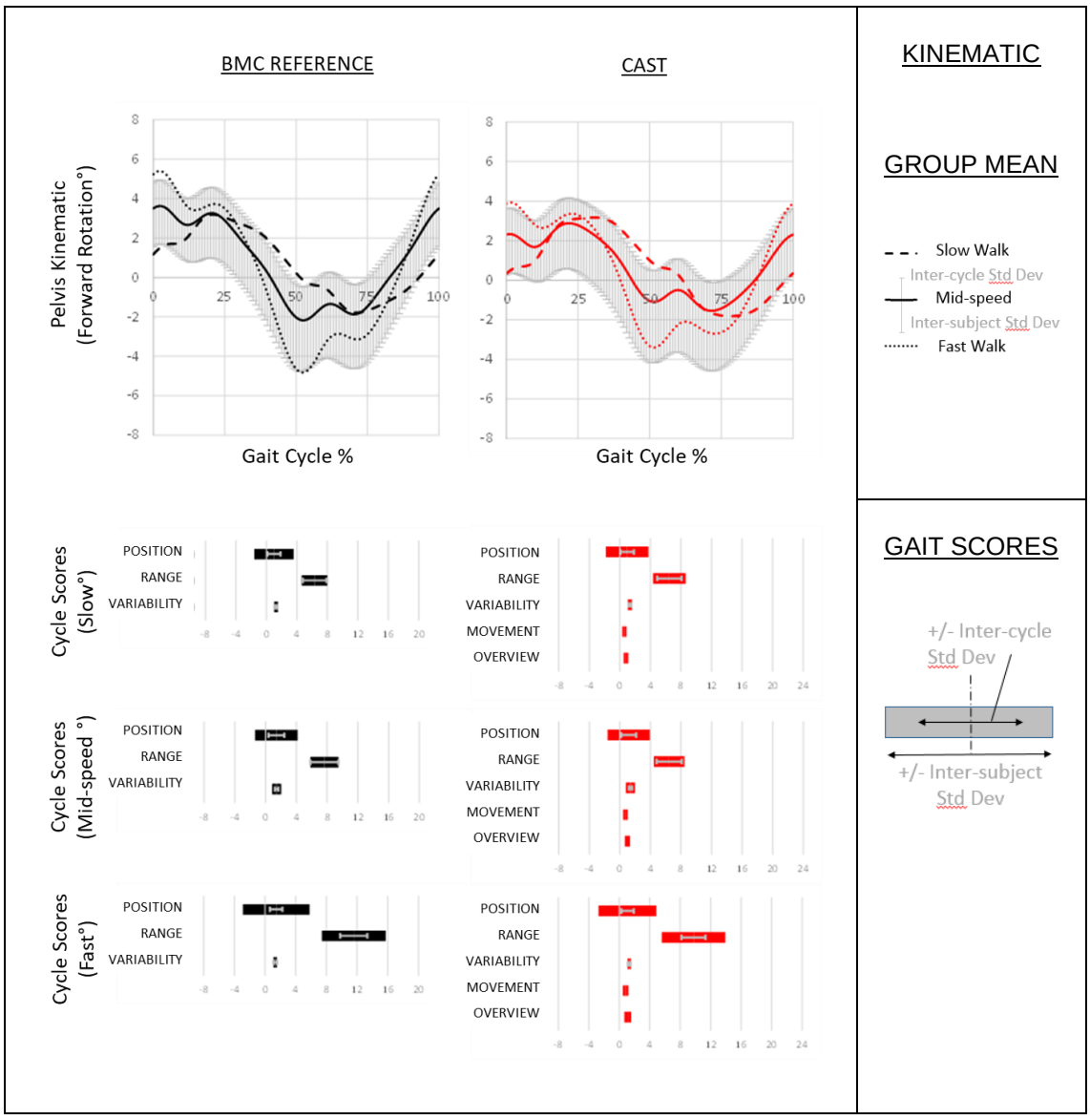

Figure 4-11 CAST tracking solution for pelvis - Transverse

Transverse plane comparison of CAST tracking solution (right column) with BMC reference (left column).

Top row shows graphical kinematic for slow (dashed line), mid-speed (solid line) and fast (dotted line) walking as depicted in the legend (right). The mid-speed typical inter-cycle, and inter-subject standard deviations are shown above and below the mid-speed graph line respectively.

Subsequent rows depict speed specific gait scores as per the legend (right bottom). Cycle position, range and variability scores represent absolute values from zero. Movement pattern and overview scores measure the difference between comparative and BMC reference values.

The CAST tracking causes an approximate 3° decrease in the average pelvic anterior tilt position at all walking speeds (Figure 4-9). This effect may have been caused by the prevalence of STA over the ASIS locations employed by the BMC, or amplification of tracking error of these locations over the separation distance to the sacral TRF employed by the CAST solution. As the difference in measured range and cycle variability between the two solutions are small and show no consistent direction in favour of one solution or the other, these scores confirm the visual impression that there is little to choose between the two solutions.

Sagittal, coronal and transverse plane RMS approximate 3°, 2° and 1° respectively. Proportionate difference in the movement pattern scores were most evident in the coronal kinematic. Visual inspection of the kinematic confirms a pattern difference during the single support and swing periods, with the BMC solutions showing a progressive decrease in obliquity during support and increase during swing, not evident in the CAST solution. Usefulness of this movement in contributing to foot clearance during swing suggest that it may be genuine, arguably tipping the balance of favouritism towards the BMC solution.

4.4.6.2 CGM Tracking Solution

Figure 4-12 compares the sagittal kinematic from the CGM tracking solution, against the BMC reference. These solutions only differ in their use of all 4 available pelvic bony landmarks (CGM solution), and the hip joint centre locations derived from this plane plus a mid-PSIS derived virtual marker (BMC solution).

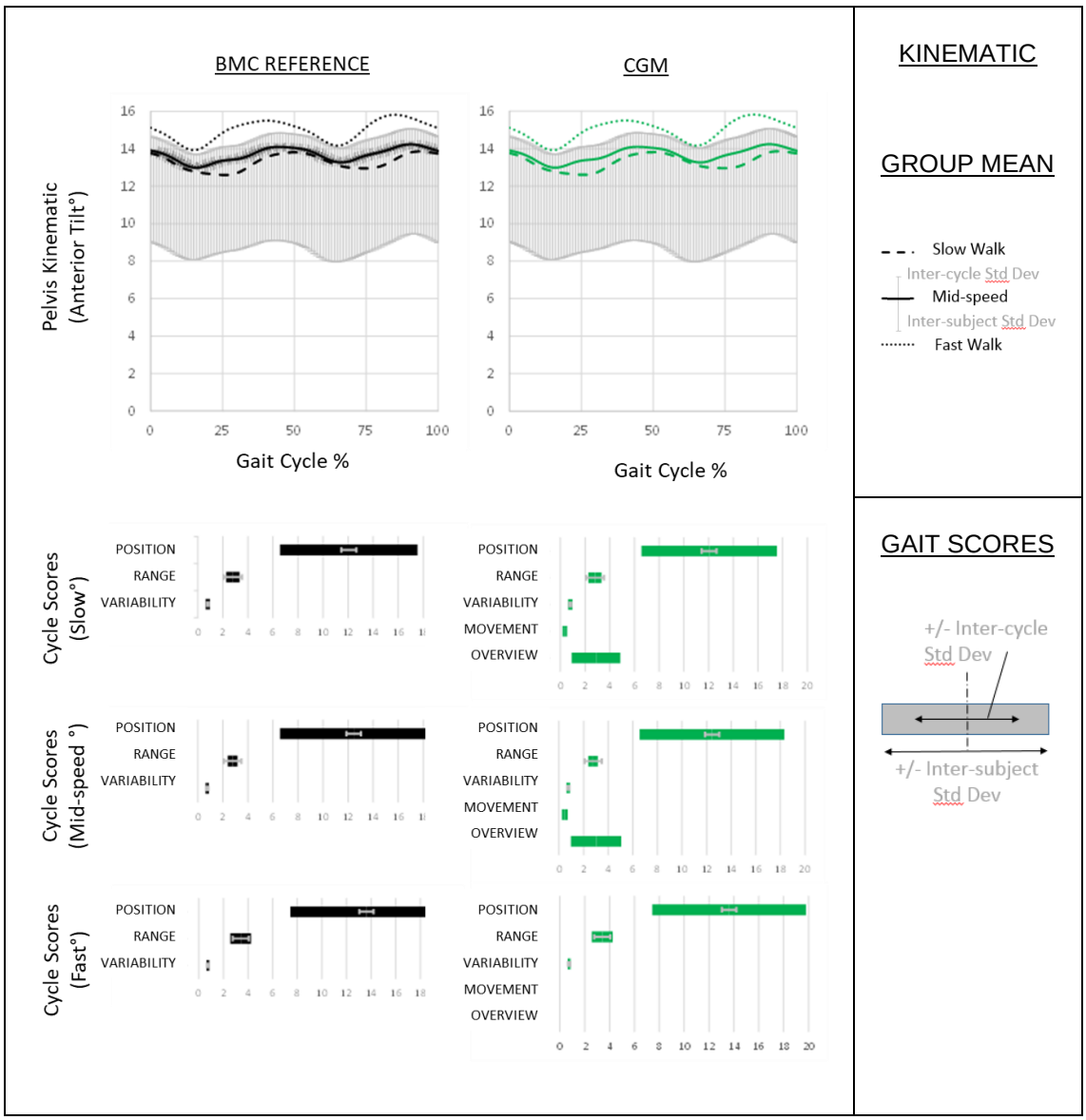

Figure 4-12 CGM tracking solution for pelvis - Sagittal

Sagittal plane comparison of CGM tracking solution (right column) with BMC reference (left column).

Top row shows graphical kinematic for slow (dashed line), mid-speed (solid line) and fast (dotted line) walking as depicted in the legend (right). The mid-speed typical inter-cycle, and inter-subject standard deviations are shown above and below the mid-speed graph line respectively.

Subsequent rows depict speed specific gait scores as per the legend (right bottom). Cycle position, range and variability scores represent absolute values from zero. Movement pattern and overview scores measure the difference between comparative and BMC reference values.

The coronal and transverse plane comparisons for the CGM solution are shown in figures 4-13 and 4-14 respectively.

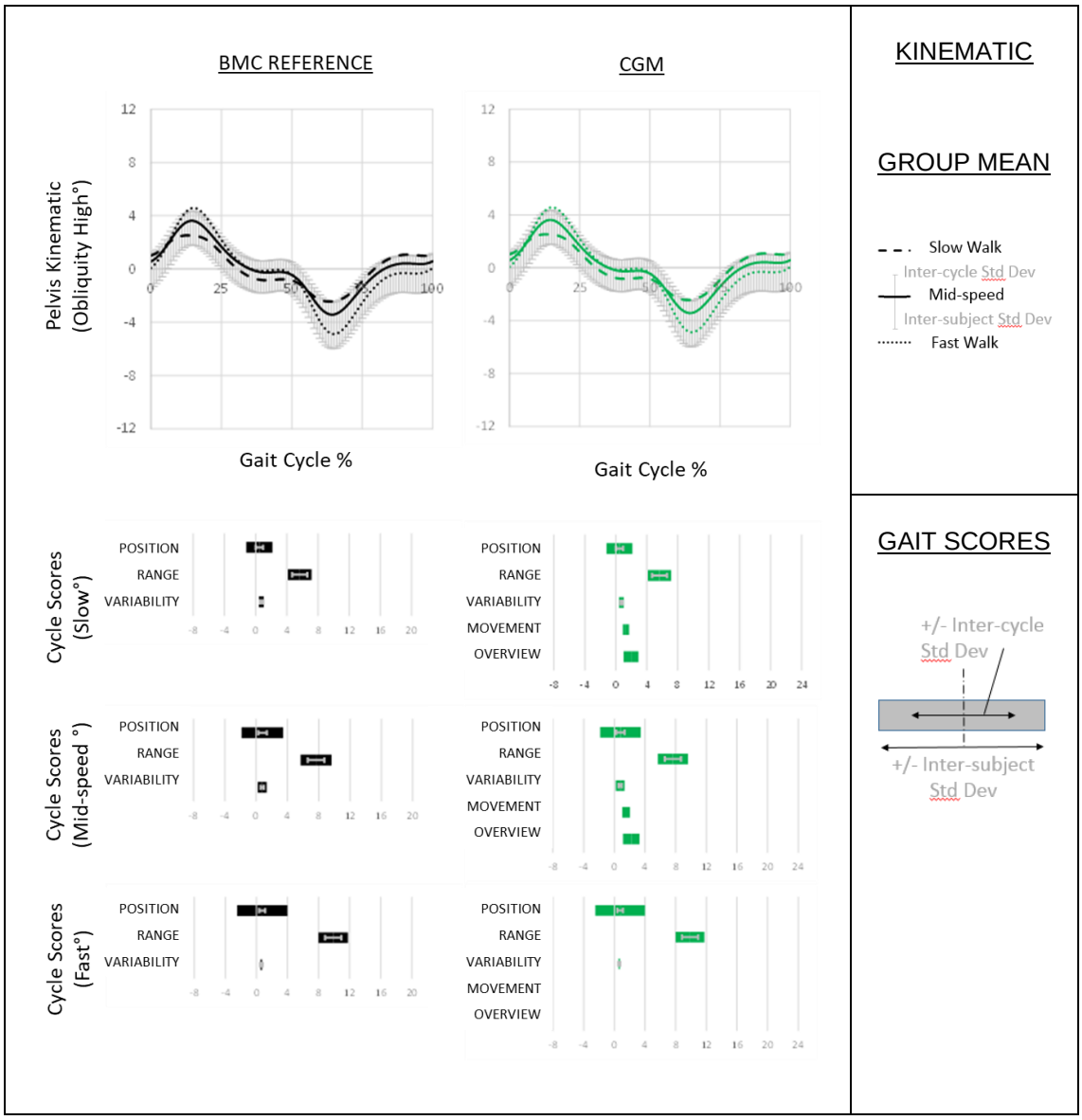

Figure 4-13 CGM tracking solution for pelvis - Coronal

Coronal plane comparison of CGM tracking solution (right column) with BMC reference (left column).

Top row shows graphical kinematic for slow (dashed line), mid-speed (solid line) and fast (dotted line) walking as depicted in the legend (right). The mid-speed typical inter-cycle, and inter-subject standard deviations are shown above and below the mid-speed graph line respectively.

Subsequent rows depict speed specific gait scores as per the legend (right bottom). Cycle position, range and variability scores represent absolute values from zero. Movement pattern and overview scores measure the difference between comparative and BMC reference values.

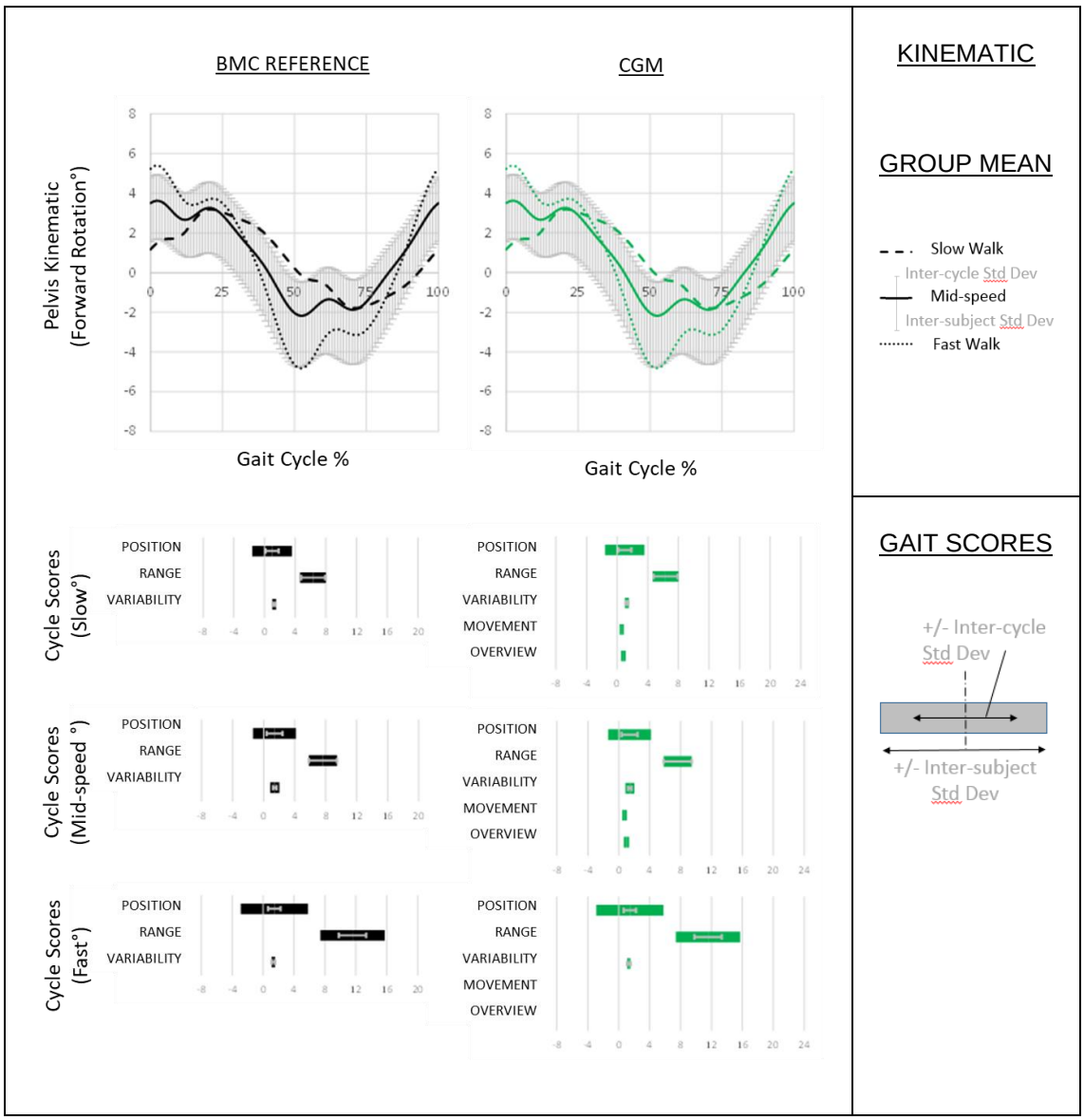

Figure 4-14 CGM tracking solution for pelvis - Transverse

Transverse plane comparison of CGM tracking solution (right column) with BMC reference (left column).

Top row shows graphical kinematic for slow (dashed line), mid-speed (solid line) and fast (dotted line) walking as depicted in the legend (right). The mid-speed typical inter-cycle, and inter-subject standard deviations are shown above and below the mid-speed graph line respectively.

Subsequent rows depict speed specific gait scores as per the legend (right bottom). Cycle position, range and variability scores represent absolute values from zero. Movement pattern and overview scores measure the difference between comparative and BMC reference values.

As expected, no observable differences are noted between the structurally similar BMC and CGM tracking solutions.

4.4.6.3 RNOH Tracking Solution

Similar, sagittal, coronal, and transverse plane comparisons of the RNOH pelvic tracking solution against the BMC reference values are depicted in figures 4-15, 4-16 and 4-17 respectively.

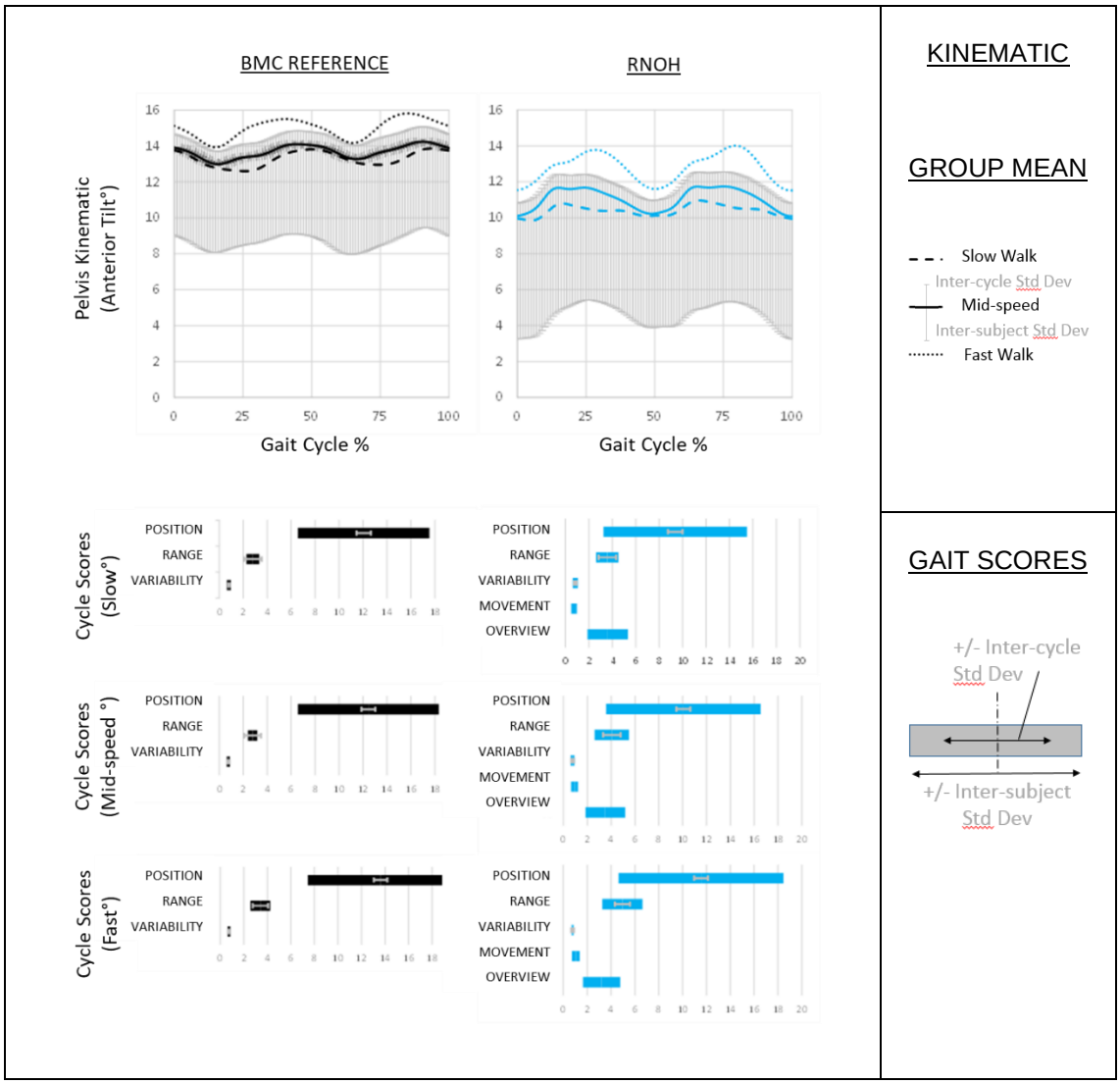

Figure 4-15 RNOH tracking solution for pelvis - Sagittal

Sagittal plane comparison of RNOH tracking solution (right column) with BMC reference (left column).
Top row shows graphical kinematic for slow (dashed line), mid-speed (solid line) and fast (dotted line) walking as depicted in the legend (right). The mid-speed typical inter-cycle, and inter-subject standard deviations are shown above and below the mid-speed graph line respectively.

Subsequent rows depict speed specific gait scores as per the legend (right bottom). Cycle position, range and variability scores represent absolute values from zero. Movement pattern and overview scores measure the difference between comparative and BMC reference values.

The RNOH pelvic tracking solution captures slightly more sagittal range of motion from a less anteriorly tilted position than the BMC reference (Figure 4-15). Although both solutions show small movement ranges, the movement patterns appear phase shifted from each other, often showing opposite movement directions at the same instance. In addition to capturing more range, the RNOH solution shows better left right reflective symmetry through the 50% cycle line.

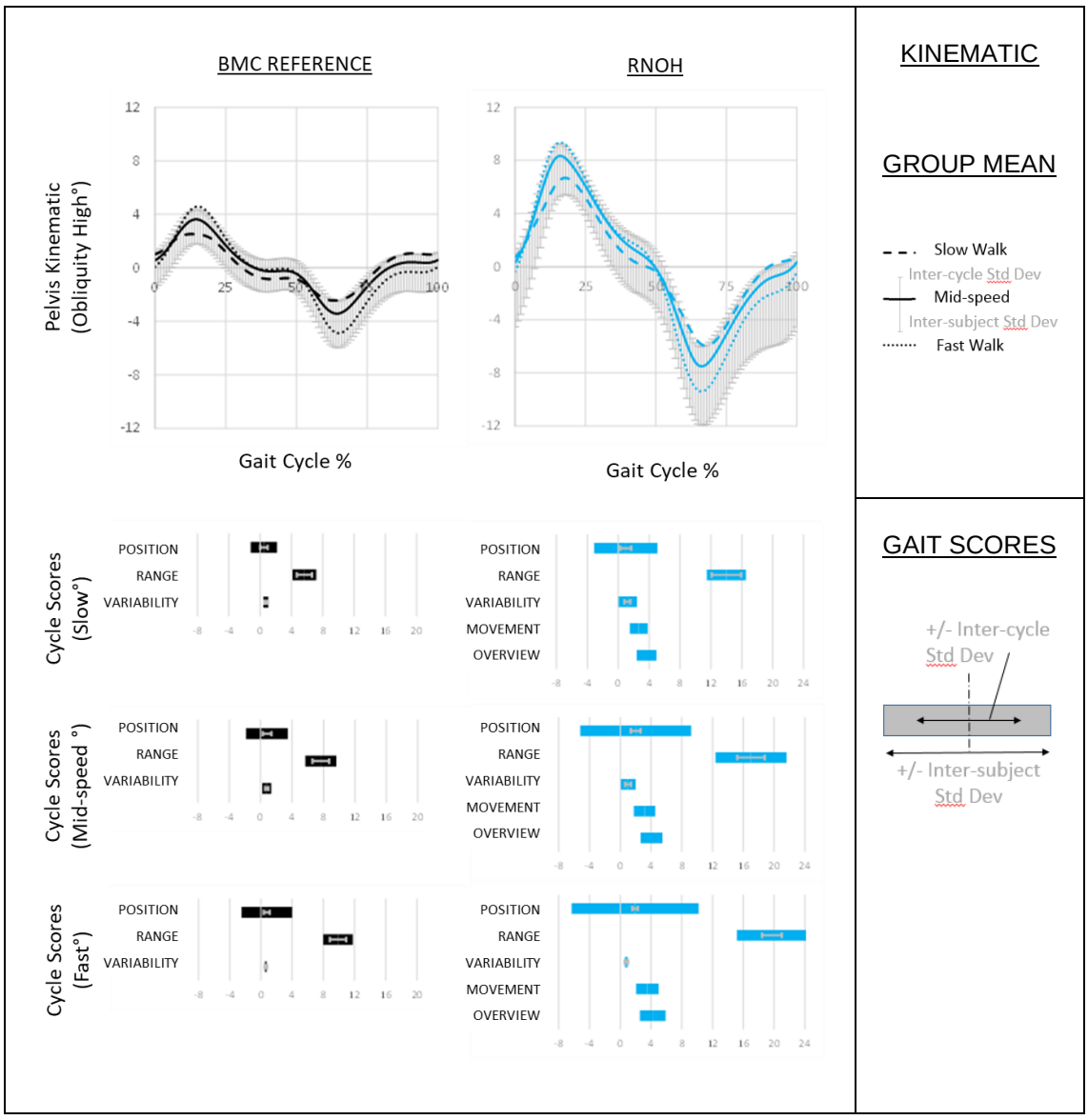

Figure 4-16 RNOH tracking solution for pelvis - Coronal

Coronal plane comparison of RNOH tracking solution (right column) with BMC reference (left column).

Top row shows graphical kinematic for slow (dashed line), mid-speed (solid line) and fast (dotted line) walking as depicted in the legend (right). The mid-speed typical inter-cycle, and inter-subject standard deviations are shown above and below the mid-speed graph line respectively.

Subsequent rows depict speed specific gait scores as per the legend (right bottom). Cycle position, range and variability scores represent absolute values from zero. Movement pattern and overview scores measure the difference between comparative and BMC reference values.

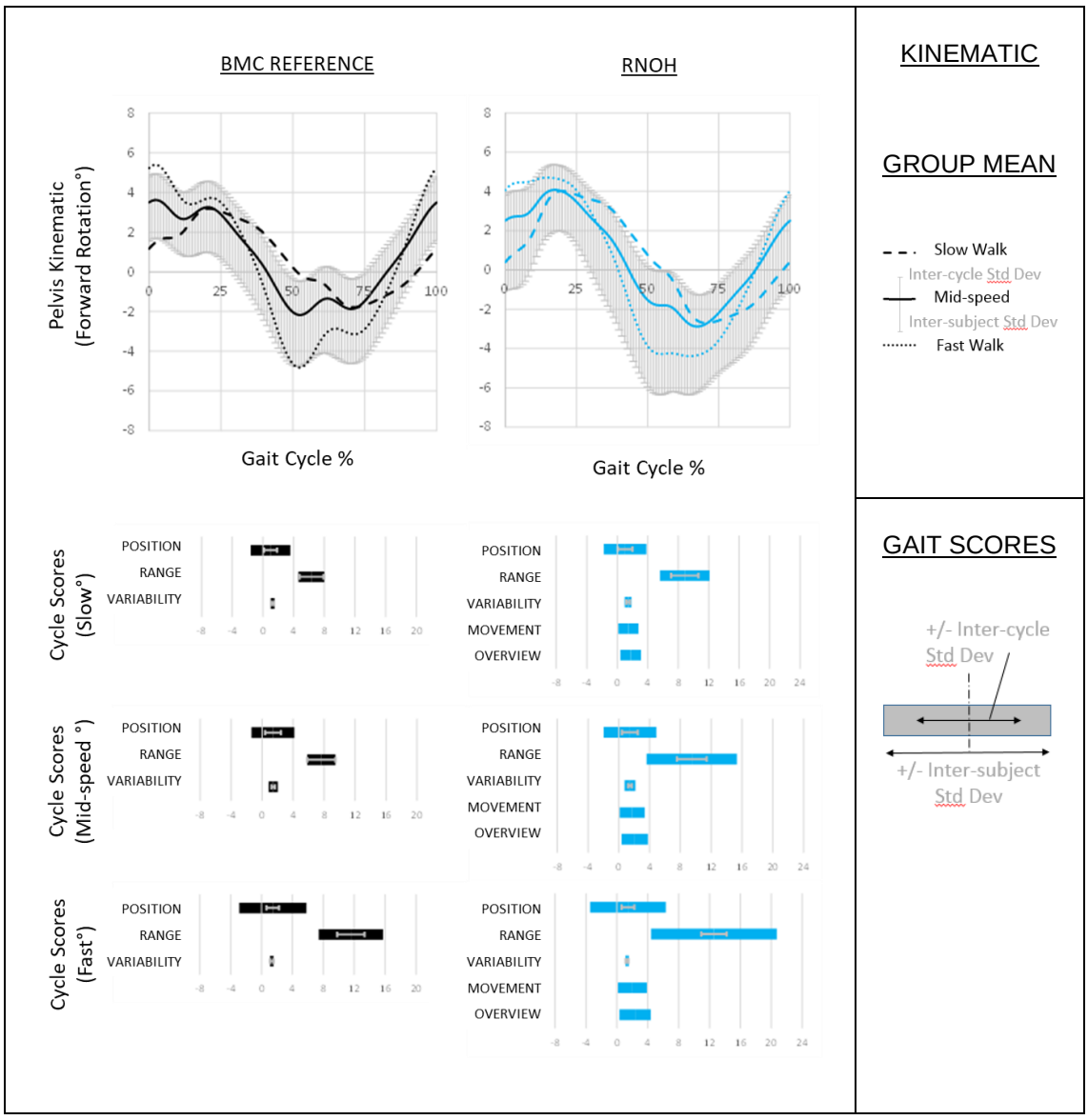

Figure 4-17 RNOH tracking solution for pelvis - Transverse

Transverse plane comparison of RNOH tracking solution (right column) with BMC reference (left column).

Top row shows graphical kinematic for slow (dashed line), mid-speed (solid line) and fast (dotted line) walking as depicted in the legend (right). The mid-speed typical inter-cycle, and inter-subject standard deviations are shown above and below the mid-speed graph line respectively.

Subsequent rows depict speed specific gait scores as per the legend (right bottom). Cycle position, range and variability scores represent absolute values from zero. Movement pattern and overview scores measure the difference between comparative and BMC reference values.

More coronal than sagittal range of motion is evident from both solutions (Figure 4-16); in this plane the RNOH range of motion is clearly increased over the BMC

reference, and no phase shift difference is observed in the movement pattern. Minimal differences are observed in the transverse plane kinematic (Figure 4-17).

4.4.6.4 BMI Effects

Correlation coefficient between gait scores for each of the tested pelvic tracking solutions and subject BMI are shown in Table 4-6.

Table 4-6 BMI correlation coefficient between gait scores from each tracking solution.

Sagittal

	Position			Range			Variability		
	Slow	MidSpeed	Fast	Slow	MidSpeed	Fast	Slow	MidSpeed	Fast
BMC	0.14	0.11	0.14	-0.42	-0.29	-0.61	-0.16	-0.25	-0.01
CAST	-0.05	-0.05	-0.02	-0.69	-0.50	-0.60	-0.19	-0.31	0.18
CGM	0.14	0.11	0.14	-0.42	-0.29	-0.61	-0.16	-0.25	-0.01
RNOH	0.31	0.28	0.29	-0.50	-0.39	-0.73	-0.24	-0.47	-0.50

	Movement			Overview		
	Slow	MidSpeed	Fast	Slow	MidSpeed	Fast
CAST	0.00	0.30	0.31	0.36	0.36	0.36
CGM	-0.09	-0.39	-0.18	-0.16	-0.33	-0.05
RNOH	-0.33	-0.19	-0.31	-0.27	-0.24	-0.26

Coronal

	Position			Range			Variability		
	Slow	MidSpeed	Fast	Slow	MidSpeed	Fast	Slow	MidSpeed	Fast
BMC	-0.09	-0.18	-0.07	-0.48	-0.17	-0.38	0.22	-0.27	0.33
CAST	0.27	0.23	0.30	-0.48	-0.38	-0.60	0.13	-0.36	-0.36
CGM	-0.09	-0.18	-0.07	-0.48	-0.17	-0.38	0.22	-0.27	0.33
RNOH	0.02	-0.06	0.10	0.10	0.39	0.25	0.25	-0.29	-0.06

	Movement			Overview		
	Slow	MidSpeed	Fast	Slow	MidSpeed	Fast
CAST	0.20	0.66	0.56	0.56	0.63	0.55
CGM	-0.58	-0.54	-0.55	-0.12	-0.09	-0.06
RNOH	0.02	0.26	0.21	0.33	0.31	0.31

Transverse

	Position			Range			Variability		
	Slow	MidSpeed	Fast	Slow	MidSpeed	Fast	Slow	MidSpeed	Fast
BMC	0.49	0.44	0.46	-0.71	-0.26	-0.46	-0.17	-0.22	-0.44
CAST	0.47	0.40	0.44	-0.64	-0.46	-0.57	-0.12	-0.36	-0.68
CGM	0.49	0.44	0.46	-0.71	-0.26	-0.46	-0.17	-0.22	-0.44
RNOH	0.49	0.39	0.45	-0.28	0.22	0.25	0.05	-0.34	-0.51

	Movement			Overview		
	Slow	MidSpeed	Fast	Slow	MidSpeed	Fast
CAST	0.05	0.35	0.56	0.35	0.60	0.64
CGM	-0.48	-0.32	-0.61	-0.01	0.02	0.02
RNOH	0.06	0.17	0.19	0.11	0.17	0.20

Overall, all solutions showed some BMI related decrease in their sagittal range of motion. The coronal range was only sensitive to the CAST solution which also showed some movement pattern and overall score BMI effects. Only the RNOH solution exhibited resistance to BMI effects in the transverse plane. Correlations in any of the CGM scores reflect mathematical artefacts in near zero scores of the order of a millionth of one-degree.

4.4.7 Hypothesis Testing

The CGM solution did not produce any measurable differences in the group average gait scores (Table 4-7).

Table 4-7 Difference between pelvic CGM and BMC reference gait scores.

	Position (°)			Range (°)			Variability (°)		
	Sagittal	Coronal	Transverse	Sagittal	Coronal	Transverse	Sagittal	Coronal	Transverse
SLOW	0.00	0.00	0.00	0.00	0.00	0.00	0.00	0.00	0.00
p-value	1.000	0.866	0.731	0.339	0.104	0.586	1.000	0.339	1.000
MIDSPEED	0.00	0.00	0.00	0.00	0.00	0.00	0.00	0.00	0.00
p-value	1.000	0.713	0.828	0.339	0.144	0.165	1.000	0.339	1.000
FAST	0.00	0.00	0.00	0.00	0.00	0.00	0.00	0.00	0.00
p-value	1.000	0.870	0.670	0.339	0.104	0.344	1.000	0.339	1.000

	Movement (°)			Overview (°)		
	Sagittal	Coronal	Transverse	Sagittal	Coronal	Transverse
SLOW	0.00	0.00	0.00	0.00	0.00	0.00
MIDSPEED	0.00	0.00	0.00	0.00	0.00	0.00
FAST	0.00	0.00	0.00	0.00	0.00	0.00

Paired t-test significance for cycle position, range and variability shown beneath each score, with p-values <0.05 highlighted.

Differences in range scores the CAST solution increased with walking speed, becoming statistically significant at the faster speeds (Table 4-8).

Table 4-8 Difference pelvic between CAST and BMC reference gait scores.

	Position (°)			Range (°)			Variability (°)		
	Sagittal	Coronal	Transverse	Sagittal	Coronal	Transverse	Sagittal	Coronal	Transverse
SLOW	-2.72	0.50	-0.01	0.12	0.01	0.15	0.04	-0.11	0.06
p-value	0.001	0.294	0.946	0.317	0.967	0.610	0.204	0.006	0.001
MIDSPEED	-2.83	0.53	-0.07	0.41	-0.45	-1.19	0.05	-0.10	-0.04
p-value	0.001	0.285	0.690	0.033	0.166	0.000	0.065	0.124	0.358
FAST	-2.59	0.57	-0.01	0.85	-0.92	-1.81	0.09	-0.07	-0.01
p-value	0.002	0.274	0.962	0.007	0.016	0.001	0.092	0.109	0.706

	Movement (°)			Overview (°)		
	Sagittal	Coronal	Transverse	Sagittal	Coronal	Transverse
SLOW	0.37	1.31	0.60	2.88	1.97	0.81
MIDSPEED	0.48	1.54	0.73	3.02	2.21	0.99
FAST	0.65	1.82	0.83	2.85	2.48	1.10

Paired t-test significance for cycle position, range and variability shown beneath each score, with p-values <0.05 highlighted.

Whilst sagittal ranges increased, coronal and transverse ranges were reduced. The largest differences were in the transverse plane; even at the fastest speed this loss was less than 2°.

Differences in range score were much larger for the RNOH solution, with statistically significant increases for the sagittal and coronal plane kinematic at all walking speeds, and a statistically significant increase in the transverse plane kinematic at the slow walking speed. Sagittal and transverse plane range scores were of similar magnitude to the CAST changes – approximately 2°, but consistently acted to increase the captured range. The coronal plane increase was substantial, ranging from more than 8° at the slow walking speed, to just short of 10° when walking fast. (Table 4-9).

Table 4-9 Difference between pelvic RNOH and BMC reference gait scores

	Position (°)			Range (°)			Variability (°)		
	Sagittal	Coronal	Transverse	Sagittal	Coronal	Transverse	Sagittal	Coronal	Transverse
SLOW	-2.88	0.21	-0.07	0.77	8.36	2.53	0.04	0.45	0.15
p-value	0.003	0.757	0.656	0.025	0.000	0.017	0.283	0.134	0.058
MIDSPEED	-2.63	0.24	-0.14	1.28	9.33	1.83	0.01	0.24	0.02
p-value	0.006	0.688	0.344	0.013	0.000	0.255	0.739	0.149	0.716
FAST	-2.20	0.07	-0.13	1.54	9.85	1.02	0.02	0.15	0.01
p-value	0.013	0.888	0.230	0.011	0.000	0.638	0.396	0.028	0.721

	Movement (°)			Overview (°)		
	Sagittal	Coronal	Transverse	Sagittal	Coronal	Transverse
SLOW	0.73	2.65	1.48	3.60	3.67	1.76
MIDSPEED	0.94	3.15	1.73	3.51	4.06	2.07
FAST	1.05	3.52	2.01	3.21	4.22	2.36

Paired t-test significance for cycle position, range and variability shown beneath each score, with p-values <0.05 highlighted.

The primary hypothesis for this chapter (Hypothesis 4B_I), that the RNOH solution will capture more coronal plane range than other solutions is therefore accepted.

A sagittal positional offset of just less than 3° towards extension is inherited from the CAST solution. This shift in the kinematic position accounts for the majority of the overall difference score. The movement pattern difference approximates a single degree for all walking speeds.

The coronal plane kinematic does not show any positional shift but shows much greater overall difference scores than the sagittal kinematic. Most of this difference is represented in the movement score, but this is heavily weighted by the large increase in range scores. Visual inspection of the kinematic confirms no major change in the shape of the kinematic pattern.

There is also no positional shift in the transverse plane kinematic. Movement difference scores are only slightly smaller than the overall difference scores, probably reflecting their absolute-mean and RMS averaging strategies. At around 2°, these scores are about the same as the increase in cyclic range. This suggest that most of the average cyclic difference occurs at the kinematic turning points. Here again, visual inspection of the kinematic confirms no major change in the shape of the kinematic pattern.

The secondary hypothesis for this chapter (Hypothesis 4B_II), that the RNOH solution will maintain the movement pattern of the BMC reference is also accepted.

4.5 Discussion

To re-quote George Box, ‘all models are wrong, but some are (remain) useful’. While the wrongness of each modelling approach is captured in the assumptions that it makes to simplify reality, their usefulness is retained by their user accepting these assumptions and outputs not violating them.

4.5.1 Model Complexity

A possible measure of tracking solution complexity is the number of surface markers it requires. In this respect, pelvic based solutions represented by BMC/CGM and CAST methods, each require the absolute minimum of 3 markers and may thus be regarded as the simplest. The Kisho Fukuchi approach tracks each thigh segment by a minimum of 3 surface markers (6 total), providing just two of the three required pelvic tracking markers. The third marker must then be located on the pelvic surface, making the solution vulnerable to the STA influences of a total of 7 surface markers. Finally, the RNOH_Pelvis requires a minimum of 3 surface markers on each shank segment to track the KJC locations (6 total), plus 3 pelvic markers to track the interim HJC locations including the principal axis spin movement, a grand total of 9 markers (Figure 4-18).

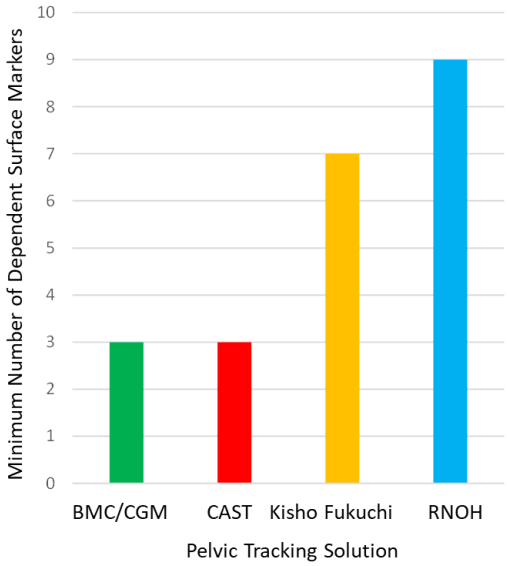

Figure 4-18 Complexity of various Pelvis Tracking Solutions

Complexity indicated by the minimum number of dependent surface markers required by each solution.

Although each surface marker is a potential source of additional noise to each tracking solution, more markers does not necessarily lead to reduced accuracy. Single segment BMC/CGM/CAST solutions, often employ additional surface markers above the minimum requirement, in the hope that STA effects will cancel each other out, rather than accumulate. In chapter 3 for example, one of the identified thorax models sought a simple 3 marker solution that could mimic, the assumed gold standard average movement of 11 (Armand et al., 2014). Once the 3D orientation of segment has been established, by any method, each additional marker will provide added complexity and noise, plus a potential improvement in signal accuracy. An optimal model should aim to find the best balance between all of these factors.

4.5.2 Model Assumptions

Face validity for each model is subjectively assessed by weighing up the accumulative reasonableness of its underlying assumptions. Assumptions required for each of the tested pelvic models are presented in table 4-10.

Table 4-10 Modelling assumptions specific to each pelvic segment modelling approach

	ARF Modelling Assumption	TRF Modelling Assumptions
BMC	A principal plane is effectively defined at the pelvic crest by anteriorly located left and right ASIS locations anteriorly, and a mid-PSIS location posteriorly. The resulting ARF provides the orthogonal directions for application of offset values to estimate HJC locations from the mid-ASIS origin. The accuracy of this estimate assumes good accuracy of the regression equation providing these offset values, and that the surface markers are able to represent the skeletal locations of the ASIS bony landmarks.	Segment tracking is via the pelvic crest markers which are assumed to move with the underlying bone. This is a known poor assumption.
CGM	In order to provide common HJC location for the CGM, CAST and RNOH methods, the pelvic origin was modified to facilitate specification of an internal location for each ASIS. Improvement of this location over the BMC requires that laterally placed ASIS surface markers transect the bony locations better than the anteriorly placed markers.	Segment tracking is as for the BMC.
CAST	The CAST method is free to adopt any ARF solution. The selected ARF orientation is then related to that of the segment's TRF during a static calibration trial. In this case the common ARF with the CGM HJC modification was employed.	Segment movement is tracked by a cluster consisting of left and right PSIS surface markers and a non-collinear sacral marker. This regional cluster avoids the most STA affected ASIS regions, and is assumed to move like the underlying pelvic bone. The pelvis skeleton is assumed rigid.
RNOH	The common ARF with the CGM HJC modification was employed. The fixed length of each thigh segment is established during the ARF –TRF calibration trial.	KJC locations representing the distal end of each thigh segment are assumed to be accurately track via the neighbouring shank segments. This requirement mostly concerns the ability of the knee to constrain axial distraction away from the thigh. The CGM HJC locations are further modified, to maintain fixed thigh lengths to the KJC locations without altering their orientation. Segment tracking is via these modified HJC locations plus an external mid-PSIS location.

Simple modelling approaches that attempt to track segmental movements by surface markers restricted to that segment, are assuming low levels of segmental STA. For the pelvis this is known to be a poor assumption. More complex modelling approaches attempt to bypass this assumption, by accepting multiple smaller assumptions. Usefulness then depends on the accumulative effect of

these assumptions being less than that of assuming low STA – a few fibs rather than one big untruth.

4.5.3 Model Face Validity

Face validity of each of the tested pelvic tracking solutions is discussed.

4.5.3.1 CAST solution

The line between two body segment surface markers, defines a randomly orientated embedded axis. The addition of a third non-collinear marker converts this axis into a plane that can represent the 3D orientation of the segment. With the condition that the markers describe a reasonably fat triangle, their instantaneous locations are all that is required to define a stable TRF. Once calibrated, any discrepancy between the segments ARF and TRF solutions occurs as a result of the interplay of soft tissue movement under each TRF surface marker location. The resulting STA may be considered as having two factors.

i. the angular discrepancy between the TRF and the true skeletal orientation
ii. the distance over which this discrepancy acts.

While the first factor suggests use of a CAST cluster that avoids relatively more STA affected ASIS surface marker locations, the second supports use of the CGM solution which spans the entire segment, rather than assuming a particular segment sub-region to represent the whole.

On balance, proximity of both critical HJC locations to the CAST sacral marker cluster, supports the choice of the CAST solution over CGM. This conclusion is also supported by its better reliability (Borhani et al., 2013); even so, significant STA over the entire pelvic surface (Fiorentino et al., 2017) inevitably limits the scope for accurate measurement by any combination of pelvic based surface markers.

4.5.3.2 Kisho Fukuchi method

The alternative paradigm considered the pelvis principal axis between left and right HJC locations, as a single link in a kinematic chain, between the respective thigh segments (Kisho Fukuchi et al., 2010). This arrangement allowed the HJC locations to be tracked via the thigh segments, while contributing to the pelvic tracking solution. This solution assumes that the HJC locations hold a common location viewed from either the pelvis or the thigh segment i.e., that there is no appreciable translational movement. In reality, the ball-and-socket anatomy of the joint makes this a seemingly reasonable assumption; any error in locating the true HJC location is, however, likely to model as a violation.

Relative complexity of the method proposed by Kisho Fuskuchi, warrants individual consideration of the STA factors at each TRF location. The pelvic based marker, which tracks principal axis spin between the two HJC locations, will suffer the same pelvic STA as the CAST solution, also located over the sacral region. For the thigh-based markers, reduced soft tissue cover thickness suggests use of a distally located cluster, while proximity to the target HJC locations suggests a proximal location. The optimal balance of these factors is likely specific to individual subject STA characteristics. However, given the known high levels of STA over the entire thigh segment (Barre et al., 2017, Fiorentino et al., 2017), performance similar to pelvic marker solutions seems likely.

4.5.3.3 RNOH solution

The proposed RNOH_Pelvis treads a fine line between the two previously presented tracking paradigms, in conjunction with constraining the thigh segments to a fixed length. This hybrid approach employs the CAST sacral cluster to track interim HJC locations but moderates these locations via the thigh while bypassing thigh-based STA effects. This is achieved by tracking distal KJC locations via the neighbouring shank segments, where relatively low STA is a fundamental premise of RNOH_model development (see Chapter 1). Although the anatomy of the knee does not anatomically constrain translational movements, these movement occur predominately perpendicular to the thigh

principal axis in an antero-posterior direction (Gray et al., 2019), and are thus expected to have minimal effect on the HJC-KJC separation distance.

Increased face validity of the RNOH_Pelvis solution over CAST, is based on the very reasonable assumption of a constant length thigh segment. The same cannot be claimed by the Kisho Fukuchi method which relies on low STA over the thigh segments. Thigh segment STA is generally greater than effects seen at the pelvis (Fiorentino et al., 2017) and known to be particularly active along the direction of its longitudinal principal axis (Barre et al., 2017).

4.5.4 RNOH Construct Validity

The RNOH_Pelvis captures approximately 9° more coronal plane range than any solution based solely on pelvic markers, which are in turn known to underestimate the true skeletal movement (Fiorentino et al., 2017). Complexity of the RNOH approach, however, falls outside of the pelvic surface marker paradigm, that all solutions will underestimate the true skeletal movement. There is therefore a possibility that the RNOH solution overestimated this value.

A single available bone-pin study, measured an average of 12mm of superior-inferior STA at the PSIS locations of typically developing walking subjects of an unspecified demographic (Rozumalski, 2008). Assuming a 50% left-right phase shift in the action of this STA gives rise to an expected 24mm differential height loss between the two PSIS markers, and representing the lost pelvic obliquity as measured by these locations. Assuming again, a PSIS separation distance of between 125mm and 75mm, results in an obliquity deficit of the CGM/BMC solution in the range of 11.1° to 18.7°. Further, because the original 12mm measurement on which this estimate is based was a cycle average rather than maximum difference, this estimate is likely still a significant underestimate of the true obliquity deficit. Available evidence therefore suggests that the average 9° increase in measured range offered by the RNOH solution can reasonably be interpreted as an accuracy benefit, and not an over-estimation of the true skeletal movement.

5 Chapter 5 – The Thigh

Identified problems concerning current methods employed to model the thigh include difficulties in specifying a suitably aligned ARF (Chapter 1 – Issue 2), and overcoming considerable STA effects particularly affecting the transverse plane kinematic (Chapter 1- Issue 3). Improved modelling of this segment therefore forms a major aim of this thesis.

5.1 Introduction

The thigh segment anatomy differs from that of the trunk and pelvis, both in the simplicity of its skeletal anatomy, and the extent of its soft tissue cover.

5.1.1 The Thigh provides a Rigid Link between the Pelvis and Shank Segments

Unlike the thorax and pelvis segments, the thigh maintains a continuous kinematic chain between neighbouring segments, without any internal articulations, by a single bone - the femur. The proximal end of the femur provides the 'ball' component of a 'ball and socket' shaped hip joint with the pelvis. This femoral head is extended medially from the femoral shaft by a short neck region of the bone. Condyles at the distal end of the femur are shaped to rollover the relatively flat tibial plateaus of the shank segment in a hinge like action of the knee.

Thigh orientation is modelled by a principal plane between a proximal HJC location inherited from the pelvis, and distal knee joint axis between medial and lateral epicondyle surface markers (Wu et al., 2002). Optimised purely for simplicity, the BMC approach developed in chapter 1 defines and tracks this plane directly from these points. The medial knee marker can however be difficult to track, particularly with early motion capture systems suffering a limited number of relatively low-resolution cameras. In the clinical setting, this marker is also easily dislodged on patients with excessive adduction/internal rotation of the thigh.

Much of the femoral surface is covered in thick musculature, with palpable bony landmarks confined to the lateral end of the femoral neck at the greater trochanter proximally, and the medial and lateral aspects of the knee joint axis over the epicondyles distally. Anteriorly the four components of the quadriceps muscle, insert into large sesamoid bone (patella), before attaching to the shank segment to effect extension of the knee. The patella acts to provide a mechanical advantage to this action and is constrained to run in an articular groove between the epicondyle landmarks. Although not directly attached to the femur, the patella provides an additional palpable bony landmark location.

5.1.2 There is a Distal to Proximal Increase in Femoral Soft Tissue Cover.

A recent comprehensive study of STA over the thigh and shank segments, employed a total of 40 surface markers distributed over both segments (Barre et al., 2017). Nineteen elderly subjects with unilateral knee prostheses were studied and principal component analysis employed to identify the primary STA movements. Results show a significant rigid component – where all surface markers move *en bloc* with respect to the underlying bone. Both shank and thigh segments suffered translational STA in the direction of their long axes. Additional STA was primarily translational along an antero-posterior axis at the shank, and rotational about a medio-lateral axis for the thigh. Thigh STA was much more correlated with the knee flexion angle than that of the shank.

The truncated cone shape of the thigh segment, gives an expectation of a distal to proximal increase in STA. Height of the CGM lateral thigh marker placement has been shown to have a significant influence on both the coronal knee and the transverse plane hip kinematic, with a proximal marker measuring less range than distal (Cockcroft et al., 2016). This study also shows that the proximal marker is less sensitive to whether the post-collection AP correction is optimised over the whole gait cycle or restricted to the mid-stance phase only. From these findings, the authors conclude that the distal thigh marker *overestimates* the thigh rotation, and that the reduced range associated with the more proximal marker is indicative of a reduction in STA effects. They also note that this conclusion is contrary to other published findings (Wren et al., 2008, Lamoreux, 1991, Cappozzo et al., 1996), but attribute this disparity to these studies looking at a pure axial rotation

task rather than functional gait activity. A more reasonable interpretation of the increased distal movement is that the proximal marker *underestimates* thigh rotation; this is actually the conclusion of the gait based analysis quoted by Cockcroft and colleagues in support of their findings (Schache et al., 2008). The Schache study of transverse plane thigh movement compared four configurations of distal thigh configuration against the CGM solution. They conclude that the CGM solution is 'inappropriate' for this purpose and recommend a distal cluster of three individual surface markers, capturing 60% of the movement 'at best'.

More recent publications employing dynamic dual fluoroscopy have indeed shown that STA in *all* thigh regions acts to *underestimate* true bone movement during gait (Barre et al., 2017), and that this is particularly a problem for tracking axial rotation of the thigh (Fiorentino et al., 2017).

5.1.3 Static Evaluation of Thigh Principal Plane

Craig's test is commonly employed during orthopaedic examination to assess the transverse plane angle at which the neck of the femur branches from the shaft (Uding et al., 2019). Excessive internal rotation in this angle is termed anteversion. Less common is excessive external rotation – retroversion (Figure 5-1).

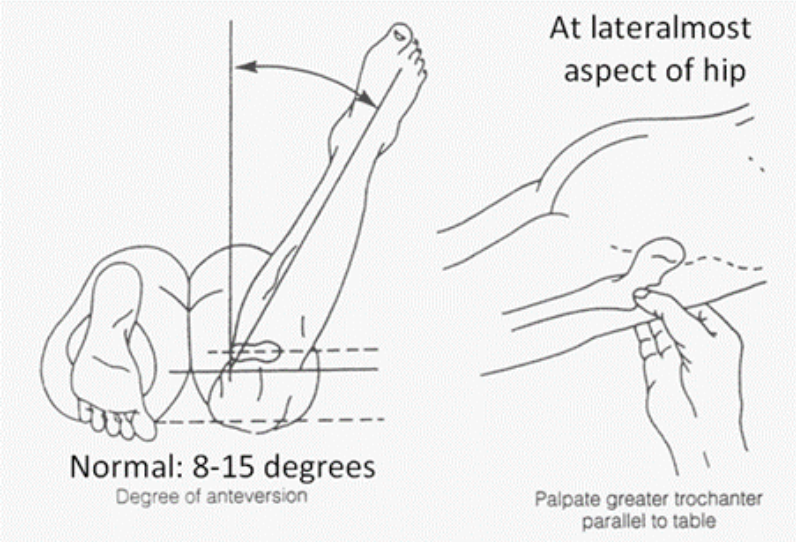

Figure 5-1 Clinical test for Femoral Anteversion (Craig's test)

Craig's test is commonly employed to estimate femoral anteversion as the shank inclination angle when the greater trochanter points laterally. The same method may be employed to estimate the internal and external rotation ranges of the extended hip with respect to a vertical shank position. Image from:https://epomedicine.com/clinical-medicine/femoral-anteversion-craigs-test/

Craig's test is performed with the patient lying prone with the knee flexed. The clinician passively rotates the thigh via the shank segment to identify the angle at which the greater trochanter bony landmark, at the lateral end of the femoral neck, becomes most prominent to palpation. In this position the inclination of the shank with respect to vertical, provides an estimate of the femoral neck anteversion angle.

An underappreciated characteristic of all gait model kinematic joint outputs, is that they include a fixed contribution that reflects any skeletal deformation of the distal segment. At the hip for example, which reports the orientation of the distal femur with respect to the proximal pelvis, the '*internal-rotation'* transverse plane output, would be less succinctly but more accurately labelled '*internal-rotation plus femoral anteversion*' Similarly, the transverse plane knee kinematic reflect both dynamic knee rotation and a fixed tibia torsion estimate.

A modified version of Craig's test uses the same inclination measure to estimate the internal and external rotation ranges in the extended hip, around neutral (shank near vertical) position. In the precise neutral position, flexion-extension

movements at the knee causes the shank to move without any medial or lateral deviation of the distal ankle, indicating that the knee joint axis is horizontal. This position reflects any deformation within the thigh segment morphology; the measured internal external rotation ranges from this neutral point, should therefore correlate with those measured by clinical gait analysis. By extension of this logic, recreating the salient features of the Craig's test during the static calibration of the gait marker-set, has the potential to inform on the required neutral rotation axial rotation position of the thigh.

5.2 Development of RNOH_Thigh model

Justification for re-employment of the thigh principal axis developed to facilitate accurate tracking of the RNOH_Pelvis (Chapter 4), precedes separate descriptions of the RNOH_Thigh full ARF definition and TRF development.

5.2.1 Justification for re-employment of the thigh Principal Axis utilised by RNOH_Pelvis

The RNOH_Pelvis (developed in chapter 4) provides a principal axis for the thigh segments, defined between modified KJC and HJC locations. Re-use of this definition for modelling an RNOH_Thigh segment is not mandatory but is consistent with the philosophy of adopting an integrated approach to model development (see chapter 1), and the avoidance of undue complexity (see chapter 2).

RNOH_Pelvis modifications to the HJC locations were employed to fix the length of the thigh segment without affecting its orientation. KJC locations continued to be defined as the mid-point of their medial and lateral epicondyle locations but were tracked via the distal shank segment. This modification will have a small effect on the orientation of the thigh as the distal end will now reflect the shank's perspective on any translation movements at the knee. These translations normally predominate in the antero-posterior direction (Gray et al., 2019), mostly affecting the sagittal plane orientation of the thigh. Fortunately, large ranges of movement in this plane will generally act to mask the smaller rotational anomaly caused by knee translation movements. A typical distal translation of 4mm (Gray

et al., 2019) over a typical thigh length of say, 500mm, would generate a flexion artefact approximating 5°, which is consistent with published expectations of constraining translations in the model (Andersen et al., 2010). High values of STA in the distal thigh region are reported to be as high as 40mm - an order of magnitude higher than the translation movements. On balance, for a general use clinical gait model, the modelling choice to constraining translational movement at the knee, outweighs the alternative required assumption of low STA tracking via the thigh segment.

5.2.2 Definition of the RNOH_Thigh TRF

The above thigh principal axis between a pelvic tracked HJC location, and a shank tracked KJC location, has previously been promoted under the guise of a 'marker less' thigh solution (Schulz and Kimmel, 2010). In this implementation, absence of any thigh surface markers made tracking of the axial rotation movement impossible. This omission reduces the knee kinematic to a sagittal output plus a secondary output that variably mixed the coronal and transverse components depending on the sagittal value. Like development of the RNOH_Pelvis (Chapter 4), conversion of the thigh principal axis into a principal plane, such that the full 3D kinematic may be restored, requires specification of a non-collinear marker, located on the segment's surface. Literature suggests that a surface marker over the patella might be optimally placed to perform this function (McMulkin and Gordon, 2009, Wren et al., 2008, Wren et al., 2013). This suggestion is consistent with the common clinical observation of squinting or frog-eyed patella being indicative of internally or externally rotated thigh segments respectively (Parikh and Noyes, 2011).

Direct use of a patella surface marker in the thigh tracking solution risks the introduction of artefactual sagittal plane movement. As the knee flexes, the patella tracks downward along the trochlear groove between the medial and lateral condyles (Li et al., 2007). Serendipitously, this vertical movement should not unduly influence the ability of a patella surface marker to track the required axial spin movement, reflected in it medio-lateral position (Figure 5-2).

Figure 5-2 Knee Joint Bony Anatomy

A groove between the medial and lateral epicondyles promotes downward vertical tracking of the patella within the bony trochlear grove with knee flexion. This should not affect the ability of a patella surface marker to track thigh axial rotation as movement perpendicular to this axis. Image: courtesy of www.MedicalGraphics.de under the creative commons licence (CC BY-ND 4.0).

This unwanted component of the patella marker movement is therefore modelled out via the creation of a virtual representation, as the projection of the mid-epicondyle KJC location on the HJC/surface-patella line. The RNOH-thigh TRF is then formed by this virtual marker plus the principal axis between pelvic tracked HJC and shank tracked KJC locations (Figure 5-3).

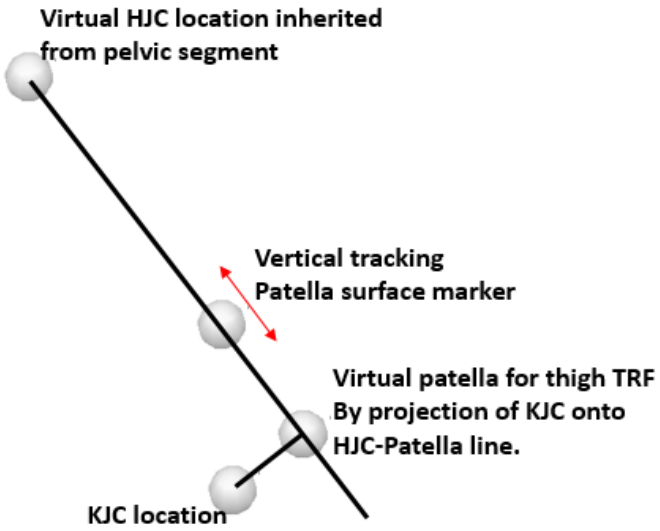

Figure 5-3 Schematic for creation of stable representation of patella tracking marker

Medio-lateral movements of the patella surface marker optimally track axial rotation of the thigh. Vertical tracking movements are however undesirable in the overall tracking solution. Projection of the KJC location on to the HJC-Patella line creates a virtual position with the intended movement only.

5.2.3 Definition of the RNOH_Thigh ARF

The clinical expectation of planar movement at the knee makes accurate alignment of the thigh segment ARF critical. If the segment principal plane is modelled too internally rotated or too externally rotated, true knee movement will be represented with an unrealistically large range in the coronal plane knee kinematic (Piazza and Cavanagh, 2000). With sufficient knee movement, the resultant excessive coronal knee kinematics is generally easy to recognise as aberrant. The primary value, however, is in alerting of an offset error in the transverse plane thigh position that without sufficient knee movement, might go unnoticed. CGM specific difficulty with this issue reflects difficulties in locating a lateral thigh marker in the desired plane (Fonseca et al., 2020). It may also be adversely affected by the visually obvious forward digression of a lateral (or medial) knee marker, as the subject moves from a seated application posture to an upright standing calibration posture. The alternative application of markers in the standing posture can create adverse clinical utility implications in some patients.

The reasonably flat coronal kinematic from the BMC solution (Figure 2-7) indicates that the desired knee axis may be suitably defined during a crouched calibration trial, by surface markers located over medial and lateral epicondyle markers when the subject was seated. This protocol may not hold however in non-typically developing subjects, or with less skilled application of the surface markers.

Unlike the ball-and-socket anatomy of the hip joint that allows rotation in any plane at the proximal end of the femur, condyles at the distal end are shaped to roll over relatively flat tibial plateaus to approximate planar movement at the knee. (Johal et al., 2005, Freeman and Pinskerova, 2005). In the weight bearing congruent knee, this approximation is largely controlled by the exact shape of the articulating surface. Reduced weight bearing reduces joint congruence (Hohe et al., 2002) and changes the relationship between concomitant planar movements (Koo and Koo, 2019).

Although the shape of the tibiofemoral articular surface is not palpable, its shape has a direct influence on the orientation of the shank segment with respect to the thigh. In the loaded knee joint the required movement axis might therefore be regarded as perpendicular to a plane containing the principal axis of both proximal and distal segments; the plane defined by hip, knee and ankle joint centres. This concept is employed by the RNOH_Thigh to axially align the ARF. For this purpose, the ankle joint centre (AJC) is defined as the mid-point of the medial and lateral malleoli surface markers. During a crouched posture static calibration trial, a virtual representation of a surface marker located over the centre of the patella, is projected into the plane defined by the three modelled joint centres. This marker then defines the anterior aspect of the thigh, thus orientating the neutral spin orientation of its principal axis.

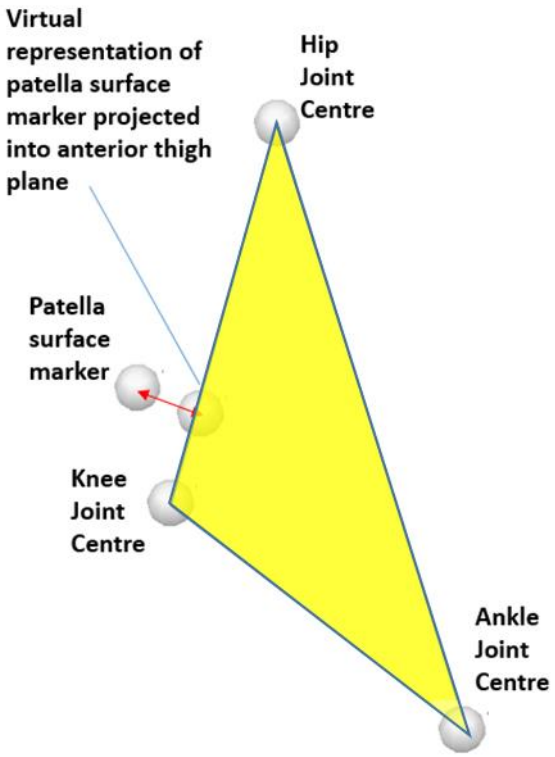

Figure 5-4 Thigh principal plane defined during a crouched calibration

Instead of defining a local coronal plane between a proximal hip joint centre location and a distal knee joint axis between medial and lateral epicondyle markers, an equivalently aligned sagittal principal plane is defined. The principal axis remains between hip and knee joint centres; the sagittal plane is then defined by the creation of virtual projection of a surface patella marker into the plane defined by the principal axis and a mid-malleoli ankle joint centre location.

Similarity between the proposed RNOH method, and that used to access transverse plane hip joint ranges during the static examination is expected to show good agreement between the two. By gleaning information about the articular orientation of the knee during a loaded static pose, it aims to avoid the need for post collection data correction based on the unloaded joint kinematic during swing. It also removes the BMC assumption that the epicondyle surface markers will accurately represent the knee movement axis. Overtime, the proposed calibration method has proved more reliable than early attempts to manually locate an anterior thigh marker, by transfer of the mid-epicondyle

location to the anterior thigh surface by alignment of an external calliper (Thornton et al., 2016).

5.3 Experiment 5A – Axial Rotation Tracking

Data was collected ex-vivo in one left-leg cadaveric specimen, and in-vivo in a single participant. For the ex-vivo testing, with the hemi-pelvis rigidly mounted, bone pins screwed into the femur and tibia allowed gold standard tracking of the thigh and shank movements via rigidly attached marker clusters.

5.3.1 Aims

The aim of this experiment was to investigate the ability of variously placed thigh segment surface markers to track the axial spin movement around the defined thigh segment principal axis.

5.3.2 Hypothesis

Primary hypothesis 5A_I - With sufficient knee flexion the ex vivo HJC-KJC-AJC plane will provide a good representation of thigh axial rotation as measured by bone pin, such that it might be employed as a gold standard measure for the in vivo testing.

Secondary hypothesis 5A_II – Axial tracking accuracy of proximally based markers will be most affected by the hip joint angle, and accuracy of the distal markers most affected by the knee joint angle.

Tertiary hypothesis 5A_III – Anteriorly placed surface markers will outperform lateral, and distal surface markers will outperform proximal in their ability to accurately capture axial rotation movement.

5.3.3 Methods

5.3.3.1 Model Specification

For both the ex vivo and in vivo experiments, distal to proximal linear arrays of 6 individual surface markers were attached on the anterior and lateral aspect of the left thigh, starting over the patella and lateral epicondyle bony landmarks

respectively, and each separated by approximately 5cm. On the lateral aspect, an extreme proximal marker was also added over the greater trochanter bony landmark.

Additional surface markers were attached over the medial epicondyle, pelvis and shank segments, in order to facilitate the calculation of the HJC and KJC locations and movement in the usual way. These locations defined the principal axis of a ‘markerless’ thigh solution (Schulz and Kimmel, 2010); the full 3D thigh kinematic could then be calculated using these locations plus one of the surface markers from either the anterior or lateral array. For the ex vivo cadaveric testing, each resulting solution was evaluated against the gold standard bone-pin measure, termed *thigh_bone*. This testing also established a *thigh_plane* solution between non-collinear hip, knee and ankle joint centres as a gold standard reference for the in vivo experiment, under the caveat of sufficient knee flexion. Detailed specification of the resulting biomechanical models are presented in table 5-1.

Table 5-1 Model Specification for ex vivo cadaver testing and in vivo mimic.

PREFIX*	NAME	PLACEMENT / CALCULATION
Surface Markers		
L or R	asis_Ant	In common with BMC, over anterior aspect of pelvic ASIS bony landmark.
L or R	medEpi	In common with BMC, at centre of medial epicondyle bony prominence at the knee.
L or R	latEpi	In common with BMC, at centre of lateral epicondyle bony prominence at the knee.
L or R	asis_Lat	Over lateral aspect of pelvic ASIS bony landmark to define true inter-ASIS bony line.
L or R	psis	Over pelvic PSIS landmarks as an alternative to a single mid-PSIS BMC marker.
	Sacrum	A few cm below mid-PSIS location to form posterior CAST tracking cluster.
L or R	antThigh	Gold standard HJC tracking 1 of 3 - On anterior aspect of thigh a few cm above patella.
L or R	medThigh	Gold standard HJC tracking 2 of 3 - On antero-medial aspect of thigh a few cm above antThigh.
L or R	latThigh	Gold standard HJC tracking 3 of 3 - On antero-lateral aspect of thigh a few cm above antThigh.
Virtual Markers		
L or R	midEpi	In common with BMC, at mid-point of latEpi and medEpi surface markers.
L or R	asis_True	Projection of asis_Ant marker onto Lasis_Lat – Rasis_Lat line.
	midAsis	Mid-point of Lasis_True and Rasis_True.
L or R	hipHarr	Posterior, lateral and inferior offsets from midAsis provided by the Harrington regression equation (Harrington et al., 2007) during the initial neutral position test; this location tracked between tests by the Lpsis, Rpsis and Sacrum cluster.
L or R	hipGold	hipHarr location from initial neutral position test, tracked via antThigh, medThigh and latThigh marker cluster which are STA insulated by the experimental design.
L or R	_HJC	Proximal end of thigh Length vector from midEpi to hipHarr.
Subject Metrics		
L or R	thigh Length	Distance from midEpi to hipHarr established during the initial neutral position test.
Anatomical Reference Frame (ARF)		
	Pelvis (All versions)	Principal axis from Lasis_True to Rasis_True with midPsis defining principal transverse plane.
Technical Reference Frame (TRF)		
	Pelvis_Gold	LhipGold, RhipGold and midPSIS virtual marker location.
	Pelvis_CGM	Pelvic crest surface markers at Lasis_Ant, Lpsis, Rasis_Ant, and Rpsis.
	Pelvis_CAST	Posterior cluster consisting of Lpsis, Rpsis and Sacrum surface markers.
	Pelvis_RNOH	L_HJC, R_HJC and midPSIS virtual marker locations.
		**** L or R corresponds to left or right side respectively***

5.3.4 Laboratory Set-up

A fresh-frozen cadaveric left leg, consisting of a hemi-pelvis, thigh, shank and foot segments with all soft tissue fully intact, was sourced from a reputable source

within the United States of America (Anatomy Gift Register). The subject was female aged 47 with a BMI of 20, ambulatory and RIP secondary to widespread cancer.

The leg was supplied in an insulated polystyrene box packed with solid carbon dioxide (dry ice). On receipt the leg was unpacked and stored in a -20°C freezer until required. One day prior to testing, it was removed from the freezer and placed in a supportive sling constructed from a polythene sheet stretched over a large open topped cardboard box. A small hole at the centre of the sheet allowed any defrosting liquids to be cleanly collected in a small polythene bag. In actuality, these liquids were minimal in volume, and the defrosting assembly performed little additional function. The whole assemble was stored overnight in a cold air-conditioned room ready for testing the next day (Figure 5-5).

Figure 5-5 Defrosting assembly for cadaveric leg

The specimen was held on a supportive polythene sheet over night to defrost.

5.3.4.1 Test Subject

Similar marker placement protocols were employed to collect data from one cadaveric leg, and on a separate occasion from the left leg of the author.

5.3.5 Data Collection

On the day of ex-vivo testing, the cadaveric leg was removed from the defrosting assembly and the medial surface of the hemi-pelvis mounted to the top of a vertical frame, such that the leg hung freely downward with unrestricted passive movement available at all articulations. Bone pins were inserted through the soft tissue on the medial aspects of the thigh and shank segments, to gain firm attachment into the femur and tibia bones. These bone pins provided two functions. Firstly, they provided attachment points for hand grips from which independent passive movements of the hip and knee joints could be applied. Second, they provided attachment points for rigid marker cluster triads, to provide a STA free, gold-standard measure of these movements. Surface markers were glued to the skin surface as per the biomechanical models (Table 5-1).

Figure 5-6 Cadaveric leg mounted in test rig

Left - femoral and tibial bone pins and glued surface markers. Right – close-up of knee region showing TRF markers attached to the bone pins, and also illustrating the relative laxity of the anterior soft tissue structures.

Prior to testing all TRFs were spatially synchronised to the common ARF during a static calibration trial with the limb hanging in a neutral posture (Figure 5-6). Full range dynamic axial rotation movements of the cadaveric thigh were then applied in various degrees of approximately fixed hip and knee flexion angles. Each movement consisted of approximately 10 full range oscillations, with each condition representing different tensioning of the femoral soft tissue covering. For each test, the applied hip and knee flexion angle was record as the average of the bone-pin measured values. Positional offset differences in the measured axial rotation between solutions were removed by subtraction of mean test value from all solutions – all results then oscillated around a zero mean. Evaluation metrics were calculated as the average absolute difference (equivalent to movement pattern score – developed in chapter 2) between the kinematic produced by each tracking solution and the gold standard bone-pin measure, through the entirety of the test movement.

In vivo testing of the axial rotation movement mimicked that of the in vitro testing, without the bone-pin gold standard measure. Testing was restricted to a single subject (the author), standing on the right leg with the left knee appropriately flexed. Surface marker placements mimicked that employed for the ex-vivo testing. In the absence of any bone-pin tracking, the thigh_plane tracking solution, validated as part of the ex vivo testing, assumed the role of a gold standard measure.

5.3.6 Data analysis

5.3.6.1 Signal Processing

A common thigh ARF was defined using the standard coronal principal plane between a HJC location inherited from the pelvis in conjunction with medial and lateral epicondyle surface markers. Multiple TRFs were defined to represent different tracking solutions to this ARF. The gold standard TRF, thigh_bone, employed a triad of three markers rigidly fixed to the thigh bone pin. All other TRFs employed the hip and knee joint centres to track the segments principal axis, plus one surface marker to track the spin of this axis. Spin tracking markers were arranged in distal to proximal linear arrays on the anterior and lateral aspect

of the thigh. Each array consisted of 6 markers labelled 0 to 5, where 0 represented the most distal anterior patella and lateral epicondyle marker of each array. These solutions were denoted thigh_ant0 and thigh_lat0 respectively, with higher integers denoting the more proximal solutions. An addition proximal marker extended the lateral array to the greater trochanter bony landmark, denoted thigh_GT.

Finally, the ability of the plane defined by hip, knee, and ankle joint centres to track the thigh axial rotation was tested with a solution denoted thigh_plane. In common with other solutions, thigh_plane tracked the segments principal axis via the pelvic tracked HJC (fixed) and shank tracked KJC locations. Axial spin was tracked via a virtual marker located along the HJC – AJC line, which forms the open boundary of the required plane. In order to minimise the effect of any inadvertent knee flexion movement during the dynamic tests, this virtual location was defined a fixed distance (200mm) from the HJC end of this line (Figure 5-7).

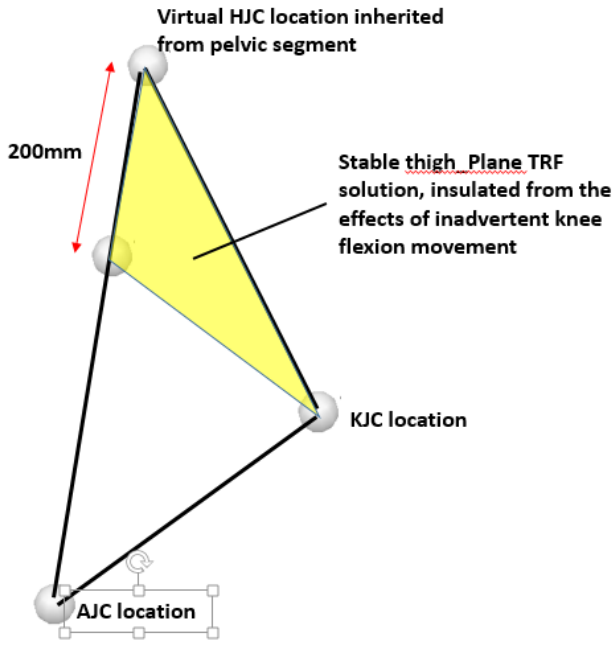

Figure 5-7 Gold standard plane for in-vivo thigh axial rotation

Like the RNOH_Thigh, the plane defined by hip, knee and ankle joint centres with the knee flexed, is assumed to track thigh axial rotation. Although all tests attempted to maintain fixed hip and knee flexion angles, the effects of any inadvertent sagittal plane movements are mitigated by creation of a stable triangle in the required plane.

5.3.6.2 Statistics

Ex vivo evaluation of HJC-KJC-AJC plane to act as a gold standard measure of thigh axial rotation movement. The average absolute-mean-difference between the HJC-KJC-AJC plane, and bone-pin tracking of thigh axial rotation were calculated for each test condition at different knee flexion angles. A threshold of 2° error was set for establishing the minimum knee flexion required to produce a stable measurement by the planar method.

The effect of knee and hip joint angle on the ability of various axial rotation tracking solutions was also investigated. Each solution consisted of common HJC and KJC locations, plus one surface marker from either the anterior or lateral array. Errors for each tracking solution were evaluated against the ex-vivo bone-pin and in vivo planar gold standard measure of thigh axial rotation. These errors where then correlated to either the hip or knee joint angle test condition.

The final testing concerned the effect of distal to proximal placement of additional TRF marker on axial tracking accuracy. Using average test values over the full range of hip and knee positions, mean and standard deviation axial tracking errors are calculated for each tracking solution. Best fit regression lines are sought to describe the relationship between marker placement height and axial rotation error, for both the anterior and lateral marker arrays. Where appropriate, linear relationships are additionally sought within a range of confined marker heights.

5.3.7 Results 1a Establishing a Non-invasive Gold Standard Measure

At high knee flexion angles, the HJC-KJC-AJC plane shows good agreement with the bone-pin gold standard measure of thigh axial rotation (Figure 5-8). At 30° of knee flexion kinematic errors average approximately 2°. Above 60°, average errors were fractions of a degree.

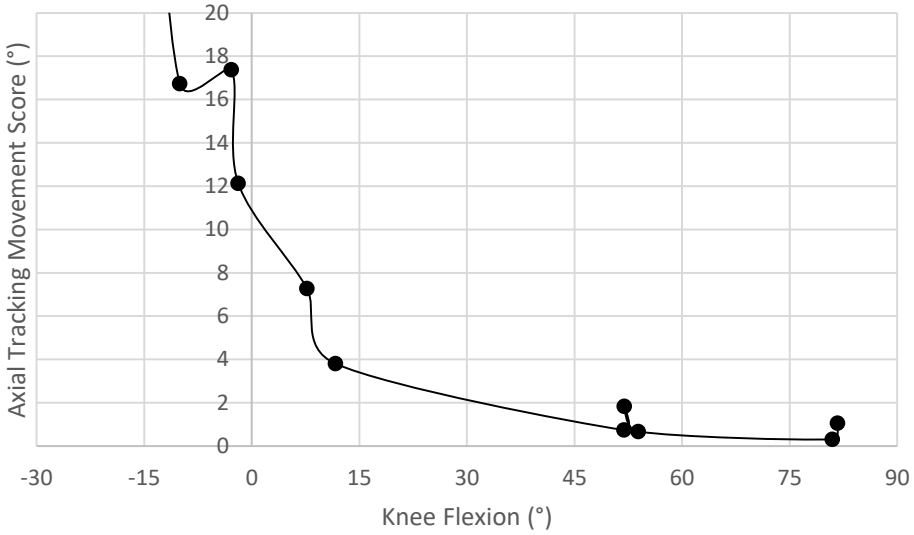

Figure 5-8 Ex vivo evaluation of HJC-KJC-AJC plane

Femoral bone pin gold standard measure of thigh axial rotation plotted against knee flexion angle Collinearity of the HJC,KJC, AJC locations at knee flexion angles of less than 30° results in significant disagreement; above this angle the defined plane is a good surrogate.

The *primary hypothesis 5A_I* for this experiment, that with sufficient knee flexion, the HJC-KJC-AJC plane can act as a reasonable representation of the thigh segment axial rotation movement is therefore accepted.

In-vivo testing, employing this measurement as a gold standard measure of thigh axial rotation, were therefore restricted to knee flexion angles of around 30° and above (Figure 5-9)

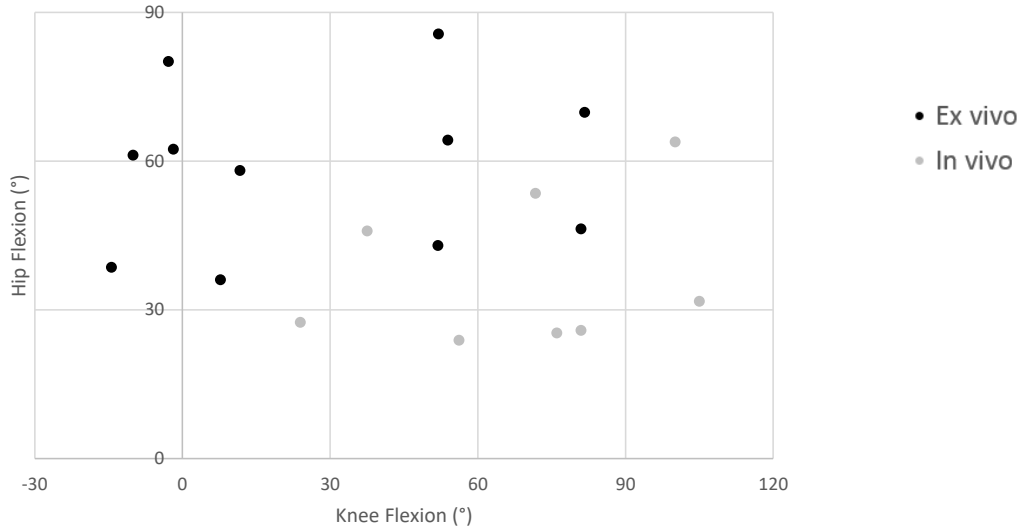

Figure 5-9 Test combinations of hip and knee angles

Each test condition creates different soft tissue tensioning during the passive application of thigh axial spin movement. Ex vivo testing was restricted to knee joint angles above 30°of flexion.

5.3.8 Results 1b Joint driven STA effects

Prior to testing, a large amount of soft tissue laxity was observed around the patella region of the cadaveric specimen (Figure 5-6 Right). This observation was taken into consideration when evaluating the performance of the patella surface marker (ant_0) in the ex-vivo results.

In the in-vivo situation, the accuracy of anterior and lateral placed markers was largely unaffected by the hip joint angle; this was particularly apparent for the lateral markers (Figure 5-10).

	Anterior Marker Array	Lateral Marker Array
Knee Flexion	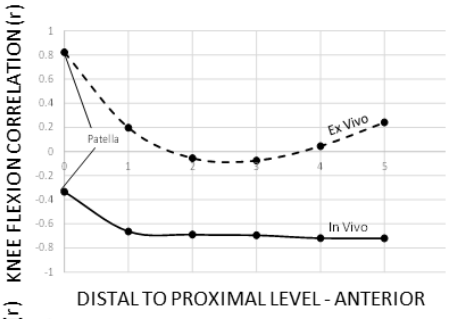	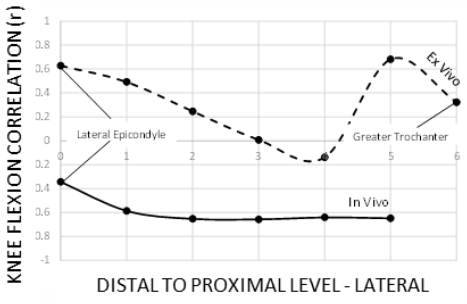
Hip Flexion	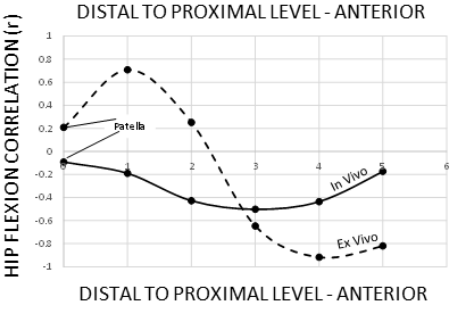	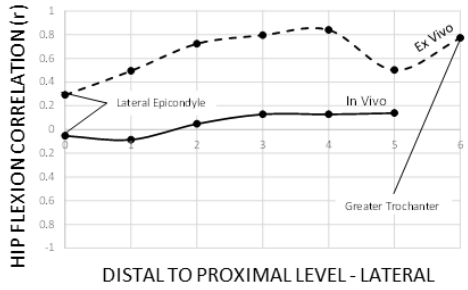

Figure 5-10 Sensitivity of each axial tracking marker to hip and knee flexion

Correlation coefficient of axial spin marker tracking error to knee joint angle (top row) and hip joint angle (bottom row) and for anterior (right column) and lateral (left row) markers at various distal to proximal heights.

In vivo, except for the most distal anterior patella marker and lateral epicondyle marker, all other markers exhibited a negative correlation (r ≈-0.6) with knee flexion angle; as the knee flexion increases tracking accuracy decreases. The patella and lateral epicondyle markers over bony landmarks appear to be insulated from these joint driven STA influences. Deformation of ex-vivo tissue in response to joint movement followed a more complex pattern. Here, correlations of axial rotation tracking errors associated with various marker locations did not follow any simple pattern.

Overall, no convincing distal to proximal axial rotation accuracy effects, of either knee or hip joint were identified. Secondary *hypothesis 5A_II* that thigh axial tracking accuracy will be most affected by the angle of the closest joint, is therefore rejected.

5.3.9 Results 1c Proximal to Distal STA influences

Regression analysis suggests that a distal to proximal in-vivo increases in axial STA effects might be modelled by a simple exponential growth for the anterior marker array (Figure 5-11). These graphs plot the distal-to-proximal placement of each marker against the axial tracking movement score developed in chapter 2. This score is the test average, absolute mean difference between the test condition and gold standard measure. STA for lateral array was well modelled by fourth order polynomial, which was also the preferred regression fit for both the anterior and the lateral ex-vivo marker arrays. All of the polynomial fits also demonstrated a linear mid-region that has the potential to inform on the required parameters for inclusion of the soft tissue movement with the biomechanical model (Andersen et al., 2012).

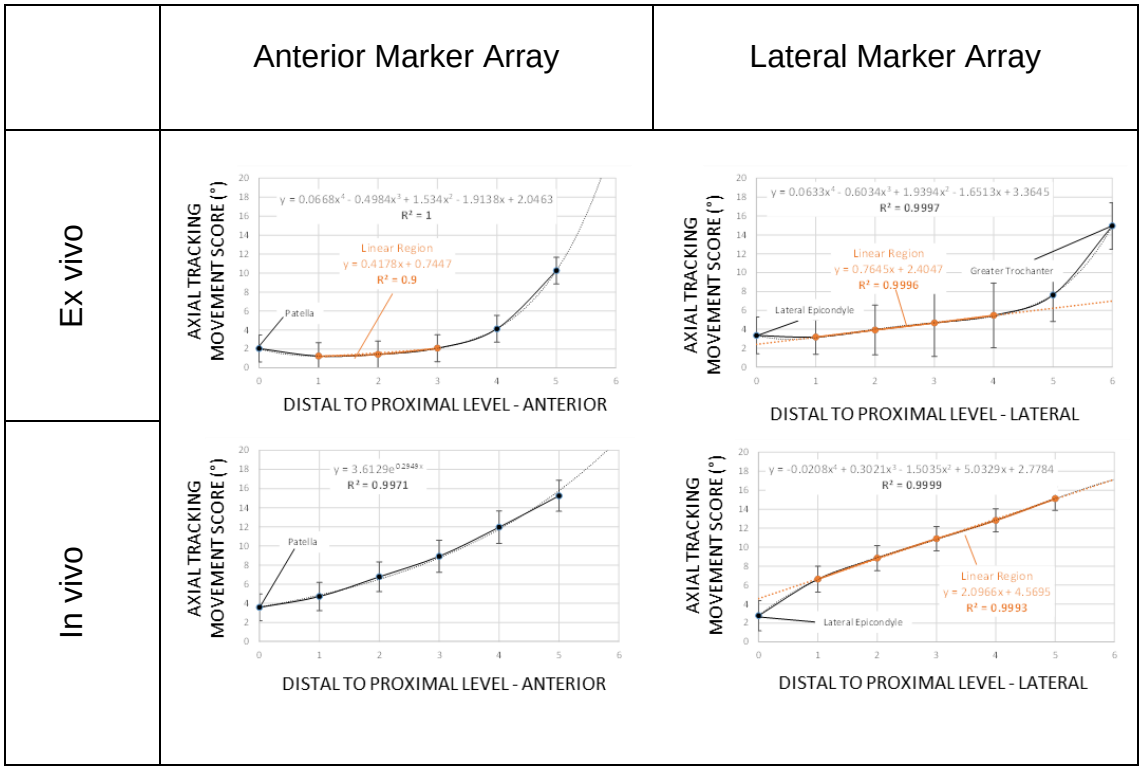

Figure 5-11 STA proximal to distal regression equation

Test average and standard deviation axial tracking error for anterior (left column) and lateral (right column) thigh surface markers at various heights. Ex-vivo results (top row) are from a single cadaveric specimen. In-vivo results are also from a single subject.

Despite different deformation characteristics of the in-vivo and ex-vivo soft tissue, both experimental conditions showed broad agreement on the distribution of STA

error in tracking axial rotation of the thigh. Generally, more proximal markers suffered more error, with the most distal anterior patella and lateral epicondyle markers performing best in the in-vivo situation. These locations were only mildly outperformed by the next most distal contender in the ex-vivo testing.

Tertiary Hypothesis 5A_III, predicting the superiority of anterior distal markers to track axial rotation of the thigh, with the patella marker proving optimal for this purpose, is therefore accepted.

5.4 Experiment 5B – Dynamic Gait Trials

5.4.1 Aims

This experiment aims to evaluate a distally located CAST tracking cluster, and the RNOH tracking solutions against the BMC reference values established in chapter 2.

The BMC-model employed the HJC location inherited form the pelvis in conjunction with surface marker located over medial and lateral epicondyle bony landmarks, to both define and track the thigh segment principal axis. This model provided direct representation of the required CGM principal plane, without the unpredictable errors associated with placement of an additional lateral thigh marker, or the associated mitigating adjustments to its placement.

An additional condition tests the combination of the development RNOH TRF, and the full RNOH TRF plus ARF (RNOH_Thigh) against the BMC reference.

5.4.2 Hypothesis

Hypothesis 5B_I. A distal thigh CAST tracking cluster will capture a similar transverse plane kinematic to the BMC solution, which also employs distal medial and lateral epicondyle markers for the same purpose. Nonrepresentation of the proximal end of the segment may well cause the CAST solution to misrepresent sagittal and coronal components.

Hypothesis 5B_II. The RNOH tracking solution will capture considerably more transverse plane rotation than the BMC solution, without fundamentally changing the kinematic form in any plane.

Hypothesis 5B_III. The RNOH axial alignment solution will show good axial alignment of the thigh segment, thus maintaining a low amplitude coronal plane knee kinematic, similar to the BMC reference value.

Hypothesis 5B_IV. Captured range of thigh motion will show a tendency to decrease with increasing subject BMI. Secondarily, the RNOH solution, which employs the minimum number of thigh surface markers will be least affected by this phenomenon.

5.4.3 Methods

5.4.3.1 Model Specification

In addition to the BMC surface markers, an additional marker was located centrally over the patella to provide the base co-ordinates for virtual representations used to axially align and track RNOH_Thigh segment. Additional TRF surface markers were also applied to low STA regions of the shank segment (Figure 5-12).

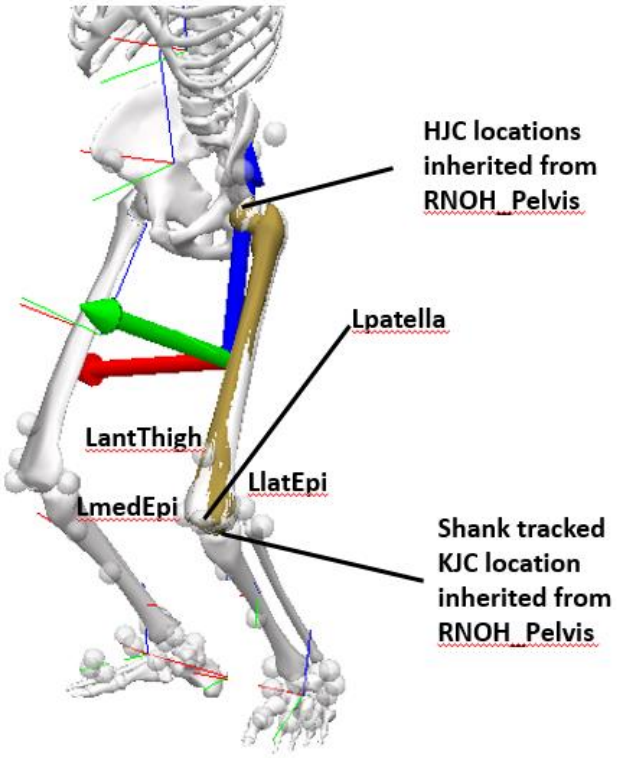

Figure 5-12 Surface marker and inherited locations employed to model left thigh segment

The principal axis of the thigh is defined between a pelvic HJC location and shank tracked KJC location. A single marker located over the patella tracks the spin of this axis.

Formal definition of all tested thigh models are outlined in table 5-2.

Table 5-2 Model specification for thigh segment dynamic gait trials

PREFIX	NAME	PLACEMENT / CALCULATION
Surface markers		
Thigh		
L or R	latEpi	In common with BMC, at the centre of lateral epicondyle bony prominence at the knee
L or R	medEpi	In common with BMC, at the centre of medial epicondyle bony prominence at the knee
L or R	patella	Central patella marker
L or R	antThigh	Additional tracking marker on anterior aspect of thigh, 5-10cm above patella marker.
Shank		
L or R	fibHead	Proximal lateral tracking marker over the fibular head bony landmark
L or R	proxShin	Proximal antero-medial tracking marker on the upper bony shin region
L or R	distShin	Distal antero-medial tracking marker on the lower bony shin region
L or R	latMal	In common with BMC, at the Tip of lateral malleoli bony prominence at the ankle
L or R	medMal	In common with BMC, at the tip of medial malleoli bony prominence at the ankle
Virtual markers		
L or R	_HJC	Hip joint centre location inherited from RNOH_Pelvis segment
L or R	midEpi	Mid-point of latEpi and medEpi surface markers
L or R	_KJC	midEpi location tracked via the shank TRF
L or R	midMal	Mid-point of latMal and medMal surface markers.
L or R	patella_align	Lpatella projected into the HJC-KJC-midmal plane during a crouched calibration trial.
L or R	patella_track	KJC projected onto HJC –patella line.
Anatomical reference frame (ARF)		
L or R	thigh_BMC	Principal axis from HJC to midEpi with latEpi defining principal coronal plane.
L or R	thigh_CAST	As for thigh_BMC
L or R	thigh_RNOH	Principal axis from HJC to KJC with patella_align defining principal sagittal plane.
L or R	shank	Principal axis from KJC to midMal with latMal defining principal coronal plane.
Technical reference frames (TRF)		
L or R	thigh_BMC	HJC virtual marker with medEpi and latEpi surface markers.
L or R	thigh_CAST	latEpi, medEpi and antThigh surface markers
L or R	thigh_RNOH	L_HJC, L_KJC and Lpatella_track virtual markers.
L or R	shank	LfibHead, LproxShin, LdistShin, LlatMal and LmedMal surface markers

L or R corresponds to left or right side respectively

5.4.4 Laboratory Set-up

Data was collected concurrently with that for the BMC reference values presented in chapter 2.

5.4.5 Data Analysis

5.4.5.1 Signal Processing

The BMC (CGM surrogate) model employed the HJC location inherited form the pelvis in conjunction with surface marker located over medial and lateral epicondyle bony landmarks, to both define and track the thigh segment principal axis. The CAST solution employed the same ARF as the BMC reference but tracked segment movement via a triad of individual surface markers around the knee (see table 5-2). The RNOH_TRF solution also employed the common ARF definition but tracked the thigh movement via a HJC location inherited from the pelvis, KJC location tracked via the shank, and the virtual representation of the patella surface marker, developed to mitigate the unrequired vertical movement component. Finally, the full RNOH solution (RNOH_Thigh) is defined by RNOH_TRF plus a similarly defined ARF that employs a different representation of the patella marker, this time projected into the local sagittal plane of the segment during the crouched static calibration pose.

Like the previously developed segments, visual inspection of the kinematic and gait scores by various tracking solutions against BMC reference values are expected to show subtle differences only. The concurrent nature of the data collection adopted for dynamic trails throughout this thesis however, ensured that these differences were caused by the choice of solution and not hidden by inter-session variation in walking pattern. Simple paired t-test and linear regression statistics are employed to highlight significant differences with the BMC reference values.

For each tested solution, data is presented for both the thigh segment orientation, and its effect on the knee joint kinematic for all three planes of movement.

5.4.5.2 Statistics

For each tracking solution under investigation. Paired t-test were applied across all gait scores, to identify statistically significant differences with BMC reference values.

Correlation coefficients were calculated for each gait score, against subject BMI. Correlations above 0.5 ($R^2 > 0.25$) are highlighted in the solution designated colour; red for the CAST, solution and blue for RNOH solutions.

5.4.6 Results 2a CAST tracking solution

5.4.6.1 CAST sagittal kinematic

Figure 5.13 compares the sagittal kinematics for the thigh segment, from the CAST tracking solution, employing a distal thigh cluster, and the BMC reference solution.

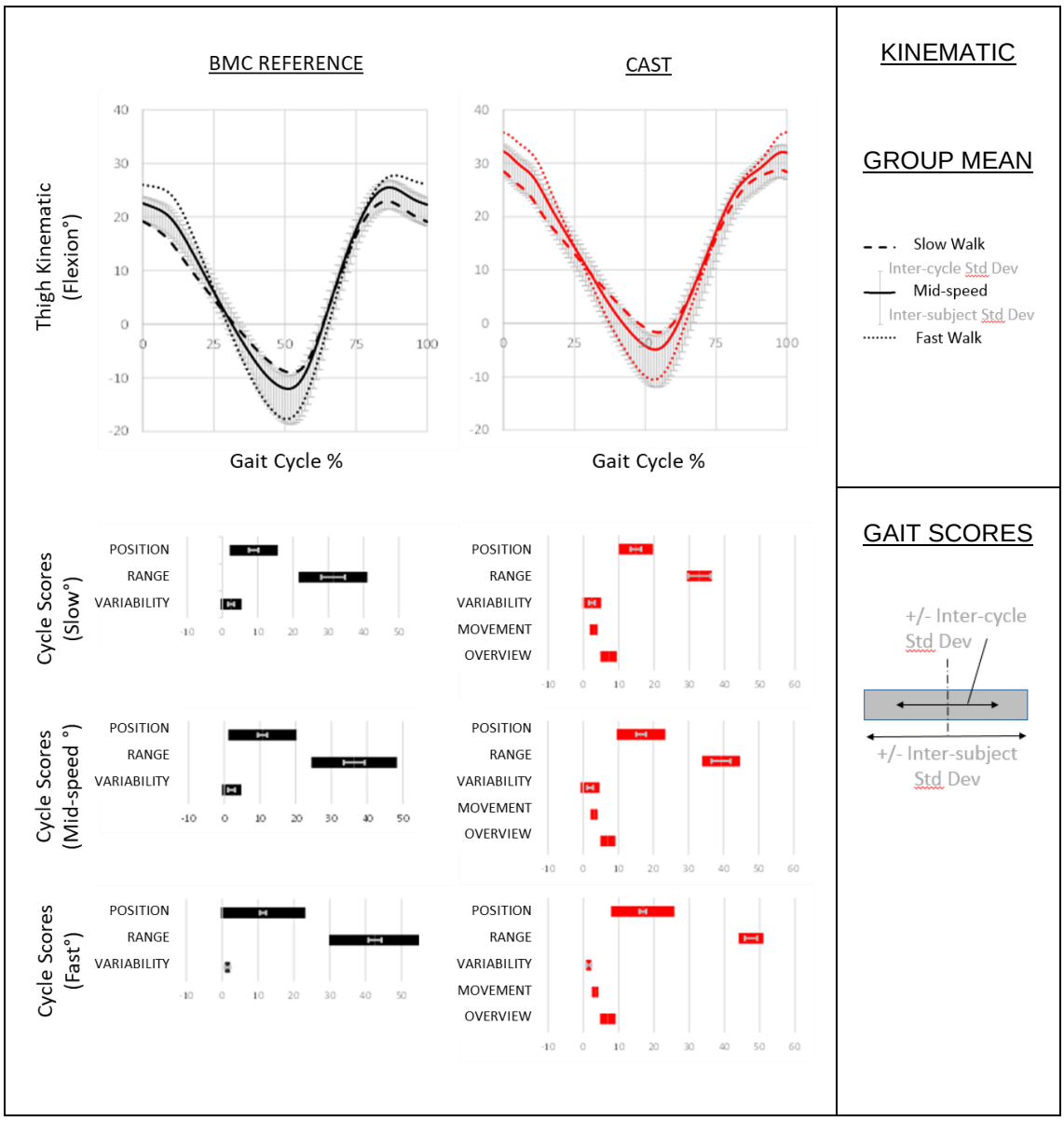

Figure 5-13 CAST tracking solution for thigh- Sagittal

Thigh sagittal plane comparison of CAST tracking solution (right column) with BMC reference (left column).

Top row shows graphical kinematic for slow (dashed line), mid-speed (solid line) and fast (dotted line) walking as depicted in the legend (right). The mid-speed typical inter-cycle, and inter-subject standard deviations are shown above and below the mid-speed graph line respectively.

Subsequent rows depict speed specific gait scores as per the legend (right bottom). Cycle position, range and variability scores represent absolute values from zero. Movement pattern and overview scores measure the difference between comparative and BMC reference values.

The CAST solution kinematic shows a clear positional offset, more extended throughout the cycle. Subtleties in the shape of late swing kinematic are also lost. The resultant sagittal knee kinematic is shown in figure 5-14.

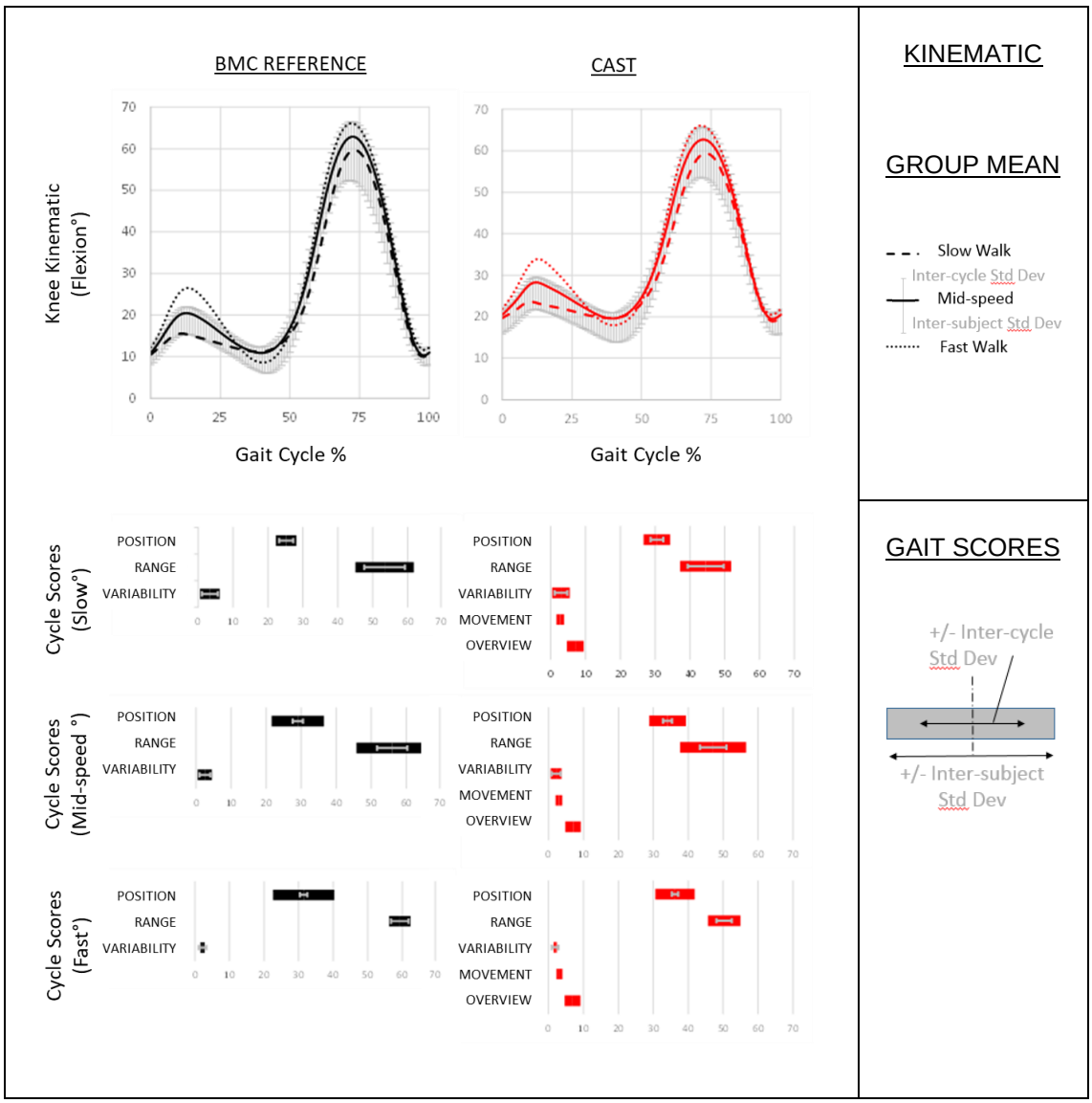

Figure 5-14 CAST tracking solution for knee- Sagittal

Knee sagittal plane comparison of CAST tracking solution (right column) with BMC reference (left column).

Top row shows graphical kinematic for slow (dashed line), mid-speed (solid line) and fast (dotted line) walking as depicted in the legend (right). The mid-speed typical inter-cycle, and inter-subject standard deviations are shown above and below the mid-speed graph line respectively.

Subsequent rows depict speed specific gait scores as per the legend (right bottom). Cycle position, range and variability scores represent absolute values from zero. Movement pattern and overview scores measure the difference between comparative and BMC reference values.

Expression of the CAST_Thigh solution extension shift in the knee kinematic results to a 20° average at initial contact. This abnormally high value confirms the impression form the sagittal thigh comparison, that the CAST solution is aberrant.

5.4.6.2 CAST coronal kinematic

Figures 5-15 and 5-16 show the CAST and BMC comparison kinematic for the thigh and knee coronal kinematics.

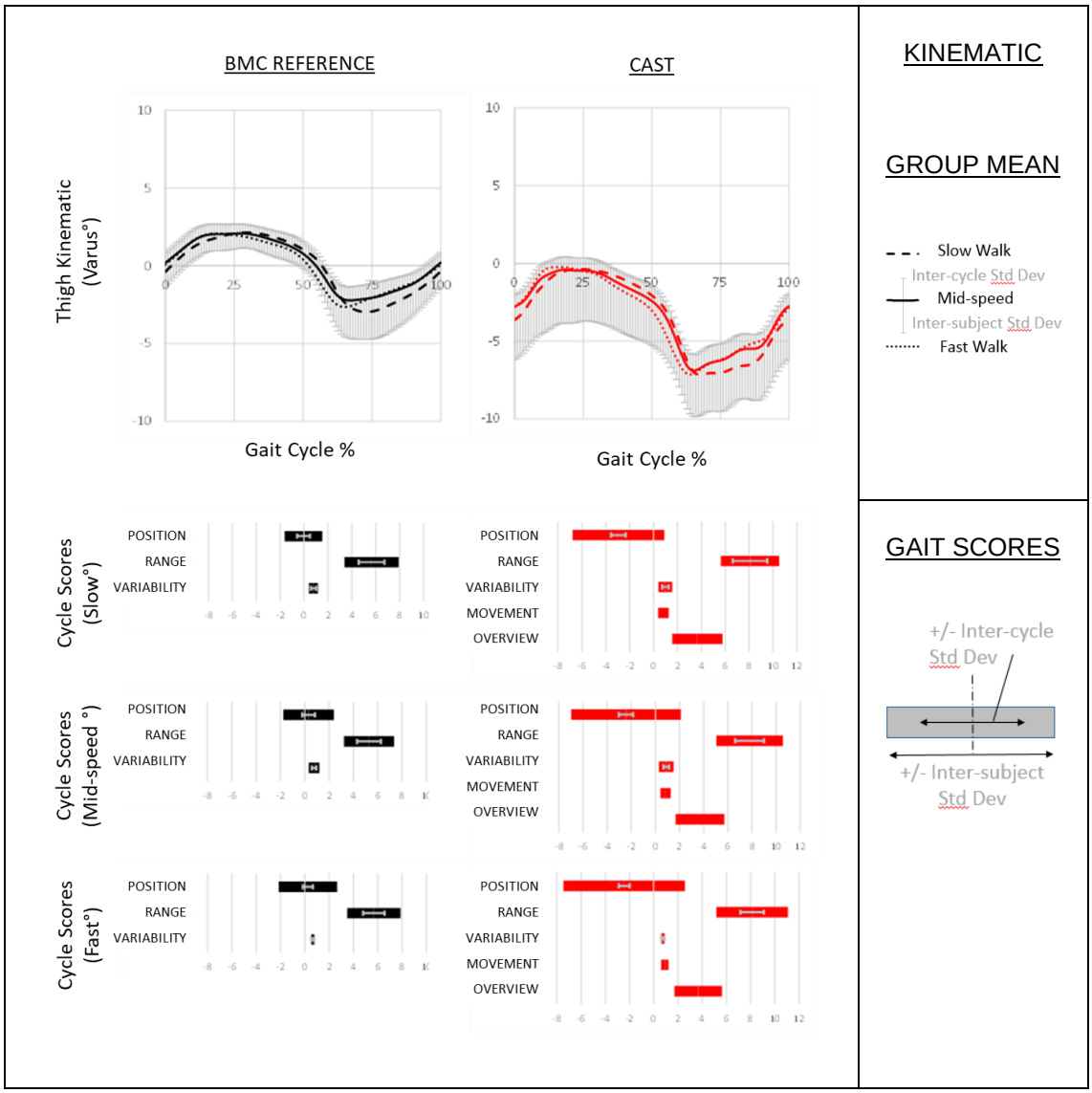

Figure 5-15 CAST tracking solution for thigh- Coronal

Thigh coronal plane comparison of CAST tracking solution (right column) with BMC reference (left column).

Top row shows graphical kinematic for slow (dashed line), mid-speed (solid line) and fast (dotted line) walking as depicted in the legend (right). The mid-speed typical inter-cycle, and inter-subject standard deviations are shown above and below the mid-speed graph line respectively.

Subsequent rows depict speed specific gait scores as per the legend (right bottom). Cycle position, range and variability scores represent absolute values from zero. Movement pattern and overview scores measure the difference between comparative and BMC reference values.

The CAST thigh kinematic looks to have introduced an increased range of motion and significant valgus offset of the BMC reference.

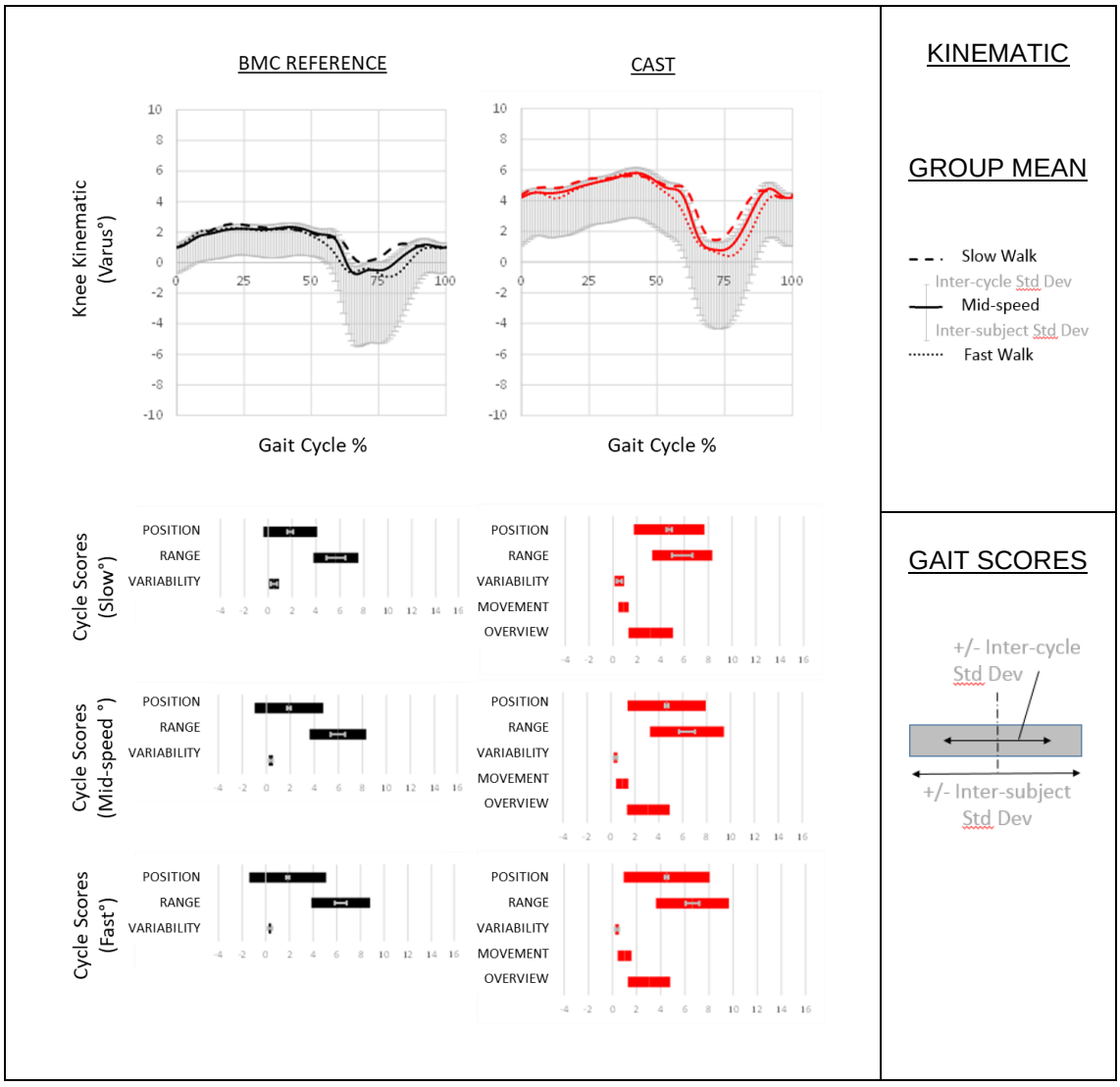

Figure 5-16 CAST tracking solution for knee- Coronal

Knee coronal plane comparison of CAST tracking solution (right column) with BMC reference (left column).

Top row shows graphical kinematic for slow (dashed line), mid-speed (solid line) and fast (dotted line) walking as depicted in the legend (right). The mid-speed typical inter-cycle, and inter-subject standard deviations are shown above and below the mid-speed graph line respectively.

Subsequent rows depict speed specific gait scores as per the legend (right bottom). Cycle position, range and variability scores represent absolute values from zero. Movement pattern and overview scores measure the difference between comparative and BMC reference values.

The valgus shift in the CAST_Thigh position results in a varus shift in the CAST knee kinematic, away from the near neutral BMC reference signal average.

5.4.6.3 CAST transverse kinematic

Transverse plane results for the CAST_Thigh and resultant knee kinematic are shown in figures 5-17 and 5-18 respectively.

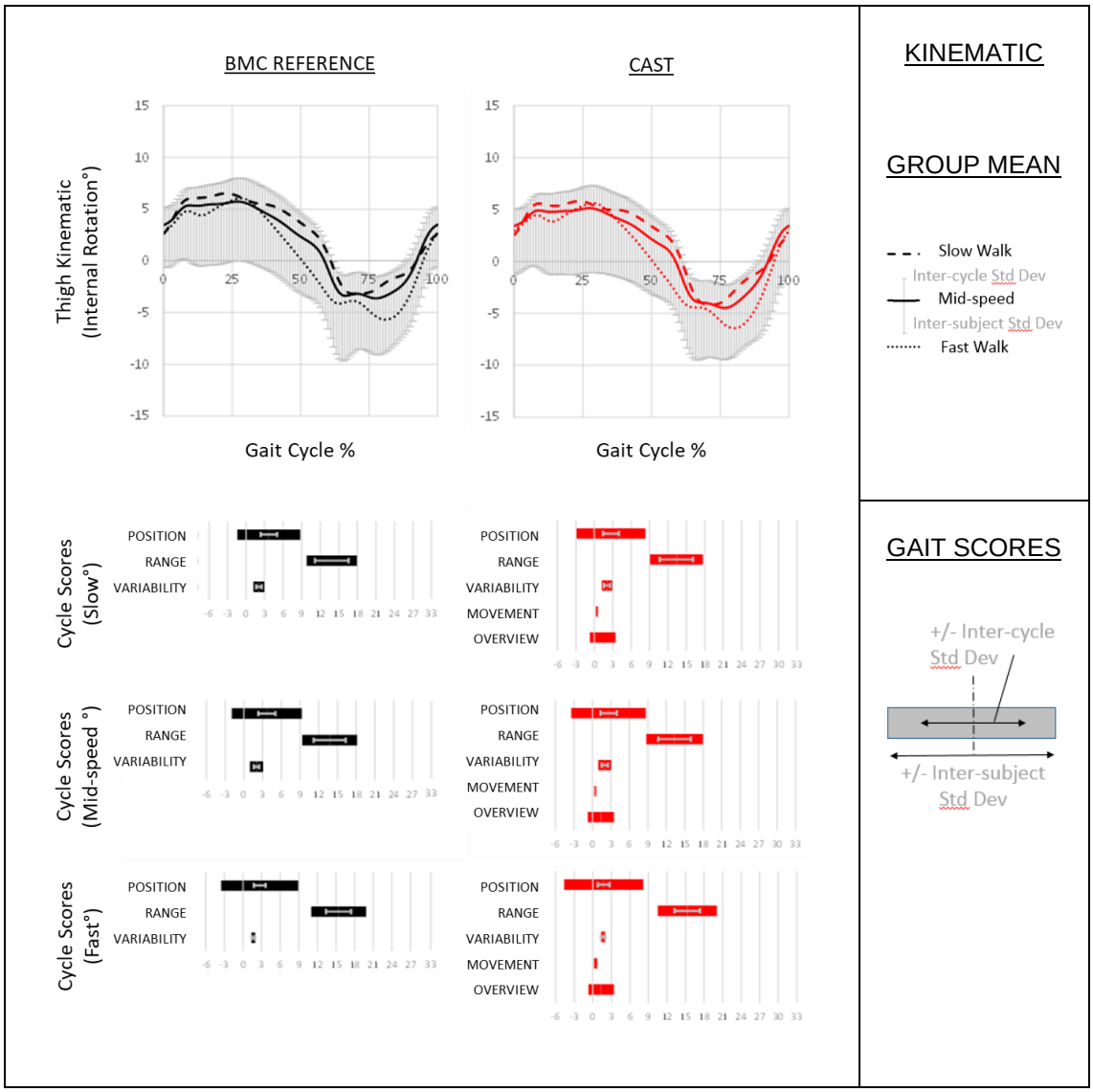

Figure 5-17 CAST tracking solution for thigh- Transverse

Thigh transverse plane comparison of CAST tracking solution (right column) with BMC reference (left column).

Top row shows graphical kinematic for slow (dashed line), mid-speed (solid line) and fast (dotted line) walking as depicted in the legend (right). The mid-speed typical inter-cycle, and inter-subject standard deviations are shown above and below the mid-speed graph line respectively.

Subsequent rows depict speed specific gait scores as per the legend (right bottom). Cycle position, range and variability scores represent absolute values from zero. Movement pattern and overview scores measure the difference between comparative and BMC reference values.

The CAST and BMI thighs both employ the distal medial and lateral epicondyle surface markers as two of the three tracking locations. The transverse plane thigh kinematic form the two solutions are visually indistinguishable.

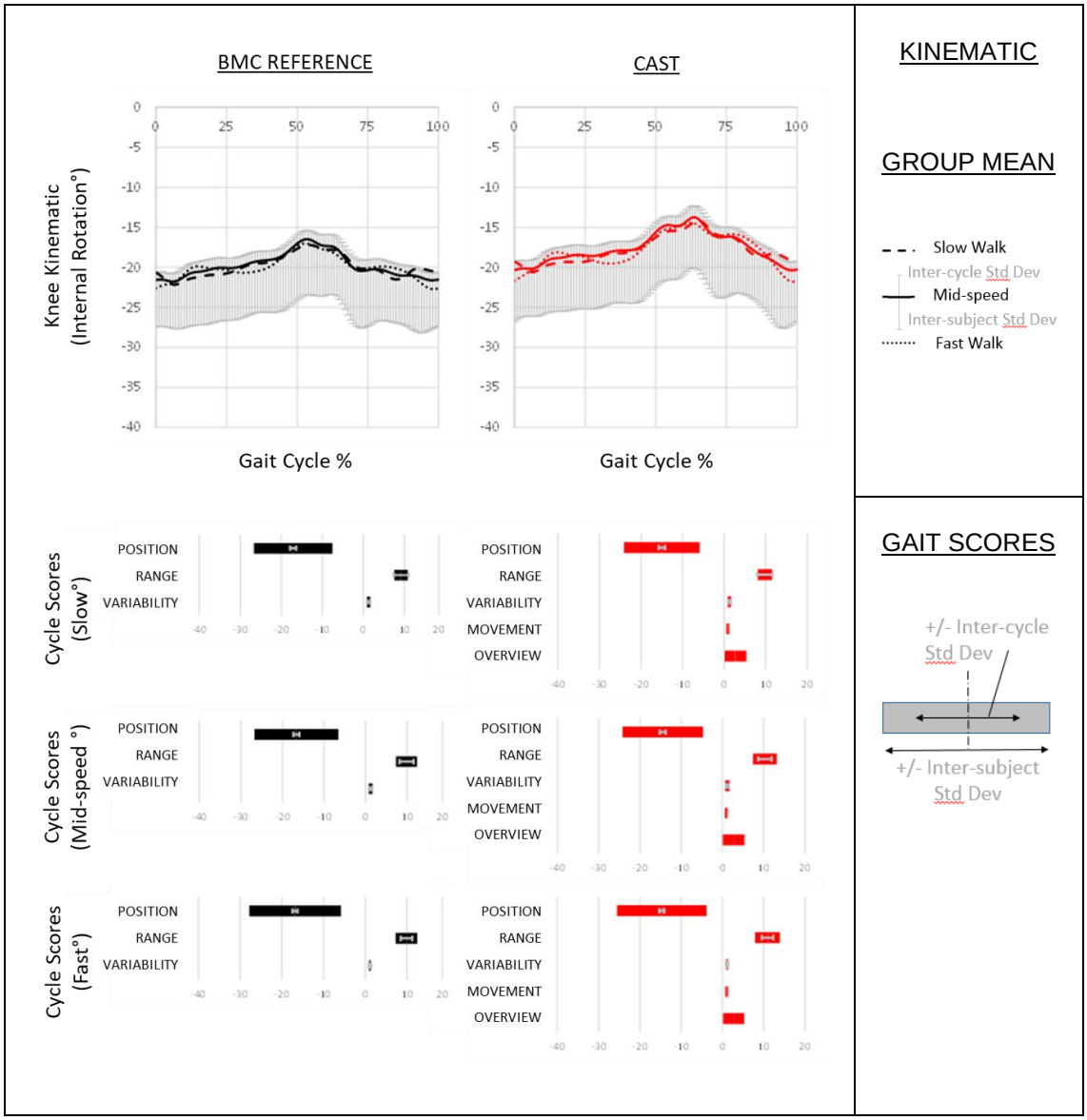

Figure 5-18 CAST tracking solution for knee- Transverse

Knee transverse plane comparison of CAST tracking solution (right column) with BMC reference (left column).

Top row shows graphical kinematic for slow (dashed line), mid-speed (solid line) and fast (dotted line) walking as depicted in the legend (right). The mid-speed typical inter-cycle, and inter-subject standard deviations are shown above and below the mid-speed graph line respectively.

Subsequent rows depict speed specific gait scores as per the legend (right bottom). Cycle position, range and variability scores represent absolute values from zero. Movement pattern and overview scores measure the difference between comparative and BMC reference values

An obvious offset difference between the CAST and BMC transverse plane knee kinematic, not visually apparent in the thigh kinematic, demonstrates sensitivity of the measured knee movement to the modelled thigh orientation.

5.4.6.4 CAST - Hypothesis Testing

Table 5-3 highlights statistically significant (p<=0.05 paired T-test) difference between the CAST and BMC reference gait scores.

Table 5-3 CAST gait scores for thigh segment and knee joint

	Thigh Position (°)			Thigh Range (°)			Thigh Variability (°)		
	Sagittal	Coronal	Transverse	Sagittal	Coronal	Transverse	Sagittal	Coronal	Transverse
SLOW	6.79	-3.10	-0.95	1.53	2.42	-0.47	-0.08	0.20	-0.01
p-value	0.000	0.001	0.289	0.607	0.001	0.528	0.547	0.023	0.858
MIDSPEED	6.53	-3.10	-1.05	2.90	2.52	-0.41	-0.08	0.14	-0.01
p-value	0.000	0.000	0.295	0.414	0.000	0.447	0.013	0.032	0.493
FAST	6.19	-3.08	-0.92	4.94	2.45	-0.11	0.02	0.11	0.03
p-value	0.000	0.000	0.334	0.233	0.000	0.798	0.758	0.000	0.490

	Thigh Movement (°)			Thigh Overview (°)		
	Sagittal	Coronal	Transverse	Sagittal	Coronal	Transverse
SLOW	2.90	0.82	0.45	7.12	3.67	1.37
MIDSPEED	3.11	0.84	0.45	7.03	3.70	1.37
FAST	3.31	0.92	0.48	6.92	3.68	1.37

	Knee Position (°)			Knee Range (°)			Knee Variability (°)		
	Sagittal	Coronal	Transverse	Sagittal	Coronal	Transverse	Sagittal	Coronal	Transverse
SLOW	6.13	2.90	2.14	-8.83	0.16	0.63	-0.44	0.05	0.00
p-value	0.000	0.000	0.028	0.000	0.848	0.068	0.001	0.208	0.980
MIDSPEED	5.92	2.80	2.15	-8.84	0.40	0.44	-0.38	0.01	0.00
p-value	0.000	0.000	0.027	0.000	0.662	0.310	0.034	0.696	0.700
FAST	5.75	2.66	2.10	-8.98	0.30	1.06	-0.30	0.03	0.00
p-value	0.000	0.000	0.026	0.000	0.746	0.020	0.000	0.331	0.943

	Knee Movement (°)			Knee Overview (°)		
	Sagittal	Coronal	Transverse	Sagittal	Coronal	Transverse
SLOW	2.73	0.88	0.89	7.07	3.17	2.61
MIDSPEED	2.94	0.94	0.95	6.97	3.13	2.66
FAST	3.13	1.01	1.03	6.90	3.03	2.68

Difference between CAST and reference BMC gait scores for the thigh orientation (top) and knee joint ankle (bottom).

Location of CAST tracking cluster over a region of relatively low soft tissue cover, was successful in capturing more coronal plane thigh movement, without an increase in the range of the coronal knee kinematic. This increase, however, come at a cost in the average cycle position scores, which show the segment

approximately 6 degrees more flexed and 3 degrees more abducted. This shift reflects the inability of the localised CAST cluster to represent movement of the whole thigh segment, resulting in an approximate 9° loss of knee joint range.

As hypothesised, there was no statistically significant difference between the transverse plane range of thigh rotation captured by the CAST tracking solution and the BMC reference. Differences were noted in both the sagittal and coronal plane kinematic; *hypothesis 5B_I* is therefore accepted.

5.4.7 Results 2b RNOH_TRF tracking solution

Data presented in this section compares the RNOH tracking solution against the BMC reference values, with both solutions employing the BMC_Thigh ARF axes definition.

5.4.7.1 RNOH TRF only sagittal kinematic

Figure 5-19 shows the RNOH – BMC sagittal comparison for the thigh.

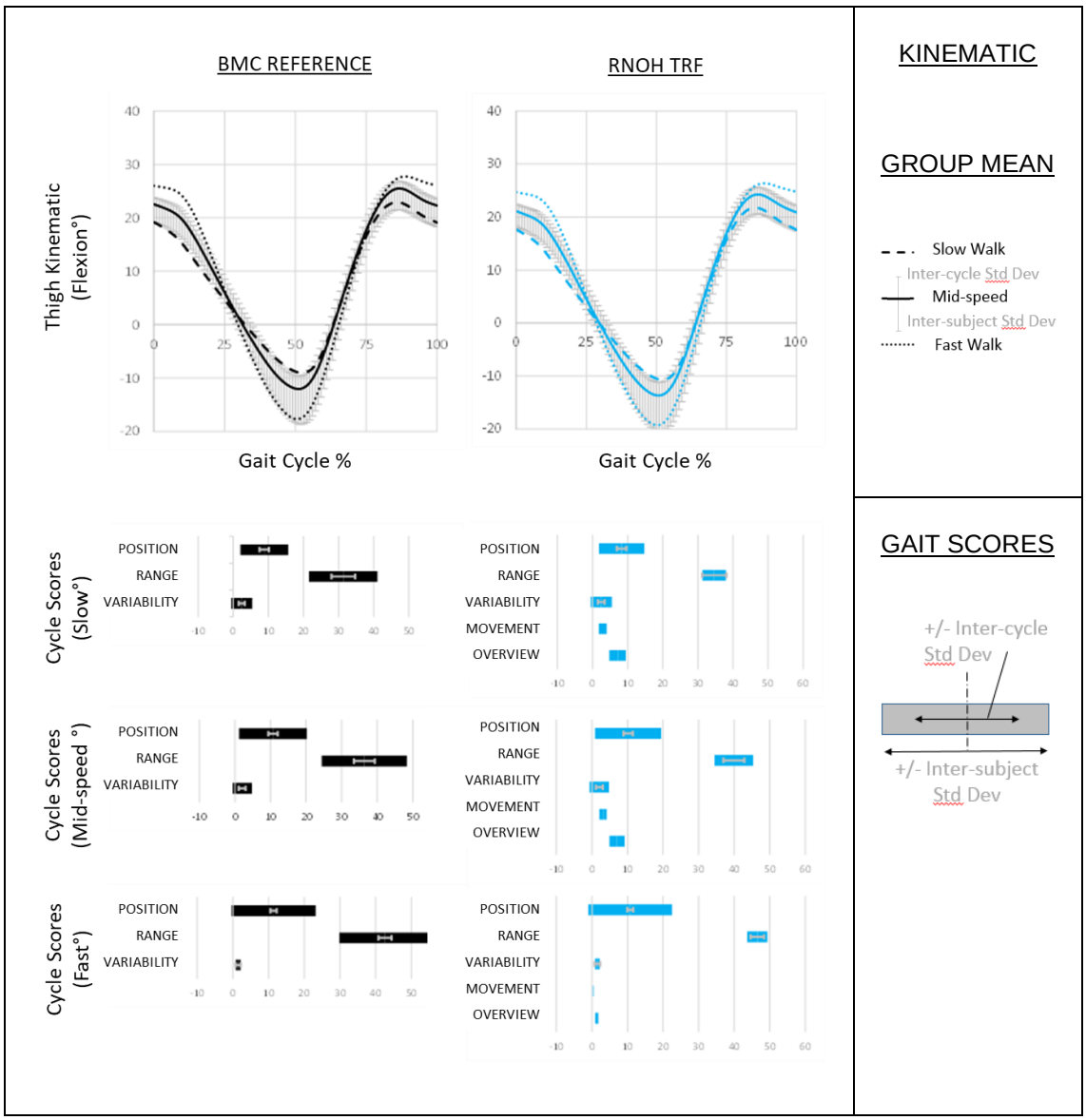

Figure 5-19 RNOH tracking solution for thigh- Sagittal

Sagittal plane comparison of RNOH tracking solution (right column) with BMC reference (left column).

Top row shows graphical kinematic for slow (dashed line), mid-speed (solid line) and fast (dotted line) walking as depicted in the legend (right). The mid-speed typical inter-cycle, and inter-subject standard deviations are shown above and below the mid-speed graph line respectively.

Subsequent rows depict speed specific gait scores as per the legend (right bottom). Cycle position, range and variability scores represent absolute values from zero. Movement pattern and overview scores measure the difference between comparative and BMC reference values.

Sagittal plane differences are small between the two solutions. Effects on the knee kinematic are shown in figure 5-20.

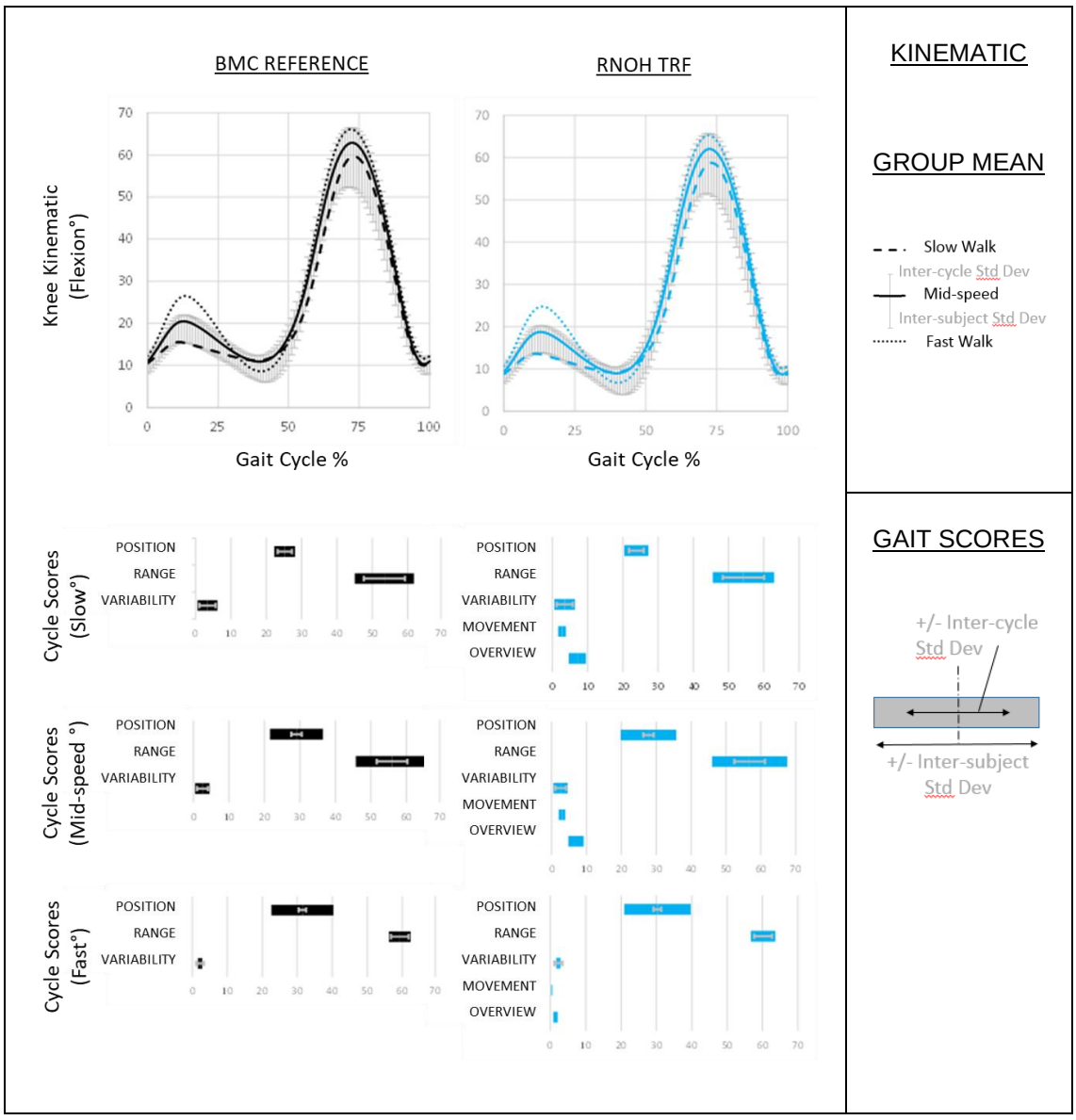

Figure 5-20 RNOH tracking solution for knee- Sagittal

Sagittal plane comparison of RNOH tracking solution (right column) with BMC reference (left column).

Top row shows graphical kinematic for slow (dashed line), mid-speed (solid line) and fast (dotted line) walking as depicted in the legend (right). The mid-speed typical inter-cycle, and inter-subject standard deviations are shown above and below the mid-speed graph line respectively.

Subsequent rows depict speed specific gait scores as per the legend (right bottom). Cycle position, range and variability scores represent absolute values from zero. Movement pattern and overview scores measure the difference between comparative and BMC reference values.

Here again, no visual differences are seen between the sagittal kinematic from the two solutions.

5.4.7.2 RNOH TRF only coronal kinematic

Figures 5-21 and 5-22 compare the RNOH thigh and knee tracking against the BMC reference values.

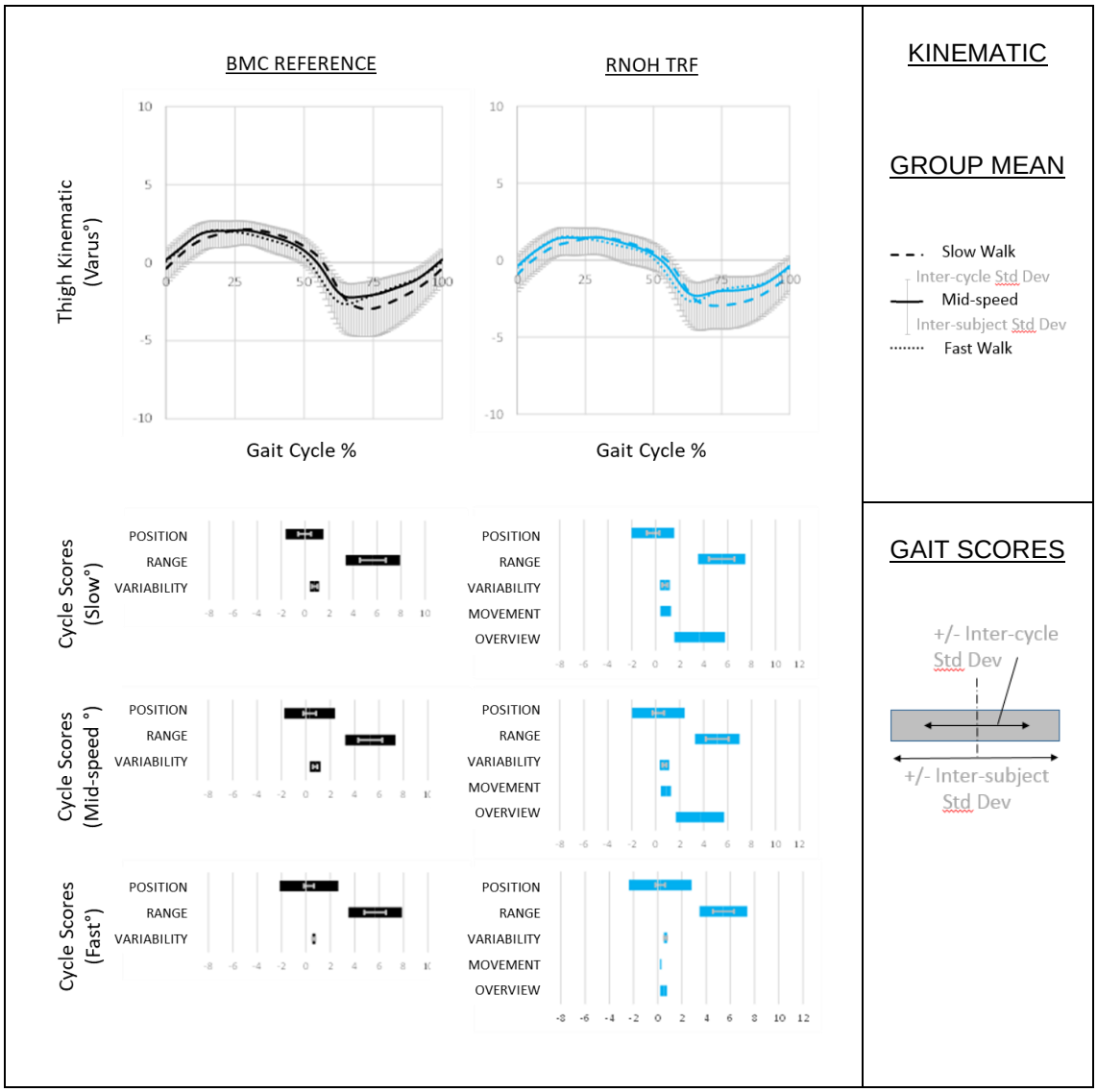

Figure 5-21 RNOH tracking solution for thigh- Coronal

Thigh coronal plane comparison of RNOH tracking solution (right column) with BMC reference (left column).

Top row shows graphical kinematic for slow (dashed line), mid-speed (solid line) and fast (dotted line) walking as depicted in the legend (right). The mid-speed typical inter-cycle, and inter-subject standard deviations are shown above and below the mid-speed graph line respectively.

Subsequent rows depict speed specific gait scores as per the legend (right bottom). Cycle position, range and variability scores represent absolute values from zero. Movement pattern and overview scores measure the difference between comparative and BMC reference values.

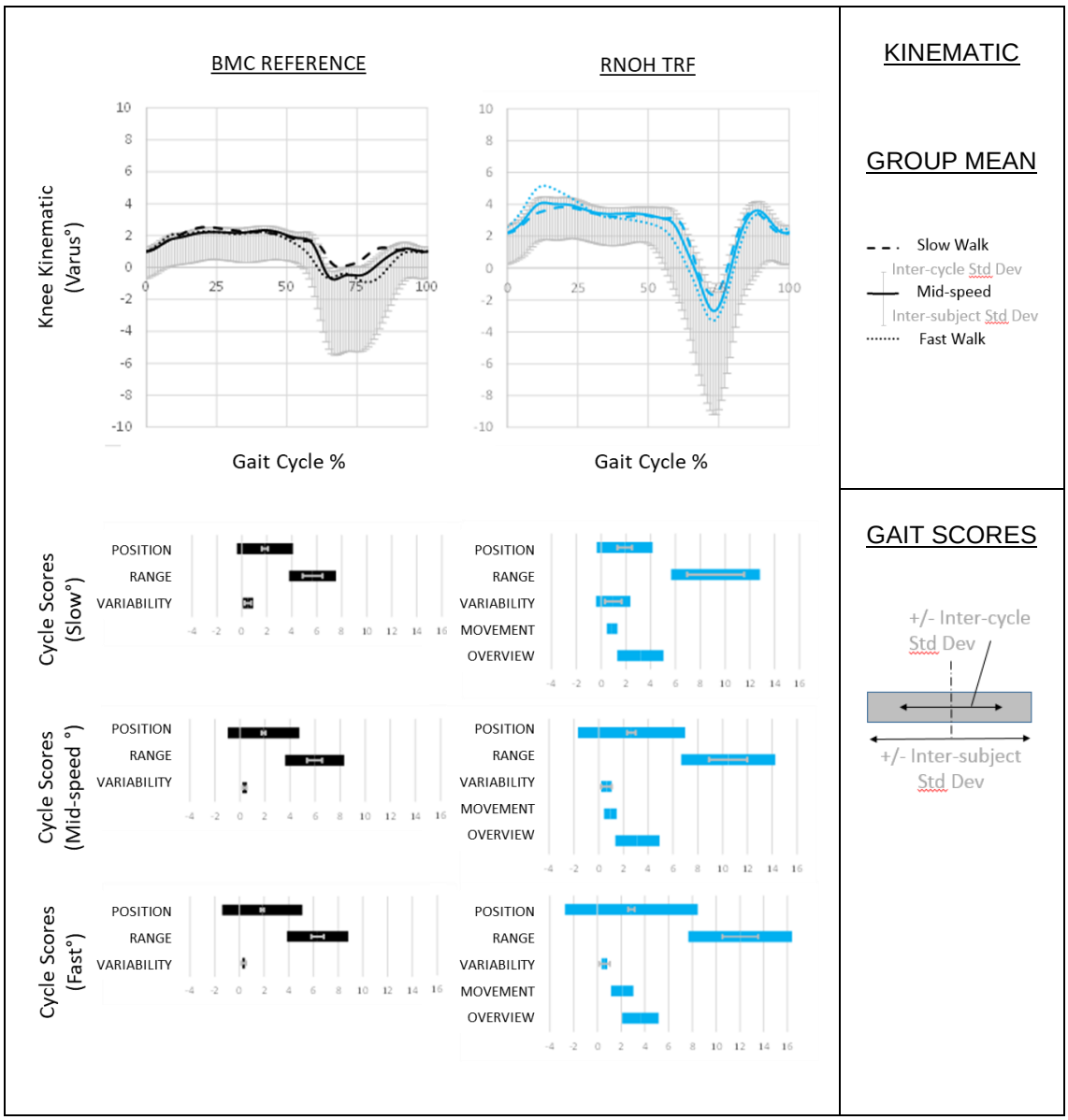

Figure 5-22 RNOH tracking solution for knee- Coronal

Knee coronal plane comparison of RNOH tracking solution (right column) with BMC reference (left column).

Top row shows graphical kinematic for slow (dashed line), mid-speed (solid line) and fast (dotted line) walking as depicted in the legend (right). The mid-speed typical inter-cycle, and inter-subject standard deviations are shown above and below the mid-speed graph line respectively.

Subsequent rows depict speed specific gait scores as per the legend (right bottom). Cycle position, range and variability scores represent absolute values from zero. Movement pattern and overview scores measure the difference between comparative and BMC reference values.

No obvious differences are seen between either the BMC and RNOH tracked thigh or knee kinematic.

5.4.7.3 RNOH TRF only – transverse kinematic

Finally, the thigh and knee transverse plane kinematics are shown if figures 5-23 and 5-24.

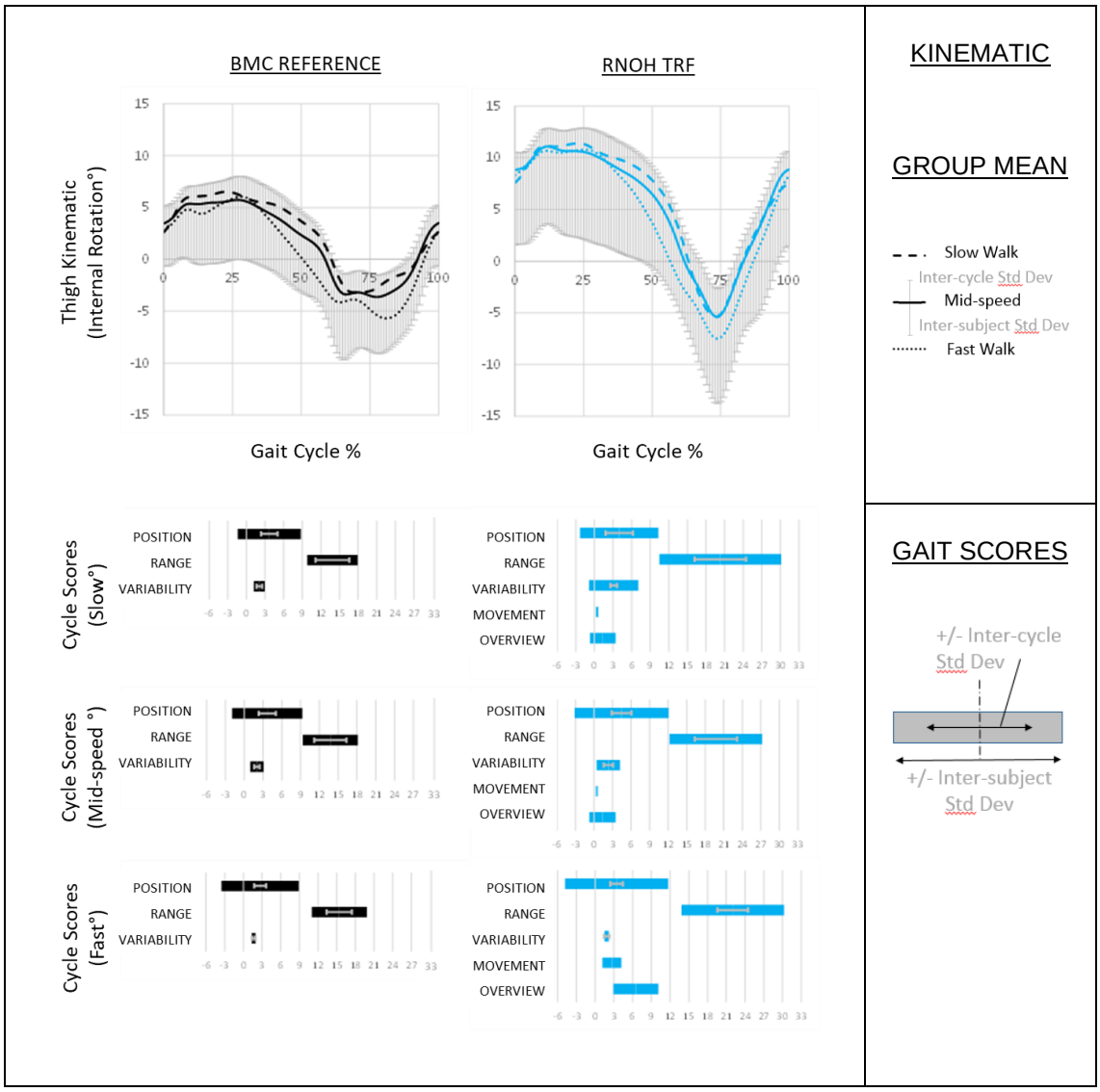

Figure 5-23 RNOH tracking solution for thigh- Transverse

Thigh transverse plane comparison of RNOH tracking solution (right column) with BMC reference (left column).

Top row shows graphical kinematic for slow (dashed line), mid-speed (solid line) and fast (dotted line) walking as depicted in the legend (right). The mid-speed typical inter-cycle, and inter-subject standard deviations are shown above and below the mid-speed graph line respectively.

Subsequent rows depict speed specific gait scores as per the legend (right bottom). Cycle position, range and variability scores represent absolute values from zero. Movement pattern and overview scores measure the difference between comparative and BMC reference values

5.4.7.4 RNOH TRF only - Knee Transverse

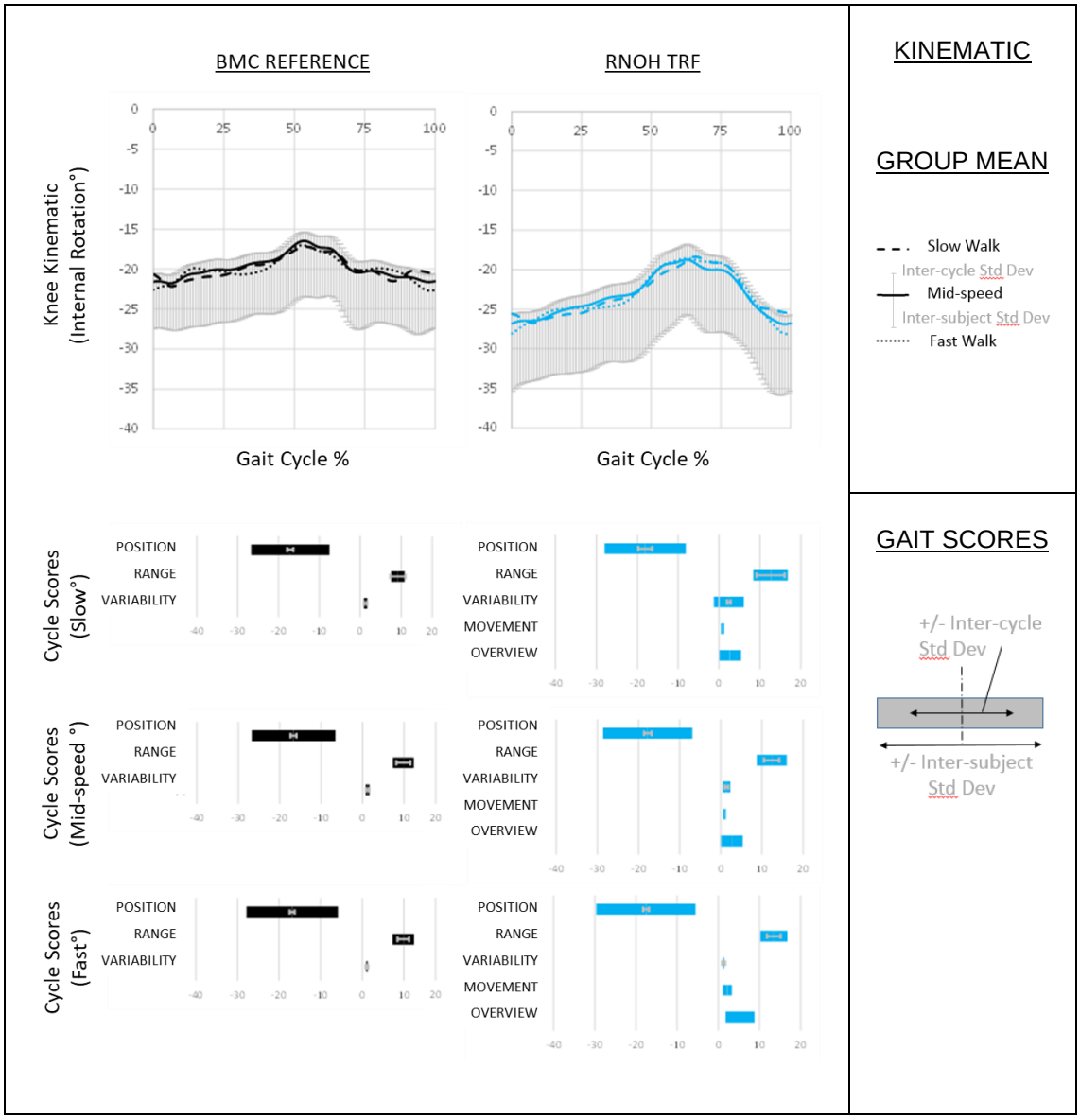

Figure 5-24 RNOH tracking solution for knee- Transverse

Knee transverse plane comparison of RNOH tracking solution (right column) with BMC reference (left column).

Top row shows graphical kinematic for slow (dashed line), mid-speed (solid line) and fast (dotted line) walking as depicted in the legend (right). The mid-speed typical inter-cycle, and inter-subject standard deviations are shown above and below the mid-speed graph line respectively.

Subsequent rows depict speed specific gait scores as per the legend (right bottom). Cycle position, range and variability scores represent absolute values from zero. Movement pattern and overview scores measure the difference between comparative and BMC reference values.

The RNOH tracking solution appears to capture more transverse plane range for both thigh and knee kinematics, than the equivalent BMC reference.

5.4.7.5 RNOH TRF only – Hypothesis Testing

This results section evaluates the RNOH_Thigh tracking solution in conjunction with the common ARF employed by the BMC and CAST solutions. The captured movements are therefore expressed around a set of common axes defining the sagittal, coronal, and transverse planes.

Table 5-4 highlight statistically significant (paired t-test p<=0.05) difference with the BMC reference gait scores in blue.

Table 5-4 Thigh/knee difference between RNOH tracking and reference BMC gait scores

	Thigh Position (°)			Thigh Range (°)			Thigh Variability (°)		
	Sagittal	Coronal	Transverse	Sagittal	Coronal	Transverse	Sagittal	Coronal	Transverse
SLOW	-0.72	-0.21	2.86	3.32	-0.15	6.45	0.07	-0.03	1.04
p-value	0.356	0.468	0.142	0.256	0.621	0.012	0.040	0.582	0.328
MIDSPEED	-0.67	-0.15	2.98	3.53	-0.15	5.98	0.02	-0.04	0.32
p-value	0.370	0.616	0.135	0.283	0.501	0.002	0.100	0.217	0.234
FAST	-0.75	-0.12	2.80	3.88	-0.25	6.63	0.03	-0.01	0.21
p-value	0.231	0.688	0.142	0.311	0.149	0.002	0.090	0.279	0.009

	Thigh Movement (°)			Thigh Overview (°)		
	Sagittal	Coronal	Transverse	Sagittal	Coronal	Transverse
SLOW	0.29	0.20	2.15	1.45	0.53	6.67
MIDSPEED	0.29	0.21	2.28	1.38	0.51	6.85
FAST	0.29	0.24	2.68	1.34	0.48	6.90

	Knee Position (°)			Knee Range (°)			Knee Variability (°)		
	Sagittal	Coronal	Transverse	Sagittal	Coronal	Transverse	Sagittal	Coronal	Transverse
SLOW	-1.69	1.01	-3.22	0.98	3.42	4.04	0.10	0.54	1.14
p-value	0.000	0.075	0.080	0.002	0.008	0.001	0.062	0.195	0.280
MIDSPEED	-1.56	1.20	-3.43	0.93	4.17	3.15	0.03	0.25	0.25
p-value	0.000	0.057	0.060	0.003	0.003	0.000	0.001	0.009	0.144
FAST	-1.51	1.25	-3.19	0.98	5.41	4.40	0.03	0.27	0.16
p-value	0.000	0.051	0.062	0.002	0.001	0.000	0.043	0.000	0.001

	Knee Movement (°)			Knee Overview (°)		
	Sagittal	Coronal	Transverse	Sagittal	Coronal	Transverse
SLOW	0.39	1.07	2.18	1.76	2.34	6.25
MIDSPEED	0.36	1.24	2.20	1.62	2.72	6.27
FAST	0.35	1.55	2.50	1.57	3.00	6.18

An approximate 6° increase in captured transverse plane range by the RNOH_Thigh tracking solution at all walking speeds represents an approximate 50% increase on the BMC solution. Movement difference scores were much less than the overall difference scores in all three planes, and visual inspection of the

kinematic confirmed that the general shape of the BMC movement pattern was maintained. *Hypothesis 5B_II*, that the tracking solution will capture considerably more transverse plane rotation than the BMC solution, without fundamentally changing the kinematic, is therefore accepted.

As both tested solutions shared a common anatomical alignment, the increase in the coronal plane (and similar transverse plane increase) knee range, can only be a consequence of the increased captured thigh movement.

A small difference in the sagittal position and range scores reflect a difference in tracking of the distal end of the segment. While BMC track the KJC location directly as the mid-point of medial and lateral epicondyle markers, the RNOH solution tracks this same point via shank-based markers.

5.4.8 Results 2c RNOH full solution

5.4.8.1 RNOH - Thigh Sagittal

Figures 5-25 compares the full RNOH_Thigh solution with the BMC reference sagittal plane kinematic. These solutions differ in both their ARF and TRF definitions.

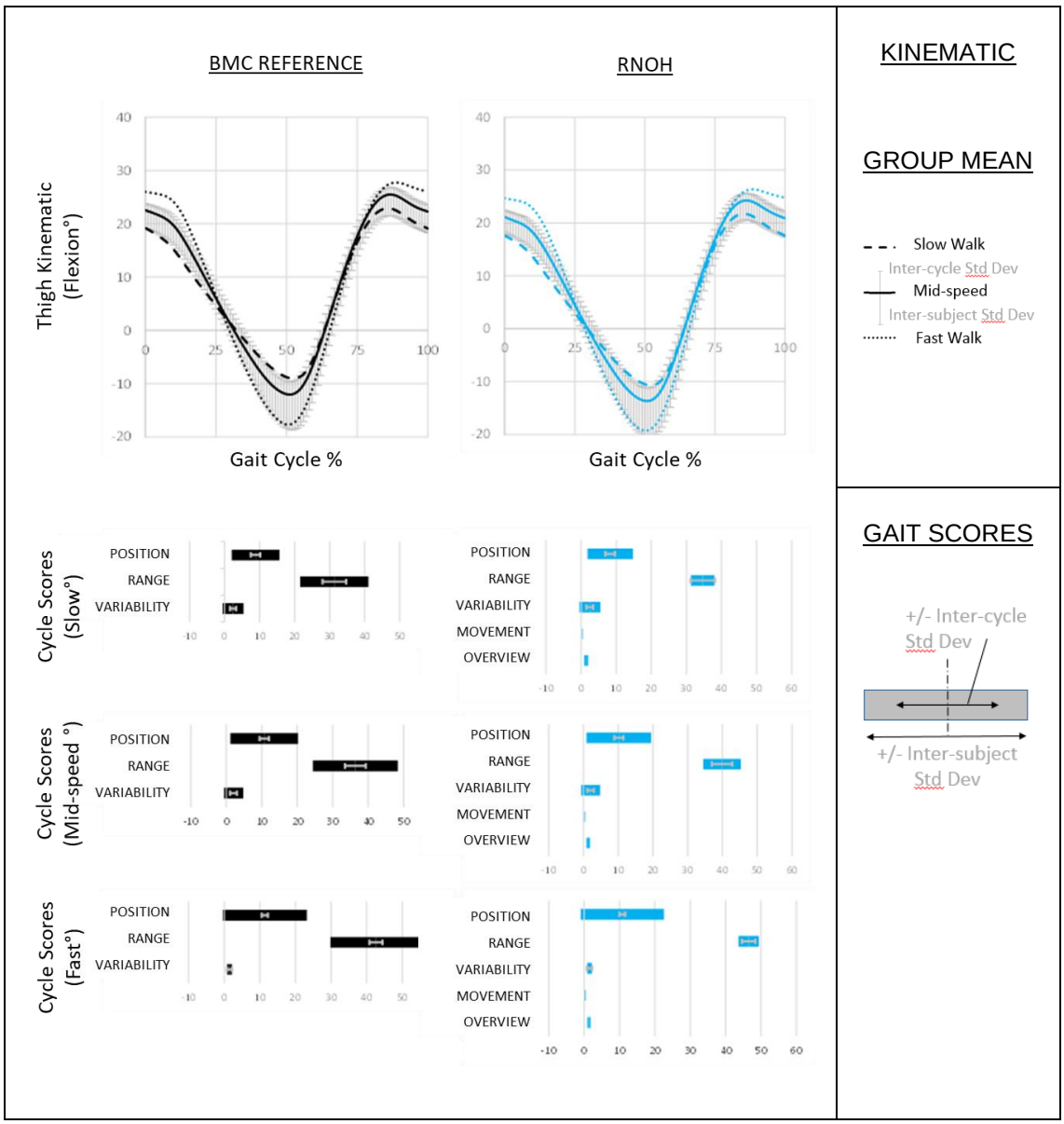

Figure 5-25 RNOH full solution for thigh - Sagittal

Sagittal plane comparison of RNOH full solution (right column) with BMC reference (left column).

Top row shows graphical kinematic for slow (dashed line), mid-speed (solid line) and fast (dotted line) walking as depicted in the legend (right). The mid-speed typical inter-cycle, and inter-subject standard deviations are shown above and below the mid-speed graph line respectively.

Subsequent rows depict speed specific gait scores as per the legend (right bottom). Cycle position, range and variability scores represent absolute values from zero. Movement pattern and overview scores measure the difference between comparative and BMC reference values.

5.4.8.2 RNOH - Knee Sagittal

Details of the resultant knee joint kinematic are presented in figure 5-26.

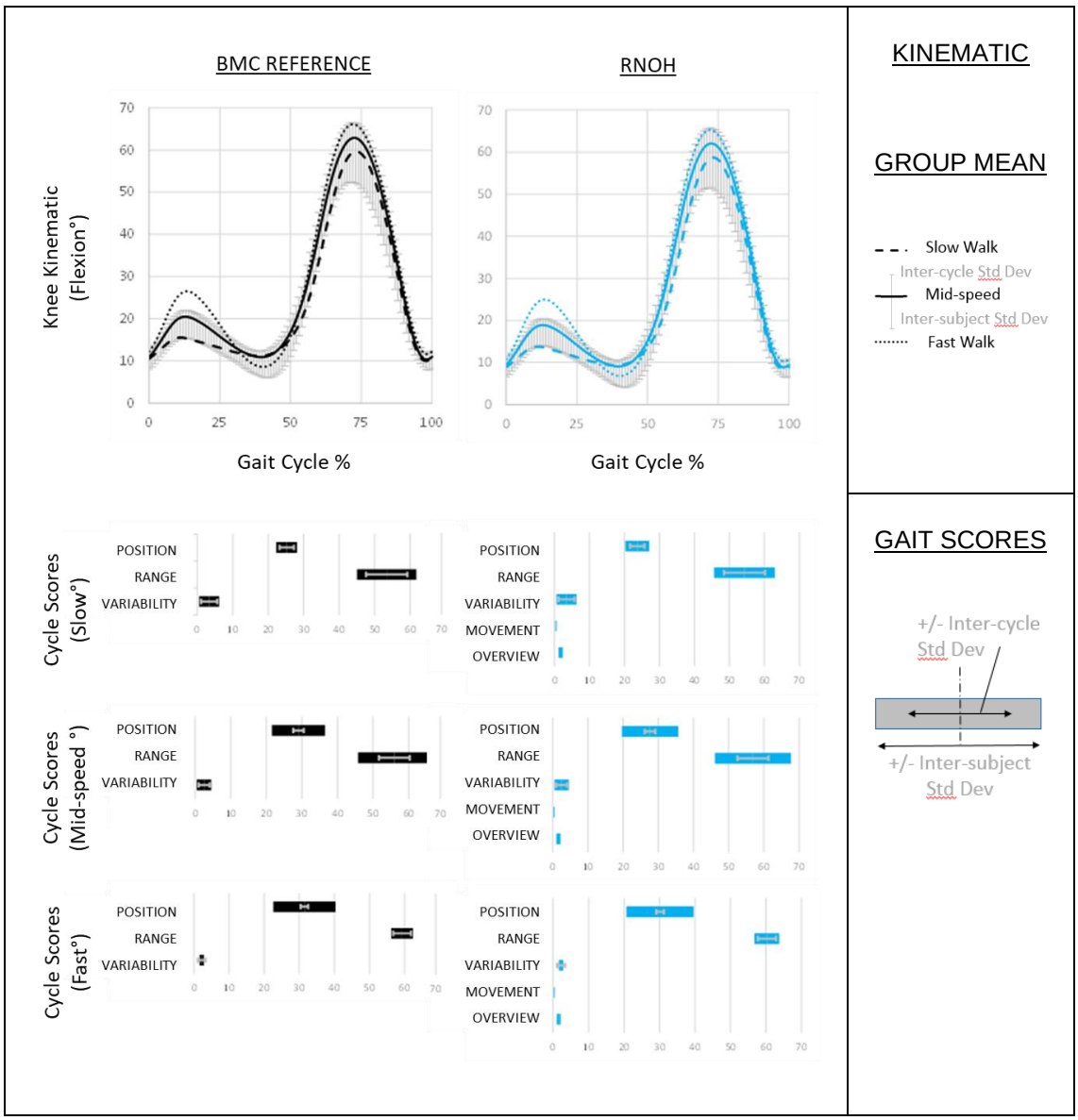

Figure 5-26 RNOH full solution for knee - Sagittal

Sagittal plane comparison of RNOH full solution (right column) with BMC reference (left column).

Top row shows graphical kinematic for slow (dashed line), mid-speed (solid line) and fast (dotted line) walking as depicted in the legend (right). The mid-speed typical inter-cycle, and inter-subject standard deviations are shown above and below the mid-speed graph line respectively.

Subsequent rows depict speed specific gait scores as per the legend (right bottom). Cycle position, range and variability scores represent absolute values from zero. Movement pattern and overview scores measure the difference between comparative and BMC reference values.

5.4.8.3 RNOH - Thigh Coronal

Figures 5-27 and 5-28 show equivalent results for the coronal plane comparison.

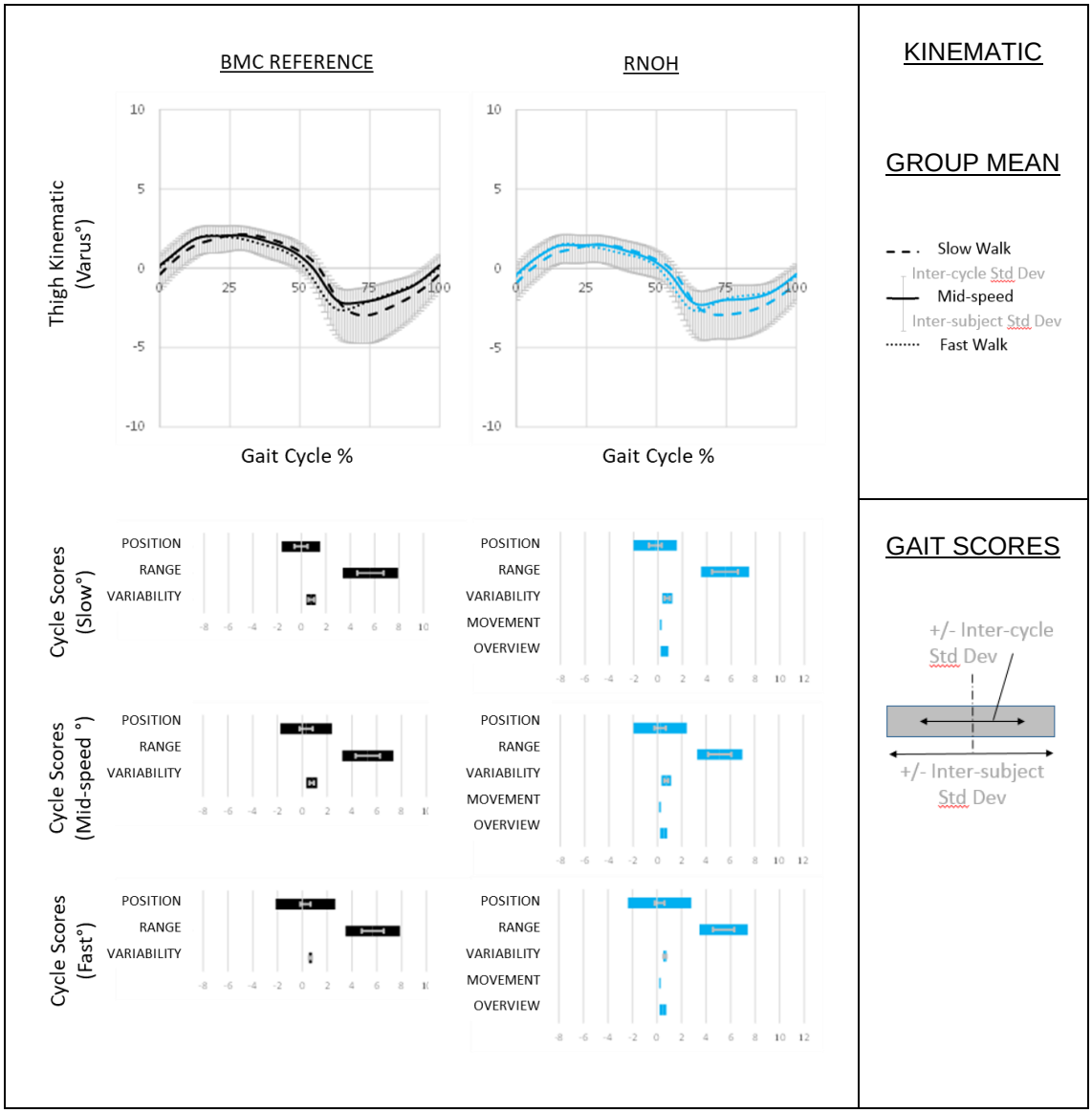

Figure 5-27 RNOH full solution for thigh - Coronal

Coronal plane comparison of RNOH full solution (right column) with BMC reference (left column).

Top row shows graphical kinematic for slow (dashed line), mid-speed (solid line) and fast (dotted line) walking as depicted in the legend (right). The mid-speed typical inter-cycle, and inter-subject standard deviations are shown above and below the mid-speed graph line respectively.

Subsequent rows depict speed specific gait scores as per the legend (right bottom). Cycle position, range and variability scores represent absolute values from zero. Movement pattern and overview scores measure the difference between comparative and BMC reference values.

5.4.8.4 RNOH - Knee Coronal

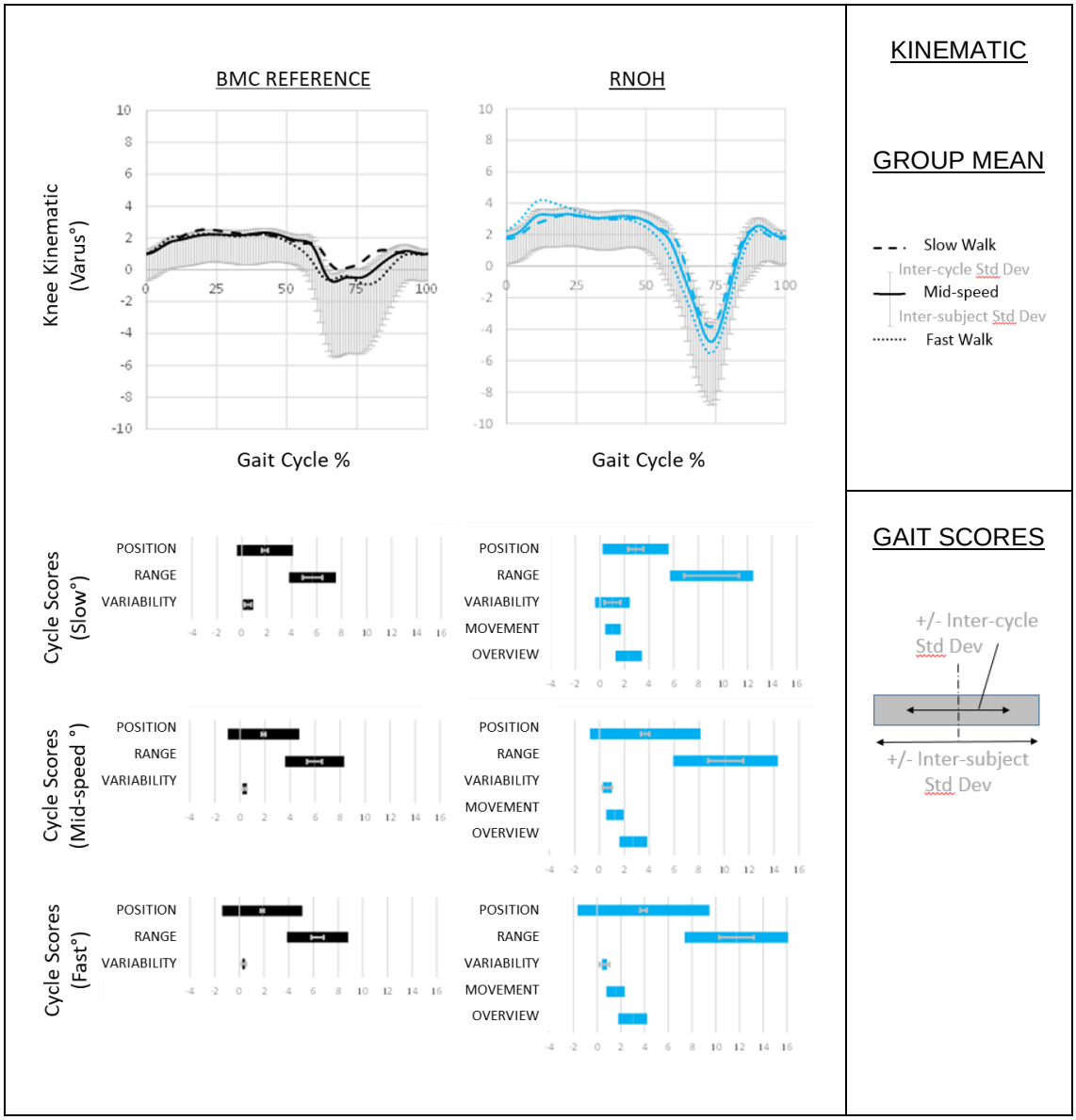

Figure 5-28 RNOH full solution for knee - Coronal

Coronal plane comparison of RNOH full solution (right column) with BMC reference (left column).

Top row shows graphical kinematic for slow (dashed line), mid-speed (solid line) and fast (dotted line) walking as depicted in the legend (right). The mid-speed typical inter-cycle, and inter-subject standard deviations are shown above and below the mid-speed graph line respectively.

Subsequent rows depict speed specific gait scores as per the legend (right bottom). Cycle position, range and variability scores represent absolute values from zero. Movement pattern and overview scores measure the difference between comparative and BMC reference values.

The increase in measured range for the RNOH solution is in keeping with the TRF change only (Figure 5-22) and therefore not related to the ARF alignment.

5.4.8.5 RNOH - Thigh Transverse

Finally, figure 5-29 shows the clear increase in transverse plane range captured by the RNOH_Thigh solution, and figure 5-30 the transverse plane knee kinematic comparison.

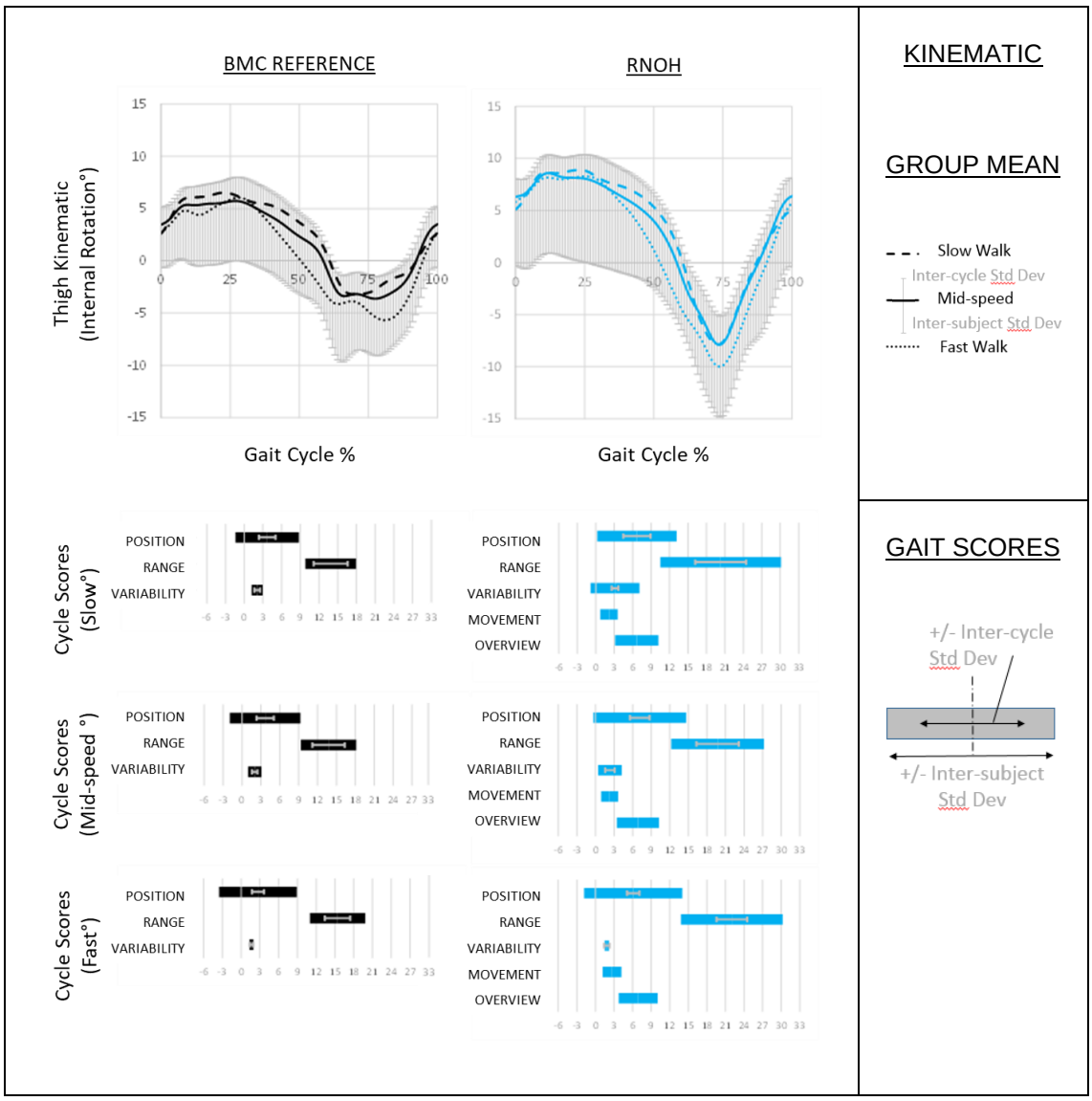

Figure 5-29 RNOH full solution for thigh - Transverse

Transverse plane comparison of RNOH full solution (right column) with BMC reference (left column).

Top row shows graphical kinematic for slow (dashed line), mid-speed (solid line) and fast (dotted line) walking as depicted in the legend (right). The mid-speed typical inter-cycle, and inter-subject standard deviations are shown above and below the mid-speed graph line respectively.

Subsequent rows depict speed specific gait scores as per the legend (right bottom). Cycle position, range and variability scores represent absolute values from zero. Movement pattern and overview scores measure the difference between comparative and BMC reference values.

5.4.8.6 RNOH - Knee Transverse

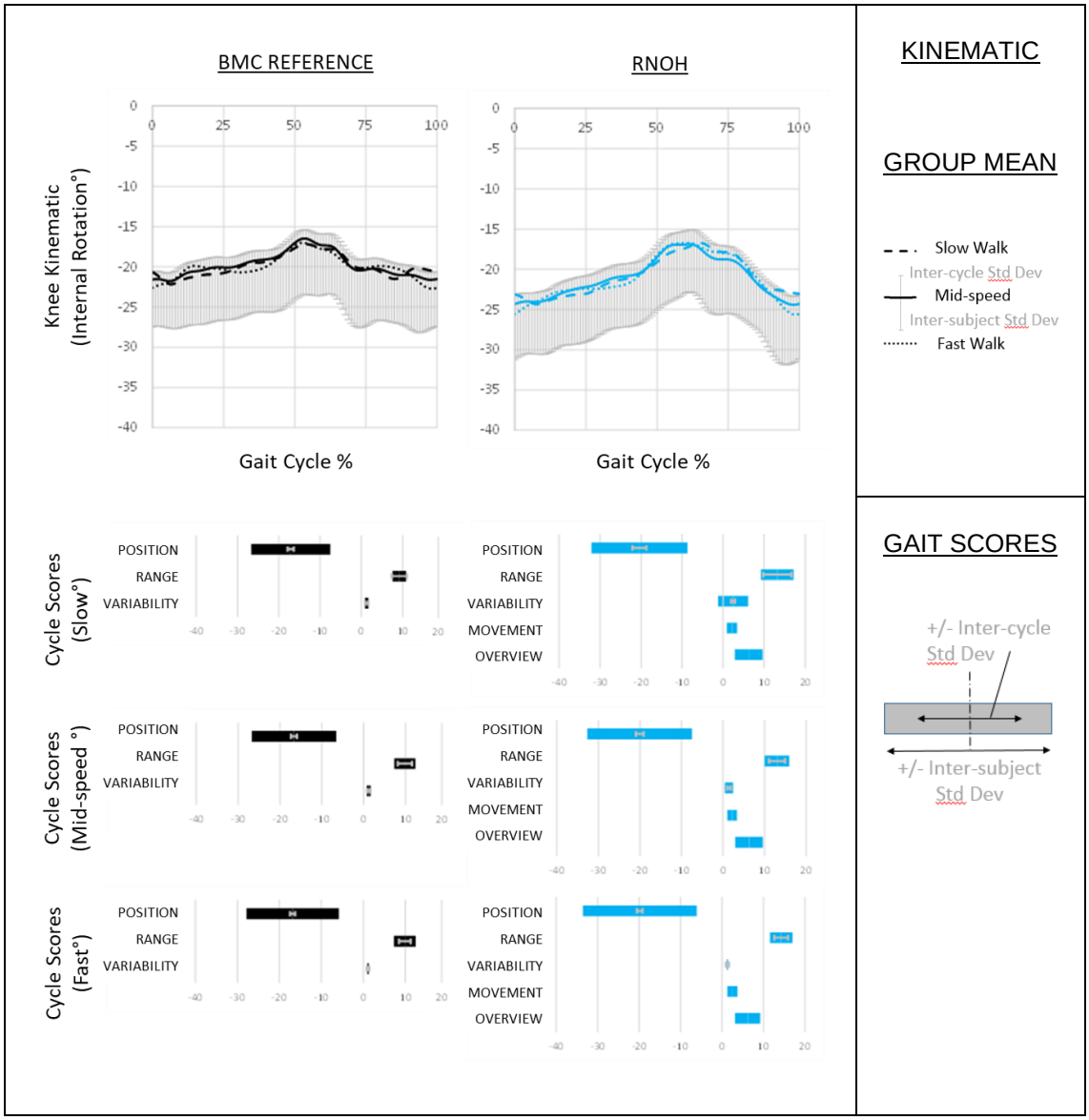

Figure 5-30 RNOH full solution for knee - Transverse

Transverse plane comparison of RNOH full solution (right column) with BMC reference (left column).

Top row shows graphical kinematic for slow (dashed line), mid-speed (solid line) and fast (dotted line) walking as depicted in the legend (right). The mid-speed typical inter-cycle, and inter-subject standard deviations are shown above and below the mid-speed graph line respectively.

Subsequent rows depict speed specific gait scores as per the legend (right bottom). Cycle position, range and variability scores represent absolute values from zero. Movement pattern and overview scores measure the difference between comparative and BMC reference values.

5.4.8.7 The Full RNOH Solution

The preceding section demonstrated superiority of the RNOH_Thigh tracking solution, in capturing significantly more transverse plane movement than either BMC or CAST solutions, without detriment to other kinematic features. This section has further incorporated this tracking solution with a modification to the segment ARF, based on the knee orientation during a crouched posture static calibration. This modification aligned the neutral axial spin of the thigh segment principal axis, with anterior in a plane defined by hip, knee, and ankle joint centres. Table 5-5 highlights statistically significant difference with the BMC reference gait scores.

Table 5-5 Difference between thigh full-RNOH and reference BMC gait scores.

	Thigh Position (°)			Thigh Range (°)			Thigh Variability (°)		
	Sagittal	Coronal	Transverse	Sagittal	Coronal	Transverse	Sagittal	Coronal	Transverse
SLOW	-0.72	-0.21	0.36	3.32	-0.15	6.45	0.07	-0.03	1.04
p-value	0.356	0.468	0.865	0.256	0.621	0.012	0.040	0.582	0.328
MIDSPEED	-0.67	-0.15	0.48	3.53	-0.15	5.98	0.02	-0.04	0.32
p-value	0.370	0.616	0.825	0.283	0.501	0.002	0.100	0.217	0.234
FAST	-0.75	-0.12	0.30	3.88	-0.25	6.63	0.03	-0.01	0.21
p-value	0.231	0.688	0.887	0.311	0.149	0.002	0.090	0.279	0.009

	Movement (°)			Overview (°)		
	Sagittal	Coronal	Transverse	Sagittal	Coronal	Transverse
SLOW	0.29	0.20	2.15	1.45	0.53	6.14
MIDSPEED	0.29	0.21	2.28	1.38	0.51	6.36
FAST	0.29	0.24	2.68	1.34	0.48	6.52

	Knee Position (°)			Knee Range (°)			Knee Variability (°)		
	Sagittal	Coronal	Transverse	Sagittal	Coronal	Transverse	Sagittal	Coronal	Transverse
SLOW	-1.56	0.10	-1.01	0.85	3.57	3.43	0.11	0.49	1.13
p-value	0.000	0.884	0.588	0.009	0.015	0.004	0.086	0.228	0.286
MIDSPEED	-1.43	0.26	-1.26	0.84	4.50	2.54	0.03	0.25	0.23
p-value	0.000	0.740	0.484	0.008	0.002	0.001	0.006	0.026	0.133
FAST	-1.38	0.28	-1.05	0.89	5.70	3.61	0.03	0.25	0.15
p-value	0.000	0.731	0.539	0.006	0.002	0.000	0.054	0.002	0.000

	Knee Movement (°)			Knee Overview (°)		
	Sagittal	Coronal	Transverse	Sagittal	Coronal	Transverse
SLOW	0.40	1.57	1.91	1.63	2.87	5.31
MIDSPEED	0.35	1.74	1.92	1.49	3.21	5.33
FAST	0.34	2.09	2.21	1.44	3.62	5.28

The RNOH_ARF alignment matches that of the BMC solution; measured difference were fractions of a degree in all planes, increases in the knee joint range match those of employing the RNOH tracking with the BMC alignment. *Hypothesis 5B_III*, that the RNOH_ARF realignment will not cause a significant increase in amplitude of the coronal knee kinematic is therefore accepted.

5.4.9 Results 2d BMI Effects

Table 5-6 collates linear correlation coefficient for each gait score with subject BMI value. RNOH values were little affected by the minimal shift in ARF position between the two tested versions; values were extracted from the fully implemented version. Once again, position, range and variability scores reflect cycle mean, minimum minus maximum, and inter-cycle standard deviation

differences with the BMC reference kinematic. The overview scores show the RMS difference between the two kinematics, and the movement score the absolute mean difference of the position normalised kinematic. Values above a magnitude of 0.5 (R^2=>0.25), accounting for at least 25% of the score variance are highlighted.

Table 5-6 Correlation of gait scores with subject BMI for each of the tracking solutions.

Sagittal

	Thigh Position			Thigh Range			Thigh Variability		
	Slow	MidSpeed	Fast	Slow	MidSpeed	Fast	Slow	MidSpeed	Fast
BMC	-0.11	-0.20	-0.17	0.00	0.19	0.07	0.20	-0.21	-0.07
CAST	-0.10	-0.23	-0.17	-0.11	0.28	0.02	0.18	-0.21	-0.01
RNOH	-0.33	-0.45	-0.35	-0.24	0.26	-0.07	0.19	-0.21	-0.09

	Thigh Movement			Thigh Overview		
	Slow	MidSpeed	Fast	Slow	MidSpeed	Fast
CAST	0.06	0.51	0.29	0.11	0.16	0.12
RNOH	-0.32	-0.23	-0.17	0.09	0.06	0.06

Coronal

	Thigh Position			Thigh Range			Thigh Variability		
	Slow	MidSpeed	Fast	Slow	MidSpeed	Fast	Slow	MidSpeed	Fast
BMC	-0.32	-0.49	-0.51	0.33	0.57	0.35	0.05	-0.29	0.15
CAST	-0.37	-0.49	-0.46	-0.02	0.31	0.13	0.13	-0.30	-0.11
RNOH	-0.31	-0.55	-0.56	0.36	0.61	0.39	0.00	-0.26	0.21

	Thigh Movement			Thigh Overview		
	Slow	MidSpeed	Fast	Slow	MidSpeed	Fast
CAST	-0.36	-0.06	-0.27	0.26	0.32	0.29
RNOH	-0.29	0.05	0.16	-0.06	-0.04	0.05

Transverse

	Thigh Position			Thigh Range			Thigh Variability		
	Slow	MidSpeed	Fast	Slow	MidSpeed	Fast	Slow	MidSpeed	Fast
BMC	-0.01	-0.11	0.00	-0.19	0.01	-0.20	0.05	-0.39	-0.49
CAST	-0.09	-0.17	-0.08	-0.19	0.03	-0.20	-0.01	-0.39	-0.49
RNOH	-0.32	-0.48	-0.44	-0.22	0.11	-0.10	-0.35	-0.40	-0.29

	Thigh Movement			Thigh Overview		
	Slow	MidSpeed	Fast	Slow	MidSpeed	Fast
CAST	-0.04	0.36	0.13	0.20	0.23	0.22
RNOH	-0.04	0.34	0.15	0.05	0.05	0.05

The CAST tracking of the thigh segment was generally insensitive to subject BMI value. Only the sagittal plane movement pattern score was highlighted, and even this score only just met the low threshold value, and only at the middle walking speed.

Correlation coefficients for the coronal thigh position approximate the same 0.5 modulus threshold for all solutions at the mid and fast walking speeds only. Lower

sensitivity at the slow walking speed indicates that the BMI effect is associated with dynamic STA components.

The strongest correlations are seen in the coronal plane range scores for the BMC and RNOH solutions at the mid walking speed. Here, lower correlations at either the faster or slow walking suggest an interplay whereby dynamic STA effects may act to compensate the static skin-sliding STA component.

Overall, no strong correlations between any gait score and subject BMI value were observed, and *hypothesis 5B_IV* predicting such a relationship is rejected.

5.5 Discussion

Like the RNOH_Trunk solution (Chapter 3), derivation of the RNOH_Thigh segment benefited from the establishment of the pro-forma simplistic BMC solution (Chapter 2). This approach differs from the CGM evolutionary development promoted elsewhere (Leboeuf et al., 2019). The BMC removed inaccuracies caused by unwarranted complexity of the CGM solution. Further model development was then focused on optimisation and clinical utility issues, with the benefit of research findings published over the 4 decades since the CGM inception.

One key publication in the RNOH_Thigh development, introduced the idea of a ‘marker-less’ thigh, where by the principal axis is tracked via its proximal and distal neighbours (Schulz and Kimmel, 2010). This solution eliminates thigh-based STA influences at the expense of not measuring the axial spin component of the kinematic. A second key publication suggested that a patella surface marker is particularly good at measuring this movement (Wren et al., 2008). The RNOH_Thigh was then able to integrate both solutions into a coherent biomechanical model.

Initial testing validated the patella location as optimal for tracking thigh axial rotation. Use of a cadaveric specimen facilitated insertion of bone pines from which true bone movement could be measured to act as a gold standard measure. In this respect, I would defend the use of the term ex-vivo (outside of

the living organism) for this type of experiment (Fleps et al., 2019, Ramo et al., 2018, Cartner et al., 2011), over the term in vitro (under glass) which the limited number of previous gait analysis specific cadaveric studies appears to favour (Nester et al., 2007b, Zhu et al., 2020).

As part of the BMC comparison common to development of all body segments, the RNOH_Thigh and an alternative CAST tracking solution were tested under dynamic gait conditions outlined in chapter 2. Each of these models requires acceptance of different underlying assumptions that directly relate to the face validity of each approach. Assumptions made by each of the thigh modelling approaches are therefore outlined in table 5-7.

Table 5-7 Modelling assumptions specific to each thigh segment modelling approach

	ARF Modelling Assumption	TRF Modelling Assumptions
BMC	A knee joint axis is defined between medial and lateral epicondyle surface markers. This direct representation of the required axis assumes that the clinician can accurately locate these rather diffuse bony landmarks and that the defined axis is representative of curvature of the articular condylar surface. The method is akin to use of a knee alignment device (KAD) sometimes employed by the CGM with the additional assumption that the KAD can be clamped across the knee to represent the required axis.	Segment tracking is via the HJC location, medial and lateral epicondyle markers.
CGM	Knee joint axis is defined in a plane defined by the HJC location, a lateral epicondyle surface marker and a lateral thigh marker. The model either assumes that the clinician is able to accurately locate the lateral thigh marker manually, or that there will be sufficient knee movement to adjust this position post data collection. In the latter case, minimising the overflow of sagittal movement into the coronal kinematic is assumed to represent a reasonable alignment; this minimising is inevitably based on the unloaded swing phase data when most of the knee movement occurs.	Segment tracking employs the same HJC, lateral epicondyle and lateral thigh surface markers are used to define the coronal principal plane. Lateral markers for the left and right thigh are located at different heights in order to facilitate software side recognition.
CAST	The CAST method is free to adopt any ARF solution. The selected ARF orientation is then related to that of the segment's TRF during a static calibration trial.	Segment tracking markers are intended for a low STA region. Any failure of this region to represent movement of the whole segment, as represented by the ARF, results in a residual error. Multiplication of this angular error by the separation distance between the tracking cluster and the segment extremities dictates a mid- segment location, which in turn is unlikely to exhibit minimal STA. Long body segments such as the thigh are therefore not best suited to application of a localised CAST tracking solution.
RNOH	An AJC location is defined as the midpoint of medial and lateral malleoli surface markers and thigh anterior aspect defined by projection of a patella surface marker into the HJC-KJC-AJC plane during a weight bearing crouched static calibration. The method therefore assume that there is no undue coronal plane deformation of the shank segment. The medio-lateral knee axis is modelled as mutually perpendicular to the thigh long axis and the anterior axis from KJC to the projected patella location.	The KJC location is tracked via the shank segment. Axial tracking of the thigh around the principal axis is achieved via another virtual projection of the patella marker. In order to suppress vertical movement, this virtual representation is calculated as the projection of the KJC onto the HJC-patella line.

5.5.1 The BMC/CGM Solutions

The BMC solution defines its principal plane directly via the HJC location and the knee joint axis anatomy promoted by ISB recommendations (Wu et al., 2002). As such, the only anatomical assumption made by the model is that these structures can be accurately represented by surface markers. Employing these markers to also monitor the segment movement, requires the additional, and less easily accepted, tracking assumption of low STA effects under all of these marker locations.

The CGM approach is similar to that of the BMC, but additionally requires the anatomical assumption that a mid-segment lateral thigh marker, can substitute the medial knee marker, both for anatomical and tracking purposes.

The direct nature of the BMC method appears to provide reasonable anatomical alignment. The extensive soft tissue-cover over the entire segment however, makes the assumption that skeletal movement may be accurately tracked by the anatomical surface markers untenable (Schache et al., 2008).

5.5.2 The CAST Solution

The alternative CAST tracking method inherited the direct anatomical orientation of the BMC solution but tracked this orientation via different surface markers. In the case of the thigh segment however, no low STA locations are available for this purpose (Fiorentino et al., 2017). A general distal to proximal increase in soft tissue cover thickness, supported use of a distal tracking cluster consisting of the anatomical marker identifying the medial and lateral ends of the knee axis, and a third marker on the distal anterior aspect of the segment, a few centimetres above the patella. As the BMC axial rotation of the segment is tracked by the same knee axis markers that contribute to the CAST cluster, the solutions were unsurprisingly well matched in their ability to capture this component of the movement. The extreme distal bias of this cluster also ensured accurate tracking of the distal KJC end of the segment's principal axis. Accurate tracking of the proximal HJC end of this axis, requires the assumption of minimal mismatch between the segment's true orientation and that of the tracking cluster, as the

subject moved away from the synchronising calibration posture. This assumption would have been helped by the mid-task-position, crouched calibration posture. The distal bias, however, still resulted in a significant angular mismatch, manifesting in the location of the tracked HJC location, after amplification over the entire length of the thigh (Figure 5-31).

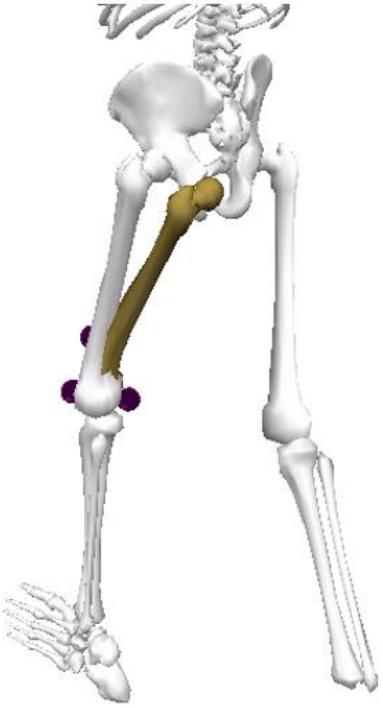

Figure 5-31 CAST tracked thigh segment (highlighted in colour) at left initial contact

The distal marker cluster consists of individual surface markers located over the medial and lateral epicondyles and an anterior distal thigh location. Small angular errors in the orientation of this cluster result in unacceptably large translational offsets in the proximal position of the HJC location.

Avoidance of the distal bias by use of a mid-segment cluster would have helped to distribute this error over both ends of the segment. These locations however are inevitably subject to dynamic STA components caused by muscle contraction. Although the employed CAST cluster may not have been the best compromise of all of these factors, the general principle that STA will cause any local sub-region to misrepresent movement of the whole, supports the decision not to implement a CAST tracking cluster for the thigh to track HJC locations for the pelvic solution (Kisho Fukuchi et al., 2010) in chapter 4.

It follows that the true value of the CAST method is in the intellectual separation of the TRF segment solution from its ARF surface markers. The other CAST characteristic of localising the TRF markers to a small sub region of the segment inevitably lead to a misrepresentation of the whole. This finding warns against the use of accelerometers to mimic segment orientations, the ultimate in localised sample data collection techniques (Zhang et al., 2013).

TRF markers should instead be distributed over the length of the segment, such that any tracking errors may be absorbed by deformation of the cluster. In this way the cluster can simultaneously reflect the location of both proximal and distal segment extremities; a reasonable objective if the segment is truly rigid. This finding substantiates the decision to extend the shank based tracking solution (Peters et al., 2009) to the proximal end of the segment, by the addition of a surface marker over the fibular head in chapter 1.

5.5.3 The RNOH solution

The RNOH tracking solution demonstrates good face validity by avoiding all high STA thigh regions. Avoiding the CGM need to correct the model based on a cosmetic fix to the knee kinematic, is another important feature for a model that claims to ‘measure’ the thigh orientation. This feature was most easily achieved by the BMC method, via the assumption of surface marker placements being able to accurately represent the articular surfaces at either end. The alternative RNOH approach attempts to glean this information, by the orientation of the pelvis-thigh-shank kinematic chain during a crouched calibration pose. This approach requires the modelling assumption that these relationships are stable over the range of crouched positions likely to be adopted during testing. This in turn requires that there must be sufficient knee flexion for the modelled hip, knee, and ankle joint centres to define a stable plane. Data from the in-vivo testing suggest that a minimum value of 30° results in <2° of error. To make the technique insensitive to precise posture adopted during the calibration pose requires the additional assumption of accurate location of all joint centres and for the knee to act as a perfect hinge joint.

The BMC and RNOH avoid the need to correct the measured orientation of the thigh, by very different modelling assumptions. Both solutions require accurate location of the HJC. Anecdotally, I would expect that in the clinical environment the RNOH requirement for KJC and AJC locations in the desired plane, is less sensitive to marker placement error than the BMC requirement for precise definition the knee joint axis. In the typically developed cohort tested here, both solutions proved equally capable.

6 Chapter 6 – The Foot

Early implementations of CGM reported the ankle kinematic in 2D only; the distal foot segment was represented as a line vector with sagittal movement reported as dorsiflexion/plantar flexion. In this paradigm, the coronal plane axial spin is presumed well correlated with the measured transverse plane component, and the combined output is often labelled as supination/pronation. More recent CGM applications have moved towards representing the foot as a 3D rigid body, in common with the other model segments.

6.1 Introduction

This chapter considers accurate modelling of the orientation of a 3D foot segment, plus the optional description of its internal shape via the application of additional surface markers. Similar to other body segment, the contribution to step formation is described by its orientation with respect to the laboratory frame. This whole foot kinematic tells, for example, whether the foot strikes the ground by the toes (equinus), entire plantar surface (flat-footed) or heel (normal). Description of this same whole foot kinematic with respect to the shank segment, are generally reported as an ankle kinematic, and relate to the length of anatomical muscles, ligaments and other soft tissue structures that cross the joint. The addition of a hind-foot sub-region as part of a multi-segment foot model (MSFM), might more precisely facilitate a shank-heel (tibiocalcaneal) kinematic. The primary purpose of a MSFM however, is to report shape changes caused by force induced deformations as the segment is loaded and unloaded through the gait cycle. Use of an instrumented treadmill can additionally facilitate investigation of the effect of speed and inclination on these deformations (Tulchin et al., 2010b, Tulchin et al., 2010a).

6.1.1 Foot Anatomy

The foot skeleton is often considered in anatomical regions. Posteriorly, the large calcaneal bone forms the familiar hind-foot region. The calcaneus does not, however, articulate directly with the proximal shank segment; instead, the intervening talus bone articulates with the shank on its top surface and the

calcaneus below. Although the talus is remotely palpable on the anterior aspect of the ankle, it does not present any realistic possibility of 3D tracking via surface markers. The trackable combination of tibio-talo movement between the shank and the talus, and subtalar movement between the talus and the calcaneus, is collectively referred to as a tibiocalcaneal joint. The rigid nature of both proximal and distal sides of this functional joint make it the most trackable intra-foot kinematic available to surface markers (Nester et al., 2007a).

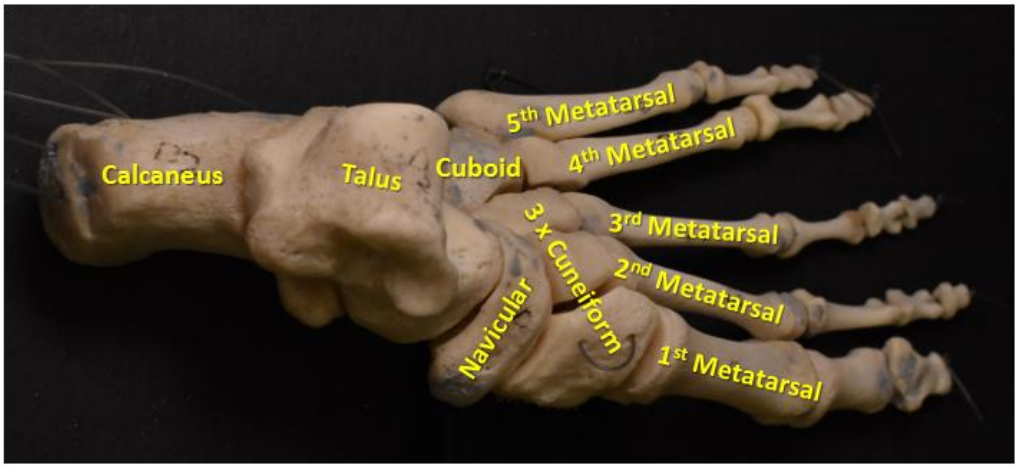

Figure 6-1 Dorsal view of articulated left foot skeleton

Hind foot consists of calcaneal heel bone below the talus located at the centre of the ankle joint. In front of these are navicular, cuboid, medial central and lateral cuneiform tarsal bones. The forefoot consists of the metatarsal bones, 1 to 5.

Anterior to the hind-foot, five small tarsal bones form a mid-foot region (tarsus). From the tarsus, five metatarsal long bones stretch forward to their respective toes. The metatarsals are identified 1-5 from medial to lateral, such that the 1st metatarsal articulates with the great toe. Flared regions at both ends of each metatarsal provide palpable bony landmark locations on their dorsal surface. The distal flares form a metatarsal-head line that separates the proximal forefoot region from the distal toes. The proximal metatarsal flares are termed ‘bases’. On the lateral side of the foot, the 4th and 5th metatarsal bases articulate with the cuboid tarsal bone; opposite this articulation, the posterior aspect of the cuboid articulates directly with the calcaneum.

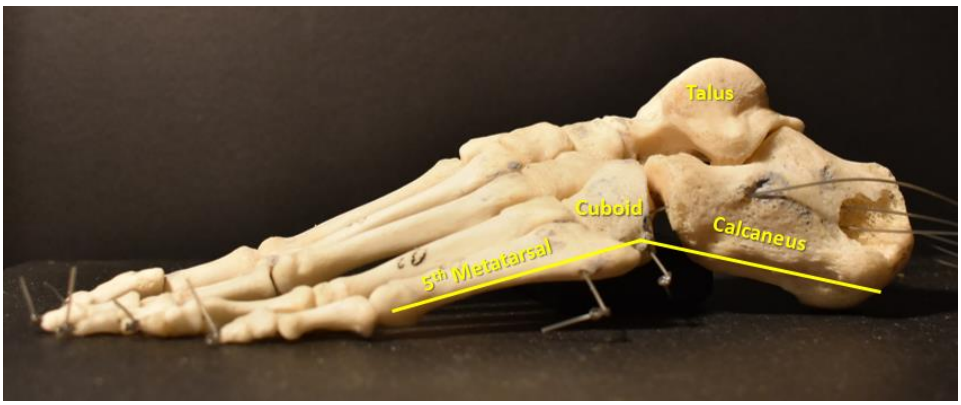

Figure 6-2 Lateral view of articulated left foot skeleton

The relatively rigid lateral longitudinal arch of the foot, apexes at the central cuboid tarsal bone, articulating directly with calcaneus posteriorly, and the 4th and 5th metatarsals anteriorly.

The 5th base is additionally easily palpable on the lateral aspect of the foot, and the cuboid, which marks the apex of the lateral foot arch, is palpable within a small depression just behind this.

On the medial side of the foot, the 1st metatarsal-base starts a kinematic chain to the medial cuneiform and navicular tarsal bones, on to the talus and ending at the calcaneus. These bones form a medial arch, with its apex palpable as a bony protrusion (tuberosity) of the navicular.

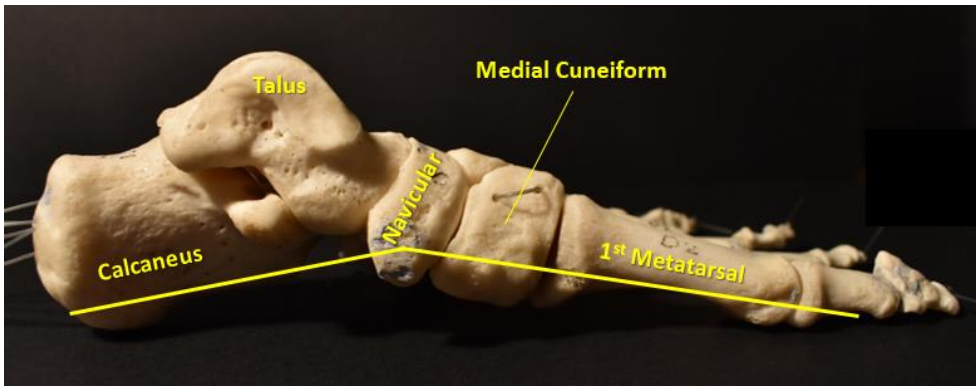

Figure 6-3 Medial view of articulated left foot skeleton

The medial longitudinal arch apexes at the tuberosity of the navicular tarsus bone. The navicular articulates with the talus posteriorly, which in turn articulates with the calcaneus via the subtalar joint. Anteriorly, the medial cuneiform intervenes between the navicular and the 1st metatarsal. With four articulations along its length, the medial longitudinal arch is more flexible than its lateral counterpart.

The angles formed around the apexes of the lateral and medial longitudinal arches are often used to describe the foot shape. The lower number of smaller articulations comprising the lateral column of foot bones, make it more rigid than its medial counterpart. Transverse arches are also commonly described, distally across the metatarsal-head line, and proximally across the tarsus.

6.1.2 Modelling the Foot Segment

Including the toes, each foot consists of 26 individual bones joined by 33 separate articulations; the internal complexity of the foot segment is only rivalled by that of the trunk. Modelling of these segments must contend with non-rigidity caused by genuine skeletal deformation, in addition to the STA influences suffered by all body segments. The RNOH_Trunk, developed in chapter 3, resolved this issue by ensuring that its tracking solution surface markers spanned the entire length of the segment; the resulting TRF was thus able to deform, to simultaneously represent the location of both the proximal and distal ends of the segment.

Analogues to the trunk, the primary aim of the foot model, remains the accurate representation of the orientation of the whole segment. Here again, the simplistic BMC solution for the foot segment provides a good starting point for development but presents with an obvious deficit. Unlike the trunk, where the identified deficit was in the tracking solution, the BMC_Foot shows an anatomical anomaly that manifests as a medial side high orientation during mid-stance (Chapter 2 Figure 2-8), where the typically developing test cohort, would reasonably be expected to show near flat ground contact. The cause of this deficit is clearly a failure to locate surface markers over the first and fifth metatarsal bases, at a common height above the plantar surface of the foot. Similar to the RNOH_Trunk, development of the whole segment RNOH_Foot will aim to apply targeted complexity to the simplistic BMC solution in order to resolve the identified deficit.

Once the whole segment orientation of the foot is described, modelling of the internal deformation by division into sub-region, requires additional mid-segment surface markers. For the trunk, the utility costs of these extra markers were judged to outweigh the value of the resultant information in the context of a clinical gait analysis. At the foot, increased accessibility, and a direct involvement in

locomotion tips this balance towards the development of a multi-segment modelling approach.

MSFM development aims to describe the internal deformation of the foot shape in response to applied forces as it is loaded and unloaded through the gait cycle. This development differs from that of previous orientation modelling where the simplest suitable solution was sought. The focus of MSFM development is on with how much of the underlying anatomical complexity is available to useful representation by surface markers.

6.1.3 The Heidelberg Foot Measurement Method (HFMM)

The HFMM takes a novel approach to modelling the foot, with the aim of outputting descriptive angles suitable for general clinical use (Simon et al., 2006). Instead of dividing the foot into 3D sub-regions, HFMM outputs describe the angle formed by line-vectors defined between various surface markers, sometimes projected onto a plane. Clinical applicability is somewhat compromised by the additional definition of separate tibiotalar and subtalar axis based on normative anatomy (Areblad et al., 1990, van den Bogert et al., 1994). Other outputs include overall and medial forefoot splay angles, medial and lateral arch angles, forefoot supination with respect to both shank and midfoot reference lines, and adduction with respect to shank and hind-foot reference lines. Another vector describes the flexion and adduction angle of the great toe (hallux). This innovative, non-orthogonal modelling approach seems applicable to the stated MSFM aim of describing the foot shape, rather than orientation, in a clinically applicable way. There are obvious comparisons to methods used to extract angular measurements from x-ray images. The somewhat arbitrary definitions of the vector lines contributing to each output, however, does not lend itself to simple description, and overall, the collection of independent outputs are more measurement than model.

6.1.4 Sensitivity of Close Proximity surface markers to Rotational Error

The vast majority of current MSFM employ the familiar Euler/Cardan/JCS type mathematics, to describe the 3D orientation of defined foot sub-regions(Bishop

et al., 2012, Deschamps et al., 2012). The small size of these sub-regions, however, confines surface markers to much smaller separation distance than for the whole segment modelling considered in previous chapters. This in turn, magnifies the angular consequence of any absolutes error in marker placement (Hyslop et al., 2010, Leardini et al., 2019). Consider, for example, the coronal plane heel alignment defined by the intersection of a KJC-AJC shank line, and vertical line bisecting the posterior heel surface. In this case, marker misplacement causing the AJC location to model say, 5mm too medial, will cause less than 1° error in the orientation of a realistically 500mm long shank segment (arcsine 5/500), but more than 5° error in the alignment of a 50mm high hind-foot segment. Current MSFM have, unreasonably, tended to pass responsibility for this modelling sensitivity to the data collection protocol, by the promoting the requirements for operator training and experience (Leardini et al., 2019).

6.1.5 Validity of current MSFM

While an early review of foot models concluded that there was insufficient evidence for the use of MSFM in clinical practice (Deschamps et al., 2012), a more recent review of largely the same models reached the opposite conclusion (Leardini et al., 2019). This latter review, identified 39 clinical models published between 1990 and 2016, suggesting a validity barrier for the introduction of new models. Both reviews concede, however, that direct validation by invasive means is challenging, that current validity claims are based largely on reliability studies/qualitative interpretation, and that the claimed reliability is based largely on widespread usage in differing populations. In this regard, the earlier review condemns widespread use of correlation indices over absolute measures of variability. These indices are considered to mask interpretation of the model's true reliability (Deschamps et al., 2012).

On the above-described basis, two prolifically used models have been highlighted as having demonstrated some level of validity (Bishop et al., 2012, Deschamps et al., 2012). The Milwaukee Foot Model (MFM(Kidder et al., 1996)), and a self-proclaimed similar marker arrangement, the Oxford Foot Model (OFM (Carson et al., 2001)), now commercially backed in modified form and incorporated into Vicon software(mOFM (Stebbins et al., 2006)). MFM model validity derives from

its novel use of X ray images to calibrated surface marker location to bony orientations The OFM attempt this calibration by surface marker directly, without the assumption of a neutral static posture employed by many other models.

6.1.6 Similarities of current MSFM

Pragmatically, there are a finite number of identifiable bony landmark foot locations, over which surface markers may be located, and that are therefore broadly common to all MSFM. The forefoot presents the distal heads and proximal bases of the metatarsals. The medial and lateral landmarks of the 1st and 5th metatarsals are commonly employed to mark the perimeter of this sub-region. A central axis may also be defined by the 2nd or 3rd metatarsal landmarks, or alternatively the by the space between them. Proximal base landmarks might alternatively be replaced by their adjacent tarsal bone of the midfoot, the navicular for the 1st base, cuboid for the 5th base. The location of other tarsal bones may be estimated relative to these identifiable landmarks, by knowledge of their general arrangement. On the anterior aspect of the ankle, the talus is faintly palpable, and some models claim to be able to establish a subtalar neutral position from this (Houck et al., 2008, Tome et al., 2006). The only individual foot bone to providing a convincing 3D tracking solution, however, is the calcaneus, which presents with relatively large, medial, posterior and lateral heel surfaces available (Nester et al., 2007b).

It has previously been suggested that the commonality between MSFM marker placements probably furnishes them all with similar reliability characteristics (Nester et al., 2014). In this respect, each MSFM may be regarded as subtly different variant to a general solution, each aiming to optimise the validity of their outputs. Five reporting standard have been suggested to this aim. (Bishop et al., 2012). The first two standards concern the challenge of defining an appropriate number of foot sub-regions and the consequently required surface marker placement. The next two concern definition of segment ARF and subsequent calculation methods. The final standard concerns demonstrating inter-session reliability as a surrogate measure of validity.

6.1.7 Segmentation and Signal to Noise Ratio

Ex-vivo (Nester et al., 2010, Nester et al., 2007b, Okita et al., 2009, Zhu et al., 2020) and in vivo (Arndt et al., 2004, Lundgren et al., 2008, Wolf et al., 2008) bone-pin investigations of individual bone movements, show distinct movement patterns in all bones. While these studies demonstrate true complexity of the foot structure, they do not inform on how much of this complexity might be usefully captured by surface markers. Models developed in major clinical centres have, however, tended to regard the tarsus/midfoot region as a joint complex between hind and fore foot sub-segments, rather than as a separate segment (Carson et al., 2001, Kidder et al., 1996, Saraswat et al., 2012, Stebbins et al., 2006).

Accurate representation of any foot sub-region by surface markers, depends on its movement being much larger than associated STA and other measurement error (Hyslop et al., 2010, Leardini et al., 2019), and on it being sufficiently large to facilitate reliable representation by surface markers. Genuine anatomical complexity makes fully realistic modelling of individual foot bones, apart from the calcaneus, outside of the scope of a surface marker-based approach. Arguments, for example, on the clinical desirability of including a mid-foot regions (De Mits et al., 2012), does not in itself, make this orientation accurately measurable by surface markers. MSFM development is therefore concerned with the question of how much of the foot's underlying complexity is usefully measurable, not on how much would be clinically desirable.

6.1.8 Modelling orientation of the Hind-foot

Although all identified MSFM include a hind-foot segment (Bishop et al., 2012, Deschamps et al., 2012, Leardini et al., 2019), accurate representation of even this segment's ARF axis by surface markers, is widely recognised as a major challenge (Hyslop et al., 2010, Leardini et al., 2007, Rattanaprasert et al., 1999, Wu et al., 2000). Coronal alignment concerns the orientation of the posterior vertical heel line. Many MSFM represent this line directly by inferior and superior placed surface markers on the posterior heel surface (Bishop et al., 2013, Bruening et al., 2012, Carson et al., 2001, Hyslop et al., 2010, Oosterwaal et al., 2016, Pohl et al., 2006, Rattanaprasert et al., 1999, Seo et al., 2014, Stebbins et

al., 2006). The close proximity of these markers, however, makes this representation extremely sensitive to marker placement error (Maurer et al., 2013). The natural curvature of the region and STA associated with the insertion of the Achilles tendon further increase the difficultly of this placement. Other models have opted to instead define a equivalent (orthogonal) medio-lateral axis via a variety of methods including, clinical judgment (Hunt et al., 2001), goniometer calibration (Saraswat et al., 2012), use of a heel alignment jig (Simon et al., 2006) or cross-hair laser (Tulchin et al., 2010a). None of these method have provided a widely recognised reliable solution.

Absence of any bony landmarks at the anterior calcaneus, also presents an additional challenge to modelling the hind-foot sagittal inclination. Even the OFM, which claims a primary objective of not assuming a neutral orientation during the static examination (Stebbins et al., 2006), makes an exception for this measurement (Carson et al., 2001). Other models that employ two minimally separated lateral markers (Jenkyn and Nicol, 2007, Rao et al., 2007, Scott and Winter, 1991), suffer similar close-proximity error sensitivity, to the use of inferior and superior heel markers for the coronal alignment.

6.2 Development of RNOH_Foot model

Modification to the BMC foot, provides a single segment representation of the whole foot orientation, prior to development of a multi-segment modelling approach.

6.2.1 RNOH_Foot Single Segment solution

Development of the single segment RNOH_Foot takes the form a modification to the BMC solution presented in chapter 2. Orientation of the single segment foot is intended to report how the plantar surface interacts with the ground. This requirement is essential if the model is to distinguish, for example, between a heel-strike, or flat-foot ground contact. Direct measurement of the required plane by markers located on the plantar surface is, of course, not possible. In theory, it is possible to represent a parallel plane by markers placed on the dorsal surface of the 5th metatarsal head, medial surface of the 1st metatarsal head and posterior

surface of the heel (the BMC model – chapter 2). This approach however presents two practical problems in its implementation. First, different curvatures on these surfaces, make judgement of equal heights above the plantar surface difficult. Second, the required marker located on the medial surface of the 1st metatarsal head, is highly susceptible to being dislodged during gait trails. This practicality often results in the marker being fixed too high on the dorsal foot surface. Although this might be resolved by implementation of a CAST method, with the additional tracking marker on the dorsal surface, this is not the approach adopted by the RNOH_Foot. Instead, both marker placement problems are resolved by the introduction of a bespoke calibration procedure, which reduces the requirement for accurate marker placement at all three locations.

With the subject seated, the calibration height of all three required markers, is measured with the planter surface flat to the floor. Experience has shown that this can usually be achieved in a single calibration for each foot. Occasionally, it is necessary to calibrate the two forefoot markers separately to the hind-foot marker. Following calibration, virtual representations of markers representing the plantar surface plane defined by the 1st and 5th metatarsal heads with the heel are easily calculated (Figure 6-4).

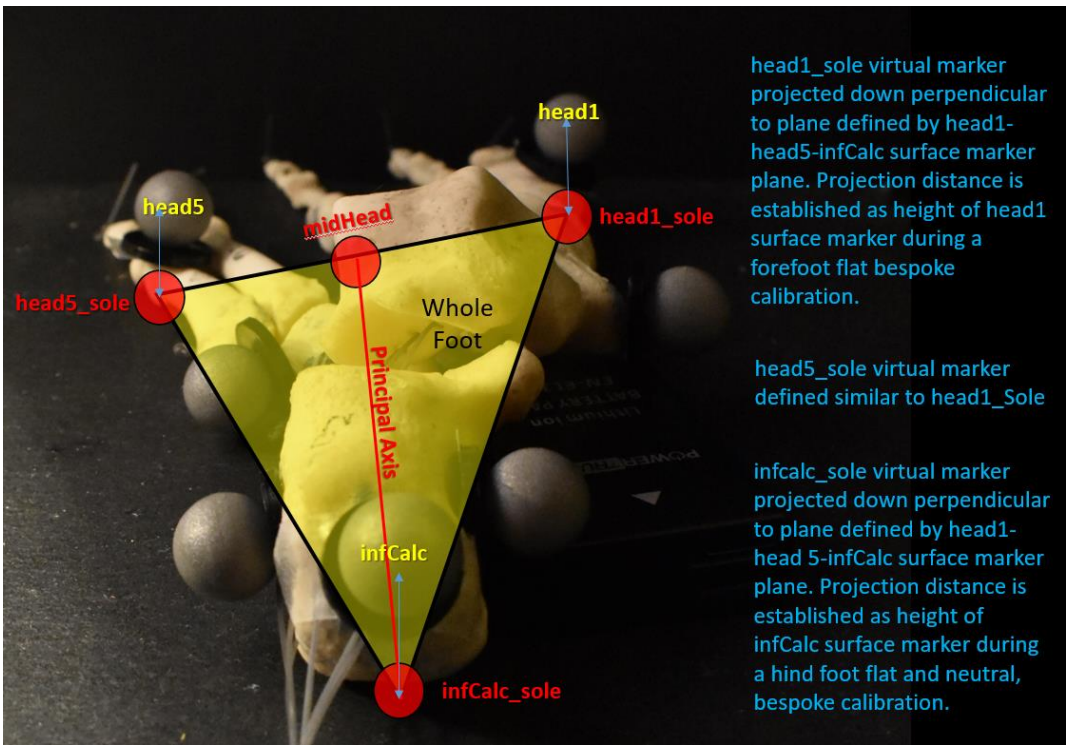

Figure 6-4 Projection of heel, head1 and head5 surface markers to Plantar Surface Plane

Posterior view of skeletal left foot, illustrated to show derivation of RNOH whole foot segment. The principal plane is calibrated to the plantar surface. This definition facilitates accurate description of the segment's orientation with respect to the ground.

To recap, the BMC_Foot represents the plantar surface of the foot by three surface markers over the posterior heel surface, 1st and 5th metatarsal head. Difficulty in fixing these markers to define a parallel plane is relinquished by re-specification of metatarsal head markers onto the dorsal foot surface and introduction of a bespoke calibration procedures for the hind and forefoot sub-segments. These calibrations relate surface marker locations to a posed neutral foot posture. For the forefoot this simply requires the metatarsal headline to make flat foot contact. In this position the height of the 1st and 5th metatarsal head markers are measured. During the static full model calibration, virtual representations of these markers are created on the plantar surface, by subtraction of these heights, perpendicular to the plane defined by all 3 of the original surface markers. The bespoke hind-foot calibration similarly requires the heel to be flat to the floor such that a plantar surface virtual representation may be created. These segment specific calibrations remove any requirement for the foot to remain neutral during the full model calibration. The three virtual

representations of their surface markers are thus calibrated to represent the required plantar surface plane; this is the principal plane of the RNOH_Foot segment.

With the plantar surface plane of the foot defined, the next section considers development of a MSFM.

6.2.2 Analysis of Existing MSFM by Complexity Groupings

Existing MSFM are considered in groups of decreasing complexity. Lessons-learned from each analysis are taken forward to the next, and identification of a clinically appropriate level of complexity sought.

Development of the RNOH_Foot into a MSFM is based on a structural analysis of thirty-nine clinical foot models identified in a recent published review (Leardini et al., 2019). Of these, the already mentioned HFMM (Simon et al., 2006), and bone-pin methods papers (Wolf et al., 2008) are rejected on the basis that they do not present a novel MSFM. Another publication is rejected on the basis of being presented as a book reference only without any peer review (Henley et al., 2008). The remaining 37 models are analysed in groups of similar complexity. Ignoring any modelling of the toes, these groups are identified by a nomenclature borrowed from the days of steam, when locomotives were recognised by the configurations of their wheels. The toy train from my childhood, with 4 wheels at the front, 6 main driving wheels and no extra wheels behind would thus be categorised as a [4-6-0] (Figure 6-5).

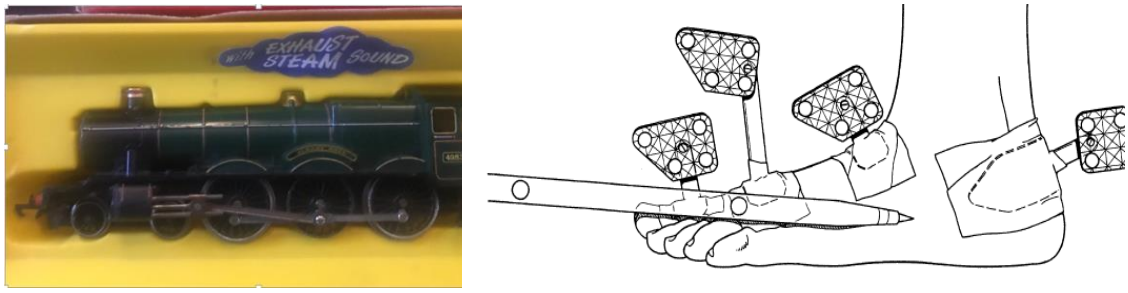

Figure 6-5 MSFM classification by number of fore, mid and hind foot subdivisions

The Whyte locomotive classification by number of wheels in front middle and rear sets has this toy locomotive (left) as [4-6-0]. A similar system is proposed to show the number of MSFM subdivisions in the forefoot (excluding toes)-midfoot-and hind-foot region. For example, complexity of a proposed CAST model (right) with single tracking clusters over forefoot, midfoot and hind-foot regions (Leardini et al., 1999), is classified as [1-1-1].

Similarly, the MSFM are here grouped by the number of further sub-divisions they employ in the forefoot, midfoot and hind-foot regions,

6.2.2.1 [5-5-2] – The Ultimate in Complexity with all Foot Bones Individually Modelled

Only one model was identified in this extreme classification, which attempts to individually model the orientation and movement of all five metatarsal bones, all five tarsal bones and both the talus and calcaneal bones of the hind-foot (Oosterwaal et al., 2016, Oosterwaal et al., 2011). The model additional outputs kinematic for movement of all toe bones. This is achieved from forty-three surface markers per foot, via a combination of true measurement, constraining some modelled joints to move in specified planes only, and others to move in assumed kinematic rhythms. The high number of surface markers and normative modelling assumption, make this model too complex for clinical applications.

6.2.2.2 [2-2-1] - Medial and Lateral Forefoot and Midfoot plus a Single hind-foot segment.

Four models are identified that employ this segmental division. One of these is a conference presentation, including segments labelled talus and cuboid, but with

marker placements only described as ‘anatomically appropriate’, and use of Euler angles without specification of a rotation sequence (Hwang et al., 2004). The second model, from the Shriners Hospital in Salt Lake City, Utah, focuses on introducing intra-foot kinetic to a MSFM (MacWilliams et al., 2003). This paper lacks details of the segmental ARF orientations, and includes an admission that further refinement is required in this respect.

The remaining two models are virtually identical presentations of a single model with a common lead author (Cobb et al., 2016, Cobb et al., 2009). The model was first presented with a clinical focus looking at patients with stiff feet. Unfortunately, complexity of the model contributed to reconstruction failure of the lateral midfoot and lateral forefoot segments. Despite this, the second publication with a more technical focus, continues to promote the mind-set that insufficient subdivision risks masking foot dysfunction. An alternative viewpoint is that this number of foot subdivision remains too complex for clinically applicable modelling by surface markers. Their testing identified the hind-foot-midfoot kinematic as the least reliable.

6.2.2.3 [2-1-1] - Single Hind and Midfoot, with Medial and Lateral Forefoot segments

Five models are identified that employ this segmental division. The complexity of three of these models limits their clinical utility in terms of their calibration procedure (Jenkyn and Nicol, 2007), nonstandard use of JCS (Arampatzis et al., 2002) and extensive surface marker requirement (Hyslop et al., 2010).

The two remaining models offer different insights into model design. A collection of normal walking data from 100 barefoot adults showed relatively little movement between mid-foot and hind-foot segments, and larger, distinct movement patterns from medial and lateral forefoot segments with respect to the midfoot (Nester et al., 2014). Taken together, these findings support division of the foot into hind, medial forefoot, and lateral forefoot segments. The final model in this group, claims to provide an optimal complexity-utility balance, but does not offer any evidence for this assertion (De Mits et al., 2012). The model’s most significant contribution was actually the concept of modelling a posterior to anterior hind-foot principal axis, from the heel to a mid-point between navicular and cuboid surface

markers This idea was independently suggested by another of the identified models, creating a midfoot joint centre for kinetic calculations (Bruening et al., 2012). In both instances, the arrangement allows the inclination angle of the hind-foot to be modelled without the need for an X-ray measurement (Kidder et al., 1996, Saraswat et al., 2012), or the assumption of a neutral orientation during the model calibration pose.

6.2.2.4 [2-0-1] - Medial and Lateral Forefoot segments direct to Hind-foot

Only three clinical publications that employ this segmental division are identified. Two of these made this division by separation of the 1st metatarsal bone from the lateral forefoot, to report a pathological cohort against a healthy control. The first of these, studied patients with tibialis posterior dysfunction by the use of a rigid tracking cluster CAST method (Tome et al., 2006). This study reported increased medial arch angle during the double support periods of the gait cycle, accompanied by excessive hind-foot eversion on loading and forefoot abduction on off-loading. The second clinical study fixed markers directly to the skin surface to report on patients with diabetic neuropathy (Rao et al., 2007). These patients showed reduced hind-foot eversion in early stance, accompanied by reduced forefoot splay; during terminal stance hind-foot plantarflexion and both medial and lateral forefoot supination were also reduced. Unfortunately, the clinical focus of both publications contributed to poor/incomplete descriptions of their underlying biomechanical models. Model outputs describe hind-foot orientation and forefoot morphology using existing clinical terminology.

The final model identified in this group, tested twenty healthy adults, and shows the arrangement to have good inter-session reliability (Seo et al., 2014). This is consistent with another study investigating the objective foot segmentation schema based on relative intra segment rigidity and intersegment mobility (Rouhani et al., 2011). Here again, the [2-0-1] configuration is suggested as a sensible upper limit for reliable kinematic outputs.

6.2.2.5 [1-1-1] - The Rizzoli Foot Models

Two MSFM from the Rizzoli Laboratory, Bologna, Italy, have been proposed by the same lead author of the review employed to identify all clinical MSFM for this critical analysis (Leardini et al., 2007, Leardini et al., 1999). The first attempt employed separate rigid clusters moulded to fit hind, midfoot and forefoot segments. Each cluster had at least 3 non-co-linear markers that would act as seemingly perfect TRF. The suitability of these frames to track the underlying bones would however be less perfect (Figure 6-5). Each cluster was related to bony landmarks locations identified by a digital pointer during an upright posture standing calibration trial (CAST method). These calibration orientations were assumed neutral; this made test-retest reliability less dependent of accurate marker placement by the clinician, at the expense of requiring a consistent standing posture by the subject. Model validity depends on this posture being truly neutral, severely limiting its application in the clinical environment.

The second Rizzoli model moved away from the CAST method, acknowledging that the rigid clusters were uncomfortable to wear, and use of the digitised pointer time-consuming. Anatomical locations were instead identified by direct placement of surface markers. Many features of the original model were retained, including a separate midfoot segment, restriction to stance phase measurement, and retention of the neutral posture assumption during the static trial. Marker placements were unremarkable, with the familiar trio of medial, posterior and lateral hind-foot markers and quartet of fifth and first metatarsal head and base markers. The long axis of the metatarsus was defined via second head and base markers.

A single hallux marker allows a vector representation with the head of the first metatarsal. Volatility of the hallux calculation is acknowledged secondary to the necessary proximity of markers on this small segment. Several other clinically relevant planar projection angles, akin to angles commonly extracted from static x-ray images, are also output. For all angles, projection artefacts are minimised through choice of minimally oblique planes. All planar angles are output as absolute values without static offset contamination of a neutral static assumption.

6.2.2.6 [1-1-1] – Other Models Employing Transverse Tarsal and Tarso metatarsal joints

One of these studies employed electromagnetic sensors to measure 3D orientation via the near field magnetic vectors of three orthogonal coils(Cornwall and McPoil, 1999). Sensors were located over the calcaneus, navicular and first metatarsal bone and stance phase orientations reported with respect to a reference sensor located over the tibia. As movements of the whole foot with respect to the tibia, was much greater than any individual difference seen by different foot sensors, all outputs were essentially representation of the ankle movement.

Two surface marker based solutions investigated diabetic feet (Sawacha et al., 2009) and kinematics of the foot-shoe combination.(Bishop et al., 2013). These models were structurally similar to the most recent model from the Rizzoli laboratory (Leardini et al., 2007).

6.2.2.7 [1-0-1] – The Milwaukie Foot Model (MFM)

Published in 1996, the Milwaukie Foot Model (MFM) is now regarded as the grandfather of the modern multi-segment approach (Kidder et al., 1996). This largely technical paper presents data from a single adult subject only. This model claims to be the first to report the full gait cycle including swing phase. The acclaimed validity of model (Bishop et al., 2012, Deschamps et al., 2011) comes at a high clinical price. Technical reference frames for each segment are referenced to the underlying skeletal anatomy using radiographic images. X-ray exposure is therefore an integral part of the required protocol. Angles not measurable from X-ray images rely on clinical determination; the coronal plane orientations of the forefoot and hallux, and the transverse plane orientation of the hind-foot are acknowledged as particularly difficult.

Marker placement consists of the familiar medial, lateral, and posterior calcaneal markers for the hind-foot, first and fifth metatarsal head plus first metatarsal base for the forefoot. The proximal phalanx of the hallux is tracked via a marker cluster triad.

6.2.2.8 [1-0-1] - The original Oxford Foot Model (OFM) and modified form (mOFM)

Evolution of OFM into the mOFM facilitated a claim of validity transference from one to the other (Stebbins et al., 2006). Validity of the original OFM however, was established in an era when other models were tending to prioritise reliability by application of a static neutral assumption. Difference between the original OFM and its modified version are at least as large as that between other published configurations. Incorporation of the mOFM into the Vicon software has enabled it to become a widely employed industry standard.

Without any testing, the principal plane of the mOFM hind-foot was redefined, to substitute the mid-malleoli location, for a mid-calcaneal location. This change requires the addition of two extra markers, which seems contrary to the stated aim of the modification to make the model suitable for use with smaller, children's feet. On this 'default' model, five more modelling variations were then accessed.

The first tested variation was to replace a mid-metatarsal head toe marker, with a virtual representation calculated between surface markers over the 1st and 5th metatarsal heads. This change, which again would have reduced the number of physical markers required on the smaller foot, was found to make no difference to model outputs but was rejected.

The second variation was to restrict tracking markers to the lateral side of the forefoot only. This resulted in a reduced range of captured movement which is interpreted as a violation of the rigid body assumption across the full forefoot region. Instead of suggesting separate medial and lateral sub-regions, however, the medial arch height with respect to the lateral plantar surface, is offered as an estimate of forefoot supination error.

The third variation concerns elimination of a wand mounted marker on the posterior aspect of the hind-foot for dynamic tracking. The wand is found to make no significant difference, but again, an opportunity to increase the model utility is missed and the wand is retained.

The fourth variation concerns substitution of a tibial defined shank segment, with the CGM definition to the mid-epicondyle KJC location. This is found to cause

offset difference in the hind-foot kinematic but is accepted to maintain compatibility with the PiG lower limb model.

Finally, the fifth variation was another consideration of the posterior hind-foot wand marker - concerning its role in defining the segment ARF. Difficulty in aligning the wand shows the only significant difference from the five tested variations, and the wand is eliminated for this purpose.

Model validity is claimed based on historic heritage without any reference to a gold standard measure, and reliability is claimed despite significant (approx. 12° and matching the movement range) inter-day variation in the example kinematic shown (see Figure 2 in (Stebbins et al., 2006)). Difficulty in replicating even this level of reliability has led others to employ alternative techniques, such as those offered by the Shriners Hospital for Children Greenville (SHCG) model.(Maurer et al., 2013).

6.2.2.9 [1-0-1] - The Shriners Hospital for Children Greenville (SHCG) foot model

The (SHCG) model, from the list of identified models, did not provide a peer review reference (Davis et al., 2006.). The provided validity reference (Maurer et al., 2013), describes how the model decreases its reliance on accurate marker placement by calibration against a 'smart surface' to represent the plantar surface of the foot. For a typically developing subject, this is simply achieved by a flat-footed contact with the floor – this appears similar to the RNOH_Foot calibration previously described. In deformed feet, that cannot achieve this posture, rather than calibrate the hind and forefoot separately, a wedge of known slope is inserted under the foot. Comparison with the mOFM showed similar interrater reliability, but improved intra-rater reliability, in a patient group requiring a hind-foot wedge to account for a midfoot break. This suggests that the technique has merit, but that use of the wedge it not consistent between different users. Insufficient detail is provided for further conclusions; the paper has a primary clinical focus. Patients with midfoot break are shown to exhibit a decreased peak hind-foot dorsiflexion angle and increased fore-foot dorsiflexion range, compared to a typically developing control group.

Another publication describes a modification to the SHCG, providing three optional method to orientate the foot sub-segment ARFs (Saraswat et al., 2012). Option 1 aligns all local ARF to the plantar surface of the foot as defined by a 'smart surface' as above. Option 2 is based on X-ray measurements of the hind-foot and forefoot orientation as championed by the MFM. Option 3 is based on a surface marker orientations orientation method as championed by the OFM.

6.2.2.10 [1-0-1] – Other simple MSFM with Hind-foot and Forefoot segments only

Models developed subsequent to the MFM have tended to remove the need for X-ray registration by instead defining ARF via surface marker locations. Like the Leardini approach, many of these models attempt to control inter-session reliability by disregarding the actual ARF orientation during the static calibration, and instead resetting this orientation as 0° around all three axes (Hunt et al., 2001, Kitaoka et al., 2006, Pohl et al., 2006, Rattanaprasert et al., 1999, Thomas et al., 2006, Wu et al., 2000). This strategy relies on the subject being able to reproduce the calibration position between sessions, more reliably that the surface markers are placed to represent the segment's true orientation. Model validity additionally requires that this pose is a meaningful neutral posture. Various jigs and positional protocols are employed to aid this. Subsequent movements are then reported around the defined axis with respect to this static calibration posture. Non-neutral hind-foot inversion-eversion is particularly difficult to control during the static calibration even in typically developing subjects. Two models correct for this, by facilitating input of a non-neutral hind-foot coronal plane orientation (Hunt et al., 2001, Rattanaprasert et al., 1999).

Other models, with a greater clinical focus, assume that all segment orientations match their surface-marker ARF orientation during the static calibration. (Bruening et al., 2012, Carson et al., 2001, Chard et al., 2013, Souza et al., 2014, Tulchin et al., 2010a, Stebbins et al., 2006). This is akin to normal practice at the larger body segments but inevitably trades model validity for test-retest reliability.

6.2.2.11 [0-0-2] - Early Models focused separation of tibiotalar and subtalar kinematic

The four earliest identified models investigated the hind-foot region only. Two of these focused on division of the tibiocalcaneal kinematic, into its separate tibiotalar and subtalar articular components (Kepple et al., 1990, Scott and Winter, 1991). Inaccessibility of the talus bone forced these, and more recent attempts not recognised in the identified list, (for example (van den Bogert et al., 1994) and the afore mentioned HFMM (Simon et al., 2006)), to employ modelling assumptions based on typically developing anatomy, that are unlikely to hold true in the clinical setting. More recently, a weight bearing computer tomography protocol has been able to establish the required anatomical division on an individual subject basis (Pena Fernandez et al., 2020). These measurements, however, remains outside of the scope of general gait analysis practice.

6.2.2.12 [0-0-1] - Early Models focused measuring the hind-foot only

A third identified early model also restricted itself to the rear foot kinematic, reporting on 14 healthy adult male subjects during the stance phase of gait (Moseley et al., 1996). This study highlights the difficulties of defining accurately aligned ARF for small sub-regions of the foot and employed a specialised jig to improve the assumption of a neutral ankle position during the static calibration procedure. While this approach improved reliability when collecting data from typically developed subjects, many patient feet are pathologically unable to adopt a neutral posture. Finally a study employing electromagnetic sensors to the hind-foot of 10 typically developing adults, and 10 with rheumatoid arthritis, was able to demonstrate the effectiveness of orthosis in normalising pronation in the feet of the pathological group (Woodburn et al., 1999).

6.2.3 Summary of MSFM Analysis

Table 6-1 summarises the above critical analysis of current MSFM by their level of complexity. Overall, this analysis supports use of the [2-0-1] configuration also suggested by a surface rigidity study (Rouhani et al., 2011). Models with more sub-divisions than this tend to require the assumption of a neutral posture during the static calibration trial in order to achieve reliability (Leardini et al., 2007).

Avoidance of a separate mid-foot region additionally facilitates use of cuboid and navicular landmarks to estimate the location of the anterior end of a hind-foot axis (Bruening et al., 2012, De Mits et al., 2012). Development of the mOFM additionally showed a clear difference in the movement of medial and lateral forefoot regions (see Figure 3 in (Stebbins et al., 2006)). Division of the foot into hind, lateral forefoot, and medial forefoot regions in consistent with clinical observations of hind-foot rigidity and forefoot medio-lateral flexibility. The introduction of posture specific calibration procedures has the potential to additionally reduce MSFM sensitivity to inaccurate marker placement (Maurer et al., 2013).

Table 6-1 Summary of lessons learned from analysis of current MSFM

Group/ Classification	Lessons Learned	References from (Leardini et al., 2019)
[5-5-2]	Kinematic outputs beyond that that can be captured by surface markers are only available through the acceptance of normative modelling assumptions.	(Oosterwaal et al., 2016, Oosterwaal et al., 2011)
[2-2-1]	Two under described models, and another that took two published attempt to achieve a full kinematic output, suggest that this configuration is unlikely to provide a sufficiently robust solution for general use.	(Cobb et al., 2016, Cobb et al., 2009, Hwang et al., 2004, MacWilliams et al., 2003)
[2-1-1]	3 models suggest that this configuration is still too complex. One of these makes the point that low amplitude kinematics are difficult to distinguish from inevitable measurement error. Another model tests 100 individual showing little movement between the hind-foot and mid foot segments, and different movements of medial and lateral forefoot segments. The final model in this set suggests use of a mid-tarsal location to orientate the inclination angle of the hind-foot.	(Arampatzis et al., 2002, De Mits et al., 2012, Hyslop et al., 2010, Jenkyn and Nicol, 2007, Nester et al., 2014)
[2-0-1]	2 models, both presented with clinical focus show difference between patient with tibialis posterior dysfunction and diabetic neuropathy respectively. Kinematic outputs are well matched to clinical terminology. A third study demonstrates good inter-session reliability.	(Rao et al., 2007, Seo et al., 2014, Tome et al., 2006)
[1-1-1]	This 3 segment configuration prioritises the anatomical description of the foot into hind-foot, mid-foot and forefoot regions, ahead of the [2-0-1] configuration suggested by surface region rigidity studies (Rouhani et al., 2011).	(Bishop et al., 2013, Cornwall and McPoil, 1999, Leardini et al., 2007, Leardini et al., 1999, Sawacha et al., 2009)
[1-0-1]	This configuration is the mainstay of current MSFM in clinical use. Models for this purpose generally trade reliability for validity by not assuming a neutral orientation of segments during the static calibration trial. Data from the mOFM provide strong evidence of the need to separate medial and lateral forefoot regions. The SHCG model shows improved reliability by the substitute of the need for accurate marker placement for bespoke calibration - similar to the BMC_Foot modification implemented at the start of this chapter.	(Bruening et al., 2012, Carson et al., 2001, Chard et al., 2013, Davis et al., 2006., Hunt et al., 2001, Kidder et al., 1996, Kitaoka et al., 2006, Pohl et al., 2006, Rattanaprasert et al., 1999, Saraswat et al., 2012, Souza et al., 2014, Stebbins et al., 2006, Thomas et al., 2006, Tulchin et al., 2010a, Wu et al., 2000)
[0-0-2]	Separation of ankle movements into talocrural and subtalar components remains outside of the scope of routine clinical gait analysis.	(Kepple et al., 1990, Scott and Winter, 1991)
[0-0-1]	Other early models, isolated the true ankle movement from general foot flexibility, by measurement of the hind-foot movement.	(Moseley et al., 1996, Woodburn et al., 1999)

6.2.4 RNOH_MSFM solution

The RNOH_MSFM aims to describe the internal shape of the foot segment, by the addition of surface markers to the whole foot model. Markers located over the medial navicular tuberosity and lateral cuboid locations, facilitating estimation of the anterior end of a hind-foot principal axis at the mid-point location (Bruening et al., 2012, De Mits et al., 2012). These locations also serve to mark the apex of the medial and lateral arches respectively; virtual representations of the 1st and

5th metatarsal head markers act as the anterior arch markers. These representations are similar to those defined to represent the plantar surface, only shifted to the mid-dorsal/plantar surface location. An equivalent posterior heel virtual marker is created at the mean height of these two virtual markers above the plantar surface.

The principal axis of the hind-foot is defined between the virtual heel marker, and the mid-navicular cuboid location. Conversion of this axis into a principal plane is achieved via an additional requirement for the posterior heel line to be vertical during the hind-foot calibration. This allows a virtual superior posterior marker to be created vertically above the real posterior heel surface marker. This real marker, plus additional medial and lateral surface markers, form a heel TRF solution that tracks the superior virtual marker position. In this way, the hind-foot principal plane is defined between the principal axis, and superior virtual markers during the full model calibration, without the need for a neutral posture assumption.

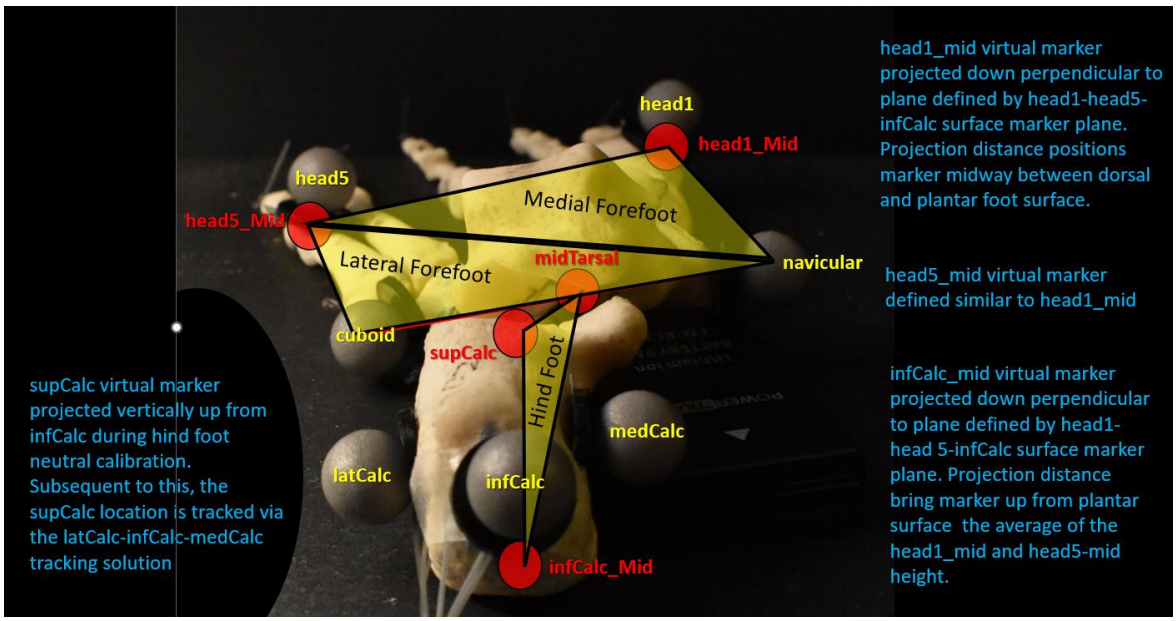

Figure 6-6 RNOH_MSFM posterior view

Posterior view of left foot skeleton, showing derivation the three RNOH_MSFM foot regions. The supCalc virtual marker is located vertically above infCalc during a hind-foot neutral posture calibration, and then tracked via a medCalc-infCalc-latCalc TRF.

Principal axis for medial and lateral forefoot segments run from the navicular and cuboid markers to the mid-segment virtual representation of the 1st and 5th metatarsal heads respectively. Application of appropriate Euler sequence as developed in chapter 2, ensures that these modelled axes are fully orientated in space, prior to specification of their axial spin orientation. Extension of the lateral forefoot principal axis to a principal plane by the navicular surface marker, allow the spin orientation to report the inversion/eversion orientation of the tarsus, without the specific inclusion of a mid-foot segment. This arrangement takes advantage of the relatively rigid anatomy, between the lateral forefoot and the tarsus. Similarly, extension of the medial forefoot principal axis to a principal plane by the 5th metatarsal head surface marker, allow the spin orientation to report the inversion/eversion orientation of the relatively flexible metatarsal-head line (Figure 6-7).

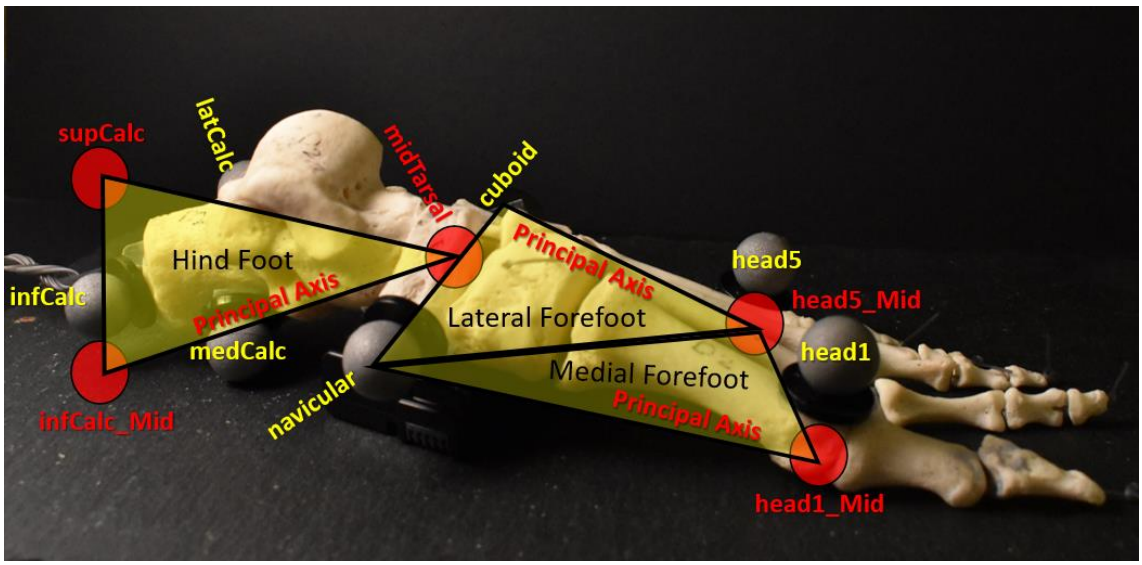

Figure 6-7 RNOH_MSFM medial view

Medial view of left foot skeleton, showing derivation the three RNOH_MSFM foot regions. The less mobile lateral division of the forefoot is grouped with the tarsal bones such that axial spin of the principal axis reports coronal plane movements of the midfoot. The same component of the medial forefoot, similarly reports the coronal plane position of the metatarsal head line.

The proposed RNOH_MSFM divides the foot into three similarly sized relatively rigid regions. This design is intended to maximise reliability. Critical marker placements are restricted to identification of navicular and cuboid locations that mark the skeletal apex of medial and lateral longitudinal arches respectively. Accurate placement of virtual anatomical representations of other surface markers is achieved via bespoke calibration procedures. This approach assumes that a clinician can place a segment into a neutral posture, more reliably than they can apply surface markers to represent segment anatomical axes.

The resultant anatomically defined ARF for each sub region facilitates model outputs that match clinical terminology. Sagittal orientation of both the lateral and medial forefoot segments, with respect to the hind foot, describe the angle of their respective longitudinal arches. Coronal components of these orientation then describe the respective tarsal and metatarsal head inversion orientations. Transverse plane components describe the lateral and medial forefoot adduction. Sagittal, coronal and transverse orientations of the medial forefoot with respect

to the lateral, describe increase in medial dorsiflexion, forefoot inversion with respect to the tarsus, and the forefoot splay angle.

6.3 Experiment 6A – Orientation of the RNOH_Foot

6.3.1 Aim

This experiment aims to evaluate effectiveness of the RNOH calibration to the BMC foot solution, in eliminating the aberrant non-neutral, coronal plane mid-stance offset.

6.3.2 Hypothesis

> Hypothesis 6A_I. The flat foot calibration applied to the BMC foot to create the RNOH_Foot, will better represent the orientation of the plantar surface of the foot. This will be demonstrated by generation of the expected near flat-foot mid-stance kinematic in the typically developing cohort.

6.3.3 Methods

6.3.3.1 Model Specification

Formal specifications of the RNOH_Foot segment are outlined in table 6-2.

Table 6-2 RNOH_Foot segments

PREFIX*	NAME	PLACEMENT / CALCULATION
Surface Markers		
L or R	infCalc	Posterior heel, similar to BMC, height no longer critical.
L or R	head1	Dorsal surface of 1st metatarsal head.
L or R	head5	Dorsal surface of 5th metatarsal head, in common with BMC.
Virtual Markers		
L or R	infCalc_Sole	infCalc projected down to plantar surface. Projected distance is the height of the marker during the bespoke hind foot calibration with the posterior flat to floor and heel vertically aligned. Projection direction is perpendicular to infCalc-head1-head5 plane.
L or R	head1_Sole	head1 projected down to plantar surface. Projected distance is the height of the marker during the bespoke forefoot calibration with the metatarsal head line flat to the floor. Projection direction is perpendicular to infCalc-head1-head5 plane.
L or R	head5_Sole	head5 projected down to plantar surface. Projected distance is the height of the marker during the bespoke forefoot calibration. Projection direction is perpendicular to infCalc-head1-head5 plane.
L or R	midToe	Mid-point of head1_Sole and head5_Sole virtual markers.
Anatomical Reference Frame (ARF)		
L or R	foot_RNOH	Principal axis from infCalc_Sole to midToe with head1_Sole defining principal transverse plane.
Technical Reference Frame (TRF)		
L or R	foot_RNOH	infCalc, head1 and head5 surface markers

**** L or R corresponds to left or right side respectively***

6.3.3.2 Laboratory Set-up

Data was collected concurrently with that for the BMC reference values presented in chapter 2. Additional surface markers were located on the dorsal surface of the 1st and 5th metatarsal head locations. Following this, and prior to the full model calibration, these markers plus the posterior heel marker were calibrated to the foot plantar surface.

The bespoke foot calibration, was performed with the subject sitting on an adjustable height bench, allowing the foot to be positioned flat to the floor. For the typically developing cohort, this posture approximated a 90° joint angle at hips, knees and ankles. In this position, control of the coronal plane foot orientation was controlled via axial rotation of the thigh segment. Separate calibration files were collected for each foot in turn, each consisting of a few seconds of data collection with the subject in a static posture.

6.3.4 Data analysis

6.3.4.1 Signal processing

The height the posterior calcaneal marker and the 1st and 5th metatarsal head markers on the dorsal surface of each foot, were extracted from their calibration trial. During the full model calibration, interim foot planes were defined between these same surface markers. Virtual representations of the three markers were then created perpendicular to this plane at the individual calibration heights. The full model calibration thereby avoided any postural requirement for a neutral foot position. The plane defined by the virtual markers, then represents the plantar surface of each foot. Orientation of this plane was expressed by three Euler angles, using a sagittal-transverse-coronal Cardan rotation sequence, constant with the antero-posteriorly defined principal axis.

6.3.4.2 Statistics

Paired t-test were applied across all gait scores, to identify statistically significant differences with BMC reference values.

Correlation coefficients were calculated for each gait score, against subject BMI. Correlations above 0.5 (R2 > 0.25) are highlighted in the solution designated colour.

6.3.5 Results 1 – Modification to BMC_Foot Segment

6.3.5.1 RNOH_Foot Kinematic

Figure 6-8 compares the BMC sagittal foot kinematic, based on a plane defined by posterior heel, 1st and 5th metatarsal head markers, with the RNOH modification which calibrated these same markers by virtual projection down to the plantar surface.

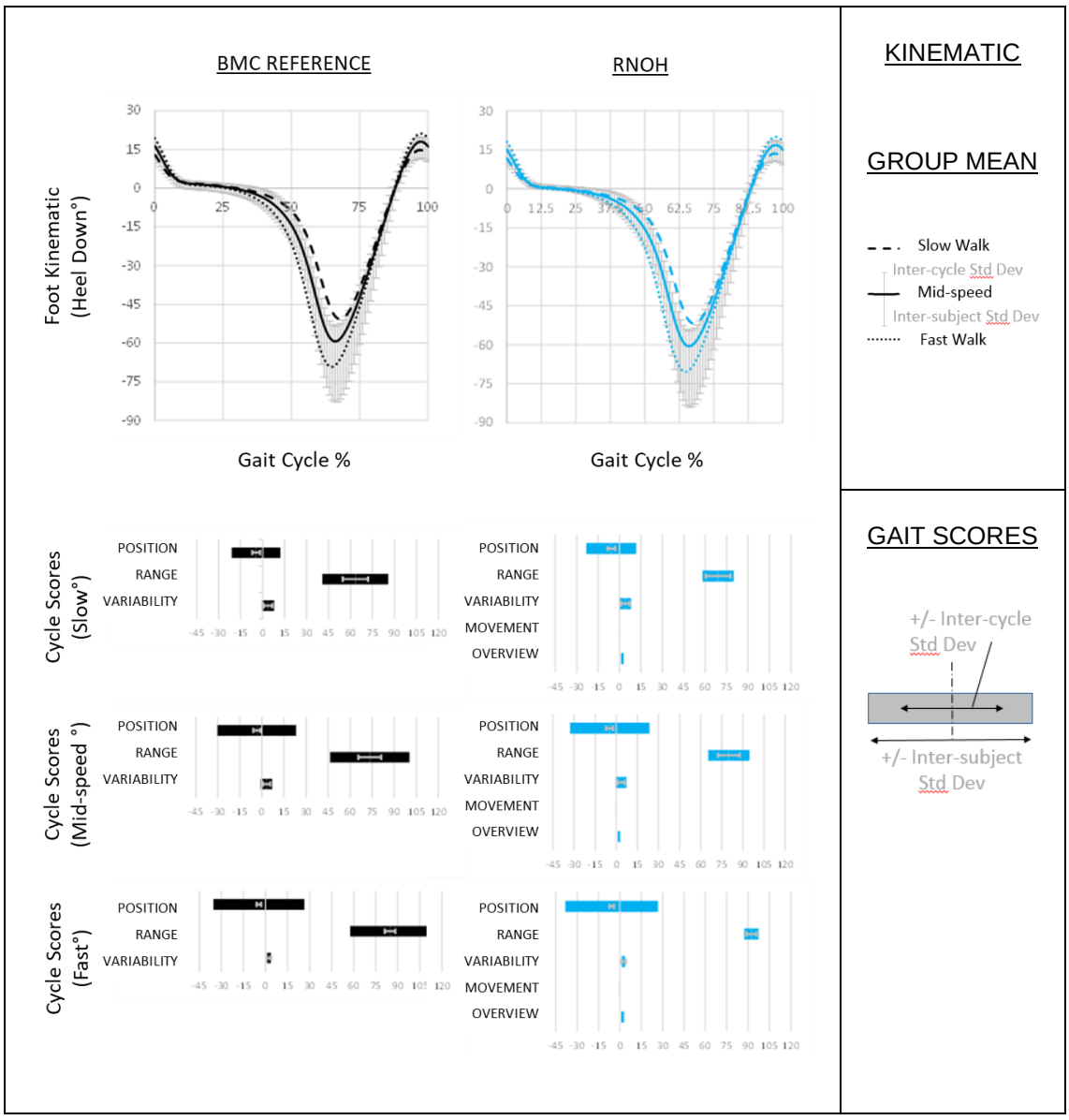

Figure 6-8 Sagittal plane comparison of RNOH calibration (right) with BMC reference (left)

Top row shows graphical kinematic for slow (dashed line), mid-speed (solid line) and fast (dotted line) walking as depicted in the legend (right). The mid-speed typical inter-cycle, and inter-subject standard deviations are shown above and below the mid-speed graph line respectively.

Subsequent rows depict speed specific gait scores as per the legend (right bottom). Cycle position, range and variability scores represent absolute values from zero. Movement pattern and overview scores measure the difference between comparative and BMC reference values.

The RNOH calibration shows no obvious effect on the sagittal kinematic. The coronal kinematic is shown in figure 6-9.

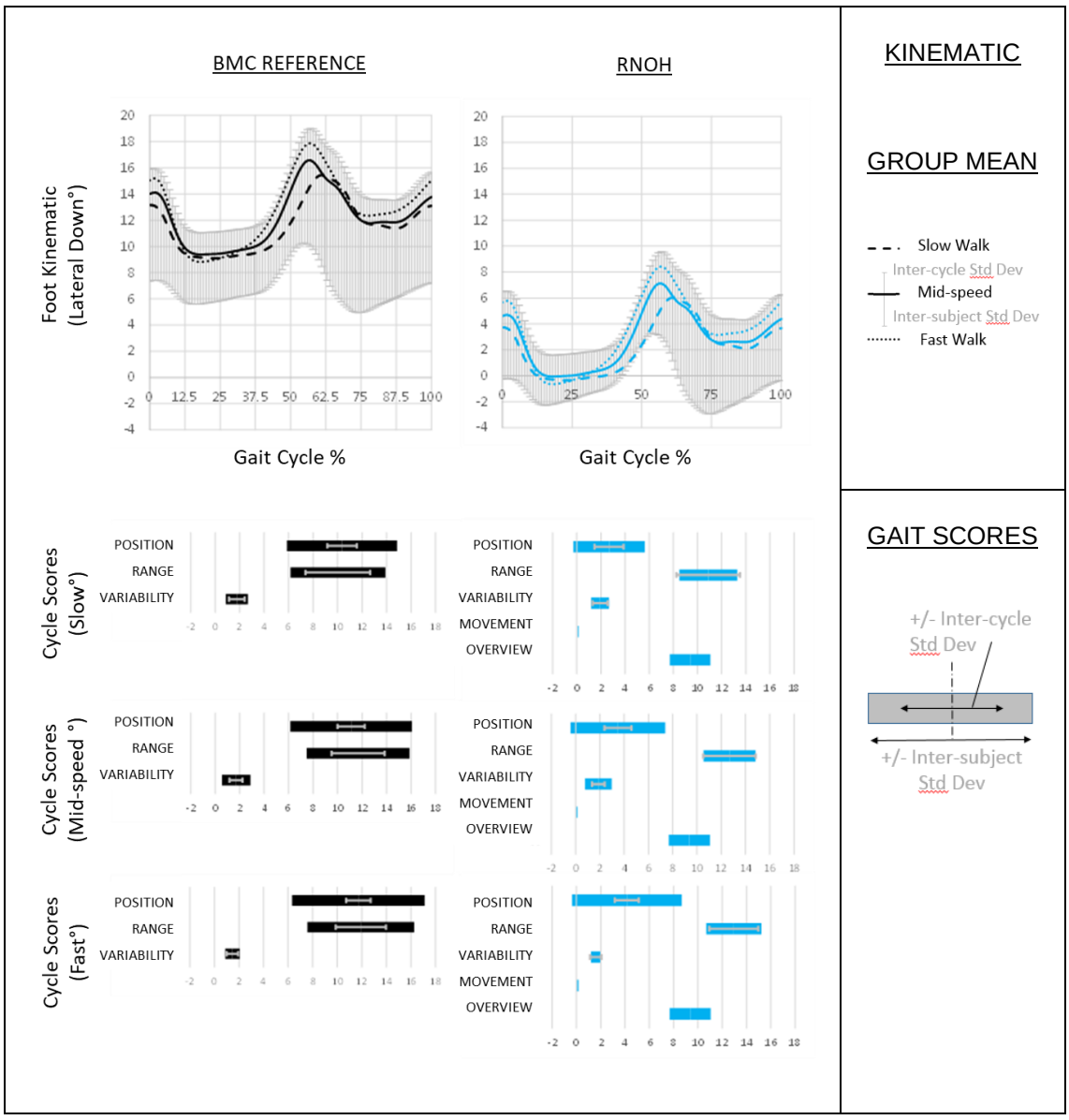

Figure 6-9 Coronal plane comparison of RNOH calibration (right) with BMC reference (left)

Top row shows graphical kinematic for slow (dashed line), mid-speed (solid line) and fast (dotted line) walking as depicted in the legend (right). The mid-speed typical inter-cycle, and inter-subject standard deviations are shown above and below the mid-speed graph line respectively.

Subsequent rows depict speed specific gait scores as per the legend (right bottom). Cycle position, range and variability scores represent absolute values from zero. Movement pattern and overview scores measure the difference between comparative and BMC reference values.

Figure 6-9 above clearly shows the expected shift in the coronal kinematic position; the RNOH calibration shows the typically developing average foot kinematic, flat to the ground, in both the sagittal and coronal components during the mid-support period. The transverse kinematic is depicted in figure 6-10 below.

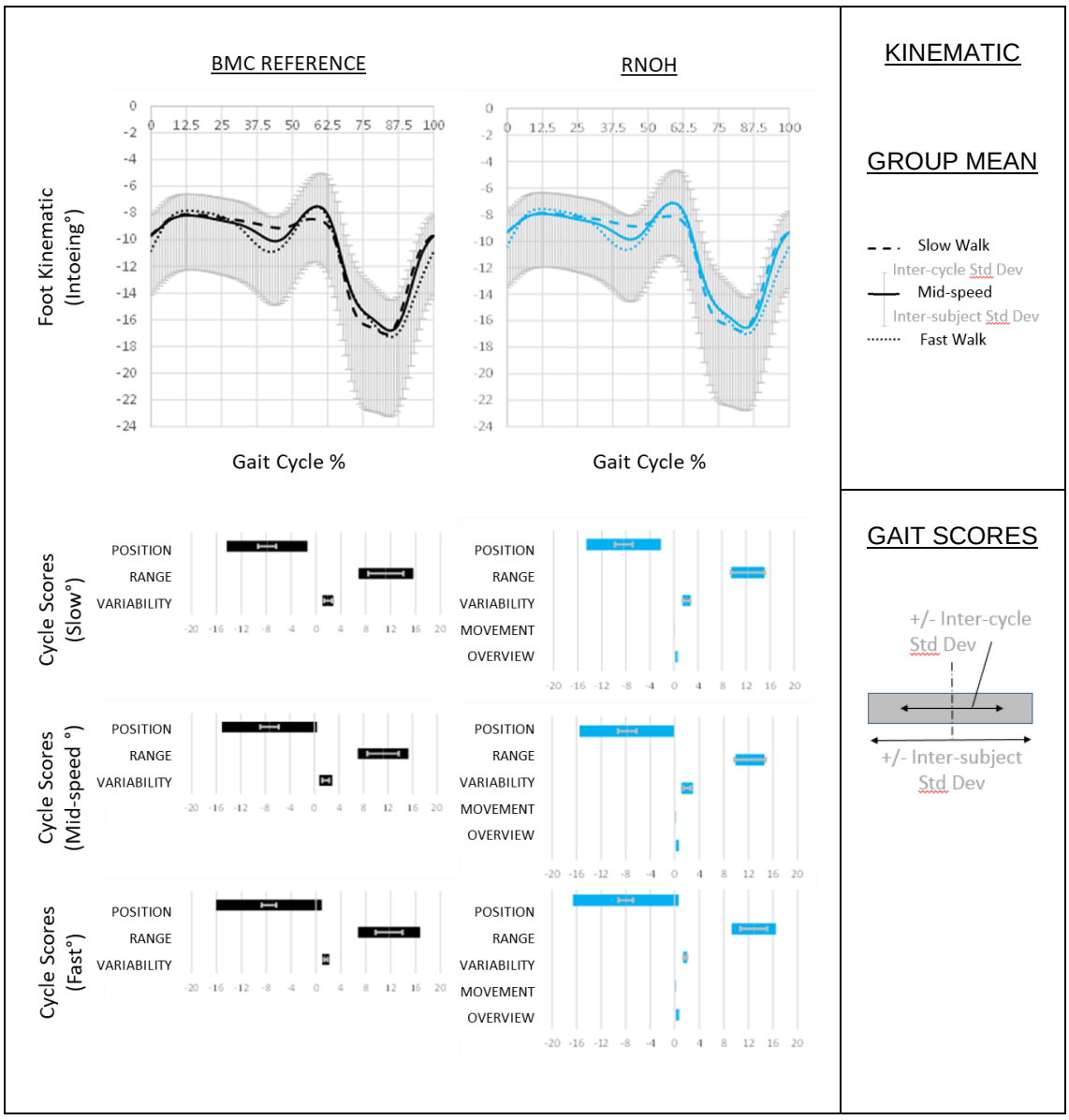

Figure 6-10 Transverse plane comparison of RNOH calibration (right) with BMC reference (left)

Top row shows graphical kinematic for slow (dashed line), mid-speed (solid line) and fast (dotted line) walking as depicted in the legend (right). The mid-speed typical inter-cycle, and inter-subject standard deviations are shown above and below the mid-speed graph line respectively.

Subsequent rows depict speed specific gait scores as per the legend (right bottom). Cycle position, range and variability scores represent absolute values from zero. Movement pattern and overview scores measure the difference between comparative and BMC reference values.

Like the sagittal kinematic, the RNOH calibration shows no obvious effect on the transverse plane kinematic.

6.3.5.2 BMI Effects

Table 6-3 shows the BMI coefficient of determination against each of the calculated gait scores.

Table 6-3 BMI correlation coefficient between gait scores from BMC and RNOH tracking solutions.

Sagittal

	Position			Range			Variability		
	Slow	MidSpeed	Fast	Slow	MidSpeed	Fast	Slow	MidSpeed	Fast
BMC	0.46	-0.07	0.15	-0.45	0.25	-0.49	0.18	-0.24	0.21
RNOH	0.43	-0.26	-0.07	-0.45	0.24	-0.50	0.18	-0.24	0.21

	Movement			Overview		
	Slow	MidSpeed	Fast	Slow	MidSpeed	Fast
RNOH	0.48	0.69	0.61	0.62	0.61	0.61

Coronal

	Position			Range			Variability		
	Slow	MidSpeed	Fast	Slow	MidSpeed	Fast	Slow	MidSpeed	Fast
BMC	0.51	0.62	0.62	0.05	0.25	0.04	-0.25	-0.65	-0.70
RNOH	0.55	0.66	0.65	0.03	0.23	0.02	-0.26	-0.65	-0.73

	Movement			Overview		
	Slow	MidSpeed	Fast	Slow	MidSpeed	Fast
RNOH	0.29	0.54	0.42	0.20	0.19	0.20

Transverse

	Position			Range			Variability		
	Slow	MidSpeed	Fast	Slow	MidSpeed	Fast	Slow	MidSpeed	Fast
BMC	-0.39	-0.41	-0.23	-0.17	0.33	-0.10	-0.27	-0.41	-0.63
RNOH	-0.36	-0.39	-0.19	-0.15	0.37	-0.07	-0.27	-0.41	-0.61

	Movement			Overview		
	Slow	MidSpeed	Fast	Slow	MidSpeed	Fast
RNOH	0.48	0.78	0.57	0.68	0.71	0.69

For the principal axis orientation, the measured sagittal and transverse average cycle position, range and variability show no strong correlations with subject BMI. BMI effects on the sagittal and transverse plane movement pattern are evident.

For the principal axis spin orientation (coronal), both the BMC and the RNOH solution show a positive correlation between subject BMI and a more supinated

average foot position. Decreased inter-cycle variability with increasing subject BMI might reflect reduced measurement error with larger feet.

6.3.6 Hypothesis Testing

Table 6-4 shows the kinematic differences causes by the RNOH_Foot calibration of the BMC reference segment. Significant differences are identified by paired T-test, and highlighted in blue.

Table 6-4 Difference between RNOH_Foot and BMC reference gait scores.

	Position (°)			Range (°)			Variability (°)		
	Sagittal	Coronal	Transverse	Sagittal	Coronal	Transverse	Sagittal	Coronal	Transverse
SLOW	-1.20	-9.39	0.26	0.00	-0.05	0.03	0.00	0.00	0.00
p-value	0.060	0.000	0.054	0.825	0.432	0.396	0.649	0.579	0.767
MIDSPEED	-1.20	-9.37	0.28	0.00	-0.05	0.05	0.00	0.00	0.00
p-value	0.060	0.000	0.050	0.898	0.378	0.474	0.311	0.622	0.576
FAST	-1.19	-9.36	0.30	-0.02	-0.05	0.07	0.00	-0.01	0.01
p-value	0.060	0.000	0.045	0.238	0.426	0.373	0.582	0.127	0.154

	Movement (°)			Overview (°)		
	Sagittal	Coronal	Transverse	Sagittal	Coronal	Transverse
SLOW	0.03	0.09	0.07	1.96	9.39	0.42
MIDSPEED	0.03	0.09	0.09	1.95	9.37	0.45
FAST	0.03	0.10	0.11	1.95	9.36	0.47

The BMC sagittal kinematic shows the expected mid-stance flat foot orientation, indicating the average height of the medial and lateral anterior markers, approximated that of the single posterior marker. The BMC coronal kinematic, however, shows an unexpected medial high offset of approximately 9° during mid-stance; this was completely resolved by the RNOH calibration. Changes in the sagittal and transverse positions were minimal, and no other significant changes were observed. *Hypothesis 6A_I,* that the RNOH foot calibration would provide a reasonable representation of the segments plantar surface is therefore accepted.

6.4 Experiment 6B – The RNOH_MSFM

6.4.1 Aim

This experiment aims to establish normative kinematic for the RNOH_MSFM

6.4.2 Hypothesis

Hypothesis 6B_I – The RNOH_MSFM joint kinematics will produce characteristic movement patterns with good left/right symmetry in the typically developed test population. This will be demonstrated by showing a predominance of no significant difference in the left versus right gait scores, and substantive left-right correlations of the same from each individual subject.

6.4.3 Method

6.4.3.1 Model Specification

Table 6-5 outlines formal specification of the RNOH_MSFM.

Table 6-5 Formal specification of RNOH_MSFM body segments.

PREFIX*	NAME	PLACEMENT / CALCULATION
Surface Markers		
L or R	infCalc	Posterior heel, similar to BMC, height no longer critical.
L or R	head1	Dorsal surface of 1st metatarsal head.
L or R	head5	Dorasl surface of 5th metatarsal head, in common with BMC.
L or R	latCalc	Lateral surface of calcaneous- tracking only, non critical placement.
L or R	medCalc	Medial surface of calcaneous- tracking only, non critical placement.
L or R	cuboid	Lateral surface of cuboid, in depression immediately posterior to palpable protrusion of 5th metatarsal base, and marking apex of longitudinal lateral foot arch.
L or R	navicular	Over palpable navicular tuberosity marking apex of longitudinal medial foot arch.
Virtual Markers		
L or R	supCalc	Located 3cm (non-critical) vertically above infCalc during the hind foot calibration, then tracked via latCalc-infCalc-medCalc tracking solution.
L or R	head1_Mid	head1_Sole projected up to the mid plantar-dorsal surface height. Projected distance = (head1_Sole projection distance - 9mm)/2. The 9mm correction represents the height of the centre of the head1 surface marker above the dorsal surface (2mm base + 7mm marker radius). Projection direction is perpendicular to infCalc-head1-head5 plane.
L or R	head5_Mid	head5_Sole projected up to the mid plantar-dorsal surface height, similar to head1_Mid
L or R	infCalc_Mid	infCalc_Sole projected up by anatomically appropriate height. Projection distance = mean of head1_Mid and head5_Mid projection distances. Projection direction is perpendicular to infCalc-head1-head5 plane.
L or R	midTarsal	Mid-point of cuboid and navicular surface markers.
Anatomical Reference Frame (ARF)		
L or R	hind_RNOH	Principal axis from infCalc_Mid to midTarsal with supCalc defining principal sagittal plane.
L or R	latFore_RNOH	Principal axis from cuboid to head5_Mid with navicular defining principal transverse plane.
L or R	medFore_RNO	Principal axis from navicular to head1_Mid with head5_Mid defining principal transverse plane.
Technical Reference Frame (TRF)		
L or R	hind_RNOH	infCalc, latCalc and medCalc surface markers
L or R	latFore_RNOH	cuboid, head5 and navicular surface markers
L or R	medFore_RNO	navicular, head1 and head5 surface markers

**** L or R corresponds to left or right side respectively***

6.4.3.2 Laboratory Set-up

Data was collected alongside the dynamic data and concurrently with the BMC reference data (presented in Chapter 2). Subject 2 did not contribute to the MSFM

modelling. Subject 1 was excluded from the left foot MSFM due to loss of the cuboid marker during the data collection.

The RNOH_MSFM calibration, required an addition specification to the subject posture, above that of the RNOH_Foot. For the RNOH_MSFM, the hind foot segment must adopt a neutral coronal plane orientation, in addition to being flat to the floor. For the typically developed cohort, this was easily achieved in conjunction with the RNOH_Foot calibration.

6.4.4 Data Analysis

6.4.4.1 Signal Processing

During the foot calibration trial, a virtual marker (supCalc) was created vertically above the posterior heel marker (infCalc). This virtual marker was tracked via the three real heel markers (infCal – medCalc – latCalc), such that there was no requirement to maintain the hind-foot neutral orientation during the full model calibration.

Like the whole foot segment, all three segment sub-regions present with antero-posterior directed principal axes, appropriate to clinical orientation description via a sagittal-transverse-coronal rotation sequence (see chapter 2), for the dynamic walking trials.

6.4.4.2 Statistics

Paired t-test are applied to left foot and right foot, position, range and variability gait score, to demonstrate minimal differences. Coefficient of determination between individual subject scores are calculated to demonstrate measurement sensitivity to individual subject symmetrical gait characteristics. The need for formalised test-retest reliability testing is acknowledged.

6.4.5 Results

6.4.5.1 Hind-foot with respect to Shank - Tibiocalcaneal Kinematic

Figure 6-11 presents the left/right comparison sagittal plane kinematic tibiocalcaneal kinematic.

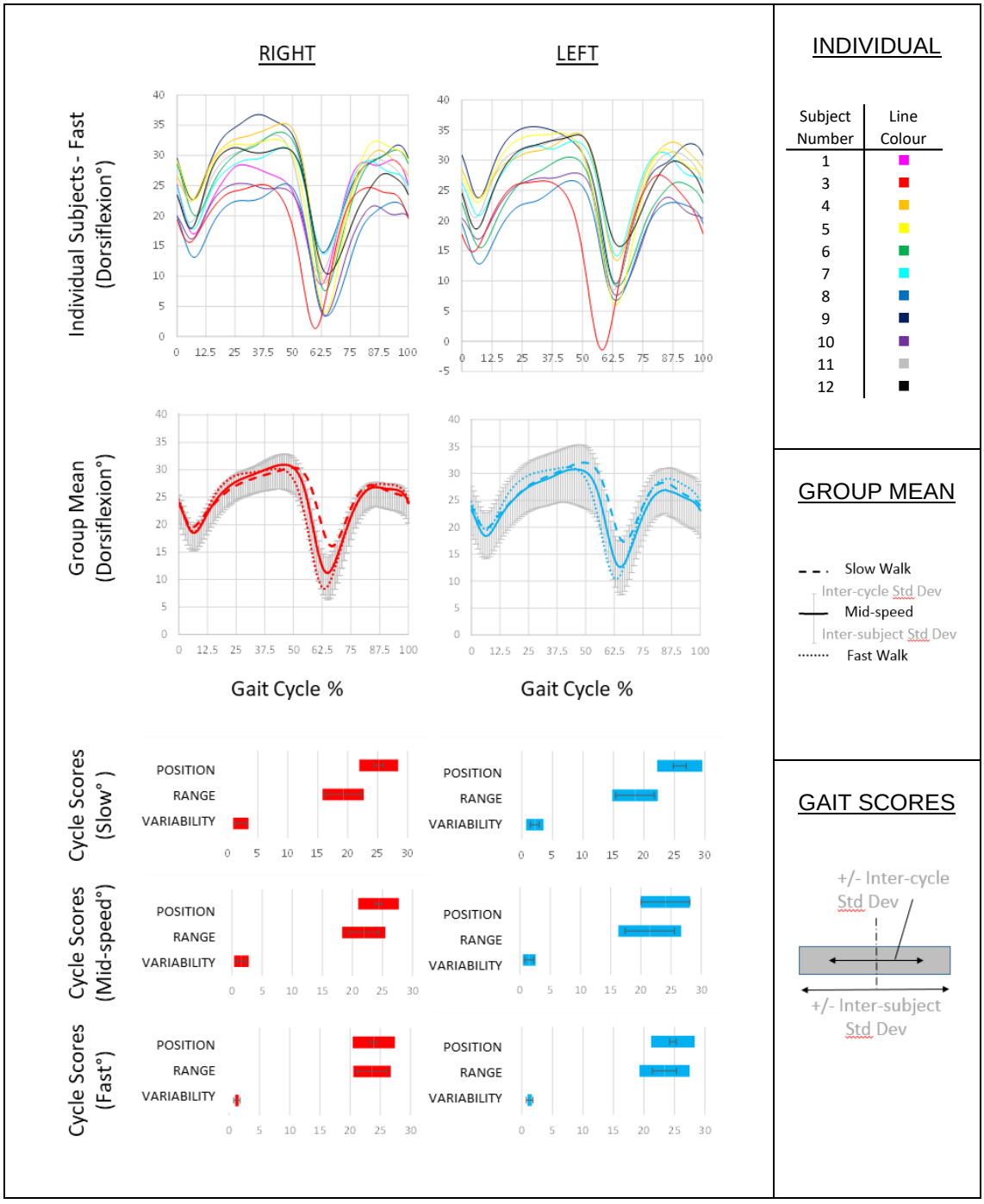

Figure 6-11 Sagittal plane comparison of left foot (right) and right foot (left) tibiocalcaneal kinematic

Top row shows individual graphical fast kinematic for 11 typically developing adults. Below this, group-mean for slow (dashed line), mid-speed (solid line) and fast (dotted line) walking. The mid-speed typical inter-cycle, and inter-subject standard deviations are shown above and below the mid-speed graph line respectively. Subsequent rows depict average cycle position, range and average cycle standard deviation gait scores in horizontal bar-chart format.

During the first eighth of the cycle, from ipsi-lateral initial contact to contra-lateral foot lift (loading), there is rapid plantar flexion to achieve foot flat orientation, followed by a transition to the dorsiflexion movement associated with tibial advancement. This dorsiflexion is rapid through early single support then slows through mid and late support. The fifth eighth of the cycle sees the strong push-off plantar flexion movement associated with double support offloading. Dorsiflexion recovery is equally rapid through early swing, plateaus in mid swing and transitions to plantar flexion prior to start of the next cycle. Common characteristic features in both the left and right kinematics of some individuals, supports the concept that a good proportion of the measured inter-subject variability was genuine, and not secondary to measurement error. Kinematics from the left and right foot of a single individual appear more similar than kinematics from different individuals. Figure 6-12 presents the data for the coronal plane tibiocalcaneal kinematic.

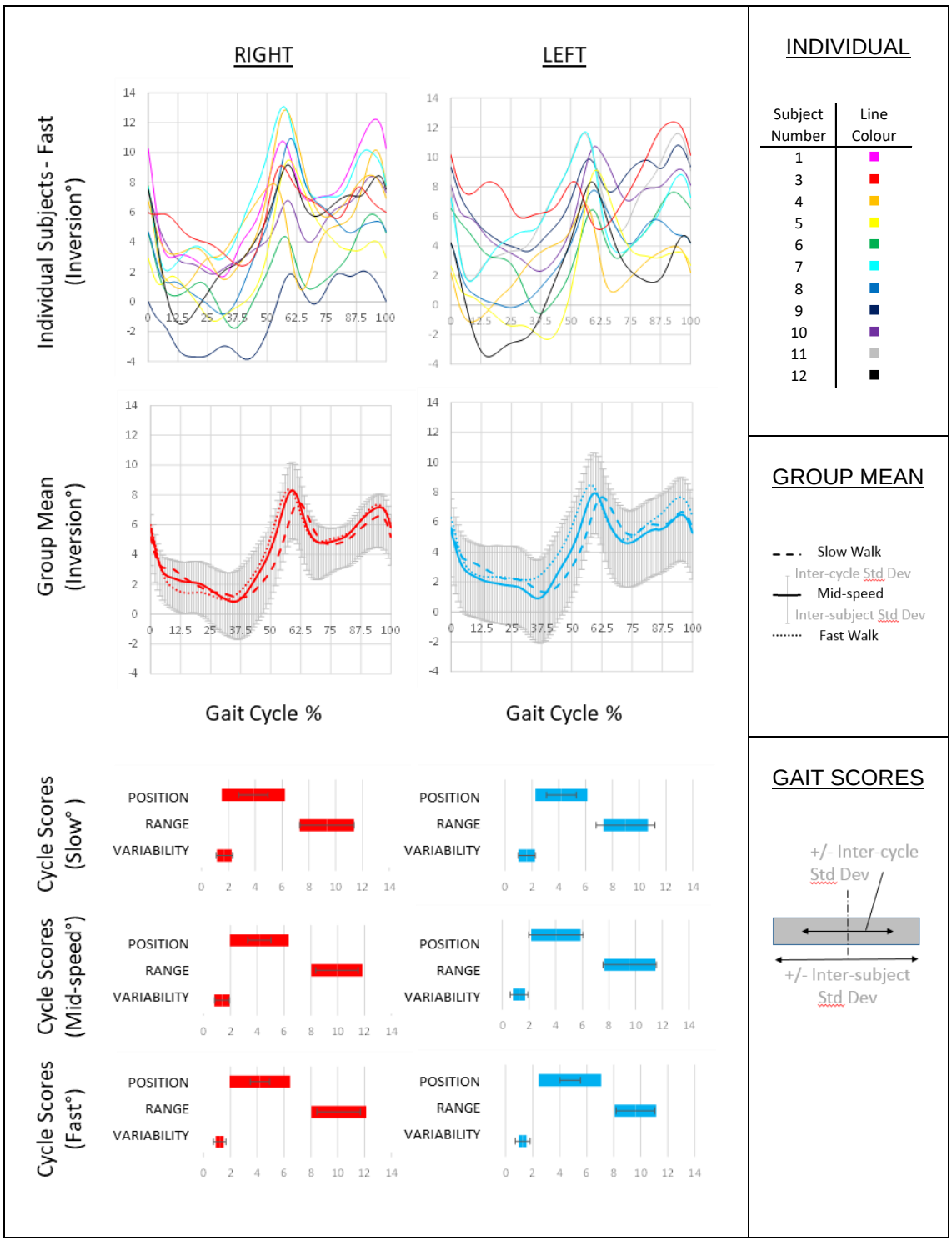

Figure 6-12 Coronal plane comparison of left foot (right) and right foot (left) tibiocalcaneal kinematic

Top row shows individual graphical fast kinematic for 11 typically developing adults. Below this, group-mean for slow (dashed line), mid-speed (solid line) and fast (dotted line) walking. The mid-speed typical inter-cycle, and inter-subject standard deviations are shown above and below the mid-speed graph line respectively. Subsequent rows depict average cycle position, range and average cycle standard deviation gait scores in horizontal bar-chart format.

Strong coronal plane eversion following initial contact, is concomitant with the strong plantar flexion movement. Slower eversion continues through early and mid-support as the tibia advances forward over the flat foot. This gives way to a strong inversion movement, which starts in late support, and continues as the strong plantar flexion movement of off-loading commences. Early swing dorsiflexion includes a strong inversion component. Fluctuation in mid and late swing includes commencement of eversion prior to the start of the next cycle.

Finally, figure 6-13 presents the transverse plane tibiocalcaneal kinematic. Although the transverse plane kinematic is largely flat, there are clear internal rotation movements, associated with the plantarflexion-eversion kinematic of the double support loading and un-loading gait phases.

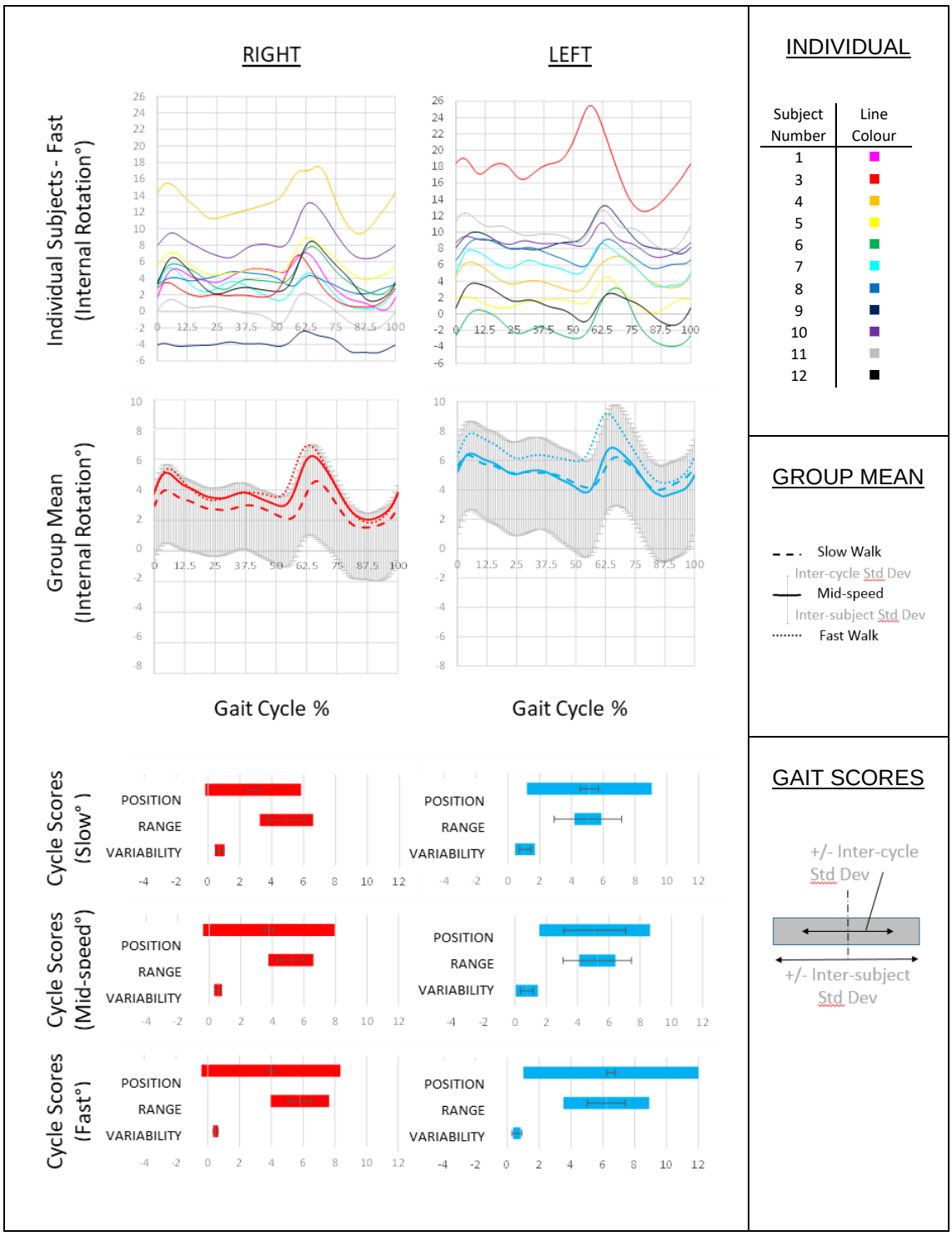

Figure 6-13 Transverse plane comparison of left foot (right) and right foot (left) tibiocalcaneal kinematic

Top row shows individual graphical fast kinematic for 11 typically developing adults. Below this, group-mean for slow (dashed line), mid-speed (solid line) and fast (dotted line) walking. The mid-speed typical inter-cycle, and inter-subject standard deviations are shown above and below the mid-speed graph line respectively. Subsequent rows depict average cycle position, range and average cycle standard deviation gait scores in horizontal bar-chart format.

6.4.5.2 Lateral Forefoot Kinematic with respect to Hind-foot

The sagittal and transverse lateral forefoot kinematic describes the orientation of a 5th ray representation from the cuboid to the 5th metatarsal head, with respect to the hind-foot. The sagittal kinematic therefore represents the lateral arch angle, and the transverse kinematic, the lateral arch adduction. The spin of this axis tracks the medial navicular, such that the coronal kinematic represents the tarsus inversion orientation.

Figure 6-14 shows data for the sagittal lateral arch angle.

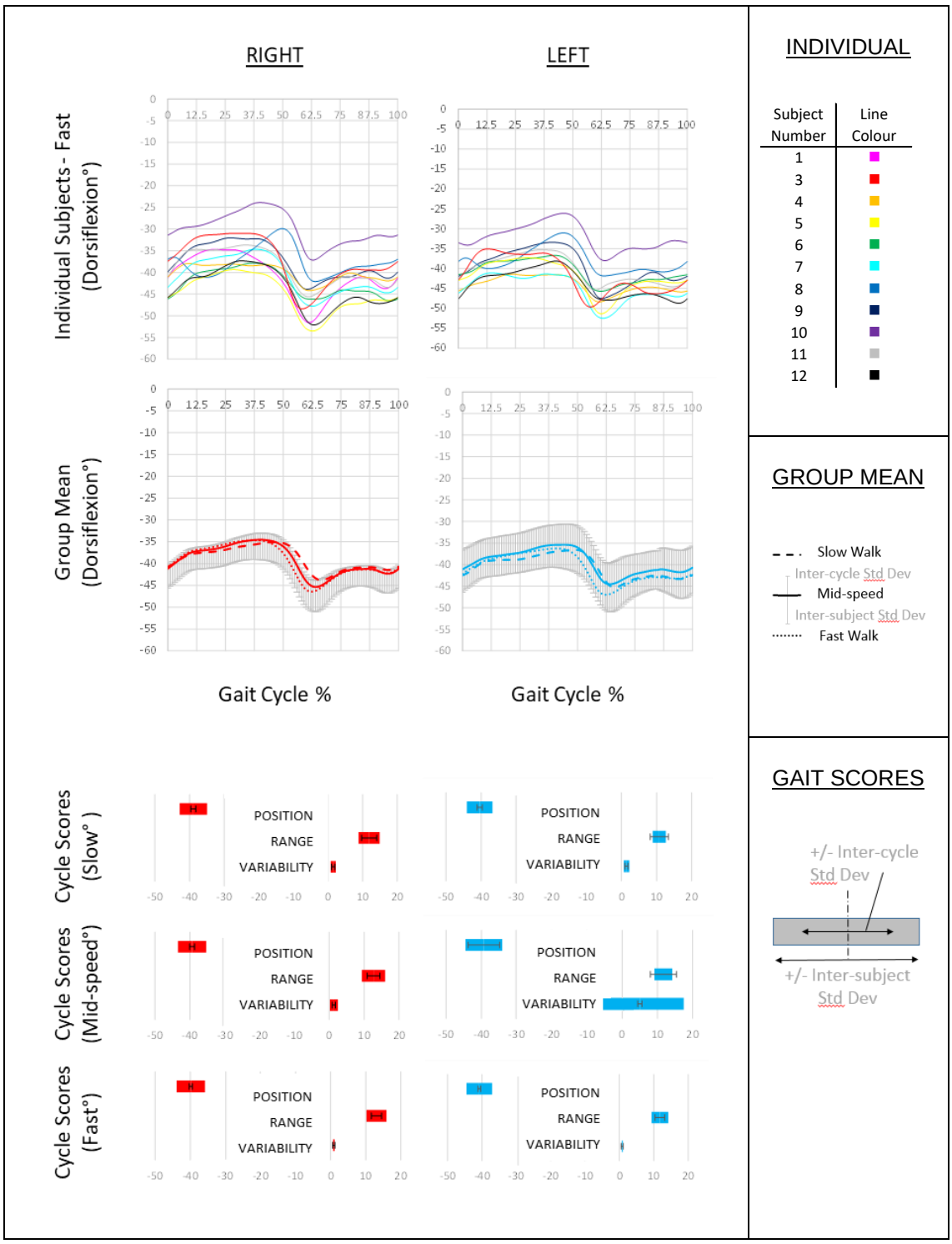

Figure 6-14 Sagittal plane comparison of left foot (right) and right foot (left) lateral arch kinematic

Top row shows individual graphical fast kinematic for 11 typically developing adults. Below this, group-mean for slow (dashed line), mid-speed (solid line) and fast (dotted line) walking. The mid-speed typical inter-cycle, and inter-subject standard deviations are shown above and below the mid-speed graph line respectively. Subsequent rows depict average cycle position, range and average cycle standard deviation gait scores in horizontal bar-chart format.

Rapid flattening of the lateral arch through loading, slows through single support, then show an even sharper re-emergence on offloading. Like the sagittal tibiocalcaneal kinematic, there are clear individual subject left right symmetries indicative of genuine differences above that of any measurement error.

Figure 6-15 show the coronal plane tarsus inversion with respect to the hind-foot.

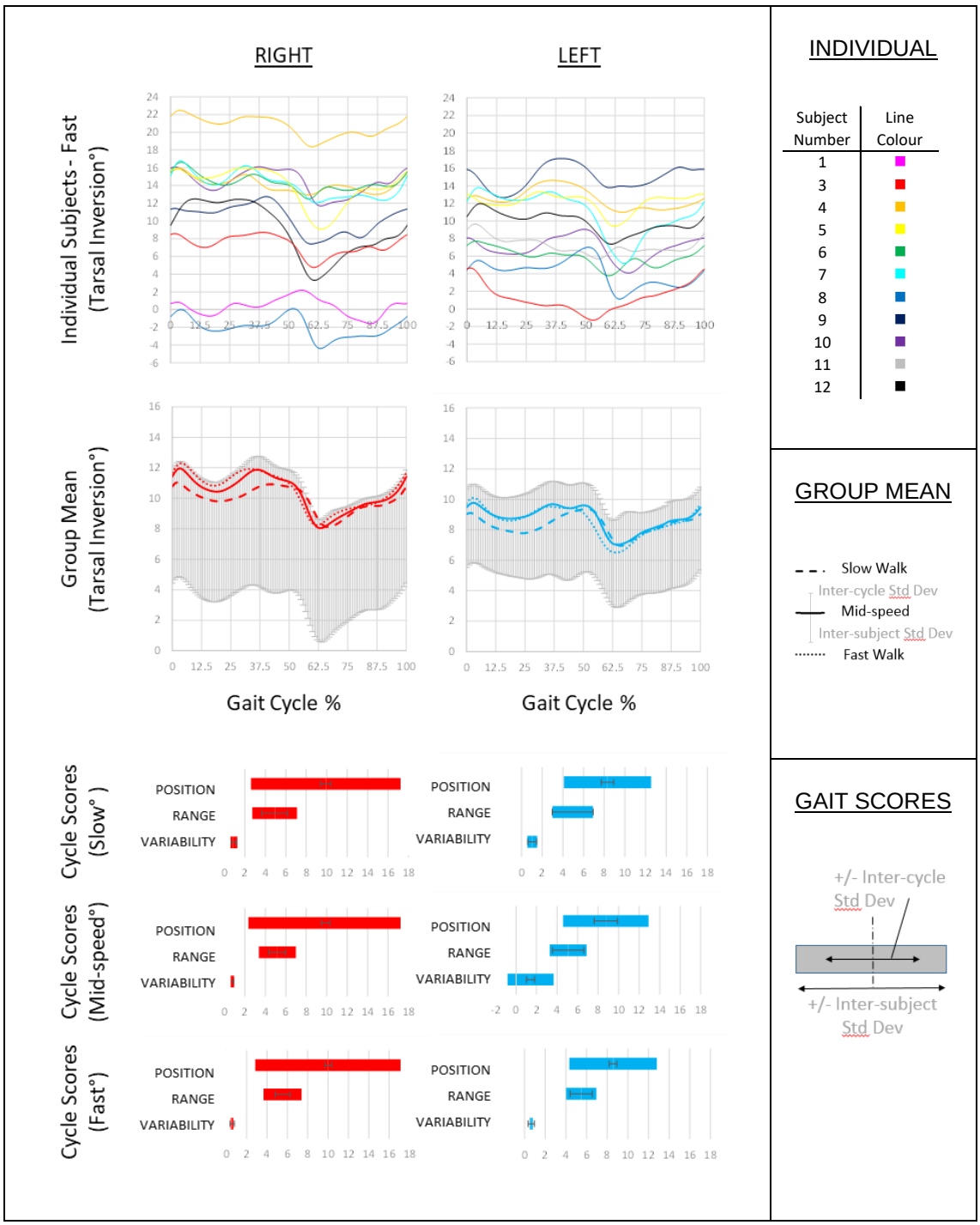

Figure 6-15 Coronal plane comparison of left foot (right) and right foot (left) lateral arch kinematic depicting the inversion of the tarsus with respect to the hind foot

Top row shows individual graphical fast kinematic for 11 typically developing adults. Below this, group-mean for slow (dashed line), mid-speed (solid line) and fast (dotted line) walking. The mid-speed typical inter-cycle, and inter-subject standard deviations are shown above and below the mid-speed graph line respectively. Subsequent rows depict average cycle position, range and average cycle standard deviation gait scores in horizontal bar-chart format.

The tarsus appears relatively fixed to the hind-foot through loading and single support. Through push-off there is strong tarsus eversion as the hind-foot transitions from an inversion to eversion movement. Progressive tarsus inversion through swing prepares the foot for the start of the next cycle.

Finally, the lateral arch adduction (transverse plane) kinematic is shown in figure 6-16.

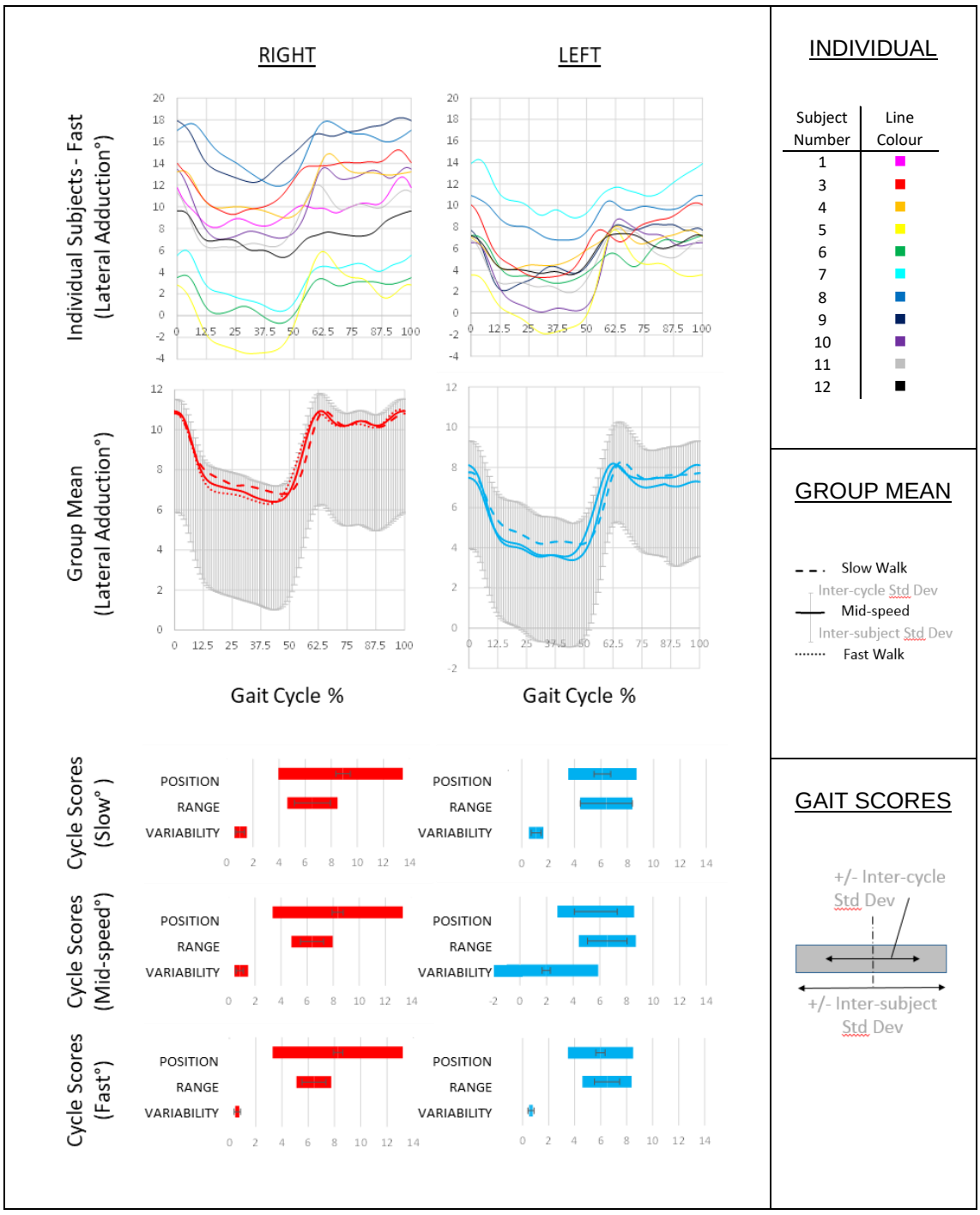

Figure 6-16 Transverse plane comparison of left foot (right) and right foot (left) lateral arch kinematic

Top row shows individual graphical fast kinematic for 11 typically developing adults. Below this, group-mean for slow (dashed line), mid-speed (solid line) and fast (dotted line) walking. The mid-speed typical inter-cycle, and inter-subject standard deviations are shown above and below the mid-speed graph line respectively. Subsequent rows depict average cycle position, range and average cycle standard deviation gait scores in horizontal bar-chart format.

There is a clear increase in lateral forefoot abduction as the arch flattens during loading, and equally strong adduction as the foot is unloaded. Overall, the lateral arch, which is expected to be the stiffer of the two longitudinal foot arches, shows clinically interpretable normal kinematic patterns in all three planes. The equivalent kinematic for the medial arch are presented in the next section.

6.4.5.3 Medial Forefoot Kinematic with respect to Hind-foot

The medial forefoot segment is based on a 1st ray axis defined from the proximal navicular to the distal head of the first metatarsal. Like the lateral arch, the sagittal and transverse plane kinematics, describe an arch and adduction angle, this time of the more mobile medial column. The spin orientation of this axis is defined by the 5th metatarsal head marker, such that it represents the inversion orientation of the metatarsal-head line, with respect to the hind-foot.

Figure 6-17 shows the sagittal medial arch kinematic.

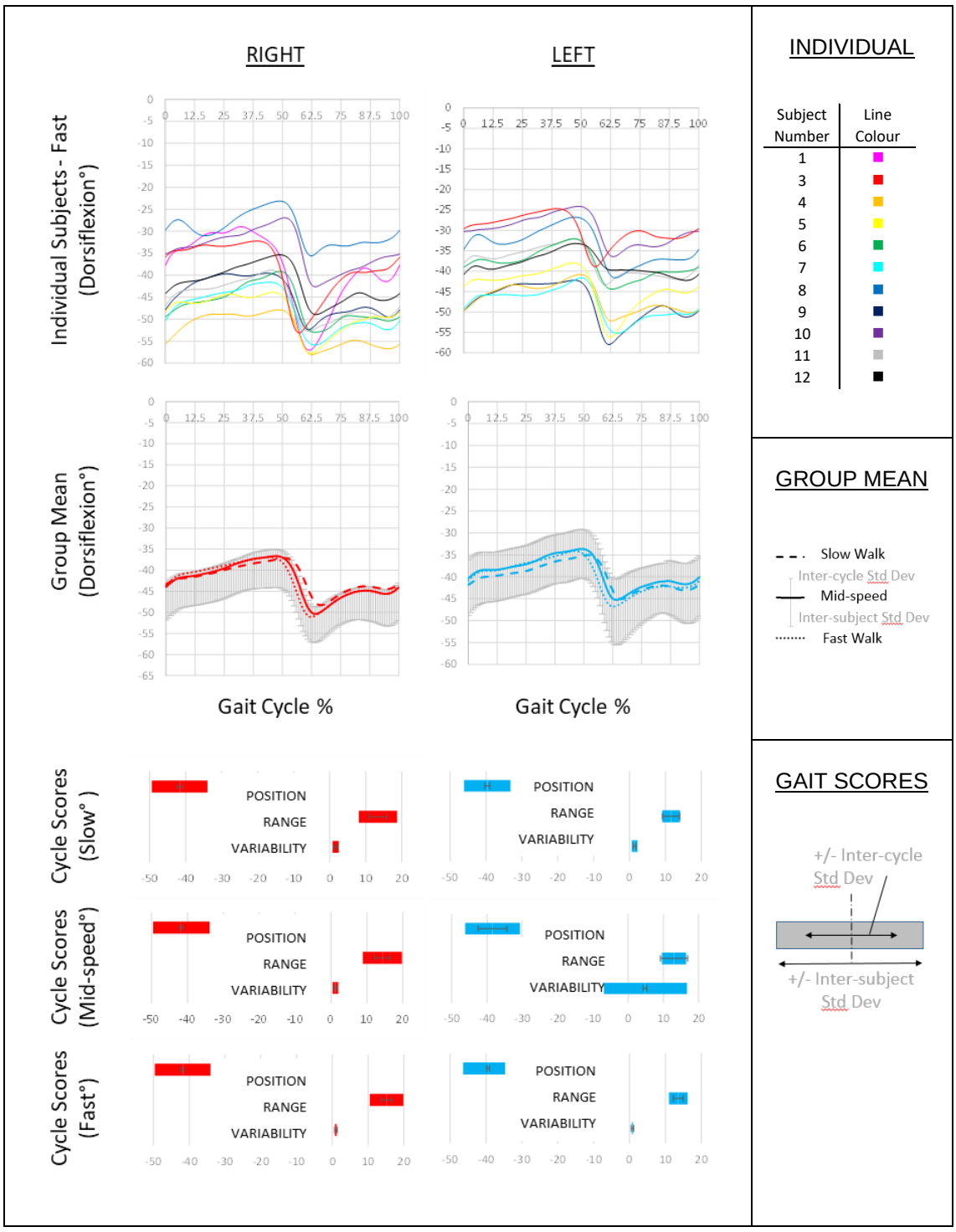

Figure 6-17 Sagittal plane comparison of left foot (right) and right foot (left) medial arch kinematic

Top row shows individual graphical fast kinematic for 11 typically developing adults. Below this, group-mean for slow (dashed line), mid-speed (solid line) and fast (dotted line) walking. The mid-speed typical inter-cycle, and inter-subject standard deviations are shown above and below the mid-speed graph line respectively. Subsequent rows depict average cycle position, range and average cycle standard deviation gait scores in horizontal bar-chart format.

In contrast to the lateral arch, which showed more rapid flattening on loading than through support, flattening of the medial arch is more progressive, and the release on off-loading an even stronger movement. A small amount of arch flattening is also apparent as the foot is pulled up during swing phase.

Figure 6-18 shows the metatarsal head inversion angle with respect to the hind-foot.

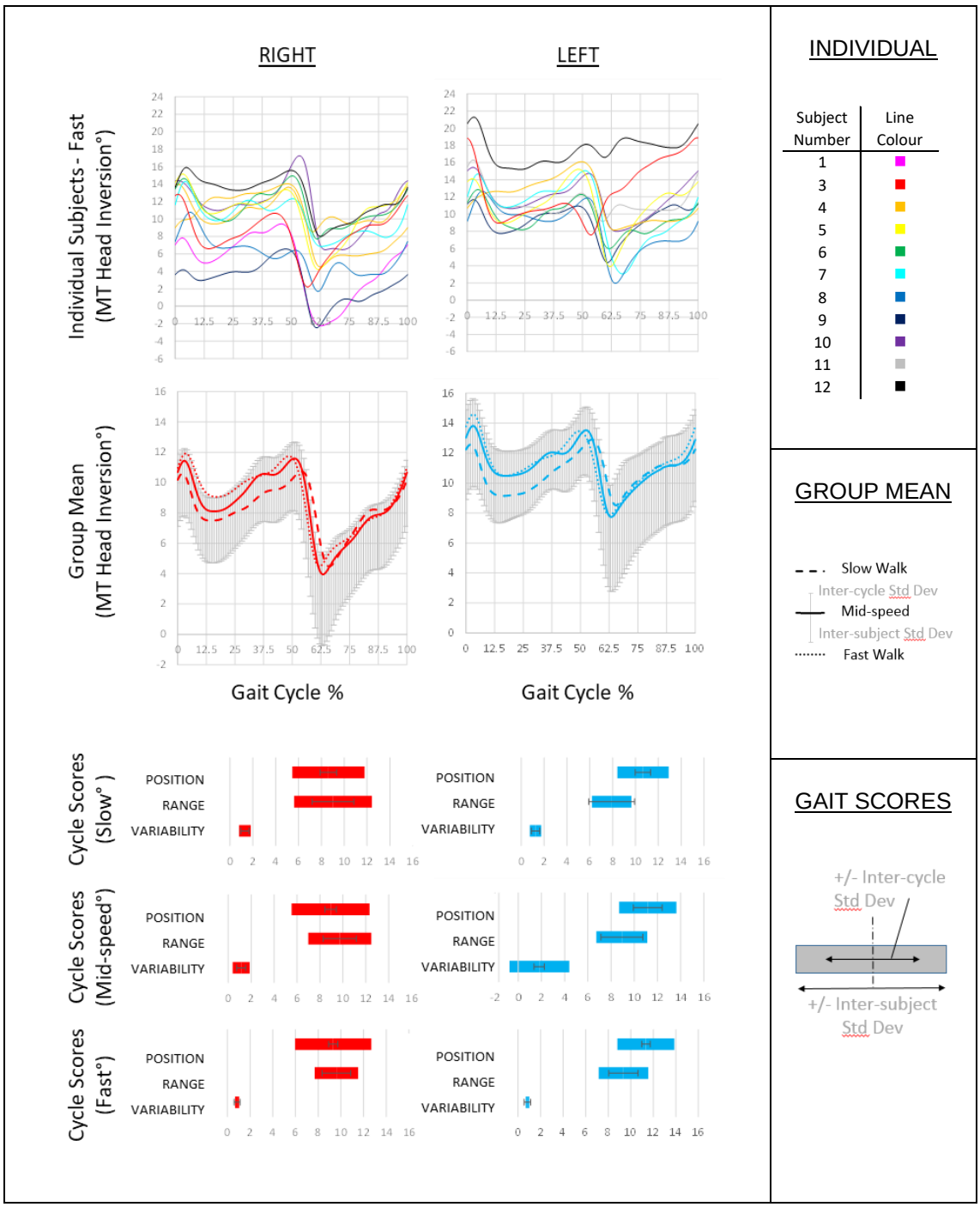

Figure 6-18 Coronal plane comparison of left foot (right) and right foot (left) medial arch kinematic depicting the inversion of the metatarsal-head line with respect to the hind foot

Top row shows individual graphical fast kinematic for 11 typically developing adults. Below this, group-mean for slow (dashed line), mid-speed (solid line) and fast (dotted line) walking. The mid-speed typical inter-cycle, and inter-subject standard deviations are shown above and below the mid-speed graph line respectively. Subsequent rows depict average cycle position, range and average cycle standard deviation gait scores in horizontal bar-chart format.

Mild inversion is held through loading and single support, lost through off-loading, and then progressively recovered through swing. Figure 6-19 shows the medial forefoot adduction kinematic with respect to the hind-foot segment.

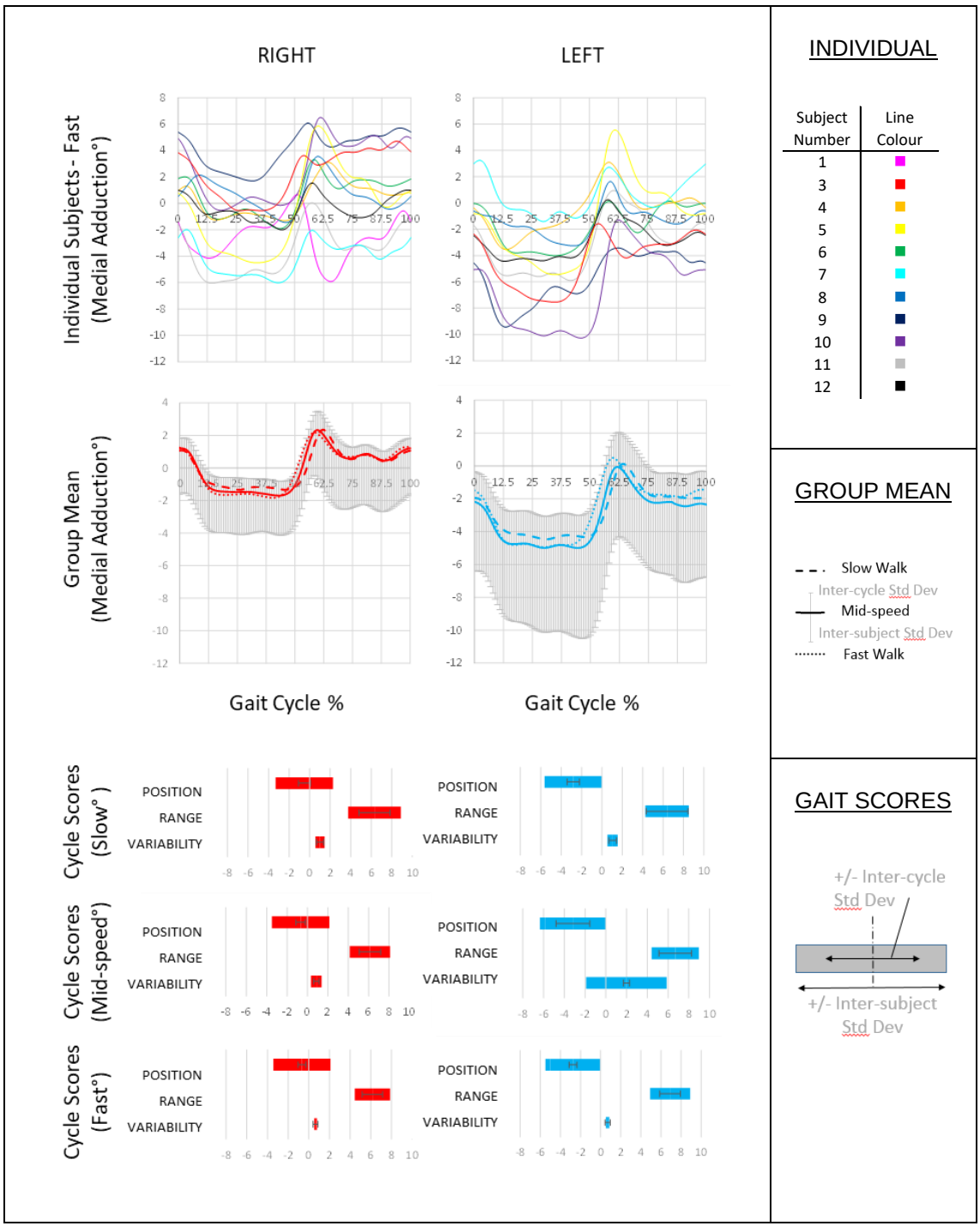

Figure 6-19 Transverse plane comparison of left foot (right) and right foot (left) medial arch kinematic

Top row shows individual graphical fast kinematic for 11 typically developing adults. Below this, group-mean for slow (dashed line), mid-speed (solid line) and fast (dotted line) walking. The mid-speed typical inter-cycle, and inter-subject standard deviations are shown above and below the mid-speed graph line respectively. Subsequent rows depict average cycle position, range and average cycle standard deviation gait scores in horizontal bar-chart format.

The transverse plane kinematic for the medial forefoot follows a similar movement pattern as that described for the lateral forefoot.

6.4.5.4 Medial Forefoot with respect to Lateral Forefoot Kinematic

This section plots movement of the medial forefoot/metatarsal head foot region, against the more rigid lateral forefoot/tarsus region. Figure 6-20 shows the medial increase in dorsiflexion.

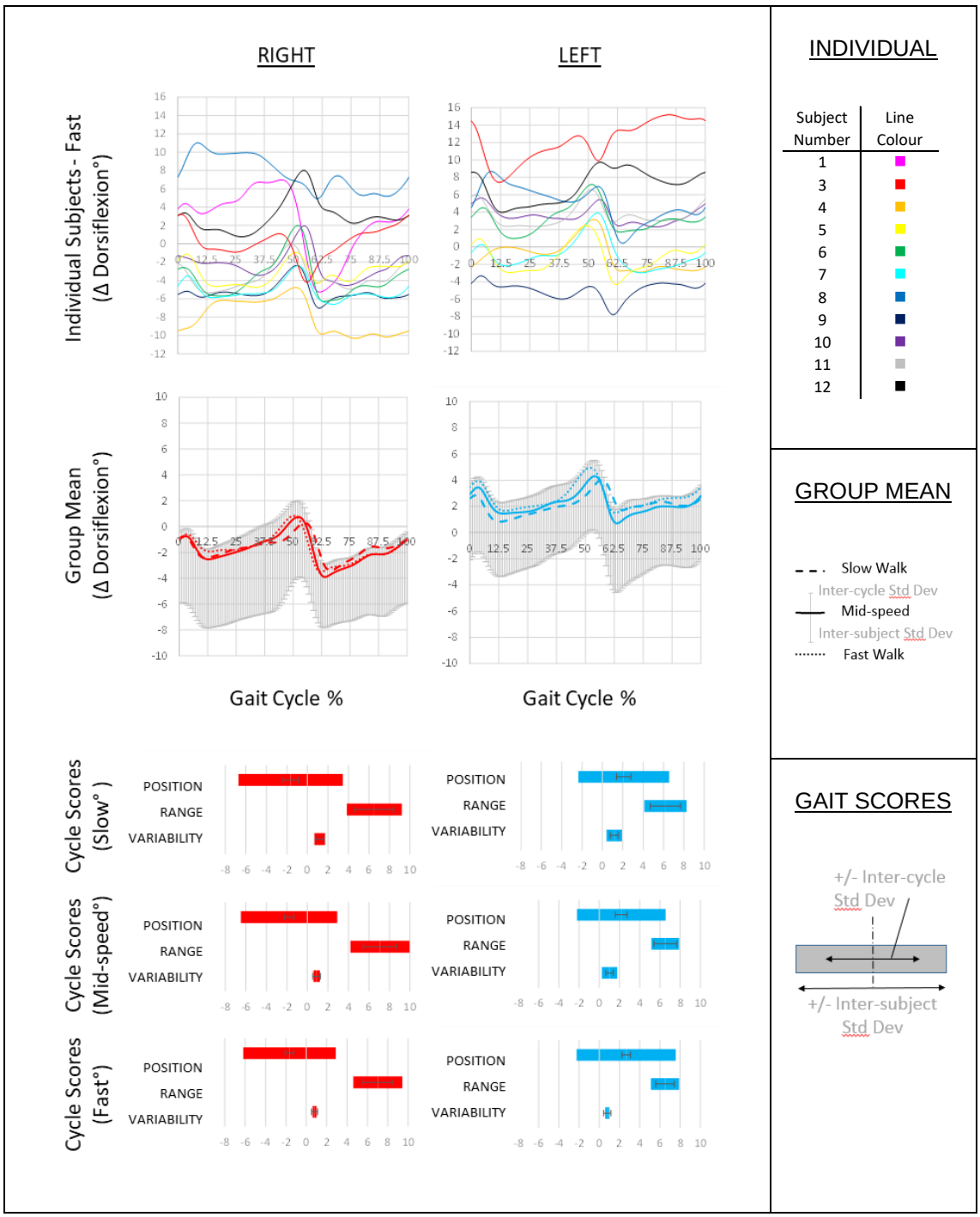

Figure 6-20 Sagittal plane comparison of left foot (right) and right foot (left) medial forefoot orientation with respect to a more rigid lateral region

Top row shows individual graphical fast kinematic for 11 typically developing adults. Below this, group-mean for slow (dashed line), mid-speed (solid line) and fast (dotted line) walking. The mid-speed typical inter-cycle, and inter-subject standard deviations are shown above and below the mid-speed graph line respectively. Subsequent rows depict average cycle position, range and average cycle standard deviation gait scores in horizontal bar-chart format.

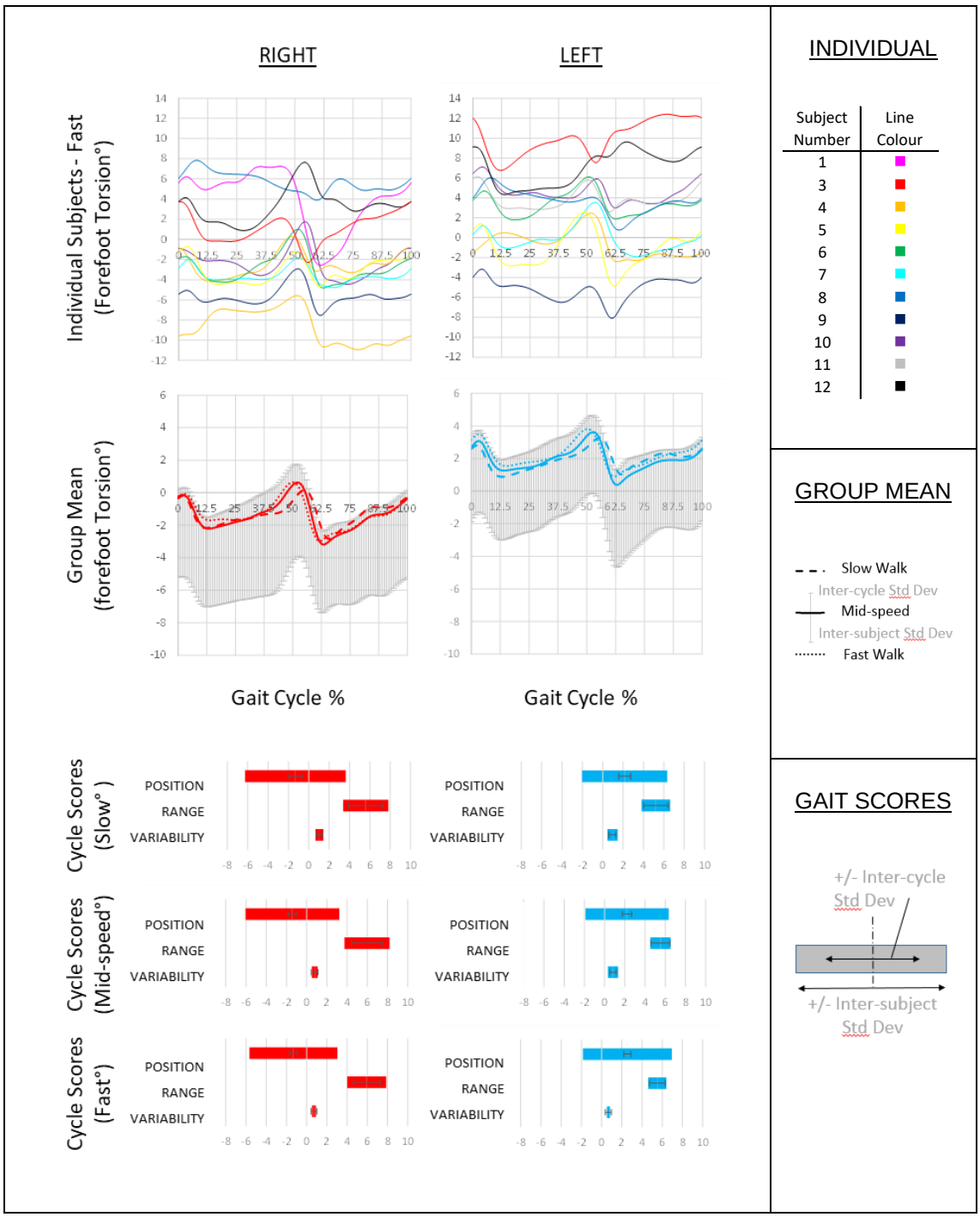

Figure 6-21 Coronal plane comparison of left foot (right) and right foot (left) medial forefoot orientation with respect to a more rigid lateral region

Top row shows individual graphical fast kinematic for 11 typically developing adults. Below this, group-mean for slow (dashed line), mid-speed (solid line) and fast (dotted line) walking. The mid-speed typical inter-cycle, and inter-subject standard deviations are shown above and below the mid-speed graph line respectively. Subsequent rows depict average cycle position, range and average cycle standard deviation gait scores in horizontal bar-chart format.

As expected, the medial forefoot exhibited slightly more dorsiflexion than the lateral. The coronal component of this kinematic (Figure 6-21) represents inversion torsion of the forefoot around the long axis of the foot (metatarsal head inversion with respect to tarsus inversion).

Finally, figure 6-22 presents the transverse plane kinematic of the medial forefoot with respect to its more rigid lateral counterpart.

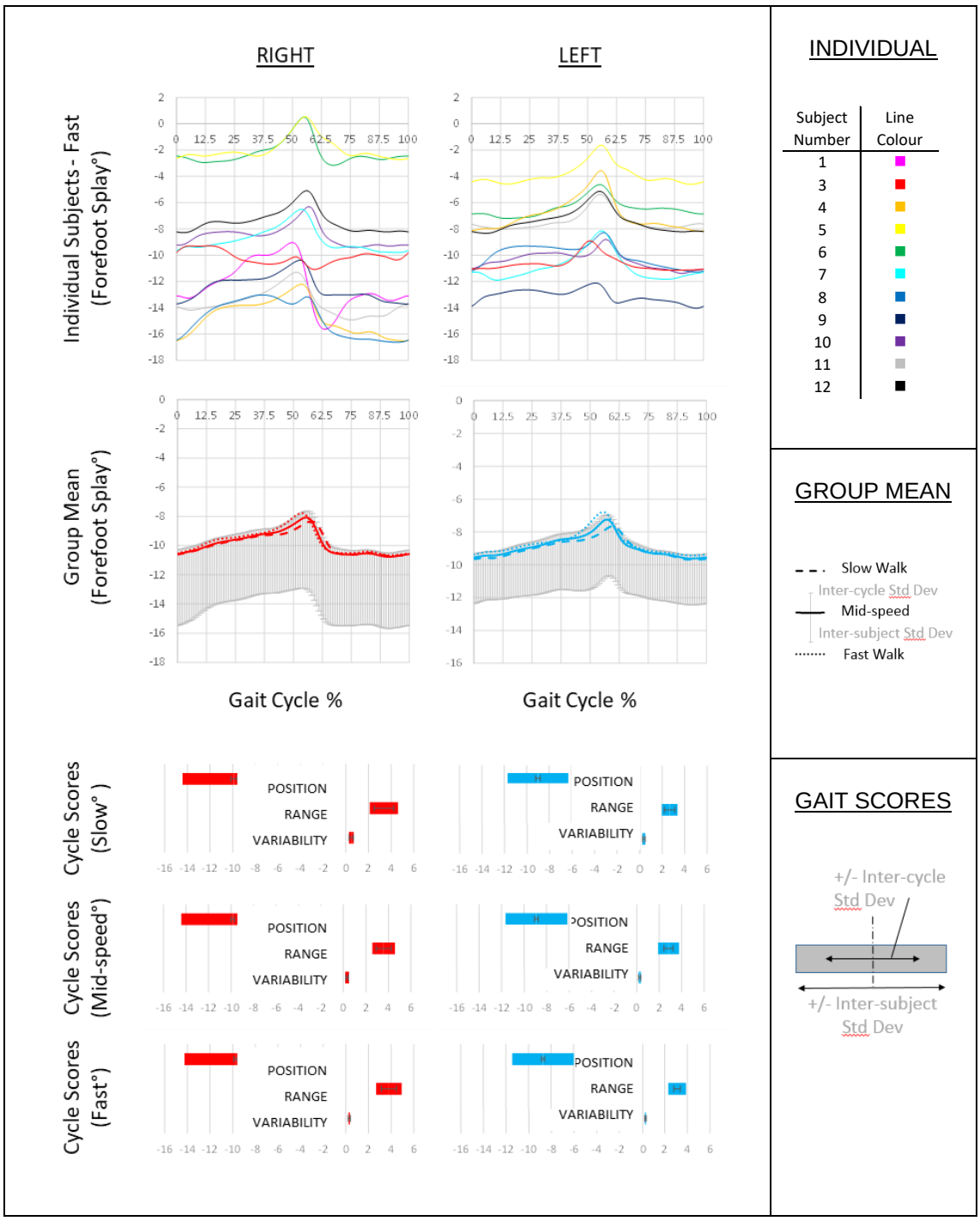

Figure 6-22 Transverse plane comparison of left foot (right) and right foot (left) medial forefoot orientation with respect to a more rigid lateral region

Top row shows individual graphical fast kinematic for 11 typically developing adults. Below this, group-mean for slow (dashed line), mid-speed (solid line) and fast (dotted line) walking. The mid-speed typical inter-cycle, and inter-subject standard deviations are shown above and below the mid-speed graph line respectively. Subsequent rows depict average cycle position, range and average cycle standard deviation gait scores in horizontal bar-chart format.

Small amplitude of the forefoot splay angles, confirms the similar movements of the separate lateral and medial kinematics.

6.4.6 Hypothesis Testing

Table 6-6 presents statistical analysis, testing for left/right symmetry of the tibiocalcaneal kinematic.

Table 6-6 Statistical analysis of RNOH_MSFM tibiocalcaneal kinematic highlighting left/right differences (top) and subject specific symmetry (bottom).

Hind Foot w.r.t. Shank (Left - Right difference, paired T-test)

	Position (°)			Range (°)			Variability (°)		
	Sagittal	Coronal	Transverse	Sagittal	Coronal	Transverse	Sagittal	Coronal	Transverse
SLOW	0.41	0.69	1.61	-0.57	-0.10	-4.05	-0.13	-0.11	-0.65
p-value	0.530	0.498	0.275	0.451	0.895	0.000	0.705	0.293	0.005
MIDSPEED	-0.46	0.09	1.18	-0.57	-0.27	-4.56	-0.10	-0.13	-0.63
p-value	0.649	0.931	0.385	0.717	0.655	0.000	0.802	0.314	0.028
FAST	0.78	0.78	2.53	-0.50	-0.35	2.53	0.01	0.05	-0.60
p-value	0.166	0.448	0.169	0.667	0.520	0.169	0.952	0.551	0.000

Hind Foot w.r.t. Shank (Left vs Right R^2)

	Position (°)			Range (°)			Variability (°)		
	Sagittal	Coronal	Transverse	Sagittal	Coronal	Transverse	Sagittal	Coronal	Transverse
SLOW	0.71	0.02	0.00	0.65	0.05	0.13	0.54	0.75	0.34
MIDSPEED	0.46	0.09	0.00	0.21	0.31	0.20	0.23	0.58	0.12
FAST	0.80	0.00	0.07	0.30	0.41	0.07	0.17	0.43	0.62

Left/right differences in the transverse plane range, highly statistically significant at the slow and mid walking speed, are likely linked with the accompany difference in inter-cycle variability. Two position, one range and four variability scores show coefficients of determination indicating good individual left/right symmetry.

Table 6-7 presents similar statistical analysis for the hind-foot/lateral forefoot kinematic.

Table 6-7 Statistical analysis of RNOH_MSFM lateral kinematic highlighting left/right differences (top) and subject specific symmetry (bottom).

Lateral Forefoot/Tarsus w.r.t. Hind foot (Left - Right difference, paired T-test)

	Position (°)			Range (°)			Variability (°)		
	Sagittal	Coronal	Transverse	Sagittal	Coronal	Transverse	Sagittal	Coronal	Transverse
SLOW	-1.59	-2.79	-2.70	-0.60	0.02	-0.31	-0.18	0.15	0.04
p-value	0.068	0.123	0.134	0.306	0.980	0.482	0.156	0.170	0.772
MIDSPEED	0.01	-2.34	-2.55	-0.34	-0.04	-0.06	3.70	0.76	1.09
p-value	0.997	0.182	0.173	0.664	0.959	0.875	0.350	0.302	0.344
FAST	-1.01	-2.41	-2.15	-0.79	-0.20	-2.15	-0.07	0.06	0.03
p-value	0.193	0.185	0.233	0.159	0.785	0.233	0.230	0.058	0.529

Lateral Forefoot/Tarsus w.r.t. Hind foot (Left vs Right R^2)

	Position (°)			Range (°)			Variability (°)		
	Sagittal	Coronal	Transverse	Sagittal	Coronal	Transverse	Sagittal	Coronal	Transverse
SLOW	0.66	0.37	0.07	0.54	0.15	0.59	0.79	0.56	0.50
MIDSPEED	0.43	0.43	0.04	0.33	0.00	0.79	0.29	0.04	0.51
FAST	0.72	0.38	0.04	0.62	0.01	0.04	0.50	0.60	0.30

No left/right difference are noted in this kinematic. Sagittal position and range scores show high subject specific left/right correlations, as do many of the variability scores.

Table 6-8 presents similar statistical analysis for the hind-foot/medial forefoot kinematic.

Table 6-8 Statistical analysis of RNOH_MSFM medial kinematic highlighting left/right differences (top) and subject specific symmetry (bottom).

Medial Forefoot/Metatarsal Heads w.r.t. Hind foot (Left - Right difference, paired T-test)

	Position (°)			Range (°)			Variability (°)		
	Sagittal	Coronal	Transverse	Sagittal	Coronal	Transverse	Sagittal	Coronal	Transverse
SLOW	2.70	1.61	-2.70	-0.39	-0.27	-0.31	-0.28	-0.06	0.04
p-value	0.078	0.055	0.134	0.668	0.695	0.482	0.122	0.531	0.772
MIDSPEED	3.81	1.75	-2.55	0.17	-0.13	-0.06	3.47	0.68	1.09
p-value	0.085	0.042	0.173	0.860	0.877	0.875	0.357	0.392	0.344
FAST	2.79	1.56	-2.15	-0.26	-0.01	-2.15	-0.13	-0.02	0.03
p-value	0.073	0.080	0.233	0.785	0.994	0.233	0.058	0.784	0.529

Medial Forefoot/Metatarsal Heads w.r.t. Hind foot (Left vs Right R^2)

	Position (°)			Range (°)			Variability (°)		
	Sagittal	Coronal	Transverse	Sagittal	Coronal	Transverse	Sagittal	Coronal	Transverse
SLOW	0.70	0.41	0.07	0.12	0.16	0.59	0.68	0.69	0.50
MIDSPEED	0.48	0.46	0.04	0.29	0.02	0.79	0.70	0.16	0.51
FAST	0.72	0.40	0.04	0.01	0.11	0.04	0.40	0.22	0.30

Only the coronal position score at the mid-speed walk met the $p<0.05$ threshold indicating a genuine left/right difference. Correlations between left and right score suggest good symmetry in the sagittal position, transverse range, slow and mid-speed variability scores.

Table 6-9 presents similar statistical analysis for the intra-forefoot kinematic.

Table 6-9 Statistical analysis of RNOH_MSFM intra-forefoot kinematic highlighting left/right differences (top) and subject specific symmetry (bottom).

Medial Forefoot/Metatarsal Heads w.r.t. Lateral Forefoot/Tarsus (Left - Right difference, paired T-test)

	Position (°)			Range (°)			Variability (°)		
	Sagittal	Coronal	Transverse	Sagittal	Coronal	Transverse	Sagittal	Coronal	Transverse
SLOW	4.30	4.15	0.67	0.42	0.22	-0.38	-0.05	-0.09	-0.12
p-value	0.003	0.003	0.611	0.571	0.640	0.122	0.819	0.494	0.136
MIDSPEED	4.55	4.32	0.74	0.15	0.13	-0.51	0.12	0.04	-0.06
p-value	0.004	0.003	0.577	0.804	0.820	0.031	0.519	0.698	0.280
FAST	4.73	4.40	0.76	0.06	0.02	0.76	-0.01	-0.05	-0.04
p-value	0.006	0.003	0.564	0.923	0.975	0.564	0.762	0.424	0.024

Medial Forefoot/Metatarsal Heads w.r.t. Lateral Forefoot/Tarsus (Left vs Right R^2)

	Position (°)			Range (°)			Variability (°)		
	Sagittal	Coronal	Transverse	Sagittal	Coronal	Transverse	Sagittal	Coronal	Transverse
SLOW	0.54	0.55	0.27	0.00	0.12	0.26	0.21	0.36	0.07
MIDSPEED	0.43	0.47	0.28	0.16	0.01	0.54	0.51	0.53	0.27
FAST	0.39	0.45	0.26	0.02	0.05	0.26	0.54	0.30	0.34

Positional offsets in both the sagittal and coronal plane ranges show significant left right differences. These difference average around 4°, similar to the offset asymmetry identified in the transverse plane tibio-calcalneal kinematic. Other identified differences were much smaller than this.

The low number of significant left/right differences identified, together with the smattering of correlations showing individual subject left-right score symmetry, is suggestive of reasonably stable measurements, for all RNOH_MSFM kinematics in the typically developing population. Hypothesis 6B_I is therefore accepted. Formal proof of reliable measurement will require formal test-retest evaluation.

6.5 Discussion

6.5.1 RNOH_MSFM normative Intra foot Kinematic

Taken together the RNOH_MSFM kinematic provides a clinically relevant description of normal foot function in all three planes.

After heel contact with the ground, tibiocalcaneal plantar flexion brings the foot flat to the floor, as load is transferred from the other leg. At about half-way through

this first eighth of the cycle, as the tibia start to move forward over the flat foot, tibiocalcaneal plantar flexion transitions to an equally rapid dorsiflexion movement. Both longitudinal foot arches angles decrease during this loading period, then show a further progressive decrease through the single support period. The rate of this arch fattening is slightly greater medially, particularly towards the end of the single support period. The off-loading push-off movement, during the fifth eighth of the cycle, sees strong plantar flexion movements in all of the measured sagittal kinematic. These movements are largely recovered during the first half of swing phase, ready for the start of the next gait cycle.

In the coronal plane, strong tibiocalcaneal eversion on loading and inversion associated with off-loading, give an overall impression of a near neutral coronal orientation during stance and a few degrees of tibiocalcaneal inversion through swing. The offloading inversion is initiated in late single support, and countered by strong eversion of the tarsus and metatarsal-head line during the fifth eight of the cycle as load is transferred from the limb. Tibiocalcaneal inversion is partially recovered through early swing, and this position is held to the start of the next cycle. Tarsal and metatarsal eversion with respect to the hind-foot, is progressive throughout swing phase.

There is little transverse plane movement in the tibiocalcaneal kinematic. A few degrees of internal rotation with the push-off movement, are fully recovered by the first half of the swing period. At the forefoot, the medial 1st ray is abducted (extoeing) with respect to the lateral 5th ray. This abduction increases by a couple of degrees through stance, recovers on off-loading and is held through swing. Both rays move together to abduct the forefoot with respect to the hind-foot on loading, adduct on off-loading, and hold their respective positions during single support and swing periods.

6.5.2 Validity of the RNOH_MSFM

Like all marker based MSFM, the described RNOH_MSFM kinematic is a surface representation of regional movements. These movements are likely similar to those of the underlying skeleton but will not be an exact match. Similarities and differences with other MSFM outputs will be directly related to their marker

placement and calculation methods (plus individual variance). Like the larger RNOH_Model segments developed in the preceding chapters, judged advantages of the RNOH_MSFM over alternative solutions, are at least partly dependent on the establishment of better face validity.

While such evaluations are necessarily subjective in nature, I personally remain confident that the proposed solutions meet this requirement. This confidence is based there being a genuine link between deficits in model face validity, and model outputs, such that overcoming the former will solve the latter.

Although the face validity of a model is based on subjective judgement, each model basis this judgement on different underlying assumptions. These assumptions in turn, are reliant on there being a further link between model outputs and the underlying skeletal structure they represent. For example, at the forefoot, the longitudinal anatomy of separate metatarsal bones, and resultant self-evident flexibility, is consistent with separate medial and lateral model subdivisions. Similarly, widely acknowledged difficulties in accurate placement of surface markers to represent the hind foot orientation, is consistent with the modelling decision to instead relate the latter to the former during a bespoke calibration. Again, while such judgements are inherently subjective, each modelling approach is based on a different set of underlying assumptions. Establishing the relative face validity of each model, relies on weighting the reasonableness of these assumptions.

7 Chapter 7 - Conclusions and Recommendation

7.1 The RNOH_model - an integration of Novel and Existing solutions

The current CGM solution for clinical gait analysis is clearly both widely accepted and fundamentally flawed. Many of its problems have been highlighted in the published literature, together with suggestion of less flawed solutions. Many of these solutions take advantage of technical improvement in mo-cap technology since the advent of the CGM solution. Advances in both the hardware and software of mo-cap systems, have shifted the development focus from practicality to more optimised solutions. PiG, the most widely used variant of CGM, employs several complexities in order to aid its practical application. Most notable of these is the requirement for accurate placement of lateral thigh markers to define a coronal thigh plane between a proximal HJC location and the knee joint axis, without the need for a medial surface marker. Placement of the lateral markers at different heights on the left and right thigh segments, in order to facilitate software identification, is another example of prioritising practicality over accuracy; clearly these markers will suffer different STA amounts one more affected than the other.(Cockcroft et al., 2016).

The BMC (chapter 2) eliminates all such anomalies, by representing the required CGM anatomy in its simplest form. The BMC is neither optimised for tracking accuracy nor compromised by practical considerations. It represents the required anatomy in the simplest most direct method possible. This approach formed the basis of the RNOH_Trunk segment (chapter 3). Comparison of a CGM representation against the simpler BMC approach, showed the latter to have both interpretative and utility advantages. The CGM approach could not therefore justify its complexity against any benefit.

Development of other segments have exploited concepts already in the published literature by amalgamation into a single coherent solution. Employing the left and right HJC locations as part of the pelvic tracking solution (chapter 4) had previously been suggested as means of avoiding the need for ASIS markers, which are easily occluded from camera view by swinging arm (Kisho Fukuchi et al., 2010). Although the author interpreted the differences between their solution

and a CGM comparison as a price worth paying for this benefit, examination of their supplementary data showed their solution to capture more range of movement than CGM. A recent fluoroscopy study implies that this feature may well make it more accurate than CGM (Fiorentino et al., 2017).

Similarly for the thigh segment (chapter 5), the removal of segment specific STA influences by the omission of local surface markers had been previously established (Schulz and Kimmel, 2010). This solution, however, was not suited to clinical gait analysis, as it represented the segment as a vector, without any axial rotation kinematic output. Amalgamation of this with another publication, promoted use of a surface patella marker to restore the missing kinematic (Wren et al., 2008). The resulting solution shifted focus of the segment's definition from that of a local coronal plane to a local sagittal plane. This in turn facilitated the introduction of a crouched calibration posture, during which the knee alignment has a direct influence on the specification of thigh orientation and eliminating the need for post data collection model adjustment.

Finally for the foot segment (chapter 6) the sensitivity of the segment orientation to precise marker placement, was reduced by the introduction of bespoke calibration procedure, similar to that previously suggested in the Shriner Hospital Model (Davis et al., 2006., Maurer et al., 2013). Further division of the foot into sub-regions was based on a critical analysis of outputs from existing foot models and consistent with published findings of surface rigidity (Rouhani et al., 2011).

7.2 Pre-Development of the RNOH_Model – the 'OctoScores' concept

Ideas presented in this thesis represents the final product of an extended development process. Previous to this, over 10 years of experience running the Clinical Gait Analysis, service at RNOH, had given rise to the idea that the traditional continuous signal outputs could easily be described by set of simple metrics or scores (Thornton et al., 2014). These scores would be based on a division of the gait cycle into eight functional phases of double support loading, 3 equal divisions of single support, double support unloading, and 3 equal divisions of swing. Temporal scores could then describe the duration and percentage of the gait cycle assigned to each phase. With these scores already accounting for

any temporal anomalies, spatial scores described, the initiating value, change in value over the phase, minimum, average and maximum values, value range and average inter-cycle variability within each phase. A movement pattern score was additionally calculated as the absolute mean difference of the signal and a functionally equivalent normal reference phase. Together these were the 'OctoScores'. The spatial OctoScores in particular, were clearly mathematically inefficient. The range score, for example, was simply calculated as the maximum minus the minimum score for that phase of the cycle; the change score was similarly calculated as the initial value of the next phase minus the initial score of the phase being described. Unlike the raw data that they described however, each OctoScore adopts a natural clinically applicable label such as, the maximum knee flexion during mid-swing, or the percentage gait cycle of the loading double support period. From a clinical perspective, equivalent scores across different datasets appeared to be functionally equivalent and therefore directly comparable. This comparison was a formalisation of the subjective interpretation of a gait graph that I had become practiced at. This link with clinical terminology provided a method for existing clinically recognised patterns to be expressed as a cocktail of scores that might be automatically detected. Temporal linkage for example, might look across the loading, early mid and late single support, and unloading phases to report an average stance value, or across the loading and unloading phases to report a temporal asymmetry. Spatial linkage might allow ranges of concurrent hip, knee and ankle flexion to be grouped into definitions of mild, moderate and severe crouch. In the longer term, it was hoped that this linkage between score and clinical terminology could also work in the opposite direction, providing the potential to clinically interpret patterns identified by a big-data analysis approach.

Two main lessons were learned during the early OctoScores development. First, a lot of numbers are generated. Eight gait phases multiplied by ten potential scores provides eighty numbers to describe a single cycle kinematic graph line. A perfectly adequate 100Hz mo-cap system might output a similar number of data points to fully describe the continuous signal itself. OctoScores are clearly not intended as a data reduction technique, but rather an additional data transformation into a clinically applicable and directly comparable format. Despite

this comparability, the sheer number of scores required to describe both legs and a normative reference over a slow mid and fast walking speed made manual interpretation laborious and ultimately impracticable. From this, it was felt that while the scores could provide a comprehensive basis for interpretation of clinical gait, some form of computerised analysis would be required to filter out redundancy and recognise/identify clinically relevant patterns.

The second lesson, however, was more damning than the first. Although the scores appeared self-consistent in their ability to describe the kinematic produced by the underlying biomechanical model, the model itself, did not always appear to be a good representation of the actual patient movement. In the old RNOH gait lab, I had been aware of the need for clinical pattern recognition above biomechanical analysis. With the move to the new treadmill-based system just prior to starting my PhD studies, I had hoped that the discrepancy between movement and model would be reduced. Instead, the ability to capture properly orthogonal video image from side and coronal views, over multiple strides, served to highlight these model anomalies. Problems were particularly apparent in the transverse plane kinematics. Often measured internal rotation of the thigh, would present as normal in the orthogonal video images, or vice versa. Sometimes, such discrepancies could be resolved by acknowledging a forward rotated pelvic segment. This evaluation was simplified by the additional calculation of segment orientation angles with respect to the laboratory frame, which could then be directly verified against video imagery.

Experiments with existing CGM variants including the Vicon PiG, Motek HBM, plus a cluster-based model suggested by Philip Rowe of the Strathclyde lab (Samala et al., 2020, Meng et al., 2020) failed to produce a convincing solution. The resulting inconsistency was a direct threat to the comparability of equivalent gait across different data collections, on which the OctoScore concept depended. In particular, if measurement remain heavily affected by individual STA, comparison across individuals would not be valid. It is ironic that the CGM solution makes no effort to reduce STA, but is widely defended as the legacy solution on the basis of maintaining this same comparability across different data sets.

7.3 Development of the RNOH_Model – a series of Data Transformations

During the period of initiating the new clinical service, experience over a range of normal and pathological gait patterns, changed the focus of my PhD studies away from OctoScore development, towards the generation of dependable kinematic signals. Anomalies between measured segment orientations, and those observed from orthogonal video images, gave rise to the segment-by-segment development approach outlined in the previous chapters.

On this journey I have spoken to many people about my project. Most of them consider the subject of gait analysis to be complicated. Many (not all) clinicians appear to deal with this complication by taking a black-box approach, with little regard for the mechanics of how inputs relate to outputs. Those of a more scientific mindset have tended to show little interest in the need for outputs to match clinical terminology, perhaps confident in their ability to extract the signal of interest from any reasonable representation of the underlying movement. On reflection, I have not changed the impression I had over a quarter of century ago as a mature undergraduate student, that gait analysis is not fundamentally complicated, and therefore does not require either of these coping paradigms. Instead, I have come to regard the process as a series of data transformations, each of which should strive to minimise loss of information. While the transformation of gait kinematics to OctoScore had not released me from the need for manual pattern recognition, this could now be attributed to the poor transformation on which the kinematic was founded.

As a patient walks, the skeletal orientation of their body segments follows a cyclic pattern. The orientation of each segment is described by one of its orthogonal planes (sagittal, coronal or transverse), which itself may be described by surface markers located over palpable bony landmarks. This process is dependent on accurate marker placement and modelling of any required virtual locations from these markers. This in turn is facilitated by building the model from a calibration trial, during which the subject remains stationary.

When a subject moves away from the static calibration posture, soft tissue structure tends to insulate surface markers from the true skeletal orientations they

represent. Some segment regions are more affected than others. Markers placed to define segment anatomy are unlikely to also be in the least affected regions. It is therefore desirable to place additional surface markers, and to track the anatomical locations from these less STA-affected regions. Calibration in a mid-task posture can further decrease movement away from the spatially synchronised bone/anatomical-marker and anatomical/tracking marker relationships. CGM failure to employ bespoke tracking specific surface markers, and use of a single upright standing calibration pose does not optimise either of these data transformations. The situation is compounded by an avoidance of medial markers, requiring segment anatomical planes to be defined indirectly, by alternative markers not over bony landmarks.

Once the moving orientation of a skeletal plane is mathematically defined, these orientations must be converted to clinical angles. This transformation has been the source of much of the perceived complexity of the gait analysis process (see Chapter 1). Euler angles are a widely used to describe the 3D orientation of one orthogonal reference frame with respect to another. They can therefore be used to describe the instantaneous orientation of one body segment with respect to its neighbour as sagittal, coronal, and transverse plane joint angles. These angles are applied sequentially from a neutral orientation to the specified orientation. The sequence of this application is critical to the angular numeric values; a sequence that provides values that match clinical terminology such as flexion/extension, ab/adduction, in/external rotation is therefore sought.

Here again I have encountered both clinical and scientific mid-sets. Clinicians tend to feel that they are perfectly able to describe the orientation of a joint without any specification of a rotation sequence. Scientists, who understand the mathematical need for the sequence, tend to explain this by concluding that the clinical terminology lacks mathematical rigour. Perhaps the real problem, is that while the Euler angles precisely describe an instantaneous 3D orientation, they are not best suited to describe the change in orientation form one instance to the next. Consider, for example, the clinical orientation of the pelvic segment, requiring specification of its sagittal tilt, coronal obliquity, and transverse rotation through the gait cycle. These angles might alternatively be measured from, frame

by frame measurements of side, front, and top mounted video camera images. In addition to being sequence independent, these true projection angles would precisely match clinical terminology, and would also retain the orthogonality of the original camera mountings.

7.4 Evaluation of the RNOH_Model

The high percentage of accepted hypothesis throughout this thesis, reflects the extensive thought that went into each segment's solution prior to formal testing (Table 7-1). These hypotheses were therefore mostly aimed at confirming solutions already designed to overcome face validity concerns of alternative approaches.

Table 7-1 Summary of Hypothesis tested throughout the RNOH_Model development

2A-I	BMC gait scores reflecting average cycle position, range of motion and inter-cycle variability, from left and right versions of each body segments, will show good symmetry.	ACCEPTED
3A_I	The RNOH_Trunk will provide similar kinematic result to the BMC reference values, but decrease the range of transverse plane movement by better representation of lumbar spine counter rotation in the tracking solution. As a secondary consideration this modification may also restore some coronal plane range.	ACCEPTED
3A-II	In the tested typically developing cohort, the CGM_Thorax will provide a reasonable representation of the holistic RNOH_Trunk solution. This will be demonstrated by the similarities in gait scores between the two solutions, indicating counter movements of the omitted superior and inferior regions by the CGM solution.	ACCEPTED
4A_I	The RNOH_Pelvis will capture more obliquity movement than either of the pelvic based tracking solutions, and thereby better match the gold standard measure.	ACCEPTED
4B_I	The RNOH_Pelvis solution will capture more coronal plane range than all of the other pelvic based tracking solutions.	ACCEPTED
4B_II	The RNOH_Pelvis solution will demonstrate a similar pattern of movement to the other pelvis based tracking solutions.	ACCEPTED
5A_I	With sufficient knee flexion the ex vivo HJC-KJC-AJC plane will provide a good representation of thigh axial rotation, such that it might be employed as a gold standard measure for the in vivo testing.	ACCEPTED
5A_II	Axial tracking accuracy of proximally based markers will be most affected by the hip joint angle, and accuracy of the distal markers most affected by the knee joint angle.	REJECTED
5A_III	Anteriorly placed surface markers will outperform lateral, and distal surface markers will outperform proximal in their ability to accurately capture axial rotation movement.	ACCEPTED
5B_I	A distal thigh CAST tracking cluster will capture a similar amount of transverse plane rotation to the BMC solution, which also employs distal medial and lateral epicondyle markers for the same purpose.	ACCEPTED
5B_II	The RNOH tracking solution will capture considerably more transverse plane rotation than the BMC solution, without fundamentally changing the kinematic form.	ACCEPTED
5B_III	The RNOH axial alignment solution will show good axial alignment of the thigh segment, thus maintaining a low amplitude coronal plane knee kinematic, similar to the BMC reference value.	ACCEPTED
5B_IV	Captured range of thigh motion will show a tendency to decrease with increasing subject BMI. Secondarily, the RNOH solution, which employs the minimum number of thigh surface markers will be least affected by this phenomenon.	REJECTED
6A_I	The flat foot calibration applied to the BMC foot to create the RNOH_Foot, will better represent the orientation of the plantar surface of the foot. This will be demonstrated by generation of the expected near flat-foot mid-stance kinematic in the typically developing cohort	ACCEPTED
6B_I	The RNOH_MSFM joint kinematics will produce characteristic movement patterns with good left/right symmetry in the typically developed test population. This will be demonstrated by showing a predominance of no significant difference in the left versus right gait scores, and substantive left-right correlations of the same.	ACCEPTED

The RNOH_Model is therefore recommended as an optimised surface marker-based solution for the transformations of body segment skeletal movement to TRF orientation, TRF orientation to ARF orientation, and ARF orientation to clinically applicable Euler Angles.

7.5 Study Limitations

7.5.1 Inter-sessional Error

Development of the RNOH-model was driven by the identification and addressing of face-validity concerns over the current CGM marker-set. Whilst it is reasonable to assume some link between these concerns and poor CGM performance, the extent of this connection remains unproven. This approach however, facilitated the prioritisation of model validity over less contentious reliability concerns, while bypassing the requirement for a ground truth measure of skeletal movement to act as a gold standard comparator. Similarly, replacement of need for accurate surface marker placement to represent anatomical axis for the thigh and whole foot body segments, by the introduction of bespoke calibration procedures, also appears reasonable, but has not been tested for inter-sessional repeatability. For these segments there are additional concerns regarding the sensitivity of the model to achieving the required calibration posture. At the foot, this requires only that the heel and metatarsal line be placed flat to the ground, either together or during separate calibrations. Following this, the position of appropriate surface markers can be related to the true plantar surface. Pragmatically, this calibration was performed with the foot unloaded and the subject in a seated posture. The calibration may therefore risks being sensitive to excessive soft tissue compression in the weight bearing foot during the stance phase of gait. Regarding the division of the whole foot into multiple segments, the proposed MSFM will be subject to the same volatility of angular output calculated from surface marker locations at small separation distances, suffered by all foot models. Here again, the development approach of the RNOH_MSFM tackles this face validity concern. Just two additional surface markers are introduced, to define the apices of the medial and lateral longitudinal arches. These, in conjunction with the three locations defining the foot plantar surface, allow the foot to be divided into three similarly sized and relatively rigid subregions, representing the hindfoot, medial

and lateral forefoot. While this approach provides good reasons to predict that the RNOH_MSFM may outperform other currently available models, the actual intersession reliability of this relatively simple MSFM remains untested, and efficacy needs to be formally established prior to clinical implementation.

Of more general concern, is the sensitivity of the crouched posture calibration employed to define the local sagittal plane of the thigh. During this calibration, the local thigh plane is considered coincidental with that defined by the modelled hip, knee and ankle joint centres. The calibration may therefore be sensitive to errors in establishing these joint centres. In particular, if the hip joint centre location is not accurately modelled, either because of poor marker placement or abnormal anatomy, the calibration is liable to be sensitive to the introduction of coronal or transverse plane hip offsets as part of the crouched posture. Here again, formal reliability and sensitivity testing are required to establish clinical efficacy.

7.5.2 Statistical Inference

The Baseline Model Concept (BMC), developed in chapter 2, provided simplistic reference values for the assessment of more sophisticated segment specific modelling tackled in chapters 3 through 6. These sophistications aimed to improve model accuracy and/or utility. While the clinical usability was largely determined by clinical expert opinion, model accuracy was inferred by solution that could maintain the basic movement pattern of the BMC output while capturing more movement range. This concept is premised on the idea that skin sliding, the primary source of tracking error, will always cause surface marker tracking solutions to underestimate true skeletal movements.

Comparison of various modelling approaches with BMC outputs, was facilitated through the development of 5 gait scores for each of the 3 planes of movement, sagittal, coronal, and transverse. The first of these scores simply measured the average cycle position. The second and third scores measured inter-cycle variability as an average standard deviation value, and the cycle range of motion respectively. Fourthly, a movement pattern score represented the area-under-the-curve differences of position normalised output – that is outputs that have been offset so that that they share a common average cycle value. Finally, an

RMS difference score is calculated as a measure of overall difference including position, range and movement pattern. This approach inevitably leads to multiple comparisons between scores from various modelling approaches and the BMC. Although these differences are small, the concurrent nature of the data collection ensures that they are directly related to that model's deviation from BMC.

The question remained however as to which of the above score differences are then worthy of highlighting. In the end I decided to employ multiple T-tests, to highlight scores where the difference holds a 95% probability of representing a genuine structural difference from the modelling approaches, rather than just the sensitivity of each approach to inter-cycle differences. This of course leaves a 5% possibility that a highlighted score does not represent a genuine structural difference in the model output with the BMC solution. In this paradigm, each score is considered individually, and scores representing true modelling differences are highlighted with an accepted false positive rate of 5% for each individual test.

An alternative paradigm to highlighting significant differences between the various modelling approaches and the BMC solution scores, would have been to distribute an acceptable false positive rate of 5% across all scores form a single modelling approach. In this case there would be a 95% chance that all the highlighted scores from that modelling approach represented a genuine structural difference. This paradigm was rejected, because it links the probability of highlighting any individual score to the number of scores that are calculated. A score that under the first paradigm may have highlighted an interesting increase in range of motion, might not be highlighted here, simply because unrelated position, variability, movement, and overall difference scores had 'used-up' some of the accepted error rate. This approach is therefore liable to provide high false negative highlighting rates, with the accompanying temptation to mitigate this effect by calculating fewer score values. In the extreme, the 5% error rate might be distributed across all scores from all modelling approaches, thus also limiting the number of modelling approach that could be sensibly investigated. This approach would of course be more suited to statistical testing where variables are rightly treated as a set all aimed at a common specified hypothesis. The difference here, is that individual scores were calculated to data-mine for any

identifiable effect of small structural changes in the modelling approaches from the BMC solution, and statistically significant differences are sought solely for the purpose of highlighting score difference that exceed an arbitrary probability threshold.

7.5.3 Sample Size

No sample size calculations were performed to justify the collection of data from the convenience sample of just 12 participants. This omission was largely driven by a lack of A priori knowledge as to the sensitivity of the individual gait scores to changes in the model, compared with the inter-cycle variability that would inevitably act to mask these differences.

7.6 Future Work – possibility of Orthogonal, sequence Independent joint angles

Selection of a rotation sequence with the stated aim of outputting angles that match clinical terminology, was incorporated into the BMC development in chapter 2. This development did not however focus on a mathematical proof of equivalence; instead seeking an intuitive understanding more suited to a clinical explanation. After considerable thought, this was finally achieved by a simple rule that linked the required sequence with the neutral orientation of the segment. A rotation sequence was then selected for each segment that first applied the major movement of the segment's principal axis, then the secondary (generally smaller) movement, and finally the axial spin movement.

Further consideration of this intuitive reasoning reveals that even these angles do not exactly match the projection angles that precisely match clinical terminology. This is best illustrated by consideration of a body segment with respect to the laboratory frame (although the same principles would apply to specification of a joint angle). In this case the sagittal orientation of the segment might be expressed as the angle formed by the projection of a segment axis against the equivalent axis of the laboratory's sagittal plane. Technically this is referred to as an axonometric projection, where the projection lines are perpendicular to the viewing plane. This is the angle observed from an orthogonally mounted sagittal facing camera. A coronal angle could similarly be

measured from a coronal facing wall camera image, and a transverse angle from a ceiling mounted camera. Together these three mutually perpendicular projection angles describe the orientation of the segment in terms that will precisely match clinical terminology.

On this realisation, my first thought was that maybe a rotation sequence was inadvertently being specified for the projection angles via the fixing of the cameras to orthogonal planar views with respect to the laboratory. If this were so, it would be akin to the specification of fixed axis rather than an explicit rotation sequence employed by the JCS. However, this is not the case here; the projection angles are fully defined by specification of the reference laboratory frame, while the Euler angle require this specification plus the specification of a rotation sequence.

The difference here is that while the projection angles precisely describe a segment's orientation, the Euler angle describe how to get to that orientation from neutral position. This subtle difference may be further illustrated by an example; consider application of the sagittal-coronal-transverse sequence to a vertically neutral segment such as the thigh. The first rotation in this intrinsic sequence might flex the segment taking the distal KJC forward of the proximal HJC. The second rotation around the no longer horizontal, anterior pointing axis may primarily abduct the segment, but because of the obliquity of the rotation axis will also extend it slightly. The first angle in the sequence will therefore have had to overstate the required flexion angle to compensate for this subsequent extension. Similarly, both the sagittal and coronal angles will need to undo any unintended consequences when the transverse plane rotation is applied around its twice reoriented axis. These compensatory additions or subtractions to the first and second applied Euler angles, means that they can never precisely match the projection angles that describe the resultant segment orientation after completion of all three rotations.

Since the development of clinical gait analysis, application of 3D geometry has become ubiquitous within the computer gaming industry. In these applications it is common to transform co-ordinates from an object frame representing a rigid body to an image frame describing the planar image of that object as might be

observed for example in a flight simulator cockpit window. Application of these transformation in gait analysis has the potential to provide outputs that precisely match clinical terminology, and genuinely deliver on the original JCS aim of being sequence independent and orthogonal. If segment orientations or joint angles were output as axonometric projection angles of the distal segment on to the planes of the proximal ARF plane, they might be calculated by any Euler sequence. The Euler method would then be restricted to describing how to orientate the distal segment from the neutral orientation, at which point the projection angles could describe that orientation with zero discrepancy between technical calculation and clinical expectation. Since coming to this conclusion, I have additionally realised, that a publication I had previously dismissed for suggesting that the Euler approach is not mathematically robust, is actually making the same point, specifically for the pelvic orientation (Wren and Mitiguy, 2007).

7.7 Final Thoughts…

Throughout this thesis I have attempted to find solutions to biomechanical problems that appealed to my dual training, first as a mechanical engineer and later as a physiotherapist. Much of the literature I encountered highlighted the problem of not having gold-standard measure of true bone movement by which one surface marker solution could prove itself over another. To me this seemed a secondary concern, a means of confirming a good solution once it had been developed. When current modelling solutions failed to produce sufficiently robust results to drive the OctoScore concept, a simple examination of their face validity was sufficient to understand why. The developed RNOH_Model attempts to overcome modelling objections at this level. Assumptions of low STA over the proximal segments, are replaced by subjectively more palatable assumptions such as a fix thigh segment. Where the accuracy of required marker placements at the foot segments appeared to make unreasonable demands on the clinician, bespoke calibrations were introduced where marker position were related to neutral postures rather than vice-versa. Similarly for the thigh segment, calibrating the model in mid-flexion posture facilitated a reduce burden for accurate marker placement to define the segment's principal plane.

From the analysis, outlined in chapter 1, it is apparent that the technical development of CGM was largely driven, or at least influenced, by clinicians. Reinterpretation of the established Euler method to describe 3D orientation into the JCS is a prime example of an attempt to bend a technical solution to the clinical mind-set, when with hindsight, a better understanding of the former reveals no disparity. It is my sincere hope that the RNOH_Model presented in this thesis can bridge the gap between technical requirements and clinical expectations. It is also my regret that it has taken so long to develop what with hindsight now seems an obvious (to me) solution to this problem, and my surprise that learning how to disseminate this information seems to have taken even longer.

8 References

ABDEL-AZIZ, Y. I., & KARARA, H.M. Direct Linear Transformation from Comparator Coordinates into Object Space Coordinates in Close-Range Photogrammetry. Proceedings of the Symposium on Close-Range Photogrammetry, 1971 Urbana, Illinois. 1-18.

ALLARD, P. C., L.; D'LIMA, D.; KIRTLEY, C.; LEARDINI, A.;, ROSENBAUM, D. S., O.; SIEGLER, S.; STOKES, I.; WHITTLE, M.; & WITTE, H. W., G. 2003. Response to Dr. Baker's letter to the editor. *Journal of Biomechanics,* 36**,** 303-304.

ALTMAN, A. R., REISMAN, D. S., HIGGINSON, J. S. & DAVIS, I. S. 2012. Kinematic comparison of split-belt and single-belt treadmill walking and the effects of accommodation. *Gait Posture,* 35**,** 287-91.

AN, K. N., BROWNE, A. O., KORINEK, S., TANAKA, S. & MORREY, B. F. 1991. Three-dimensional kinematics of glenohumeral elevation. *J Orthop Res,* 9**,** 143-9.

ANDERSEN, M. S., BENOIT, D. L., DAMSGAARD, M., RAMSEY, D. K. & RASMUSSEN, J. 2010. Do kinematic models reduce the effects of soft tissue artefacts in skin marker-based motion analysis? An in vivo study of knee kinematics. *J Biomech,* 43**,** 268-73.

ANDERSEN, M. S., DAMSGAARD, M., RASMUSSEN, J., RAMSEY, D. K. & BENOIT, D. L. 2012. A linear soft tissue artefact model for human movement analysis: proof of concept using in vivo data. *Gait Posture,* 35**,** 606-11.

ANDRIACCHI, T. P. & ALEXANDER, E. J. 2000. Studies of human locomotion: past, present and future. *J Biomech,* 33**,** 1217-24.

ARAMPATZIS, A., BRUGGEMANN, G. P. & KLAPSING, G. M. 2002. A three-dimensional shank-foot model to determine the foot motion during landings. *Med Sci Sports Exerc,* 34**,** 130-8.

AREBLAD, M., NIGG, B. M., EKSTRAND, J., OLSSON, K. O. & EKSTROM, H. 1990. Three-dimensional measurement of rearfoot motion during running. *J Biomech,* 23**,** 933-40.

ARMAND, S., SANGEUX, M. & BAKER, R. 2014. Optimal markers' placement on the thorax for clinical gait analysis. *Gait Posture,* 39**,** 147-53.

ARNDT, A., WESTBLAD, P., WINSON, I., HASHIMOTO, T. & LUNDBERG, A. 2004. Ankle and subtalar kinematics measured with intracortical pins during the stance phase of walking. *Foot Ankle Int,* 25**,** 357-64.

AURAND, A. M., DUFOUR, J. S. & MARRAS, W. S. 2017. Accuracy map of an optical motion capture system with 42 or 21 cameras in a large measurement volume. *J Biomech,* 58**,** 237-240.

BAKER, R. 1999. A new approach to determine the hip rotation profile from clinical gait analysis data. *Human Movement Science,* 18**,** 655-667.

BAKER, R. 2001. Pelvic angles: a mathematically rigorous definition which is consistent with a conventional clinical understanding of the terms. *Gait Posture,* 13**,** 1-6.

BAKER, R. 2003. Letter to the editor regarding ISB recommendation on definition of joint coordinate systems for the reporting of human joint motion-part I: ankle, hip and spine. *J Biomech,* 36**,** 300-2; author reply 303-4.

BAKER, R. 2006. Gait analysis methods in rehabilitation. *J Neuroeng Rehabil,* 3**,** 4.

BAKER, R. 2013. *Measuring Walking: A Handbook of Clinical Gait Analysis*, Wiley.

BAKER, R., ESQUENAZI, A., BENEDETTI, M. G. & DESLOOVERE, K. 2016. Gait analysis: clinical facts. *Eur J Phys Rehabil Med,* 52**,** 560-74.

BAKER, R., MCGINLEY, J. L., SCHWARTZ, M., THOMASON, P., RODDA, J. & GRAHAM, H. K. 2012. The minimal clinically important difference for the Gait Profile Score. *Gait Posture,* 35**,** 612-5.

BAKER, R., MCGINLEY, J. L., SCHWARTZ, M. H., BEYNON, S., ROZUMALSKI, A., GRAHAM, H. K. & TIROSH, O. 2009. The gait profile score and movement analysis profile. *Gait Posture,* 30**,** 265-9.

BAKER, R. L., F.; REAY, J.; SANGEUX, M. 2018. *The Conventional Gait Model - Success and Limitations*, Springer, Cham.

BARRE, A., AISSAOUI, R., AMINIAN, K. & DUMAS, R. 2017. Assessment of the lower limb soft tissue artefact at marker-cluster level with a high-density marker set during walking. *J Biomech,* 62**,** 21-26.

BAUDET, A., MORISSET, C., D'ATHIS, P., MAILLEFERT, J. F., CASILLAS, J. M., ORNETTI, P. & LAROCHE, D. 2014. Cross-talk correction method for knee kinematics in gait analysis using principal component analysis (PCA): a new proposal. *PLoS One,* 9**,** e102098.

BELL, A. L., PEDERSEN, D. R. & BRAND, R. A. 1990. A comparison of the accuracy of several hip center location prediction methods. *J Biomech,* 23**,** 617-21.

BELLEMARE, F., JEANNERET, A. & COUTURE, J. 2003. Sex differences in thoracic dimensions and configuration. *Am J Respir Crit Care Med,* 168**,** 305-12.

BENOIT, D. L., RAMSEY, D. K., LAMONTAGNE, M., XU, L., WRETENBERG, P. & RENSTROM, P. 2006. Effect of skin movement artifact on knee kinematics during gait and cutting motions measured in vivo. *Gait Posture,* 24**,** 152-64.

BISHOP, C., PAUL, G. & THEWLIS, D. 2012. Recommendations for the reporting of foot and ankle models. *J Biomech,* 45**,** 2185-94.

BISHOP, C., PAUL, G. & THEWLIS, D. 2013. The reliability, accuracy and minimal detectable difference of a multi-segment kinematic model of the foot-shoe complex. *Gait Posture,* 37**,** 552-7.

BONCI, T., CAMOMILLA, V., DUMAS, R., CHEZE, L. & CAPPOZZO, A. 2014. A soft tissue artefact model driven by proximal and distal joint kinematics. *J Biomech,* 47**,** 2354-61.

BONNET, V., RICHARD, V., CAMOMILLA, V., VENTURE, G., CAPPOZZO, A. & DUMAS, R. 2017. Joint kinematics estimation using a multi-body kinematics optimisation and an extended Kalman filter, and embedding a soft tissue artefact model. *J Biomech,* 62**,** 148-155.

BORHANI, M., MCGREGOR, A. H. & BULL, A. M. 2013. An alternative technical marker set for the pelvis is more repeatable than the standard pelvic marker set. *Gait Posture,* 38**,** 1032-7.

BOX, G. E. P. 1976. Science and Statistics. *Journal of the American Statistical Association,* 71**,** 791-799.

BRATEN, M., TERJESEN, T. & ROSSVOLL, I. 1992. Femoral anteversion in normal adults. Ultrasound measurements in 50 men and 50 women. *Acta Orthop Scand,* 63**,** 29-32.

BRUENING, D. A., COONEY, K. M. & BUCZEK, F. L. 2012. Analysis of a kinetic multi-segment foot model. Part I: Model repeatability and kinematic validity. *Gait Posture,* 35**,** 529-34.

CALAPRICE, A. 2000. *The Expanded Quotable Einstein,* Princeton, Princeton University Press.

CAMOMILLA, V., BONCI, T. & CAPPOZZO, A. 2017a. Soft tissue displacement over pelvic anatomical landmarks during 3-D hip movements. *J Biomech,* 62**,** 14-20.

CAMOMILLA, V., DUMAS, R. & CAPPOZZO, A. 2017b. Human movement analysis: The soft tissue artefact issue. *J Biomech,* 62**,** 1-4.

CAPPELLO, A., STAGNI, R., FANTOZZI, S. & LEARDINI, A. 2005. Soft tissue artifact compensation in knee kinematics by double anatomical landmark calibration: performance of a novel method during selected motor tasks. *IEEE Trans Biomed Eng,* 52**,** 992-8.

CAPPOZZO, A., CAPPELLO, A., DELLA CROCE, U. & PENSALFINI, F. 1997. Surface-marker cluster design criteria for 3-D bone movement reconstruction. *IEEE Trans Biomed Eng,* 44**,** 1165-74.

CAPPOZZO, A., CATANI, F., CROCE, U. D. & LEARDINI, A. 1995. Position and orientation in space of bones during movement: anatomical frame definition and determination. *Clin Biomech (Bristol, Avon),* 10**,** 171-178.

CAPPOZZO, A., CATANI, F., LEARDINI, A., BENEDETTI, M. G. & CROCE, U. D. 1996. Position and orientation in space of bones during movement: experimental artefacts. *Clin Biomech (Bristol, Avon),* 11**,** 90-100.

CARSON, M. C., HARRINGTON, M. E., THOMPSON, N., O'CONNOR, J. J. & THEOLOGIS, T. N. 2001. Kinematic analysis of a multi-segment foot model for research and clinical applications: a repeatability analysis. *J Biomech,* 34**,** 1299-307.

CARTNER, J. L., HARTSELL, Z. M., RICCI, W. M. & TORNETTA, P., 3RD 2011. Can we trust ex vivo mechanical testing of fresh--frozen cadaveric specimens? The effect of postfreezing delays. *J Orthop Trauma,* 25**,** 459-61.

CEREATTI, A., BONCI, T., AKBARSHAHI, M., AMINIAN, K., BARRE, A., BEGON, M., BENOIT, D. L., CHARBONNIER, C., DAL MASO, F., FANTOZZI, S., LIN, C. C., LU, T. W., PANDY, M. G., STAGNI, R., VAN DEN BOGERT, A. J. & CAMOMILLA, V. 2017. Standardization proposal of soft tissue artefact description for data sharing in human motion measurements. *J Biomech,* 62**,** 5-13.

CHAI, T. & DRAXLER, R. R. 2014. Root mean square error (RMSE) or mean absolute error (MAE)?: - Arguments against avoiding RMSE in the literature. *Geosci. Model Dev,* 7**,** 1247-1250.

CHAO, E. Y. 1980. Justification of triaxial goniometer for the measurement of joint rotation. *J Biomech,* 13**,** 989-1006.

CHARD, A., GREENE, A., HUNT, A., VANWANSEELE, B. & SMITH, R. 2013. Effect of thong style flip-flops on children's barefoot walking and jogging kinematics. *J Foot Ankle Res,* 6**,** 8.

COBB, S. C., JOSHI, M. N. & POMEROY, R. L. 2016. Reliability of a Seven-Segment Foot Model with Medial and Lateral Midfoot and Forefoot Segments During Walking Gait. *J Appl Biomech,* 32**,** 608-613.

COBB, S. C., TIS, L. L., JOHNSON, J. T., WANG, Y. T., GEIL, M. D. & MCCARTY, F. A. 2009. The effect of low-mobile foot posture on multi-segment medial foot model gait kinematics. *Gait Posture,* 30**,** 334-9.

COCKCROFT, J., LOUW, Q. & BAKER, R. 2016. Proximal placement of lateral thigh skin markers reduces soft tissue artefact during normal gait using the Conventional Gait Model. *Comput Methods Biomech Biomed Engin,* 19**,** 1497-504.

COLLINS, S. H., ADAMCZYK, P. G., FERRIS, D. P. & KUO, A. D. 2009a. A simple method for calibrating force plates and force treadmills using an instrumented pole. *Gait Posture,* 29**,** 59-64.

COLLINS, T. D., GHOUSSAYNI, S. N., EWINS, D. J. & KENT, J. A. 2009b. A six degrees-of-freedom marker set for gait analysis: repeatability and comparison with a modified Helen Hayes set. *Gait Posture,* 30**,** 173-80.

CORNWALL, M. W. & MCPOIL, T. G. 1999. Three-dimensional movement of the foot during the stance phase of walking. *J Am Podiatr Med Assoc,* 89**,** 56-66.

DABIRRAHMANI, D. & HOGG, M. 2017. Modification of the Grood and Suntay Joint Coordinate System equations for knee joint flexion. *Med Eng Phys,* 39**,** 113-116.

DAMSGAARD, M., RASMUSSEN, J., CHRISTENSEN, S. T., SURMA, E. & DE ZEE, M. 2006. Analysis of musculoskeletal systems in the AnyBody Modeling System. *Simulation Modelling Practice and Theory,* 14**,** 1100-1111.

DAVIDS, J. R., MARSHALL, A. D., BLOCKER, E. R., FRICK, S. L., BLACKHURST, D. W. & SKEWES, E. 2003. Femoral anteversion in children with cerebral palsy. Assessment with two and three-dimensional computed tomography scans. *J Bone Joint Surg Am,* 85**,** 481-8.

DAVIS, R. B., JAMESON, E. G., DAVIDS, J. R., CHRISTOPHER, L. M., RGOZINSKI, B. R. & ANDERSON, J. P. 2006. *The Design, Development and Initial Evaluation of a Multi-segment Foot Model for Routine Clinical Gait Analysis*, CRC Press.

DAVIS, R. B., OUNPUU, S., TYBURSKI, D. & GAGE, J. R. 1991. A gait analysis data collection and reduction technique. *Human Movement Science,* 10**,** 575-587.

DE MITS, S., SEGERS, V., WOODBURN, J., ELEWAUT, D., DE CLERCQ, D. & ROOSEN, P. 2012. A clinically applicable six-segmented foot model. *J Orthop Res,* 30**,** 655-61.

DECAVEL, P., MOULIN, T. & SAGAWA, Y., JR. 2019. Gait tests in multiple sclerosis: Reliability and cut-off values. *Gait Posture,* 67**,** 37-42.

DELLA CROCE, U., CAPPOZZO, A. & KERRIGAN, D. C. 1999. Pelvis and lower limb anatomical landmark calibration precision and its propagation to bone geometry and joint angles. *Med Biol Eng Comput,* 37**,** 155-61.

DELP, S. L., ANDERSON, F. C., ARNOLD, A. S., LOAN, P., HABIB, A., JOHN, C. T., GUENDELMAN, E. & THELEN, D. G. 2007. OpenSim: open-source software to create and analyze dynamic simulations of movement. *IEEE Trans Biomed Eng,* 54**,** 1940-50.

DEMPSTER, W. T. 1955. Space requirements of the seated operator. University of Michigan.

DESCHAMPS, K., STAES, F., BRUYNINCKX, H., BUSSCHOTS, E., JASPERS, E., ATRE, A. & DESLOOVERE, K. 2012. Repeatability in the assessment of multi-segment foot kinematics. *Gait Posture,* 35**,** 255-60.

DESCHAMPS, K., STAES, F., ROOSEN, P., NOBELS, F., DESLOOVERE, K., BRUYNINCKX, H. & MATRICALI, G. A. 2011. Body of evidence supporting the clinical use of 3D multisegment foot models: a systematic review. *Gait Posture,* 33**,** 338-49.

DUFFELL, L. D., HOPE, N. & MCGREGOR, A. H. 2014. Comparison of kinematic and kinetic parameters calculated using a cluster-based model and Vicon's plug-in gait. *Proc Inst Mech Eng H,* 228**,** 206-10.

DUMAS, R., CAMOMILLA, V., BONCI, T., CHEZE, L. & CAPPOZZO, A. 2014. Generalized mathematical representation of the soft tissue artefact. *J Biomech,* 47**,** 476-81.

EBERHART, H. D. & INMAN, V. T. 1951. An evaluation of experimental procedures used in a fundamental study of human locomotion. *Ann N Y Acad Sci,* 51**,** 1213-28.

EICHELBERGER, P., FERRARO, M., MINDER, U., DENTON, T., BLASIMANN, A., KRAUSE, F. & BAUR, H. 2016. Analysis of accuracy in optical motion capture - A protocol for laboratory setup evaluation. *J Biomech,* 49**,** 2085-2088.

FIORENTINO, N. M., ATKINS, P. R., KUTSCHKE, M. J., FOREMAN, K. B. & ANDERSON, A. E. 2016. In-vivo quantification of dynamic hip joint center errors and soft tissue artifact. *Gait Posture,* 50**,** 246-251.

FIORENTINO, N. M., ATKINS, P. R., KUTSCHKE, M. J., GOEBEL, J. M., FOREMAN, K. B. & ANDERSON, A. E. 2017. Soft tissue artifact causes significant errors in the calculation of joint angles and range of motion at the hip. *Gait Posture,* 55**,** 184-190.

FLEPS, I., FUNG, A., GUY, P., FERGUSON, S. J., HELGASON, B. & CRIPTON, P. A. 2019. Subject-specific ex vivo simulations for hip fracture risk assessment in sideways falls. *Bone,* 125**,** 36-45.

FLUX, E., VAN DER KROGT, M. M., CAPPA, P., PETRARCA, M., DESLOOVERE, K. & HARLAAR, J. 2020. The Human Body Model versus conventional gait models for kinematic gait analysis in children with cerebral palsy. *Hum Mov Sci,* 70**,** 102585.

FONSECA, M., GASPARUTTO, X., LEBOEUF, F., DUMAS, R. & ARMAND, S. 2020. Impact of knee marker misplacement on gait kinematics of children with cerebral palsy using the Conventional Gait Model-A sensitivity study. *PLoS One,* 15**,** e0232064.

FREEMAN, M. A. & PINSKEROVA, V. 2005. The movement of the normal tibio-femoral joint. *J Biomech,* 38**,** 197-208.

GARLING, E. H., KAPTEIN, B. L., MERTENS, B., BARENDREGT, W., VEEGER, H. E., NELISSEN, R. G. & VALSTAR, E. R. 2007. Soft-tissue artefact assessment during step-up using fluoroscopy and skin-mounted markers. *J Biomech,* 40 Suppl 1**,** S18-24.

GRAY, H. A., GUAN, S., THOMEER, L. T., SCHACHE, A. G., DE STEIGER, R. & PANDY, M. G. 2019. Three-dimensional motion of the knee-joint complex during normal walking revealed by mobile biplane x-ray imaging. *J Orthop Res,* 37**,** 615-630.

GROOD, E. S. & SUNTAY, W. J. 1983. A joint coordinate system for the clinical description of three-dimensional motions: application to the knee. *J Biomech Eng,* 105**,** 136-44.

GUTIERREZ, E. M., BARTONEK, A., HAGLUND-AKERLIND, Y. & SARASTE, H. 2003. Centre of mass motion during gait in persons with myelomeningocele. *Gait Posture,* 18**,** 37-46.

HARA, R., MCGINLEY, J., BRIGGS, C., BAKER, R. & SANGEUX, M. 2016. Predicting the location of the hip joint centres, impact of age group and sex. *Sci Rep,* 6**,** 37707.

HARA, R., SANGEUX, M., BAKER, R. & MCGINLEY, J. 2014. Quantification of pelvic soft tissue artifact in multiple static positions. *Gait Posture,* 39**,** 712-7.

HARRINGTON, M. E., ZAVATSKY, A. B., LAWSON, S. E., YUAN, Z. & THEOLOGIS, T. N. 2007. Prediction of the hip joint centre in adults, children, and patients with cerebral palsy based on magnetic resonance imaging. *J Biomech,* 40**,** 595-602.

HASENBOEHLER, E. A., CHOUDHRY, I. K., NEWMAN, J. T., SMITH, W. R., ZIRAN, B. H. & STAHEL, P. F. 2007. Bias towards publishing positive results in orthopedic and general surgery: a patient safety issue? *Patient Saf Surg,* 1**,** 4.

HENLEY, J. R. J., HUDSON, D., CHRUCH, C., COLEMAN, S., KERSTETTER, L. & MILLER, F. 2008. Reliability of a clinically practical multi-segment foot marker set. *Foot Ankle Motion Anal. Clin. Treat. Technol.*: CRC Press.

HILL, K. D., MANN, S. D., CARBONI, M. P., DOYLE, T. P., IDRISS, S. F., JANSSEN, D. F., NICHOLSON, G. T., SATHANANDAM, S. & FLEMING, G. A. 2018. Variability in radiation dose and image quality: A comparison across fluoroscopy-system vendors, generations of equipment and institutions. *Catheter Cardiovasc Interv,* 92**,** E471-E477.

HOF, A. L., GAZENDAM, M. G. & SINKE, W. E. 2005. The condition for dynamic stability. *J Biomech,* 38**,** 1-8.

HOHE, J., ATESHIAN, G., REISER, M., ENGLMEIER, K. H. & ECKSTEIN, F. 2002. Surface size, curvature analysis, and assessment of knee joint incongruity with MRI in vivo. *Magn Reson Med,* 47**,** 554-61.

HOLDEN, J. P., ORSINI, J. A., SIEGEL, K. L., KEPPLE, T. M., GERBER, L. H. & STANHOPE, S. J. 1997. Surface movement errors in shank kinematics and knee kinetics during gait. *Gait & Posture,* 5**,** 217-227.

HOLLMAN, J. H., BREY, R. H., ROBB, R. A., BANG, T. J. & KAUFMAN, K. R. 2006. Spatiotemporal gait deviations in a virtual reality environment. *Gait Posture,* 23**,** 441-4.

HOLLMAN, J. H., WATKINS, M. K., IMHOFF, A. C., BRAUN, C. E., AKERVIK, K. A. & NESS, D. K. 2016. A comparison of variability in spatiotemporal gait parameters between treadmill and overground walking conditions. *Gait Posture,* 43**,** 204-9.

HOUCK, J. R., TOME, J. M. & NAWOCZENSKI, D. A. 2008. Subtalar neutral position as an offset for a kinematic model of the foot during walking. *Gait Posture,* 28**,** 29-37.

HULLEMAN, C. S., SCHRAGER, S. M., BODMANN, S. M. & HARACKIEWICZ, J. M. 2010. A meta-analytic review of achievement goal measures: different labels for the same constructs or different constructs with similar labels? *Psychol Bull,* 136**,** 422-49.

HULLEY, S. B. M., J.N. CUMMINGS,S.R. 2001. Planning the Measurements: Precision and Accuracy. *Designing Clinical Research.* Second ed.: Lippincott Williams & Wilkins.

HUNT, A. E., SMITH, R. M., TORODE, M. & KEENAN, A. M. 2001. Inter-segment foot motion and ground reaction forces over the stance phase of walking. *Clin Biomech (Bristol, Avon),* 16**,** 592-600.

HWANG, S. J., CHOI, H. S. & KIM, Y. H. 2004. Motion analysis based on a multi-segment foot model in normal walking. *Conf Proc IEEE Eng Med Biol Soc,* 2004**,** 5104-6.

HYSLOP, E., WOODBURN, J., MCINNES, I. B., SEMPLE, R., NEWCOMBE, L., HENDRY, G., RAFFERTY, D., DE MITS, S. & TURNER, D. E. 2010. A reliability study of biomechanical foot function in psoriatic arthritis based on a novel multi-segmented foot model. *Gait Posture,* 32**,** 619-26.

JENKYN, T. R. & NICOL, A. C. 2007. A multi-segment kinematic model of the foot with a novel definition of forefoot motion for use in clinical gait analysis during walking. *J Biomech,* 40**,** 3271-8.

JOHAL, P., WILLIAMS, A., WRAGG, P., HUNT, D. & GEDROYC, W. 2005. Tibio-femoral movement in the living knee. A study of weight bearing and non-weight bearing knee kinematics using 'interventional' MRI. *J Biomech,* 38**,** 269-76.

JOHNSON, R. T. & DICKERSIN, K. 2007. Publication bias against negative results from clinical trials: three of the seven deadly sins. *Nat Clin Pract Neurol,* 3**,** 590-1.

KADABA, M. P., RAMAKRISHNAN, H. K. & WOOTTEN, M. E. 1990. Measurement of lower extremity kinematics during level walking. *J Orthop Res,* 8**,** 383-92.

KAINZ, H., GRAHAM, D., EDWARDS, J., WALSH, H. P. J., MAINE, S., BOYD, R. N., LLOYD, D. G., MODENESE, L. & CARTY, C. P. 2017. Reliability of four models for clinical gait analysis. *Gait Posture,* 54**,** 325-331.

KAINZ, H., MODENESE, L., LLOYD, D. G., MAINE, S., WALSH, H. P. J. & CARTY, C. P. 2016. Joint kinematic calculation based on clinical direct kinematic versus inverse kinematic gait models. *J Biomech,* 49**,** 1658-1669.

KENDALL, F. P., MCCREARY, K. E. & PROVANCE, P. G. 1993. Posture: Alignment and Muscle Balance. *Muscles: testing and function.* 4th ed.: Williams and Wilkins.

KEPPLE, T. M., STANHOPE, S. J., LOHMANN, K. N. & ROMAN, N. L. 1990. A video-based technique for measuring ankle-subtalar motion during stance. *J Biomed Eng,* 12**,** 273-80.

KIDDER, S. M., ABUZZAHAB, F. S., JR., HARRIS, G. F. & JOHNSON, J. E. 1996. A system for the analysis of foot and ankle kinematics during gait. *IEEE Trans Rehabil Eng,* 4**,** 25-32.

KIERNAN, D., MALONE, A., O'BRIEN, T. & SIMMS, C. K. 2015. The clinical impact of hip joint centre regression equation error on kinematics and kinetics during paediatric gait. *Gait Posture,* 41**,** 175-9.

KISHO FUKUCHI, R., ARAKAKI, C., VERAS ORSELLI, M. I. & DUARTE, M. 2010. Evaluation of alternative technical markers for the pelvic coordinate system. *J Biomech,* 43**,** 592-4.

KITAOKA, H. B., CREVOISIER, X. M., HANSEN, D., KATAJARVI, B., HARBST, K. & KAUFMAN, K. R. 2006. Foot and ankle kinematics and ground reaction forces during ambulation. *Foot Ankle Int,* 27**,** 808-13.

KONG, M., JO, H., LEE, C. H., CHUN, S. W., YOON, C. & SHIN, H. 2018. Change of Femoral Anteversion Angle in Children With Intoeing Gait Measured by Three-Dimensional Computed Tomography Reconstruction: One-Year Follow-Up Study. *Ann Rehabil Med,* 42**,** 137-144.

KOO, S. & KOO, Y. J. 2019. Three-dimensional kinematic coupling in the knee during normal walking. *J Biomech Eng*.

KURU, P., CAKIROGLU, A., ER, A., OZBAKIR, H., CINEL, A. E., CANGUT, B., IRIS, M., CANBAZ, B., PICAK, E. & YUKSEL, M. 2016. Pectus Excavatum and Pectus Carinatum: Associated Conditions, Family History, and Postoperative Patient Satisfaction. *Korean J Thorac Cardiovasc Surg,* 49**,** 29-34.

LAMOREUX, L. W. Errors in Thigh Axial Rotation Measurements using Skin Mounted Markers. International society of Biomechanics XIII Congress, 1991.

LATASH, M. L., SCHOLZ, J. P. & SCHONER, G. 2002. Motor control strategies revealed in the structure of motor variability. *Exerc Sport Sci Rev,* 30**,** 26-31.

LEARDINI, A., BENEDETTI, M. G., BERTI, L., BETTINELLI, D., NATIVO, R. & GIANNINI, S. 2007. Rear-foot, mid-foot and fore-foot motion during the stance phase of gait. *Gait Posture,* 25**,** 453-62.

LEARDINI, A., BENEDETTI, M. G., CATANI, F., SIMONCINI, L. & GIANNINI, S. 1999. An anatomically based protocol for the description of foot segment kinematics during gait. *Clin Biomech (Bristol, Avon),* 14**,** 528-36.

LEARDINI, A., BIAGI, F., BELVEDERE, C. & BENEDETTI, M. G. 2009. Quantitative comparison of current models for trunk motion in human movement analysis. *Clin Biomech (Bristol, Avon),* 24**,** 542-50.

LEARDINI, A., BIAGI, F., MERLO, A., BELVEDERE, C. & BENEDETTI, M. G. 2011. Multi-segment trunk kinematics during locomotion and elementary exercises. *Clin Biomech (Bristol, Avon),* 26**,** 562-71.

LEARDINI, A., CARAVAGGI, P., THEOLOGIS, T. & STEBBINS, J. 2019. Multi-segment foot models and their use in clinical populations. *Gait Posture,* 69**,** 50-59.

LEARDINI, A., CHIARI, L., DELLA CROCE, U. & CAPPOZZO, A. 2005. Human movement analysis using stereophotogrammetry. Part 3. Soft tissue artifact assessment and compensation. *Gait Posture,* 21**,** 212-25.

LEBOEUF, F., BAKER, R., BARRE, A., REAY, J., JONES, R. & SANGEUX, M. 2019. The conventional gait model, an open-source implementation that reproduces the past but prepares for the future. *Gait Posture,* 69**,** 126-129.

LI, G., PAPANNAGARI, R., NHA, K. W., DEFRATE, L. E., GILL, T. J. & RUBASH, H. E. 2007. The coupled motion of the femur and patella during in vivo weightbearing knee flexion. *J Biomech Eng,* 129**,** 937-43.

LIEW, B. X. W., MORRIS, S., ROBINSON, M. A. & NETTO, K. 2016. Performance of a lateral pelvic cluster technical system in evaluating running kinematics. *J Biomech,* 49**,** 1989-1993.

LU, T. W. & O'CONNOR, J. J. 1999. Bone position estimation from skin marker co-ordinates using global optimisation with joint constraints. *J Biomech,* 32**,** 129-34.

LUNDGREN, P., NESTER, C., LIU, A., ARNDT, A., JONES, R., STACOFF, A., WOLF, P. & LUNDBERG, A. 2008. Invasive in vivo measurement of rear-, mid- and forefoot motion during walking. *Gait Posture,* 28**,** 93-100.

MACWILLIAMS, B. A., COWLEY, M. & NICHOLSON, D. E. 2003. Foot kinematics and kinetics during adolescent gait. *Gait Posture,* 17**,** 214-24.

MACWILLIAMS, B. A. & DAVIS, R. B. 2013. Addressing some misperceptions of the joint coordinate system. *J Biomech Eng,* 135**,** 54506.

MAIWALD, C., ARNDT, A., NESTER, C., JONES, R., LUNDBERG, A. & WOLF, P. 2017. The effect of intracortical bone pin application on kinetics and tibiocalcaneal kinematics of walking gait. *Gait Posture,* 52**,** 129-134.

MANAL, K., MCCLAY DAVIS, I., GALINAT, B. & STANHOPE, S. 2003. The accuracy of estimating proximal tibial translation during natural cadence walking: bone vs. skin mounted targets. *Clin Biomech (Bristol, Avon),* 18**,** 126-31.

MANTOVANI, G., NG, K. C. & LAMONTAGNE, M. 2016. Regression models to predict hip joint centers in pathological hip population. *Gait Posture,* 44**,** 48-54.

MAURER, J. D., WARD, V., MAYSON, T. A., DAVIES, K. R., ALVAREZ, C. M., BEAUCHAMP, R. D. & BLACK, A. H. 2013. A kinematic description of dynamic midfoot break in children using a multi-segment foot model. *Gait Posture,* 38**,** 287-92.

MCCAHILL, J., SCHALLIG, W., STEBBINS, J., PRESCOTT, R., THEOLOGIS, T. & HARLAAR, J. 2021. Reliability testing of the heel marker in three-dimensional gait analysis. *Gait Posture,* 85**,** 84-87.

MCCLELLAND, J. A., WEBSTER, K. E., GRANT, C. & FELLER, J. 2010. Alternative modelling procedures for pelvic marker occlusion during motion analysis. *Gait Posture,* 31**,** 415-9.

MCDERMOTT, A., BOLGER, C., KEATING, L., MCEVOY, L. & MELDRUM, D. 2010. Reliability of three-dimensional gait analysis in cervical spondylotic myelopathy. *Gait Posture,* 32**,** 552-8.

MCMULKIN, M. L. & GORDON, A. B. 2009. The effect of static standing posture on dynamic walking kinematics: comparison of a thigh wand versus a patella marker. *Gait Posture,* 30**,** 375-8.

MENG, L., MILLAR, L., CHILD, C. & BUIS, A. 2020. A Cluster-based Model Using Functional Methods Requires Less Operator Experience for Reliable Gait Analysis: A Preliminary Study of Intra- and Inter-assessor Reliability. *Annu Int Conf IEEE Eng Med Biol Soc,* 2020**,** 3154-3157.

MENTIPLAY, B. F. & CLARK, R. A. 2018. Modified conventional gait model versus cluster tracking: Test-retest reliability, agreement and impact of inverse kinematics with joint constraints on kinematic and kinetic data. *Gait Posture,* 64**,** 75-83.

MOSELEY, L., SMITH, R., HUNT, A. & GANT, R. 1996. Three-dimensional kinematics of the rearfoot during the stance phase of walking in normal young adult males. *Clin Biomech (Bristol, Avon),* 11**,** 39-45.

MOTION LAB SYSTEMS, I. 1998. *Knee Alignment Device User Manual* [Online]. Available: https://www.motion-labs.com/pdf/kneealignment_ug.pdf [Accessed].

NAGYMATE, G. & KISS, R. M. 2019. Affordable gait analysis using augmented reality markers. *PLoS One,* 14**,** e0212319.

NAIR, S. P., GIBBS, S., ARNOLD, G., ABBOUD, R. & WANG, W. 2010. A method to calculate the centre of the ankle joint: a comparison with the Vicon Plug-in-Gait model. *Clin Biomech (Bristol, Avon),* 25**,** 582-7.

NEPTUNE, R. R., SASAKI, K. & KAUTZ, S. A. 2008. The effect of walking speed on muscle function and mechanical energetics. *Gait Posture,* 28**,** 135-43.

NESTER, C., JONES, R. K., LIU, A., HOWARD, D., LUNDBERG, A., ARNDT, A., LUNDGREN, P., STACOFF, A. & WOLF, P. 2007a. Foot kinematics during walking measured using bone and surface mounted markers. *J Biomech,* 40**,** 3412-23.

NESTER, C. J., JARVIS, H. L., JONES, R. K., BOWDEN, P. D. & LIU, A. 2014. Movement of the human foot in 100 pain free individuals aged 18-45: implications for understanding normal foot function. *J Foot Ankle Res,* 7**,** 51.

NESTER, C. J., LIU, A. M., WARD, E., HOWARD, D., COCHEBA, J. & DERRICK, T. 2010. Error in the description of foot kinematics due to violation of rigid body assumptions. *J Biomech,* 43**,** 666-72.

NESTER, C. J., LIU, A. M., WARD, E., HOWARD, D., COCHEBA, J., DERRICK, T. & PATTERSON, P. 2007b. In vitro study of foot kinematics using a dynamic walking cadaver model. *J Biomech,* 40**,** 1927-37.

NORMAN, G. R. & STREINER, D. L. 2000. Describing the data with numbers. *Biostatistics - The bare essentials.* London: B.C. Decker Inc.

NWOHA, P. U. 1995. The anterior dimensions of the pelvis in male and female Nigerians. *Afr J Med Med Sci,* 24**,** 329-35.

OKITA, N., MEYERS, S. A., CHALLIS, J. H. & SHARKEY, N. A. 2009. An objective evaluation of a segmented foot model. *Gait Posture,* 30**,** 27-34.

OOSTERWAAL, M., CARBES, S., TELFER, S., WOODBURN, J., TORHOLM, S., AL-MUNAJJED, A. A., VAN RHIJN, L. & MEIJER, K. 2016. The Glasgow-Maastricht foot model, evaluation of a 26 segment kinematic model of the foot. *J Foot Ankle Res,* 9**,** 19.

OOSTERWAAL, M., TELFER, S., TORHOLM, S., CARBES, S., VAN RHIJN, L. W., MACDUFF, R., MEIJER, K. & WOODBURN, J. 2011. Generation of subject-specific, dynamic, multisegment ankle and foot models to improve orthotic design: a feasibility study. *BMC Musculoskelet Disord,* 12**,** 256.

OUDE LANSINK, I. L. B., VAN KOUWENHOVE, L., DIJKSTRA, P. U., POSTEMA, K. & HIJMANS, J. M. 2017. Effects of interventions on normalizing step width during self-paced dual-belt treadmill walking with virtual reality, a randomised controlled trial. *Gait Posture,* 58**,** 121-125.

PARIKH, S. & NOYES, F. R. 2011. Patellofemoral disorders: role of computed tomography and magnetic resonance imaging in defining abnormal rotational lower limb alignment. *Sports Health,* 3**,** 158-69.

PARK, S. W., MARINO, H., CHARLES, S. K., STERNAD, D. & HOGAN, N. 2017. Moving slowly is hard for humans: limitations of dynamic primitives. *J Neurophysiol,* 118**,** 69-83.

PASSMORE, E. & SANGEUX, M. 2018. O 002- Is it the right moment to change how we report kinetics? *Gait & Posture,* 26**,** 3-4.

PENA FERNANDEZ, M., HOXHA, D., CHAN, O., MORDECAI, S., BLUNN, G. W., TOZZI, G. & GOLDBERG, A. 2020. Centre of Rotation of the Human Subtalar Joint Using Weight-Bearing Clinical Computed Tomography. *Sci Rep,* 10**,** 1035.

PERRY, J. B. J. M. 1992. *Gait Analysis: Normal and Pathological Function*.

PETERS, A., SANGEUX, M., MORRIS, M. E. & BAKER, R. 2009. Determination of the optimal locations of surface-mounted markers on the tibial segment. *Gait Posture,* 29**,** 42-8.

PIAZZA, S. J. & CAVANAGH, P. R. 2000. Measurement of the screw-home motion of the knee is sensitive to errors in axis alignment. *J Biomech,* 33**,** 1029-34.

POHL, M. B., MESSENGER, N. & BUCKLEY, J. G. 2006. Changes in foot and lower limb coupling due to systematic variations in step width. *Clin Biomech (Bristol, Avon),* 21**,** 175-83.

PREECE, S. J., WILLAN, P., NESTER, C. J., GRAHAM-SMITH, P., HERRINGTON, L. & BOWKER, P. 2008. Variation in pelvic morphology may prevent the identification of anterior pelvic tilt. *J Man Manip Ther,* 16**,** 113-7.

RAGHU, S. L., KANG, C. K., WHITEHEAD, P., TAKEYAMA, A. & CONNERS, R. 2019. Static accuracy analysis of Vicon T40s motion capture cameras arranged externally for motion capture in constrained aquatic environments. *J Biomech,* 89**,** 139-142.

RAMO, N. L., SHETYE, S. S., STREIJGER, F., LEE, J. H. T., TROYER, K. L., KWON, B. K., CRIPTON, P. & PUTTLITZ, C. M. 2018. Comparison of in vivo and ex vivo viscoelastic behavior of the spinal cord. *Acta Biomater,* 68**,** 78-89.

RAMSEY, D. K., WRETENBERG, P. F., BENOIT, D. L., LAMONTAGNE, M. & NEMETH, G. 2003. Methodological concerns using intra-cortical pins to measure tibiofemoral kinematics. *Knee Surg Sports Traumatol Arthrosc,* 11**,** 344-9.

RAO, S., SALTZMAN, C. & YACK, H. J. 2007. Segmental foot mobility in individuals with and without diabetes and neuropathy. *Clin Biomech (Bristol, Avon),* 22**,** 464-71.

RATTANAPRASERT, U., SMITH, R., SULLIVAN, M. & GILLEARD, W. 1999. Three-dimensional kinematics of the forefoot, rearfoot, and leg without the function of tibialis posterior in comparison with normals during stance phase of walking. *Clin Biomech (Bristol, Avon),* 14**,** 14-23.

REINSCHMIDT, C., VAN DEN BOGERT, A. J., MURPHY, N., LUNDBERG, A. & NIGG, B. M. 1997. Tibiocalcaneal motion during running, measured with external and bone markers. *Clin Biomech (Bristol, Avon),* 12**,** 8-16.

RICHARD, V., CAPPOZZO, A. & DUMAS, R. 2017. Comparative assessment of knee joint models used in multi-body kinematics optimisation for soft tissue artefact compensation. *J Biomech,* 62**,** 95-101.

ROCKWELL, S., KIMLER, B. F. & MOULDER, J. E. 2006. Publishing negative results: the problem of publication bias. *Radiat Res,* 165**,** 623-5.

ROUHANI, H., FAVRE, J., CREVOISIER, X., JOLLES, B. M. & AMINIAN, K. 2011. Segmentation of foot and ankle complex based on kinematic criteria. *Comput Methods Biomech Biomed Engin,* 14**,** 773-81.

ROZUMALSKI, A. S., M.H.; NOVACHECK, T. F.; WERVEY, R.; SWANSON, A. DYKES, D. C. 2008. Quantification of Pelvic Soft Tissue Artifact. *In: Gait and Clinical Movement Analysis Society.*

SADEGHI, H., ALLARD, P., SHAFIE, K., MATHIEU, P. A., SADEGHI, S., PRINCE, F. & RAMSAY, J. 2000. Reduction of gait data variability using curve registration. *Gait Posture,* 12**,** 257-64.

SAMALA, M., ROWE, P., RATTANAKOCH, J. & GUERRA, G. 2020. A Comparison of the Conventional PiG Marker Method Versus a Cluster-Based Model when recording Gait Kinematics in Trans-Tibial Prosthesis Users and the Implications for Future IMU Gait Analysis. *Sensors (Basel),* 20.

SARASWAT, P., MACWILLIAMS, B. A. & DAVIS, R. B. 2012. A multi-segment foot model based on anatomically registered technical coordinate systems: method repeatability in pediatric feet. *Gait Posture,* 35**,** 547-55.

SAWACHA, Z., CRISTOFERI, G., GUARNERI, G., CORAZZA, S., DONA, G., DENTI, P., FACCHINETTI, A., AVOGARO, A. & COBELLI, C. 2009. Characterizing multisegment foot kinematics during gait in diabetic foot patients. *J Neuroeng Rehabil,* 6**,** 37.

SCHACHE, A. G. & BAKER, R. 2007. On the expression of joint moments during gait. *Gait Posture,* 25**,** 440-52.

SCHACHE, A. G., BAKER, R. & LAMOREUX, L. W. 2006. Defining the knee joint flexion-extension axis for purposes of quantitative gait analysis: an evaluation of methods. *Gait Posture,* 24**,** 100-9.

SCHACHE, A. G., BAKER, R. & LAMOREUX, L. W. 2008. Influence of thigh cluster configuration on the estimation of hip axial rotation. *Gait Posture,* 27**,** 60-9.

SCHACHE, A. G., BAKER, R. & VAUGHAN, C. L. 2007. Differences in lower limb transverse plane joint moments during gait when expressed in two alternative reference frames. *J Biomech,* 40**,** 9-19.

SCHULZ, B. W. & KIMMEL, W. L. 2010. Can hip and knee kinematics be improved by eliminating thigh markers? *Clin Biomech (Bristol, Avon),* 25**,** 687-92.

SCOTT, S. H. & WINTER, D. A. 1991. Talocrural and talocalcaneal joint kinematics and kinetics during the stance phase of walking. *J Biomech,* 24**,** 743-52.

SEO, S. G., LEE, D. Y., MOON, H. J., KIM, S. J., KIM, J., LEE, K. M., CHUNG, C. Y. & CHOI, I. H. 2014. Repeatability of a multi-segment foot model with a 15-marker set in healthy adults. *J Foot Ankle Res,* 7**,** 24.

SIMON, J., DOEDERLEIN, L., MCINTOSH, A. S., METAXIOTIS, D., BOCK, H. G. & WOLF, S. I. 2006. The Heidelberg foot measurement method: development, description and assessment. *Gait Posture,* 23**,** 411-24.

SINITSKI, E. H., LEMAIRE, E. D. & BADDOUR, N. 2015. Evaluation of motion platform embedded with dual belt treadmill instrumented with two force plates. *J Rehabil Res Dev,* 52**,** 221-34.

SLATER, A. A., HULLFISH, T. J. & BAXTER, J. R. 2018. The impact of thigh and shank marker quantity on lower extremity kinematics using a constrained model. *BMC Musculoskelet Disord,* 19**,** 399.

SLOOT, L. H., VAN DER KROGT, M. M. & HARLAAR, J. 2014. Self-paced versus fixed speed treadmill walking. *Gait Posture,* 39**,** 478-84.

SONG, S., CHOI, H. & COLLINS, S. H. 2020. Using force data to self-pace an instrumented treadmill and measure self-selected walking speed. *J Neuroeng Rehabil,* 17**,** 68.

SOUZA, T. R., FONSECA, H. L., VAZ, A. C., ANTERO, J. S., MARINHO, C. S. & FONSECA, S. T. 2014. Between-day reliability of a cluster-based method for multisegment kinematic analysis of the foot-ankle complex. *J Am Podiatr Med Assoc,* 104**,** 601-9.

STAGNI, R., FANTOZZI, S. & CAPPELLO, A. 2006. Propagation of anatomical landmark misplacement to knee kinematics: performance of single and double calibration. *Gait Posture,* 24**,** 137-41.

STAGNI, R., FANTOZZI, S. & CAPPELLO, A. 2009. Double calibration vs. global optimisation: performance and effectiveness for clinical application. *Gait Posture,* 29**,** 119-22.

STAGNI, R., FANTOZZI, S., CAPPELLO, A. & LEARDINI, A. 2005. Quantification of soft tissue artefact in motion analysis by combining 3D fluoroscopy and stereophotogrammetry: a study on two subjects. *Clin Biomech (Bristol, Avon),* 20**,** 320-9.

STEBBINS, J., HARRINGTON, M., THOMPSON, N., ZAVATSKY, A. & THEOLOGIS, T. 2006. Repeatability of a model for measuring multi-segment foot kinematics in children. *Gait Posture,* 23**,** 401-10.

STIEF, F., BOHM, H., MICHEL, K., SCHWIRTZ, A. & DODERLEIN, L. 2013. Reliability and accuracy in three-dimensional gait analysis: a comparison of two lower body protocols. *J Appl Biomech,* 29**,** 105-11.

STRAUSS, K. J. 2019. Advancing Safety: Role of Equipment Design and Configuration Change in Pediatric Fluoroscopy. *Health Phys,* 116**,** 256-262.

SUTHERLAND, D. H. & HAGY, J. L. 1972. Measurement of gait movements from motion picture film. *J Bone Joint Surg Am,* 54**,** 787-97.

TAYLOR, W. R., EHRIG, R. M., DUDA, G. N., SCHELL, H., SEEBECK, P. & HELLER, M. O. 2005. On the influence of soft tissue coverage in the determination of bone kinematics using skin markers. *J Orthop Res,* 23**,** 726-34.

TESIO, L. & ROTA, V. 2008. Gait analysis on split-belt force treadmills: validation of an instrument. *Am J Phys Med Rehabil,* 87**,** 515-26.

THEUNISSEN, K., VAN HOOREN, B., PLASQUI, G. & MEIJER, K. 2021. Self-paced and fixed speed treadmill walking yield similar energetics and biomechanics across different speeds. *Gait Posture,* 92**,** 2-7.

THOMAS, R., DANIELS, T. R. & PARKER, K. 2006. Gait analysis and functional outcomes following ankle arthrodesis for isolated ankle arthritis. *J Bone Joint Surg Am,* 88**,** 526-35.

THORNTON, M. J., DELANEY, R. M. & EASTWOOD, D. M. 2016. A new method to track the thigh segment which combines the advantages of two long established techniques. *ESMAC.* Seville: Gait & Posture.

THORNTON, M. J., MORRISSEY, M. C. & COUTTS, F. J. 1998. Some effects of camera placement on the accuracy of the Kinemetrix three-dimensional motion analysis system. *Clin Biomech (Bristol, Avon),* 13**,** 452-4.

THORNTON, M. J., RICHARDS, R. E. & DELANEY, R. M. R. 2014. Highlighting subtle changes in gait—A new scoring system. *Gait & Posture,* 39**,** S25-S26.

TOME, J., NAWOCZENSKI, D. A., FLEMISTER, A. & HOUCK, J. 2006. Comparison of foot kinematics between subjects with posterior tibialis tendon dysfunction and healthy controls. *J Orthop Sports Phys Ther,* 36**,** 635-44.

TOPLEY, M. & RICHARDS, J. G. 2020. A comparison of currently available optoelectronic motion capture systems. *J Biomech,* 106**,** 109820.

TULCHIN, K., ORENDURFF, M. & KAROL, L. 2010a. A comparison of multi-segment foot kinematics during level overground and treadmill walking. *Gait Posture,* 31**,** 104-8.

TULCHIN, K., ORENDURFF, M. & KAROL, L. 2010b. The effects of surface slope on multi-segment foot kinematics in healthy adults. *Gait Posture,* 32**,** 446-50.

UDING, A., BLOOM, N. J., COMMEAN, P. K., HILLEN, T. J., PATTERSON, J. D., CLOHISY, J. C. & HARRIS-HAYES, M. 2019. Clinical tests to determine femoral version category in people with chronic hip joint pain and asymptomatic controls. *Musculoskelet Sci Pract,* 39**,** 115-122.

VAN DEN BOGERT, A. J., GEIJTENBEEK, T., EVEN-ZOHAR, O., STEENBRINK, F. & HARDIN, E. C. 2013. A real-time system for biomechanical analysis of human movement and muscle function. *Med Biol Eng Comput,* 51**,** 1069-77.

VAN DEN BOGERT, A. J., SMITH, G. D. & NIGG, B. M. 1994. In vivo determination of the anatomical axes of the ankle joint complex: an optimization approach. *J Biomech,* 27**,** 1477-88.

VICON 2017a. Full body modelling with Plug-in Gait. *Plug-in Gait Reference Guide.*

VICON 2017b. Lower body modeling with Plug-in Gait. *Plug-in Gait Reference Guide.* Vicon Motion Systems Ltd.

VICON, O. M.-. 1999. *Plug-In Gait Manual Ver 1* [Online]. Available: http://www.irc-web.co.jp/vicon_web/news_bn/PIGManualver1.pdf [Accessed].

WARRENER, A. G., LEWTON, K. L., PONTZER, H. & LIEBERMAN, D. E. 2015. A wider pelvis does not increase locomotor cost in humans, with implications for the evolution of childbirth. *PLoS One,* 10**,** e0118903.

WELL, D. S., MEIER, J. M., MAHNE, A., HOUSENI, M., HERNANDEZ-PAMPALONI, M., MONG, A., MISHRA, S., ZHUGE, Y., SOUZA, A., UDUPA, J. K., ALAVI, A. & TORIGIAN, D. A. 2007. Detection of age-related changes in thoracic structure and function by computed tomography, magnetic resonance imaging, and positron emission tomography. *Semin Nucl Med,* 37**,** 103-19.

WILLMOTT, C. J. & MATSUURA, K. 2005. Advantages of the mean absolute error (MAE) over the root mean square error (RMSE) in assessing average model performance. *Clim Res,* 30**,** 79-82.

WITTMAN, A. B. & WALL, L. L. 2007. The evolutionary origins of obstructed labor: bipedalism, encephalization, and the human obstetric dilemma. *Obstet Gynecol Surv,* 62**,** 739-48.

WOLF, P., STACOFF, A., LIU, A., NESTER, C., ARNDT, A., LUNDBERG, A. & STUESSI, E. 2008. Functional units of the human foot. *Gait Posture,* 28**,** 434-41.

WOODBURN, J., TURNER, D. E., HELLIWELL, P. S. & BARKER, S. 1999. A preliminary study determining the feasibility of electromagnetic tracking for kinematics at the ankle joint complex. *Rheumatology (Oxford),* 38**,** 1260-8.

WREN, T. A., DO, K. P., HARA, R. & RETHLEFSEN, S. A. 2008. Use of a patella marker to improve tracking of dynamic hip rotation range of motion. *Gait Posture,* 27**,** 530-4.

WREN, T. A., GORTON, G. E., 3RD, OUNPUU, S. & TUCKER, C. A. 2011. Efficacy of clinical gait analysis: A systematic review. *Gait Posture,* 34**,** 149-53.

WREN, T. A., LENING, C., RETHLEFSEN, S. A. & KAY, R. M. 2013. Impact of gait analysis on correction of excessive hip internal rotation in ambulatory children with cerebral palsy: a randomized controlled trial. *Dev Med Child Neurol,* 55**,** 919-25.

WREN, T. A. & MITIGUY, P. C. 2007. A simple method to obtain consistent and clinically meaningful pelvic angles from euler angles during gait analysis. *J Appl Biomech,* 23**,** 218-23.

WU, G. & CAVANAGH, P. R. 1995. ISB recommendations for standardization in the reporting of kinematic data. *J Biomech,* 28**,** 1257-61.

WU, G., SIEGLER, S., ALLARD, P., KIRTLEY, C., LEARDINI, A., ROSENBAUM, D., WHITTLE, M., D'LIMA, D. D., CRISTOFOLINI, L., WITTE, H., SCHMID, O., STOKES, I., STANDARDIZATION & TERMINOLOGY COMMITTEE OF THE INTERNATIONAL

SOCIETY OF, B. 2002. ISB recommendation on definitions of joint coordinate system of various joints for the reporting of human joint motion--part I: ankle, hip, and spine. International Society of Biomechanics. *J Biomech,* 35**,** 543-8.

WU, G., VAN DER HELM, F. C., VEEGER, H. E., MAKHSOUS, M., VAN ROY, P., ANGLIN, C., NAGELS, J., KARDUNA, A. R., MCQUADE, K., WANG, X., WERNER, F. W., BUCHHOLZ, B. & INTERNATIONAL SOCIETY OF, B. 2005. ISB recommendation on definitions of joint coordinate systems of various joints for the reporting of human joint motion--Part II: shoulder, elbow, wrist and hand. *J Biomech,* 38**,** 981-992.

WU, W. L., SU, F. C., CHENG, Y. M., HUANG, P. J., CHOU, Y. L. & CHOU, C. K. 2000. Gait analysis after ankle arthrodesis. *Gait Posture,* 11**,** 54-61.

ZAJAC, F. E. & GORDON, M. E. 1989. Determining muscle's force and action in multi-articular movement. *Exerc Sport Sci Rev,* 17**,** 187-230.

ZATSIORSKY, V. M. 1998a. 1.2.1 Fixation of a Local System With a Rigid Body. *Kinematics of Human Motion.* Human Kinetics.

ZATSIORSKY, V. M. 1998b. 2.1.2 The Clinical Reference System. *Kinematics of Human Motion.* Human Kinetics.

ZENI, J. A., JR. & HIGGINSON, J. S. 2010. Gait parameters and stride-to-stride variability during familiarization to walking on a split-belt treadmill. *Clin Biomech (Bristol, Avon),* 25**,** 383-6.

ZENI, J. A., JR., RICHARDS, J. G. & HIGGINSON, J. S. 2008. Two simple methods for determining gait events during treadmill and overground walking using kinematic data. *Gait Posture,* 27**,** 710-4.

ZHANG, J. T., NOVAK, A. C., BROUWER, B. & LI, Q. 2013. Concurrent validation of Xsens MVN measurement of lower limb joint angular kinematics. *Physiol Meas,* 34**,** N63-9.

ZHU, G., WANG, Z., YUAN, C., GENG, X., YU, J., ZHANG, C., HUANG, J., WANG, X. & MA, X. 2020. In vitro study of foot bone kinematics via a custom-made cadaveric gait simulator. *J Orthop Surg Res,* 15**,** 346.